THE UNIVERSITY *of* EDINBURGH

Field spectroscopy and spectral reflectance modelling of *Calluna vulgaris*

Alasdair A. Mac Arthur

THE UNIVERSITY
of EDINBURGH

Thesis submitted in fulfilment of
the requirements for the degree of
Doctor of Philosophy
to the
University of Edinburgh — 2011

Declaration

I declare that this thesis has been composed solely by myself and that it has not been submitted, either in whole or in part, in any previous application for a degree. Except where otherwise acknowledged, the work presented is entirely my own.

Alasdair Mac Arthur

August 2011

Abstract

Boreal peatlands store carbon sequestered from the atmosphere over millennia and the importance of this and the other ecosystem services these areas provide is now widely recognised. However, a changing climate will affect these environments and, consequently, the services they provide to the global population. The rate and direction of environmental change to peatlands is currently unclear and they have not yet been included in many climate models. This may in part be due to the ecological heterogeneity and spatial extent of these areas and the sparse sampling survey methods currently adopted. Hyperspectral remote sensing from satellite platforms may in future offer an approach to surveying and do so at the high spectral and spatial resolutions necessary to infer ecological change in these peatlands. However, work is required to develop methods of analysis to determine if hyperspectral data can be used to measure the overstorey vegetation of these areas. This will require an understanding of how annual and inter-annual cyclical changes affect the peatland plant canopy reflectances that would be recorded by hyperspectral sensors and how these reflectances can be related to state variable of interest to climate scientists, ecologists and peatland managers.

There are significant areas of peatland within Scotland and, as it is towards the southern extreme of the boreal peatlands, these may be an early indicator of environment change to the wider boreal region. *Calluna vulgaris*, a hardy dwarf shrub, is the dominant overstorey species over much of these peatlands and could

serve as a proxy for ecological, and consequently, environmental change. However, little has been done to understand how variations in leaf pigments or canopy structural parameters influence the spectral reflectance of *Calluna* through annual and inter-annual growth and senescence cycles. Nor has much work been done to develop methods of analysis to enable images acquired by hyperspectral remote sensing to be utilised to monitor change to these *Calluna* dominated peatlands over time.

To advance understanding of the optical properties of *Calluna* leaves and canopies and develop methods to analyse hyperspectral images laboratory, field and modelling studies have been carried out in time series over a number of years. The leaf and canopy parameters significantly affecting reflectance have been identified and quantified. Differences between published Chlorophyll$_{(a+b)}$ *in vivo* absorption spectra and those determined were found. Carotenoids and Anthocyanins were also identified and quantified. The absorption spectra of these pigments were incorporated into a canopy reflectance model and this was coupled to a *Calluna* growth model. This combined model enabled the reflectance of *Calluna* canopies to be modelled in daily increments through annual and inter-annual growth and senescence cycles. Reasonable results were achieved in spectral regions where reflectance changed systematically but only for homogeneous *Calluna* stands.

However, it was noted during this research that the area of support for the spectral measurements appeared to differ from that assumed from the specification provided by the spectroradiometer manufacturers. The directional response functions (DRFs) of two spectroradiometers were investigated and wavelength, or wavelength region, specific spatial dependences were noted. The effect that the DRFs of the spectroradiometers would have on reflectances recorded from *Calluna* canopies was investigated through a modelling study. Errors and inaccuracies in the spectra that would be recorded from these canopies, and commonly used biochemical indices derived from them, have been quantified.

Acknowledgements

I wish to thank the many individuals and organisations who have assisted during this research: Charlie Woodward, Terry Robinson and Alan Brown of Clyde Muirshiel Regional Park, for assistance initiating this research and for access to ecological records; Iain Duff and David Patterson, for access to Hardridge Farm; Jim McLeod and Robin Pakeman, of the Macaulay Land Use Research Institute (MLURI) for their assistance with the adaptation of HeathMod; Andrew Nolan and Andy Dalziel of the MLURI for their assistance with biomass sampling; Hartmut Lichtenthaler for taking time out from his retirement to discuss leaf pigments-in-complex; the staff at ASD and SVC who assisted me gain a fuller understanding of their spectroradiometers; Mark Danson of the University of Salford for loan of a SunScan; Edmund Potter of Delta-T Devices and John Wood of Peak Design for their advice on interpreting SunScan data; and Guillaume Drolet for discussions on LAI optical measurements. I would also like to thank Terry Dawson and Andres Kuusk for advice on using their reflectance models, LIBERTY and ACRM respectively, Gary Llewellyn for the Matlab version of LIBERTY, and Stephen Jacquemoud for informative discussions on radiative transfer modelling.

In the UK we are fortunate to have a number of organisations funded by central government to support academic research. I wish to thank: the staff at the Met Office in Edinburgh and British Atmospheric Data Centre for access to

meteorological archives; the Natural Environment Research Council (NERC) Geophysical Equipment Facility (GEF) for a loan of a differential GPS and GEF staff, Alan Hobbs and Colin Kay, for assistance with a GPS field survey; the NERC Airborne Research and Survey Facility for numerous "flights over Inverclyde" at times 'above and beyond the call of duty'; the NERC Field Spectroscopy Facility (FSF) for loans of field spectroradiometers and my colleague at FSF Chris MacLellan for collaborating in some aspects of this research and his support and advice on the 'peculiarities' of the measurement of light. I would also like to acknowledge my appreciation for the support and encouragement given to me by Lin Kay and the NERC Services and Facilities management team.

At the School of Geosciences we are particularly fortune to have a great team of Computing Officers whose professionalism and support often seems to be overlooked. I would like to thank this team for their advice, assistance and support over the years. In particular, I would like to acknowledge the support and assistance given to me by Magnus Hagdorn; through his development of various bits of computer code used in this thesis; for encouraging me to write in LaTeX; and for introducing me to Linux. I would also like to thank fellow, and former students students John Downs, Rachel Gaulton, Karin Viergever for their assistance with field work. My thanks also to Iain Woodhouse, my supervisor for the latter period of my research.

I also wish to thank Tim Malthus my supervisor from near and from far. His support, guidance and friendship have been invaluable. My love and thanks too my cousin Carole Tyson for her support, to expansive to mention in any detail. My love and thanks also too my sister, Katherine Taylor and my children, Sandy and Mike, for their love and support, again to expansive to mention, over many, many years. My love and thanks to my parents, who are unfortunately no longer with us - this is in memory of you. Finally to my wife for her love, patience, support and encouragement - I could not have done it without you, Suk Han.

Contents

List of Tables

List of Figures

List of abbreviations and symbols

ACRM	Analytical Canopy Reflectance Model
ANOVA	Analysis of variance
Antho.	Anthocyanins
ARSF	Airborne Research and Survey Facility
ASD	Analytical Spectral Devices
Avg.	Average
BRDF	Bidirectional reflectance distribution function
cm	centimetres
CO_2	Carbon dioxide
Dia.	Diameter
DRF	Directional response function
EO	Earth observation
FO	Fore optic
FOP	Fibre optic probe
FOV	Field-of-view
FSF	Field Spectroscopy Facility
FWHM	Full width half maximum
g	grams
GEF	Geophysical Equipment Facility
GUI	Graphical user interface
ha	Hectares
HPLC	High performance liquid chromatography
IFOV	Instantaneous field-of-view
InGaAs	Indium gallium arsenide
kg	Kilogram
km	Kilometre
LAI	Leaf area index
LEAFMOD	Leaf Experimental Absorptivity Feasibility MODel
LIBERTY	Leaf Incorporating Biochemistry Exhibiting Reflectance and Transmittance Yields
LIBERTY3p	LIBERTY with 3 pigment components
LIDAR	Light detection and ranging
m	metres
MCRM	Marlov chain canopy reflectance model
MLURI	Macaulay Land Use Research Institute

μg	micrograms
μm	micrometres
mg	milligrams
mm	millimetres
ND	Normalised difference
n.d.	no date
NERC	Natural Environment Research Council
NIR	Near infra-red
nm	nanometre
NS	Natural Surface
NVC	National Vegetation Classification
PAR	Photosynthetically active radiation
PROSPECT	Leaf radiative transfer model
PSF	Point spread function
PSRI	Plant senescence reflectance index
QA	Quality assurance
RAMI	Radiation transfer Model intercomparison
REP	Red edge position
RMSE	Root mean squared error
RS	Remote sensing
RT	Radiative transfer
SAIL	Scattering by Arbitrarily Inclined Leaves
SD	Standard deviation
SIPI	Structure-insensitive pigment index
SNH	Scottish Natural Heritage
SPA	Special Protected Area
SR	Simple ratio
SVC	Spectra Vista Corporation
SWIR	Short wave infra-red
SWIR-1	Short wave infra-red region 1 (1,000 nm to 1,800 nm)
SWIR-2	Short wave infra-red region 1 (1,800 nm to 2,500 nm)
VNIR	Visible near infra-red (400 nm to 1,000 nm)
4SAIL2	SAIL with two canopy layers
A_{Antho}	Anthocyanins absorption coefficient
$A_{Caroten}$	Carotenoids absorption coefficient
A_{Chloro}	Chlorophyll$_{(a+b)}$ absorption coefficient
$A_{LigCell}$	Lignin and cellulose absorption coefficient
$A_{protein}$	Nitrogen absorption coefficient
A_{water}	Water absorption coefficient
B	Baseline absorption coefficient
C_{Antho}	Anthocyanins content
$C_{Caroten}$	Carotenoids content

C_{Chloro}	Chlorophyll$_{(a+b)}$ content
$C_{LigCell}$	Lignin and cellulose content
$C_{LigCell}$	Lignin and cellulose content
$C_{protein}$	Nitrogen content
C_{water}	Water content
f_{Albino}	Albino factor
λ	Wavelength
$Tcoeff$	Total absorption coefficient

Chapter 1

Introduction

1.1 *Calluna vulgaris* and the environment within which it grows

The upland moors of Scotland are "one of the most distinctive habitats found in Europe" (Thompson *et al.*, 1995). These areas are of significant economic, aesthetic and nature conservation value nationally and internationally (Mackey *et al.*, 2001) and are "intimately linked to the major environmental interactions of our planet such as climate change" (Lindsay, 1995). The flowering and pattern of *Calluna vulgaris* (heather, as it is known colloquially) on these moors dominates the landscape and forms the back drop to much of the history of Scotland and contributes to the cultural identity of many Scots (Paterson, 2002).

Calluna vulgaris, henceforth referred to as *Calluna*, is a hardy dwarf shrub which grows in cool temperate climates such as Scotland's. Though adaptive, *Calluna* prefers to grow in moist acid soils in cool climates and some areas of the world's temperate peatlands fulfil this requirement. Peat has accumulated over millennia

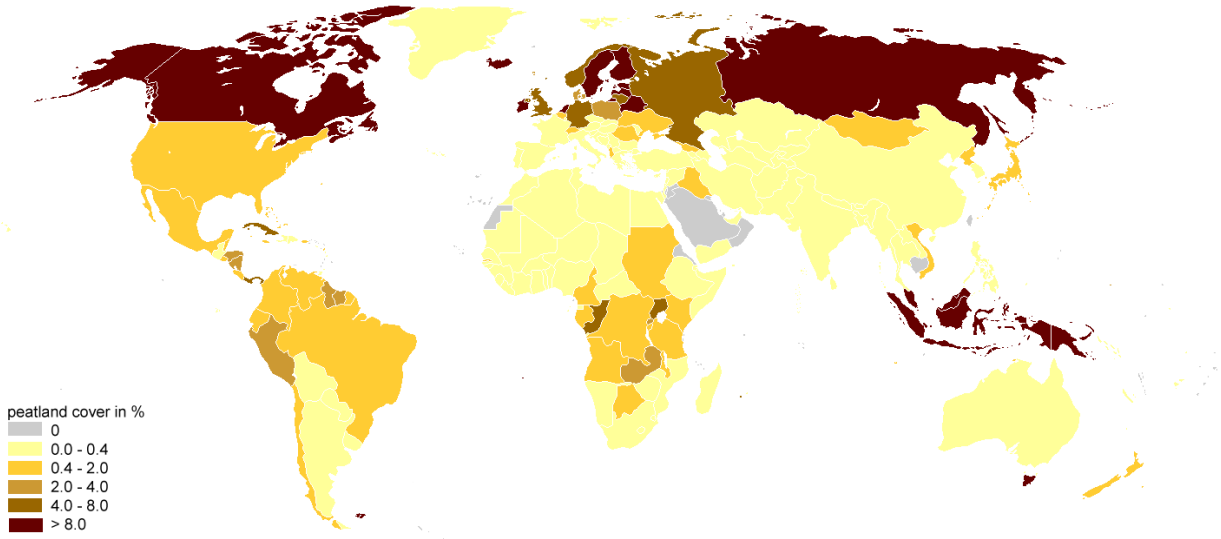

Figure 1.1: Global distribution of peatlands
Adapted from Joosten, H. (2010).

in areas with predominantly wet cool climates and where aerobic decomposition of dead vegetation is limited. The greatest proportion of the world's peat is in the boreal peatland ecosystems of the Earth's northern hemisphere (Figure 1.1) (Joosten, 2010) and the extensive services these peatlands provide is increasingly being recognised (Joosten and Clarke, 2002; Rochefort and Lode, 2006; Baird *et al.*, 2009; Bonn *et al.*, 2009a). The importance of the status and dynamics of peatlands, their place in the carbon cycle and their sensitivity to allogenic change is of global importance (Charman, 2002; Harris and Bryant, 2009b; Kurbatova *et al.*, 2009). However, these areas are under threat from a range of environmental and societal pressures (Joosten and Clarke, 2002; Rochefort and Lode, 2006; Baird *et al.*, 2009; Bonn *et al.*, 2009b). Yet the status and dynamics of these areas is not fully understood and they have not yet been incorporated into many Earth surface/atmosphere gas exchange and climate models (Limpens *et al.*, 2008; Baird *et al.*, 2009; Billett *et al.*, 2010). Dwarf shrubs form the overstorey on extensive areas of boreal peatlands, with some species being endemic or regionally distinct. As species dominance and mix are influenced by geographical,

environmental and ecological conditions dwarf shrubs may be used as an indicator of these conditions (Vitt, 2006). As the UK's peatlands are towards the southern extreme of the global boreal peatland distribution (MacDonald *et al.*, 2006), they may be particularly susceptible to environmental change driven by current or potential global climate variations. Developing quantitative methods to measure the status and dynamics of these peatlands would enable them to be monitored and inform management and policy decision and may also enable these areas to be incorporated into Earth/atmosphere flux and climate models. The *Calluna* dominated peatlands of Scotland may serve as a suitable environment in which such methods can be developed.

Optical remote sensing (RS) from airborne or satellite platforms offers one practical approach to survey extensive areas such as peatlands. Nevertheless, achieving acceptable levels of classification accuracy has been problematic due to the 'coarse' spectral and spatial resolutions of the optical imaging sensors used (Bird *et al.*, 2000; Earth Observation for Natura, 2000). Hyperspectral imaging sensors are now available on airborne platforms which can measure at far greater spectral and spatial resolutions and there are plans to mount similar sensors on satellite platforms in the coming decade. To realise the full potential of hyperspectral sensors on satellite platforms for quantitative RS in the future, a greater understanding of the interaction of light with the overstorey vegetation on peatlands is required.

1.2 Overview of this thesis

1.2.1 Objective

In order to better use hyperspectral remote sensing to characterise *Calluna* dominated peatlands, both to improve classifications and to measure biological and physiological processes, it is necessary to have a greater understanding of the interaction of light with photosynthesising *Calluna* shoots and leaves and its canopy structure and the influence that field spectroradiometer characteristics have on the areas sampled and spectra recorded. It is also necessary to develop methods to enable the changing *Calluna* canopy structure to be quantitatively and replicably measured and canopy reflectance to be modelled through its annual and inter-annual growth and senescence cycles. This thesis sets out to increase this understanding and begin canopy reflectance model development to enable *Calluna* to be used as an indicator of ecological and environmental change in global monitoring studies and to inform local and regional management decision making.

1.3 Peatlands

1.3.1 Formation of the boreal peatlands and their significance

Boreal peatland ecosystems cover only approximately 3% of the Earth's land surface, yet they contain approximately 30% of the world's terrestrial soil carbon (Wieder and Vitt, 2006). This carbon has been sequestered from the atmosphere over millennia primarily by bryophytes (but also, although to a lesser extent, by

vascular plants) during respiration and growth, since the retreat of the glaciers which covered these areas some 10,000 to 25,000 years ago (Lindsay, 1995; Kuhry and Turunen, 2006). *Sphagnum* species in particular, the primary component of peat, began to colonise and accumulate some time after glacial retreat at the end of the last Ice Age. It is one of the few plant species to thrive under cold, wet and low nutrient conditions (Glime, 2007). *Sphagnum* by its presence acidifies its environment through ion exchange with water being held within the plant's tissue, lowering the pH to around 4 (Lindsay, 1995). Due to this acidity, microbial induced plant tissue decay is limited allowing senescing and dead *Sphagnum* carbon compounds to accumulate, building up peatland at up to 1mm per year in some areas (Lindsay, 1995), as long as accumulation exceeds erosion. This acidity also restricts the higher plant species that can exist in these areas, allowing acid tolerant bryophytes to colonise and form a surface layer. However, ericaceous species, such as *Calluna*, some graminoids and acid tolerant woody shrubs, such as *Salix* and *Betula* species, can form an overstorey layer in areas which are not waterlogged.

Current or potential global warming will affect the northern hemisphere (Hansen *et al.*, 2006) including boreal peatlands (Gorham, 1991), although there are indications that there may be regional anomalies (some areas may cool) (Trenbeth, 1990; Chase *et al.*, 2000; Petoukhov and Semenov, 2010). A rise in mean temperature in the northern hemisphere may activate a strong carbon-cycle/climate feedback in peatland areas (Billett *et al.*, 2004; Davidson and Janssens, 2006; Dorrepaal *et al.*, 2009) and there is reason to believe in the near future that peatlands may become a significant source of atmospheric carbon (Archer, 2010). This may occur if the long term carbon sequestration function of peatlands is impeded by the rise in temperature, increasing microbial decomposition, or if there is a significant reduction in precipitation, causing these areas to dry and particulate carbon to oxidise more readily. The results of such environmental change may be

evident in changes to the characteristics of overstorey vegetation components and canopies or species assemblages, the primary indicators of ecological condition (Rodwell, 1991; Schwartz, 2003; Gu *et al.*, 2009; Hudson and Keatley, 2010).

Peatlands are responsive ecosystems whose structural components and physical properties cause their form and extent to be regulated by prevailing environmental and climatic conditions (Charman, 2002; Baird *et al.*, 2009; Lindsay, 2010). Peatlands have not yet been included in many global models of terrestrial-atmosphere CO_2 exchange (Le Quéré *et al.*, 2009; Billett *et al.*, 2010) and it remains unclear whether peatlands are currently a source or sink of carbon as this may depend on local management decisions (Billett *et al.*, 2004). One of the reasons for this uncertainty may be the sparse spatial sampling as a result of current field survey methods (Voßbeck *et al.*, 2010). For example, the soil carbon analysis of the UK conducted by Bradley *et al.* (2005) was based on a 1:250,000 scale soil map derived from data collected on a 1km sampling grid. An increase in scientific understanding and improvement in measurement methods is needed to determine if peatlands remain a sink for, or are becoming a source of, atmospheric carbon and to enable this information to be incorporated into climate models that account for the fine spatial detail which reflects local management decisions (Ostle *et al.*, 2009).

Due to their areal extent, much remains to be known of the rate and direction of ecological change in peatlands and a better understanding of both their significance and the interaction of societal and natural processes is necessary (Scottish Natural Heritage, 2002; Holden *et al.*, 2007). Developing methods to monitor and measure the dynamics and direction of change of these extensive ecosystems would therefore be of significant benefit (Egan *et al.*, 2000; Harris and Bryant, 2009b; Bonn *et al.*, 2010; Anderson *et al.*, 2010). As the UK peatlands are a microcosom of those of the northern hemisphere they may serve as an environment in which such methods can be researched and developed.

1.3.2 The UK's peatlands and *Calluna* - a potential ecological indicator

Peatland ecosystems, including fens, their ecological precursor (Lindsay, 1995), cover approximately 4.66 x 10^6 ha, approximately 18% of the UK's land area (Haines-Young *et al.*, 2000) and the distribution of these carbon rich organic soils is shown in Figure 1.2. As ecosystems they are a critical natural resource and provide key ecosystem services for human welfare, climate regulation and biodiversity (Alcamo and Bennett, 2003; Charman, 2002; Erwin, 2009; Bonn *et al.*, 2009a; Harris and Bryant, 2009b; Haines-Young and Potschin, 2009; Bonn *et al.*, 2010) and in many locations provide a critical hydrological buffer (Price *et al.*, 2003; Holden *et al.*, 2004; Charman, 2002; Schumann and Joosten, 2008). The services provided by peatlands can be categorised as supporting, provisioning, regulating, and cultural (Bonn *et al.*, 2009b, 2010), subdivided further in Table 1.1, and with direct and indirect effects on human well-being. These services may be considered at a global scale but many have utility at local and regional scales (Joosten and Clarke, 2002).

Table 1.1: Ecosystem services provided by peatlands

Supporting	**Provisioning**	**Regulating**	**Cultural**
Nutrient recycling	Food	Climate	Aesthetic
Soil formation	Fresh water	Flood	Spiritual
Primary production	Wood and fibre	Disease	Educational
	Fuel	Water quality	Recreational

Developed from Bonn (2010).

Expanding on Table 1.1, the UK's peatlands support human and societal well-being through nutrient recycling, the formation and conditioning of soils, sediment transportation and as an environment for primary production (Bonn *et al.*, 2010). They provide a source of energy, through the harvesting and burning of dried

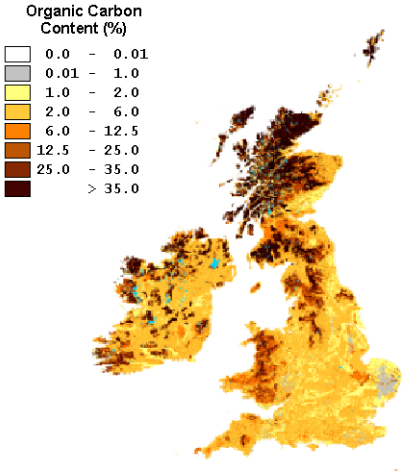

Figure 1.2: Distribution of peatlands in the UK and Eire

Adapted from Montanarella *et al.*, (2006).

peat; a source of nutrition, through their use for agricultural grazing or, in drier areas, food crop cultivation and in some areas fibre production; fresh water storage and, as a hydrological buffer, alleviation from flooding and regulating river flow as peat is hygroscopic; filtration of atmospheric pollutants, such as nitrous oxides, from rainfall (Joosten and Clarke, 2002; Bonn *et al.*, 2010). They also help regulate local and regional climates through evapotranspiration (Joosten and Clarke, 2002). As the UK's peatlands are towards the southern extreme of the boreal peatland's distribution (MacDonald *et al.*, 2006) they may be particularly susceptible to climate change in the northern hemisphere. Scotland has the greatest proportion of upland moors in the UK as they cover some 38% of its land area.

1.3.3 Growth and form of *Calluna*

Scotland's temperate oceanic climate, high levels of precipitation and the predominance of uplands favours the development of dwarf shrub and bog ecological

communities (Haines-Young *et al.*, 2000). Dwarf shrub sub-communities form on the dryer areas while bogs develop across the wetter areas and waterlogged areas. These sub-communities may be mutually exclusive and often form in complex mosaics (Rodwell, 1991) or form ecological gradients (Gimingham, 1989; Trodd, 1996). Furthermore, they are colonised by a limited range of plant species but *Calluna* may grow and develop to be the dominant over-story species across much of their extent, if the areas into which it roots are not permanently waterlogged (Gimingham, 1972).

Calluna is a sclerophyllous dwarf woody shrub annually producing shoots with microphyllous leaves 1 mm to 2 mm in length in decussate pairs (leaves arranged in opposite pairs on a stem, each pair at right angles to the pair above and below). These leaves start to become evident in the upper canopy in late spring (Figure 1.3(a)). Then during the summer months the leaves gradually becoming more prominent as more emerge and they develop a distinct light green colour (Figure 1.3(b)). Each year, from mid July to early August, distinctive densely packed purple flowers form (Figure 1.3(c)), set seed in late summer and die, with clusters of dead light brown flowers remaining attached over winter (Figure 1.3(d)). By the end of winter there are few if any green leaves evident in the upper canopy of *Calluna* shrubs (Figure 1.3(e)), although approximately two thirds of the foliage present the previous year will have survived winter desiccation in the lower canopy layers.

Distinct growth phases of *Calluna* have been identified and these are generally classified after Watt (1947) as; 'pioneer'; 'building'; 'mature'; and 'degenerate'. In the pioneer stage laterals shoots develop, also in decussate pairs, from phanerophyte growth buds (although many buds remain dormant) with the plant developing to display a pyramidal form. As *Calluna* continues to grow through the pioneer and building phases a fucate branching structure develops, with leading shoots being replaced by two or three new ones, increasing shoot

(a) May - spring greening

(b) Late June - early summer 'shoots and leaves' cover canopy greening

(c) August - late summer flowering

(d) October - early winter dying flowers and onset of senescence

(e) April - winter desiccation

Figure 1.3: Visual change to a 'building' *Calluna* canopy through a growth and senescent cycle

density and, consequently, ground cover. Lower laterals, that developed initially from the prostrate shoots, also continue to grow and adopt an ascending habit, leading to the development of a sympodial growth form (shoots growing laterally then vertically to form additional leading shoots, developing other axes for plant growth). At the end of the building phase, in favourable conditions, the *Calluna* canopy closes but leaf and shoot development continues, increasing photosynthesising biomass density to use available light and shading out ground cover species. In such areas extensive even aged *Calluna* stands, with continuous ground canopy cover, develop until in maturity the shallow rooting system begins to be unable to support the weight of the shrub. After some 25 to 30 years *Calluna* begins to degenerate and adopt a prostrate habit, allowing light in to the ground layer and enabling shorter lived species to grow. In the degenerate stage fewer new shoots are produced and the central branches collapse completely opening up the centre of the shrub, forming a characteristic spoked 'wheel' with some green shoots on the periphery (Gimingham, 1972).

While the foregoing describes the life cycle of *Calluna* under optimal conditions, *Calluna* can display considerable phenotypic plasticity under the influence of ecological and environmental determinants (Grant and Hunter, 1962; Gimingham, 1972; MacDonald *et al.*, 1995). There is evidence that the rates of growth, flowering densities and possibly leaf moisture content may vary between different ecological communities (Gimingham, 1972). In each of the recognised growth phases of *Calluna* two state variable ranges (canopy height and percentage ground cover) have been selected by biologists and ecologists to assist in the classification of *Calluna* ground cover (Watt, 1947; Gimingham, 1972; Grant and Armstrong, 1993; Macaulay Institute, 2003). However, these growth stages are not mutually exclusive and the development of *Calluna* forms a continuum with height and ground cover affected by ecological and environmental determinants, as well as age. For example, MacDonald *et al.* (1995) identified 'layering' as a condition of

Calluna growth and stand development in certain ecological communities where adventurous lateral branches could root into the substrate and propagate across the landscape, without following the cyclical process presented by Gimingham (1972).

A schematic of the growth forms that *Calluna* can adopt under different ecological and environmental conditions is presented in Figure 1.4. These characteristic forms of growth and stand development are used in field surveys to classify *Calluna* and could possibly be used as an indicator of peatland condition and environmental change if they can be reliably and replicably measured.

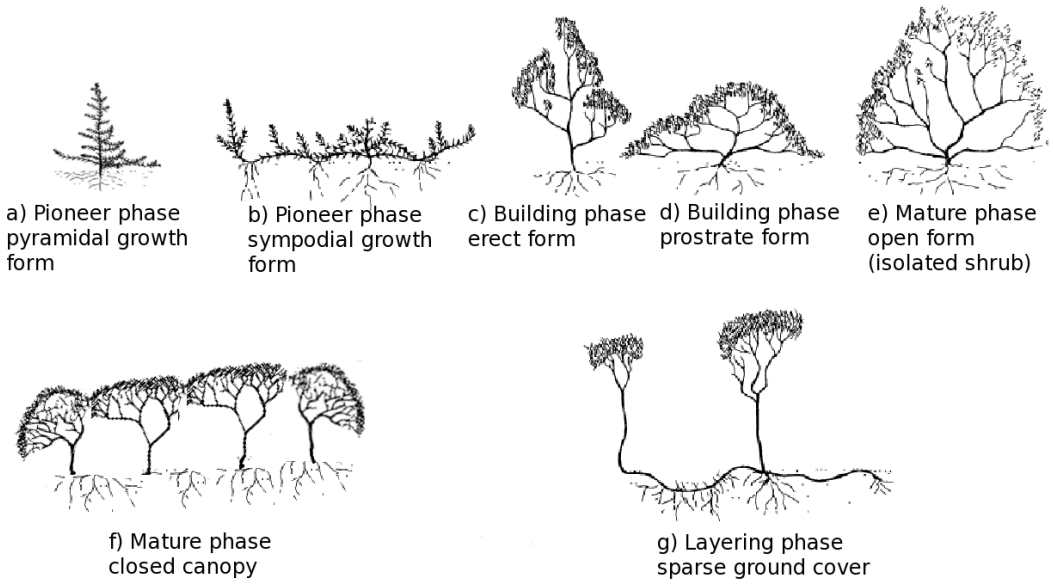

Figure 1.4: *Calluna* phenotypic plasticity

Adapted from MacDonald *et al.*, (1995).

1.4 Management and surveying of Scotland's dwarf shrub heath

In addition to their place in the natural carbon cycle, Scotland's *Calluna* dominated upland moors are utilised for agricultural, sporting and recreational activities and these areas are of international importance for biodiversity conservation (Scottish Natural Heritage, 2003; Thompson *et al.*, 1995; Mackey *et al.*, 2001; Usher *et al.*, 2001; Warren, 2002). Historically these moors were primarily used for the purposes of sheep grazing and grouse and deer shooting from the Victorian era through to the 1960s and 1970s. Management for these purposes, along with climatic and geomorphological factors, have shaped the landscape pattern and vegetation assemblages. However, there has been a dramatic decline in internationally important bird populations in these areas since the beginning of the 1970s. This has, in part, been attributed to a reduction in the extent and quality of moorland due to drainage, Sitka forest planting, excessive grazing and other current moorland management practices (Thompson *et al.*, 1995; Mackey *et al.*, 2001). Excessive grazing can lead to loss of vegetation and subsequent erosion in sensitive upland landscapes (Gordon *et al.*, 2001; MacDonald *et al.*, 1998) with consequent effects on wildlife. Thompson *et al.* (1995) advise that "Current management practices must change ... to avoid the demise of one of Britain's most distinctive landscapes and habitats".

1.4.1 Management of upland moors for agriculture, conservation and recreational purposes

Despite their importance, generally there has been an increase in grazing pressure from herbivores across Scotland's upland moors over time (Mackey *et al.*, 2001).

The adverse effects of this over grazing have been compounded by a reduction in manpower deployed in the management of the moors with consequent reduction in activities such as muirburn (the managed cyclical burning of *Calluna* to encourage regeneration). These factors have caused a change to the ecological dynamics of the moors. *Calluna* is a cyclical dominant, rather than a climax community, and its dominance is maintained by management intervention. Without this intervention the overstorey vegetation of many of these peatlands would revert to a mix of dwarf shrub and woody scrub over acid tolerant graminoids and peat forming bryophytes (Gimingham, 1972). Intervention may take the form of: controlling the number and duration of grazing herbivores on the moor; muirburn, to remove mature and degenerate *Calluna* and encourage the regeneration of young *Calluna* shrubs which produce more fresh green shoot per unit area and hence provide forage to support greater herbivore numbers; or the application of fertiliser. Recent government policy, driven in part by EU regulation, has recognised that management for agricultural production alone is detrimental to moorland value and the diverse ecosystem services they provide and has started to change the way these areas are managed. Payment for farm support is now based on good environmental management and verifiable farming practice rather than on livestock numbers and the control of deer numbers is being encouraged (Warren, 2002; Scottish Natural Heritage, 2003, 2005). However, the impact of land management decisions, such as the changing of stock densities (be it increased or decreased) or frequency of muirburn, on these peatland communities needs to be considered. As an aid to this process a suite of decision support tools, HillPlan, has been developed by the Macaulay Land Research Institute (MLURI).

Knowledge of an area's vegetation species composition, geographical location, herbivore species and numbers, and the temporal periods during which the herbivores are present are required as inputs to the HillPlan model. The software then models the availability of graminoids, the moorland herbivores preferred

Table 1.2: HillPlan *Calluna* growth and grazing model input variables

Category	Input variable	Category	Input variable
Graminoids	Graminoid species Species mix (%) Spatial extent (ha)	Herbivores	Herbivore species Quantity Weight Duration on area (days)
Calluna	Age class Spatial extent (ha) Ground cover (%) Density of ground cover (%) Ecological community class	Environment	Location Altitude (m) Aspect Soil type
Temporal	Ground cover (%) Reporting cycle (days) Duration of model run in annual cycles	Management	Fertiliser application Muirburn cycle

forage, the growth of digestible *Calluna* biomass and the utilisation of these resources by the levels of herbivores present and does so in daily increments per unit area. Consequently, the model can be used to forecast changes to vegetation assemblages and their extent and the condition of *Calluna* cover under a range of stocking regimes and management strategies (Macaulay Institute, 2003). Input to the model requires extensive areas of upland to be surveyed for each farm or estate and detailed habitat descriptions and vegetation assemblages quantified, as listed in Table 1.2. However, due to the extent and remoteness of moorland areas acquiring field survey data can be problematic (Wright *et al.*, 1997; Macaulay Institute, 2003). Condition assessment field surveys are either detailed, objective and replicable but impractical over large areas, or generally, subjective and unable to be replicated with enough precision to allow ecological change to be assessed, at least at five or ten year intervals[1].

[1]The author's personal experience from conservation management and planning of extensive areas of moorland within Scotland's Regional Park system

1.4.2 Ecological field surveys of the *Calluna* dominated upland moors of Scotland

Although a range of surveying techniques has been developed to monitor the condition of *Calluna* dominated moors (MacDonald *et al.*, 1998; Egan *et al.*, 2000; Macaulay Institute, 2003), acquiring accurate and replicable inventories of landscapes in general (Cherrill and McClean, 1999) and upland vegetation in particular (Earth Observation for Natura, 2000; Egan *et al.*, 2000) have been found to be problematic using traditional ecological surveying techniques. These survey techniques tend to rely on subjective visual assessments of small areas and on these spot surveys being representative of vastly greater areas. The UK's peatlands and *Calluna* dominated upland moors are extensive (with enclosures measured in hundreds or thousands of hectares) but for practical purposes field study methods sample a restricted number of locations, each of limited spatial extent (possibly less than a square metre to at most tens of square metres), with data being interpolated or extrapolated across the wider area of interest when maps are produced or inferences made (Bullock, 2006). This approach has been criticised by some ecologists particularly when assessment of change over time is being considered, as variations of up to 20% have been found to be due to observer differences (Bullock, 2006). Measures can be taken to minimise errors, such as observers working in pairs and using standard protocols such as those developed by MacDonald *et al.* (1998). However, it remains difficult to acquire reliable data and for surveys to be replicated and errors quantified. However, quantitative and replicable measures of the areal extent, growth phase and ground cover of *Calluna*, and its change over time is necessary both to assess the status and dynamics of peatlands and to serve as inputs to HillPlan. Field studies and ecological surveys of *Calluna* dominated peatlands would benefit from objective, replicable methods to characterise and quantify *Calluna* canopies over wide areas and methods which would also enable errors to be quantified.

As objective field survey methods, such as destructive sampling, are time consuming subjective field survey methods continue to be adopted (MacDonald *et al.*, 1998; Egan *et al.*, 2000; Rich *et al.*, 2005), which makes replicating the work or monitoring change over time problematic (Mücher *et al.*, 2010). The *Calluna* classes developed by Watt (1947) and MacDonald *et al.* (1995) continue to be used and are often assigned based on a canopy height and percentage ground cover (Barclay-Estrup and Gimingham, 1969; Egan *et al.*, 2000; Macaulay Institute, 2003). Egan *et al.* (2000) proposed a rapid objective method to classify *Calluna* canopies by height and predict standing biomass. However, although Davies *et al.* (2008) used a similar method to estimate *Calluna* biomass fuel load, it has not been widely adopted. Measuring *Calluna* canopy height due to its variability within a canopy (smaller areas of continuous cover) or a stand (a large single physiographic unit which may have gaps in its ground cover) is problematic, not least because of the mobility of shoots and leaves in windy conditions. In addition, the height of a *Calluna* canopy is influenced by factors other than just age, as is acknowledged by the "wind-clipped" (Gimingham, 1975) and "layering" (MacDonald *et al.*, 1995) growth classifications that have been developed. The ecological and environmental conditions in which *Calluna* is growing will influence its rate of development and canopy morphology, just as they will affect the development and morphology of any plant (Taiz and Zeiger, 2002). Following Egan *et al.* (2000), no further work has been reported on the development of a method to objectively classify *Calluna* canopies.

Non-destructive allometric methods have been developed by the forestry community to estimate tree physical variables and stem diameter is frequently used to predict standing woody biomass. However, although stem diameter can be easily measured, *Calluna* stem growth, and hence diameter, is influenced by the prevailing environmental and ecological conditions, just as canopy height is. Knowledge of these conditions would still be required to enable stem diameter to be related

to age, even after correlations were made between stem diameter and age using dendrochronological methods. An alternative non destructive, objective approach to characterise *Calluna* is the use optical methods of vegetation survey either in the field or by measurement from airborne or satellite platforms.

1.4.3 Field spectroscopy and optical surveys of the *Calluna* dominated upland moors of Scotland

One optical measurement approach is to use instruments to measure the photosynthetically active radiation (PAR) penetrating a *Calluna* canopy or stand then to estimate structural parameters, such as canopy gap fraction, or infer leaf area index (LAI) from this data. LAI, defined as half the leaf surface area per unit ground area (Chen and Black, 1992), can be used as an indicator of the development of vegetation canopies in physiological studies (Cournède *et al.*, 2007); to indicate productivity in crop growth models (Johnson and Thornley, 1983); and in studies of biochemical compound cycling (Jordan, 1969).

In this work two PAR canopy analysing systems were available, a LAI-2000 (LI-COR, 1992) and a Delta-T SunScan (Potter *et al.*, 1996), both marketed as plant canopy analysers. The LAI-2000 uses a series of concentric PAR sensors behind a 'fish-eye' lens located at the end of a probe (LI-COR, 1992) and measures the light incident through the canopy. To make multiple measurements the operator moves under the canopy, or through the canopy if *Calluna* was being surveyed, stops, makes a measurement then moves on to make the next measurement. The SunScan instrument is of a different configuration, having a one metre long probe which can be inserted or placed below a canopy. The SunScan may be particularly suited to *Calluna* studies as the probe has 64 photo-diodes along its length each measuring PAR and these values can be recorded individually, without necessarily having to walk through and disturb the *Calluna* canopy to make

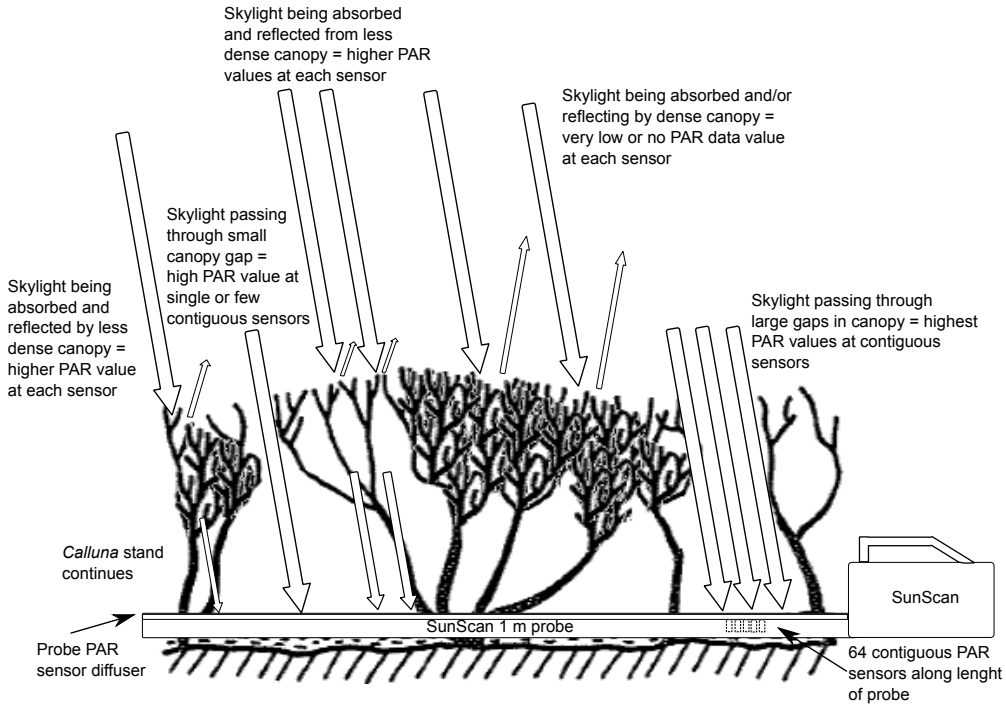

Figure 1.5: *Calluna* canopy and stand SunScan measurement schematic

multiple measurements. LAI and information of the density of *Calluna* canopies (the amount of photosynthesising biomass present and directly related to the LAI) can be estimated. It may also be possible to classify *Calluna* canopies and stands and infer spatial structural variables such as *Calluna* canopy or stand cover and gap fraction, as indicated in Figure 1.5, and use such data as inputs to HillPlan. Measurement of the reflectance of light from *Calluna* by field spectroscopy offers another objective ground survey method and one that may complement below canopy PAR measurements. By measuring light that has interacted with an Earth surface, and been reflected or transmitted, we can acquire data that can be used to infer surface structure, composition and processes within it (Milton, 2009).

In a review of the Russian literature available to the University of Zurich, and covering the period 1947 to 1966, Steiner and Gutermann (1966) report on the

extensive use of field spectroscopy (both laboratory and field based) to measure the spectral reflectance of boreal forests and peatland Earth surfaces to aid interpretation of data acquired by optical sensors deployed on airborne platforms of these areas. This Russian research recognised the advantages of measuring both across the spectral range of human vision (approximately 400 nm to 700 nm) and the near infra red range (approximately 700 nm to 1,000 nm) which, although measured in a limited number of spectral bands and with airborne data was acquired at course spatial resolutions, enabled the "separability of *(Earth surface)* objects by means of photo tone" Steiner and Gutermann (1966). In this work measurements were made of an extensive range of biotic and abiotic Earth surfaces and included peatlands ecosystems. The species composition and soil and rock surface types were recorded for these Earth surfaces and attempts made to establish and explain relationships between reflectance factors and reflecting sample chemical and physical state variables. More recently, however, field spectroscopy instruments technology has advanced and these instruments can make measurements across a greater spectral range and at higher spectral and spatial resolutions, now normally acquiring greater than 200 spectral bands from between 400 nm to 1,000 nm or 400 nm to 2,500 nm, and from Earth surface areas normally less than 1 m^2.

High spectral and spatial resolution field spectroscopy is now often used to gain an understanding of the interaction of light with Earth surfaces to facilitate hyperspectral image analysis (Milton *et al.*, 2009) and to relate biological and physiological processes to the reflectance of plant leaves and canopies and to characterise floristic communities in a diverse range of environments (Ustin *et al.*, 2009) and has been used for these purposes in some research in northern boreal peatlands. For example, field spectroscopy was used in the Boreal Ecosystem Atmosphere Study (BOREAS), along with hyperspectral images acquired by sensors mounted on airborne and satellite platforms, to measure Earth surface

reflectance factors (Gamon *et al.*, 2004). This reflectance data was used to improve biome albedo estimates and improve land cover estimates, by defining spectral endmembers (of floristic communities) for linear mixture modelling and to develop spectral libraries. Although the need for a more "rigorous experimental" design was identified as a constraint on an "objective and comprehensive comparison" of RS products being conducted, the BOREAS project did enable thematic maps to be generated and accuracy assessments to be made (Gamon *et al.*, 2004). Kuusk *et al.* (2008) used by field, laboratory and imaging spectroscopy of measure the spectral reflectance of a boreal forest ecosystem at a range of component scales from forest stand to individual needles, leaves, woody components and understorey reflectances in an database along with geographic, allometric and species metadata. This work was primarily to provide 'benchmark' data for the validation of radiative transfer models of forest stands (Kuusk *et al.*, 2009), although spectral measurements of understorey bryophytes and graminoids were included.

However, little has been done in detail to investigate the reflectance of plant leaves and canopies or to characterise floristic communities using field spectroscopy in dwarf-shrub dominated heath and peatland environments. Wardley *et al.* (1987) used field spectroscopy to characterise plant canopies in a heathland and noted the need for an understanding of the impact of three dimensional form and phenological change on spectral reflectance. Milton and Rollin (1988) investigated the directional reflectance of *Calluna* canopies and noted the need to consider view angle, the effects of inter-canopy shadowing and seasonal change on reflectance. Trodd (1996) used field spectroscopy to characterise heathland vegetation and landscape patterns and observed that methods need to be developed to characterise ecotones. Atkinson (1999) used field spectroscopy to investigate the relation between the scale of spatial variation and spectral wavelength of the overstorey vegetation on two heathland ecosystems and advised

that different sample spacings may be necessary to optimise data collection for the visible and the near infra-red regions of the spectrum when a grid sampling approach is being adopted. Lang *et al.* (2002) did compile a library of the spectral reflectance of sub-boreal forests understorey species and included *Calluna* in this. However, detail of importance in the management and monitoring of *Calluna* such as percentage ground cover, age class and canopy density were not included. Armitage *et al.* (2004) used field spectroscopy to investigate floristic composition and the spectral reflectance of semi-natural vegetation and noted that it was not possible to map the spectral characteristics of these floristic communities to National Vegetation Classification standard (NVC) classes. Schaepman-Strub *et al.* (2008) tried to quantify the fractional cover of three major plant functional types in peatlands, using field reflectance measurements, with varying degrees of success. Harris and Bryant (2008) used field spectroscopy to determine that field reflectance measurements of *Sphagnum* could be used as as proxy indicator of near-surface hydrology in peatlands but noted that surface heterogeneity needed to be investigated further. Kalaitzidis *et al.* (2008) determined that field spectroscopy could be used to monitor nitrogen status of *Calluna* foliage. Mills (2005) used field spectroscopy to determine that less than ten spectral bands were required to classify peatland vegetation at high spatial resolution but did not investigate biophysical or biological processes and their effect on reflectance.

Mac Arthur and Malthus (2006) and Nichol and Grace (2010) investigated the use of spectral indices to indicate the pigment content of *Calluna* leaves and canopies, respectively. Although such indices, based on statistical relationships between leaf biochemical concentrations and spectral reflectance features, have been demonstrated to be useful in studies of a wide variety of plant functional types (Sims and Gamon, 2002; Moorthy *et al.*, 2003; Ustin *et al.*, 2004a) the correlations between pigment content, determined by wet chemistry, by Mac Arthur and Malthus (2006), and High Performance Liquid Chromatography, by

Nichol and Grace (2010), and the indices presented by Sims and Gamon (2002) were in the main weak.

The difficulties reported by some of the authors above in using field spectroscopy to infer biophysical and physiological state variables and to characterise overstorey vegetation on heaths and peatlands may in part be due to surface heterogeneity. Areas of semi-natural vegetation in general, and *Calluna* canopies and stands in particular, are structurally and floristically heterogeneous, and comprised of multiple components each with spectrally distinct reflectances, individually discernible but at varying scales. Therefore detailed knowledge of the extent of the area of measurement support and the spectral response of the spectroradiometer across this area will be necessary to proportion the different components to the integrated reflectance recorded by a field spectroradiometer. In addition, as the area of measurement support is the sampling spatial resolution, knowledge of the spatial extent of this area and the scale of surface heterogeneity is required to enable sampling strategies to be developed (Atkinson and Curran, 1997; Curran and Atkinson, 1999; Rahman *et al.*, 2003; Atkinson and Aplin, 2004).

While field spectroscopy may offer a quantifiable approach to characterise floristic communities in peatlands and to infer biophysical and physiological state variables, the area of support for each measurement is defined by the fore optic used, the optical design of the instrument and the height of the instrument above the area of interest. Typically, this only enables areas normally less that 1 m^2 to be measured and therefore requires multiple measurements to be made to characterise a landscape surface. A potential complementary approach to survey extensive *Calluna* dominated peatland, and possibly to extrapolate or interpolate field survey results in an objective manner, is optical remote sensing (RS) from satellite or airborne platforms.

1.4.4 Remote sensing surveys of the *Calluna* dominated upland moors of Scotland

Earth observation (EO) by remote sensing has offered unprecedented opportunities to classify and map the surface of the Earth. As observations are spatially extensive, can be repeated and measurements replicated, remote sensing has led to a greater understanding of the Earth's climatic, aquatic and terrestrial systems' dynamics than ever before (Ustin *et al.*, 2004a). Data acquired by RS can be used to construct models (as abstractions of reality) of Earth surface 'scenes'. These models can be considered to be simple or complex "discrete" representing "classes" of scene elements or "continuous" where the interaction of light with an element or elements is used to infer elemental properties (Strahler *et al.*, 1986). However, these model types are not mutually exclusive but provide a continuum and framework through which RS data analysis can develop and assimilate and be assimilated with other research domains (Strahler *et al.*, 1986) and this is particularly the case with the development of hyperspectral RS.

Hyperspectral remote sensing has furthered understanding of Earth surface processes by enabling specific absorption and reflectance characteristics to be measured and relationships between these characteristics and Earth surfaces' physical and chemical state variables to be established (van der Meer *et al.*, 2001; Kumar *et al.*, 2001; Schaepman *et al.*, 2009) and both continuous and discrete models to be constructed and processes investigated. As it is now recognised that terrestrial ecosystem biological processes significantly influence climatic conditions (Heimann and Reichstein, 2008), measuring and modelling ecosystems' form, function and change over time is particularly of interest.

RS enables a synoptic view to be taken and offers an approach to assessing vegetative cover that can be objective, replicable and practical in covering extensive areas such as peatlands. Some RS research to classify the *Calluna*

cover of upland moors has been conducted (Wardley *et al.*, 1987; Belward *et al.*, 1990; Csaplovics, 1992; Foody and Trodd, 1993; Trodd, 1996; Wright *et al.*, 1997; Robertson *et al.*, 2003). However, acquiring an adequate level of detail and accuracy of classification has proved problematic due to the comparatively 'coarse' spatial and spectral resolutions used (Wright *et al.*, 1997; Bird *et al.*, 2000; Earth Observation for Natura, 2000). Satellite optical sensors with higher spatial resolutions are now available and Mills (2005), for example, demonstrated the utility of IKONOS imagery to classify upland areas but in similar work Mehner *et al.* (2004) noted low spectral resolution and classifications based on ecological taxonomy to be a constraint. Milton *et al.* (2005) used IKONOS imagery for the classification of lowland raised bogs but recommended the use of airborne Light Detection and Ranging (LIDAR) and/or aerial photographic instruments to improve classifications of bog condition and also highlighted that RS surveys can be constrained by the predominance of cloud cover in the UK. Similar work was conducted by (Anderson *et al.*, 2010) and these researchers demonstrated that a geostatistical approach to the analysis of LIDAR data, when combined with standard multispectral analysis of IKONOS images, of an ombrotrophic peatland improved thematic classifications. However, this analysis classified different surface types rather than quantified biological or physiological processes and these processes may be an indicator of of the health and vigour of the peatland vegetation hence, if measured over time, be used to infer ecosystem dynamics.

Hyperspectral RS can enable quantitative assessment of Earth surface properties (Liang, 2004) rather than solely discriminating or classifying different surface types as Kooistra *et al.* (2009) and Chan *et al.* (2010) reported. Hyperspectral RS, primarily from airborne platforms, has been used to quantify vegetation pigments (e.g. Blackburn (1998), Blackburn (2007), le Maire *et al.* (2008) and others); assess physiological status (see Blackburn (2007), Naumann *et al.* (2008) and others); assess hydrological condition (Harris *et al.* (2006), Harris and Bryant

(2009a) and others); monitor stress (see Baret *et al.* (2007), Ren *et al.* (2008) and others); monitor phenology (see Ge *et al.* (2006), Castro-Esauand and Kalacska (2008) and others); and estimate productivity (photosynthesising biomass) (see Thenkabail *et al.* (2000), le Maire *et al.* (2008), Delalieux *et al.* (2008), Biewer *et al.* (2009) and others) all across a diverse range of vegetation phenotypes (Ustin *et al.*, 2004b; Schaepman *et al.*, 2009; Ustin *et al.*, 2009). Hyperspectral RS, therefore, potentially offers a method to quantifiably measure and monitor *Calluna* cover over extensive peatland areas and, hence, enable *Calluna* to be used as an indicator of the status and dynamics of peatlands where it is the dominant overstorey species. To develop tools to enable this would be particularly relevant in the coming decade as the EnMap (Germany), Hyper-X (Japan) and potential HyspIRI (US) hyperspectral sensor satellites are deployed.

For any optical RS method the issue of cloud cover frequently obscuring the Earth's surface and interfering with optical field and remote sensing surveys remains. One potential approach to infer *Calluna* state variables at times of cloud cover would be to develop models of canopy reflectance which would enable data acquired at times of clear skies to be interpolated or extrapolated across annual and inter-annual growth and senescence cycles (forward modelling). In addition, such models, if invertible, could be used to infer *Calluna* state variables from images acquired by hyperspectral sensors on satellite platforms enabling extensive peatlands to be surveyed.

1.5 Modelling the reflectance of *Calluna* dominated uplands

A strong synergistic potential exists when RS observations and ecological models can be combined (Barrett and Curtis, 1999) as Baret *et al.* (2007) have demonstrated by combining a radiative transfer (RT) reflectance model and an agricultural crop model to investigate nitrogen induced stress. Applied to *Calluna* such an approach could allow canopy reflectance to be forward modelled through annual and inter-annual growth and senescence cycles from field survey data collected at discrete temporal intervals, or for certain key model state variables to be constrained to better infer the remaining state variables when models are inverted (Lewis, 2007). To enable the reflectance of *Calluna* to be modelled through annual and inter-annual growth and senescence cycles it may be possible to couple the HillPlan ecological growth model to a canopy reflectance model and to model the reflectance of the *Calluna* and do so for specific growth classes and ecological and environmental conditions.

1.5.1 *Calluna* canopy growth and senescence modelling

Calluna develops a complex canopy structure as it grows and its spatial distribution, canopy morphology and health and vitality are affected by ecological and environmental determinants, management influences and utilisation by herbivores (Gimingham, 1972). HillPlan incorporates the vegetation production and herbivore grazing empirically-based model produced by Grant and Armstrong (1993) and further developed by Palmer (1997) and Milne *et al.* (2002). This is based on research into animal grazing behaviour, plant growth and competition, and the response of plants to grazing on hill farm ecosystems. The HillPlan decision support tool has been produced to assist in the development of prescriptions to

determine sheep stocking densities and minimise over grazing to facilitate conservation of upland vegetation assemblages. Hence, HillPlan can be used to model intra-seasonal and inter-seasonal variation in *Calluna* photosynthesising biomass. There is a direct relationship between the leaf area present, normally expressed as LAI, and photosynthesising biomass and LAI, along with photosynthesising rate, are key variables in global climate studies (Myneni and Running, 1997).

For this research the HillPlan *Calluna* growth kernel, and the data used to derive it, were made available by MLURI[2]. The *Calluna* growth kernel requires to be parameterised with the environmental, ecological and *Calluna* specific variables listed in Table 1.3. These variables are used in the model to simulate *Calluna* photosynthesising biomass production on a daily basis, with seasonal variations accounted for, and the daily results accumulated throughout an annual cycle, with a proportion removed on a daily basis if the impact of grazing herbivores is included. However, HillPlan was developed for application in the moors on the east coast of Scotland where the climate tends to be colder and substrate drier and, hence, will require validation for west coast uplands of Scotland which tend to be warmer and wetter. It will also be necessary to couple it to a canopy reflectance model to enable the change in the reflectance of *Calluna* over time to be modelled.

Table 1.3: *Calluna* growth kernel model input variables

Environmental/Ecological	***Calluna* specific**
Mean annual temperature	Age class
Community class	Percentage ground cover
Soil density	Biomass at model initiation
	Growth start and end dates

[2]Prof. R. Pakeman made the data available and supplied an explanation of the model's development (personal communication 17/09/2009) and J. McLeod, also of MLURI, supplied both HillPlan and its *Calluna* growth kernel (15/09/2009).

1.5.2 Modelling *Calluna* canopy reflectance and its change over time

RT models are used to describe the physical interaction of light with media when transmission, absorption and scattering are present (Rees, 2004). RT theory has been simplified (because, for example, the structure of, and biochemical distribution within, leaves is incompletely understood) and adapted by a number of authors to model the interaction of light with photosynthesising components and vegetation canopies (e.g. Jacquemoud, 2006). Using these models leaf reflectances have been forward modelled and leaf biochemistry and anatomical structure inferred through their inversion (Jacquemoud and Ustin, 2001). PROSPECT (Jacquemoud *et al.*, 1996), developed to represent planar leaves, and LIBERTY (Dawson *et al.*, 1998), developed to represent conifer needles, are the most frequently used leaf reflectance models (Ustin *et al.*, 2004a). Dawson *et al.* (1998) considered the cellular structure of needles to be better represented by powders (grains with inter-granular air cavities) than turbid plates with lambertian reflecting surfaces (the approach adopted in PROSPECT) and used Melamed's (Melamed, 1963) theory of the interaction of light with powders to develop needle optical properties. LIBERTY has been used extensively in both forward and inverted mode (see Barton (2001), Moorthy *et al.* (2003), Nilson *et al.* (2003), Rochdi and Fernandes (2004), Peddle *et al.* (2004), Schlerf and Atzberger (2006), Blackburn and Ferwerda (2008), and Di Vittorio (2009) for examples).

Of course, optical remote sensing measurements made by near ground field spectroscopy methods, or imaging spectroscopy from airborne or satellite platforms, measures reflectance from vegetation canopies rather than from individual leaves. As the morphology of canopies influences the reflectance measured and biotic

or abiotic understorey reflectances may be integrated in the gross canopy reflectance measurement recorded due to gaps in the canopy structure and transmission through leaves (Kuusk, 2001; Verhoef and Bach, 2003), multi-layer canopy reflectance models have been developed.

Canopy reflectance models incorporate canopy structural variables and one or more leaf RT models, to model the reflectance of either different canopy leaf layers or a canopy leaf layer and an understorey vegetation layer, and may include another reflectance layer to represent abiotic reflectances such as from soils. Liang (2004) offers an extensive review of the diverse approaches to canopy reflectance modelling and suggests that radiative transfer approaches are the most suitable for dense canopies. One such canopy modelling approach is the Scattering by Arbitrarily Inclined Leaves (SAIL) turbid medium model (Verhoef, 1984). SAIL has subsequently been developed to model heterogeneous canopies by developing a two-layer version (4SAIL2) (Verhoef and Bach, 2007) and has been the most widely used by the RS community when coupled with the PROSPECT leaf RT model (Jacquemoud *et al.*, 2009). A further advance has been the development of 3D numerical solutions to compute radiation transport through canopies (Lewis, 2007) and, when coupled with leaf RT models, is the hybrid modelling approach discussed by Liang (2004). Disney *et al.* (2006) adopted such an approach to model the reflectance of electromagnetic radiation from coniferous forest canopies and incorporated the LIBERTY needle reflectance RT model. However, although the 3D model developed by Disney *et al.* (2006) can be inverted, it may not be appropriate for modelling *Calluna* canopy reflectances as the canopy structure sub model requires the spatial distribution of the tree trunks and branching statistics to be specified and these are unknown for *Calluna*.

Another approach to canopy reflectance modelling is the invertible Analytical Canopy Reflectance Model (ACRM), a two-layer model developed by Kuusk (2003). This model was developed in 2001 due to concerns at that time that

ignoring the vertical structure of canopies may lead to misinterpretation of the red edge position (Kuusk, 2001). ACRM is a turbid medium RT model based on the homogeneous multispectral canopy model (MCRM) and the Markov chain canopy reflectance model developed previously (Kuusk, 2003). ACRM was the most computationally efficient model tested during the RAMI (RAdiation transfer Model Intercomparison) model inter comparison experiment (Widlowski *et al.*, 2007). Either PROSPECT or LIBERTY leaf RT models can be coupled to the ACRM canopy layers and the model parameterised for canopy structural variables, Sun zenith and view angles, and a ground reflectance layer incorporated. The input variables for the coupled ACRM/LIBERTY model combination are listed in Table 1.4. The combined ACRM/LIBERTY or the ACRM/PROSPECT models can be inverted and used to determine biophysical state variables from hyperspectral data (Kuusk, 2003).

ACRM/LIBERTY was considered to be the most appropriate model for this research as *Calluna* leaves more closely resemble conifer needles, which LIBERTY has been developed to model, than broadleaves, for which PROSPECT has been developed. It also seemed and it may be possible to couple the HillPlan biomass output variable to the ACRM/LIBERTY LAI input variable.

The models discussed so far only model reflectance for a given set of leaf and canopy structure state variables and, if coupled to an ecological growth model, for change in these state variables over time. However, *Calluna* is a flowing species and its flowers may dominate the visible reflectance during late summer and their profusion be an indicator of ecological condition. Hence, this additional *Calluna* canopy reflectance parameter needs to be considered.

Calluna comes into flower in late July and early August (Figure 1.3(c)) and flowers are more profuse during the shrub's building phase and where *Calluna* is growing under more favourable ecological and environmental conditions (Gimingham,

Table 1.4: ACRM/LIBERTY radiative transfer reflectance model input variables

ACRM	**LIBERTY biochemical**	**LIBERTY biophysical**
Leaf area index	Chlorophylls	Average internal cell diameter
Leaf size parameter	Water	Inter cellular airspace
Markov clumping parameter	Nitrogen	Leaf thickness
Leaf ellipsoidal distribution	Lignin	Baseline absorption
Angstrőm turbidity coefficient	Cellulose	
understorey reflectance		
Sun zenith		
View angle		

1972). By determining the contribution of the flowers to the gross canopy reflectance it may be possible to infer these conditions by field spectroscopy or RS. However, no RT models have been developed to model the interaction of light with *Calluna* flowers. An alternative approach is linear spectral mixture modelling. In a spectral mixture modelling approach individual scene component reflectances are acquired and numerically convolved in proportions representative of the scene of interest and has been used by many researchers to model the composite reflectance of heterogeneous vegetation canopies (Hobbs, 2003) and flowering canopy reflectances (Chen *et al.*, 2009; Shen *et al.*, 2010). A linear mixture modelling approach may be appropriate to incorporate the flowering of *Calluna* into RT canopy reflectance modelling as the flowers are spectrally distinct from the other canopy components and their presence can be visually determined and relative proportion estimated with the aid of digital photographs.

This research will investigate the optical properties of *Calluna* leaves and whether the changes of reflectance of *Calluna* canopies of different ages and in different ecological communities can be modelled through annual and inter-annual growth, senescent and phenological cycles. In addition, prior to measuring canopy reflectances in the field using field spectroscopy, it was necessary to determine the spatial and spectral characteristics of spectroradiometers that define the area of

measurement support, and the effect that these have on reflectance measurements, to enable field spectroscopy sampling strategies to be developed.

1.6 Aims of this research and an outline of the thesis

The aims of this research are:

1 to investigate the pigment content and optical properties of *Calluna* shoots and leaves to enable the reflectance of these, and their change in reflectance over time, to be modelled

2 to investigate the spatial extent of the area of measurement support for field spectroradiometric measurements, the uniformity of spectral response across this area and to compare these with those assumed by field spectroscopists, given the specifications provided by instrument manufacturers

3 to determine the impact of actual measurement support on assumed spectral response, given the specifications provided by instrument manufacturers

4 to link a *Calluna* ecological growth model to a canopy reflectance model and model reflectance through a number of annual and inter-annual growth and senescence cycles

To achieve these aims, research has been carried out both in the field and in laboratories and modelling studies have been conducted. This work is presented as research papers in the following four chapters with further discussion in Chapter 6 and conclusions are drawn in Chapter 7.

1.6.1 Chapter 2 (Paper 1): Determining the biochemical and biophysical content of *Calluna vulgaris* that influences reflectance and the radiative transfer modelling of reflectance

Some research has been carried out to characterise and classify *Calluna* dominated upland by remote sensing but with limited success. This may in part be because little has been done to understand the optical properties of *Calluna* and how the biophysical and biochemical state variables that influence its reflectance change through growth and senescence cycles. This chapter sets out to increase understanding of the photo-active pigments within *Calluna* leaves and how these influence reflectance and change over time by conducting destructive and non-destructive field surveys, laboratory studies and radiative transfer modelling.

The aims of this paper were:

- to determine the biochemical and biophysical content of *Calluna* and the change of these state variables over growth and senescence cycles.
- to determine the photo-active pigments present within *Calluna* shoots and leaves and their change over growth and senescent cycles.
- to estimate the specific *in vivo* absorption spectra of photo-active pigments within *Calluna* to enable them to be incorporated into a radiative transfer model.

The work presented in this chapter has been accepted for publication in the *International Journal of Remote Sensing*.

During the course of this work the wavelength calibration and signal-to-noise characteristics of the Spectra Vista Corporation (SVC) GER 3700 spectroradiometer

used for reflectance measurements and the wavelength and radiometric calibration of the Perkin Elmer Lambda 40 UV/Vis spectrophotometer used for *in vitro* pigment absorption spectra determination were verified. In addition, the spatial characteristics of the light environment used in the laboratory reflectance measurements were determined. These calibration verifications and light environment characteristics are presented in Appendix A. The laboratory light environment in which the spectral reflectance of the *Calluna* shoots and leaves samples were made was also verified and these data are presented in Appendix B.

1.6.2 Chapter 3 (Paper 2): Characterising field spectroradiometers for high spatial resolution measurement of heterogeneous Earth surfaces

During the course of the laboratory measurements of reassembled Calluna canopies, difficulties were discovered relating the spectra recorded to the biophysical or biochemical state variables of the samples being measured. As the samples and measurement configuration used presented a heterogeneous surface (open Calluna canopy with woody, photosynthesising and senescing components over a black background) and the surface did not fully fill the field-of-view, it was considered that it may be a property of the spectroradiometer that was causing anomalies observed. Knowledge of spectroradiometer characteristics was also required to define the field sampling resolution and consequently to determine the field measurement strategy. To gain an understanding of the spectroradiometer characteristics that influence the area of measurement support, the directional response functions of two commonly used full wavelength spectroradiometers, an Analytical spectral Devices (ASD) FieldSpec Pro and a SVC GER 3700, were investigated in an optical darkroom.

The main aims of this paper were:

- to investigate if the field-of-view of two spectroradiometers, defined by the nominal included angle of the fore optic specified by manufacturers, was an adequate parameter to define the areal extent of the area of measurement support
- to investigate if there were any spatially determined wavelength dependencies across the areal extent of the area of measurement support

The work presented in this chapter has been accepted for publication in *IEEE Transactions in Geosciences and Remote Sensing.*

1.6.3 Chapter 4 (Paper 3): The effect on reflectance measurement of the directional response function of two spectroradiometers

It was demonstrated in the previous paper that the field-of-view of two commonly used field spectroradiometers was a wholly inadequate parameter to describe the area of measurement support and the responsivity of these instruments to light from locations within this area. However, it was unclear from this previous work how the area of measurement support and responsivity reported in Chapter 3 would affect the reflectance spectra recorded from heterogeneous Earth surface targets such as *Calluna* canopies. This paper addressed these deficiencies through the use of modelling studies.

The main aims of this paper were:

- to determine the impact that the differences between the actual area of

measurement support and area of measurement support assumed from specifications provided by instrument manufacturers have on spectra recorded from a number of modelled *Calluna* canopies

- to determine the effects that the differences in directional response function wavelength dependencies would have on the spectra recorded from a number of modelled *Calluna* canopies

- through the use of modelling studies, to compare differences between the spectra measured by each of the spectroradiometers and the biophysical and biochemical indices derived from these spectra

The work presented in this chapter has been prepared for submission to *IEEE Transactions in Geosciences and Remote Sensing* and addresses questions raised by two reviewers of the previous chapter when it was submitted to this journal.

1.6.4 Chapter 5 (Paper 4): Determining the structure and modelling the reflectance of *Calluna vulgaris* canopies

The intention of this thesis has been to advance understanding of the interaction of light with *Calluna* and to determine if the reflectance of *Calluna* canopies and stands can be modelled through annual and inter-annual growth and senescence cycles. To do so quantitative field survey methods will need to be developed and a photosynthesising biomass growth model coupled to a multi layer canopy and leaf radiative transfer reflectance model. If the reflectance of *Calluna* canopies and stands can be forward modelled, it is hypothesised that in future hyperspectral images will be able to be used to estimate the biological and physiological state variables influencing reflectance and their change over time through inversion of

the combined model developed in this work. The inversion outputs could then be validated by the field methods also developed in this work. This may then enable *Calluna* to be used as an indicator of peatland ecological condition and consequently environmental change.

The main aims of this paper were:

- to determine if optical field survey methods could be used to classify *Calluna* stands of different growth stages and in different ecological communities
- to assess if optical field survey methods could be used to quantifiably determine *Calluna* canopy and stand structural parameters
- to calibrate and validate a *Calluna* photosynthesising growth model for the Smeath Hill research site
- to determine if a RT model could be coupled to a *Calluna* growth model to model the reflectance of *Calluna* stands through annual and inter-annual growth and senescence cycles

It is intended to submit the work presented in this chapter to the *International Journal of Remote Sensing*.

During the course of the work for this chapter wavelength calibration and signal-to-noise characteristics of the SVC HR-1024 spectroradiometer used for the field reflectance measurements were verified and these are presented in Appendix A. The SunScan PAR measurement data for each research plot at each sampling interval is presented in Appendix D. The meteorological data accessed from the UK Met. Office and used during the analysis for this chapter are presented in Appendix C. In addition, an assessment of the field spectroscopy spatial positioning accuracy and precision of repeat measurements has been made and is presented in Appendix E.

1.7 Research site and methods

The field work for this research was undertaken at a site designated as a Special Protected Area (SPA)[3] within Clyde Muirshiel Regional Park, located in west central Scotland adjacent to the Clyde Estuary. A 120 hectare upland enclosure, known as Smeath Hill, located at an elevation of approximately 270 metres, within the 1,700 hectare tenanted agricultural holding of Hardridge Farm and Ducal Moor was selected for location of the research plots. This area contained a range of *Calluna* age classes and ecological communities typical of the upland peatlands of Scotland. An ecological survey of the area was conducted on behalf of Scottish Natural Heritage (SNH) during 1994 and a record of this survey was made available for this research. The communities, their spatial extent and the survey points used to derive the NVC ecological classifications from this survey are shown in Figure 1.6. The upland areas of the farm have historically been managed for grazing by Scottish blackface sheep (*Ovis aries*) and recreational red grouse (*Lagopus lagopus*) shooting. Highland longhorn cattle have recently been introduced to increase grazing diversity and to improve financial viability. Although there is evidence of extensive use of muirburn to manage these areas in the past, none has been carried out for over 15 years. However, a muirburn programme has now been initiated and payment from Government is being received for this and the other conservation management measures being undertaken.

Within the Smeath Hill enclosure research plots typical of specific *Calluna* age classes and growth forms were located in two distinct ecological communities representative of the surrounding moorlands. These plots were selected by stratified sampling and fenced to exclude grazers. In each research plot a point

[3]SPAs are areas proposed for protection as being of international conservation importance in accordance with Article 4 of the EC Directive on the conservation of wild birds (79/409/EEC). This Directive also allows for protection of the habitats.

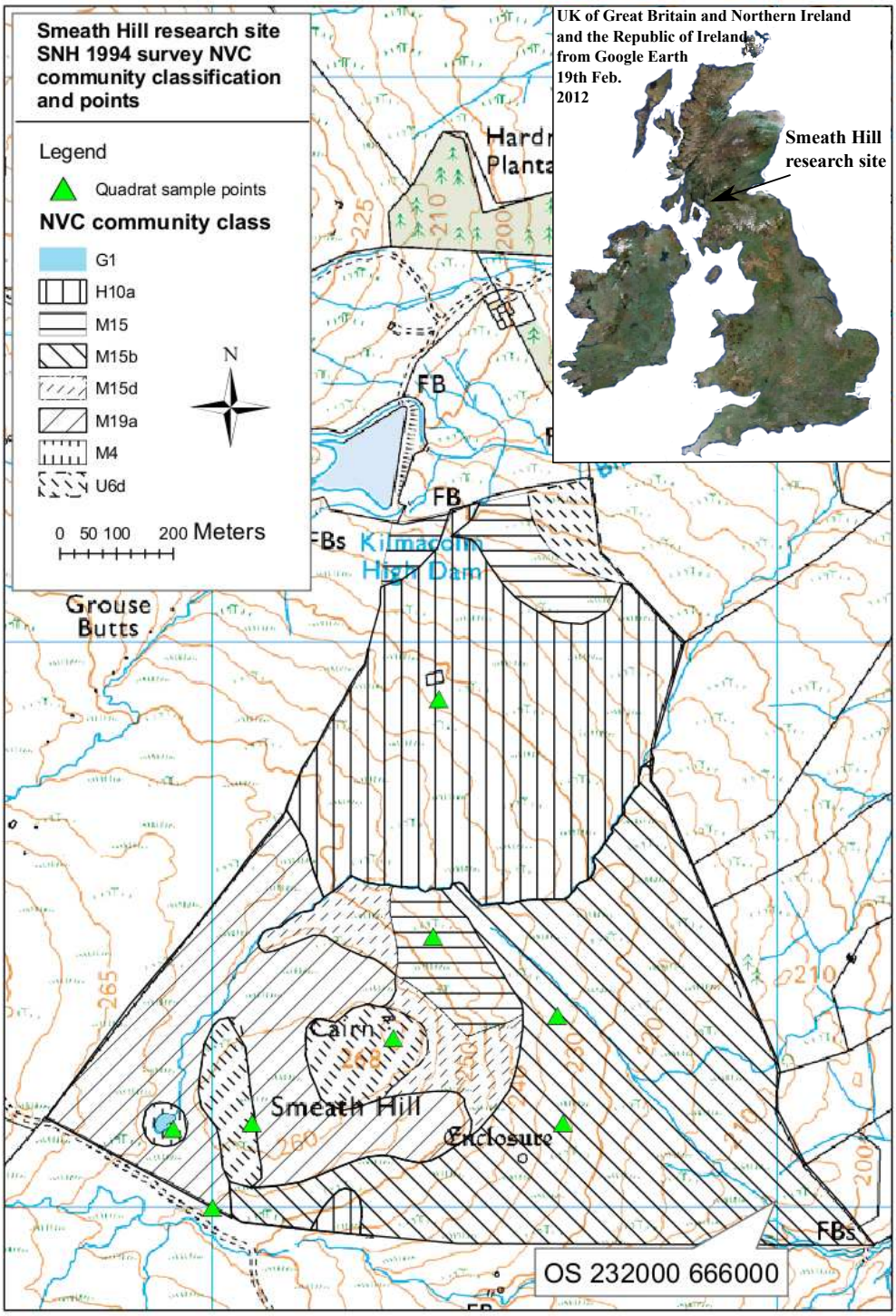

Figure 1.6: Research site location map and NVC classifications and survey points from Smeath Hill 1994 survey by Green Associates for SNH displayed on 1:25,000 scale digitised map extracted from UK Ordnance Survey sheet ns36.

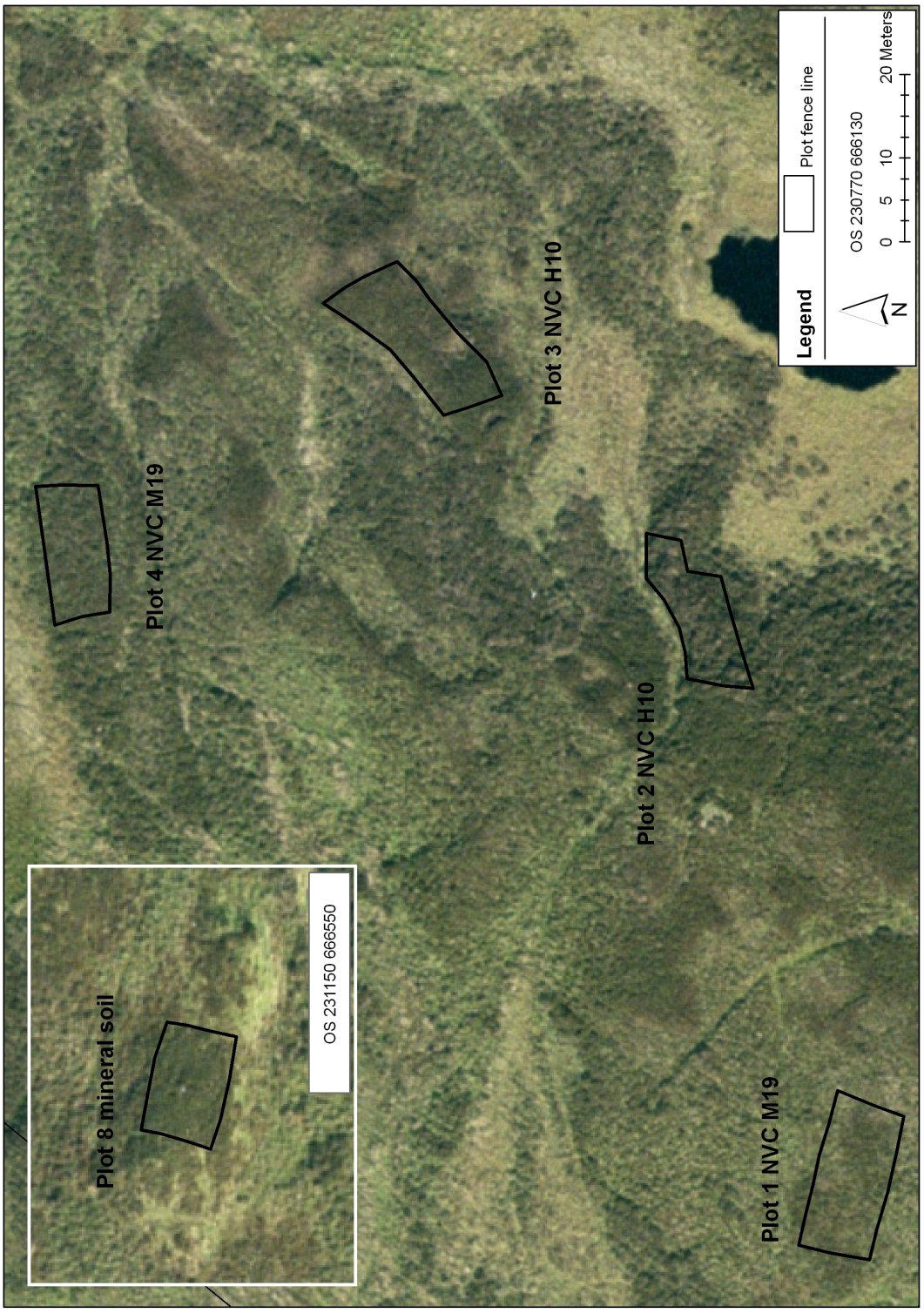

Figure 1.7: Smeath Hill research plots where the difference in 'texture' between each *Calluna* stand can be seen. Digitised and georeferenced RGB image acquired 10th July 2007 by Wild RC010 large format camera mounted on NERC ARSF aircraft and research plots delineated by differential GPS 20th June 2007.

was randomly selected and a four metre long transect fixed in place, oriented East to West, starting from this point. This transect was graduated along its length to enable repeat field spectroscopic measurements to be made of the same vegetation surface area within each research plot at each temporal sampling interval. The location and extent of the plots and each transect were positioned by differential GPS and are indicated in Figure 1.7, where distinct differences in image 'texture', related to canopy and stand gross morphology, can be seen.

In addition to the transect overstorey reflectance measurements, measurements of understorey vegetation reflectances were made at each temporal sampling interval where these could be acquired without the reflectance of *Calluna* being included. *Calluna* canopy samples were selected at random from within the plots by use of standard quadrats, taking care not to interfere with the transect sampling areas. The stems were cut where they protruded from the understorey, the cut ends wrapped in *Sphagnum* and sealed in plastic bags to minimise drying, and transferred to a field laboratory established in a building close to the research site. This field laboratory was established to enable reflectance measurements and destructive physical measurements (biomass and water content measurement and canopy component determination) of the samples to be made as soon as possible after collection. Leaf pigments were also extracted and stored for determination and quantification by wet chemistry methods in another laboratory equipped with a scanning spectrophotometer.

Chapter 2

Calluna vulgaris foliar pigment and spectral reflectance modelling

A. Mac Arthur[1] and T. Malthus[2]

[1] NERC Field Spectroscopy Facility, School of Geosciences, University of Edinburgh, Edinburgh, EH9 3JW UK.

[2]Environmental Earth Observation Program, CSIRO Land and Water, Black Mountain,ACT 2601, Australia.

This chapter has been published and should be cited as: Alasdair Mac Arthur and Tim Malthus (2012): *Calluna vulgaris* foliar pigments and spectral reflectance modelling, *International Journal of Remote Sensing*, 33:16, 5214-5239.

2.1 Introduction

In ecosystems dominated by higher plants, the reflectance of electromagnetic radiation from vegetation canopies is primarily influenced by the optical properties of leaves (Jacquemoud *et al.*, 1996), although canopy morphology and understorey reflectances may contribute significantly (Kumar *et al.*, 2001). The optical properties of leaves depend on the presence and quantity of proximate pigments, water, nitrogen, cellulose and lignin, as well as cellular and surface structure features (Jacquemoud *et al.*, 1996; Dawson *et al.*, 1998; Kumar *et al.*, 2001; Jacquemoud and Ustin, 2008) and are indicative of photosynthesis and plant physiological processes (Taiz and Zeiger, 2002). To further understand the interaction of light and leaves and, hence, photosynthesis and plant physiology, a number of approaches to modelling leaf reflectances have been developed and Kumar *et al.* (2001) and Jacquemoud and Ustin (2008) offer extensive reviews of these. Studies based on radiative transfer models, which attempt to account for the interaction of light and the biophysical structure and biochemical processes that influence leaf reflectance, have been published extensively in the remote sensing literature. Nevertheless, there remains an increasing need to understand plant pigments and photosynthetic processes and their interaction with light. This is needed at scales from leaf to biome (Schaepman *et al.*, 2009) and radiative transfer models can assist in this.

Radiative transfer models such as PROSPECT (Jacquemoud and Baret, 1990), LEAFMOD (Ganapol *et al.*, 1998), LIBERTY (Dawson *et al.*, 1998) and Raytran (Govaerts and Verstraete, 1998) each take a different approach to the application of radiative transfer theory to the components and physical structure of leaves. PROSPECT treats leaves as a series of turbid plates with gaps between and with Lambertian reflecting surfaces. LEAFMOD also considers a leaf to be planar but with a homogeneous mixture of biochemical components with isotropic scattering

occurring within plates rather than at plate boundaries. LIBERTY was developed to model the reflectance of conifer needles and considers their cellular structure to be better represented by powders (grains with inter granular air cavities) than homogeneous plates and uses Melamed's theory of the interaction of light with powders (Melamed, 1963) to develop needle optical properties. Raytran adopts a ray-tracing approach with radiative-transfer calculations following a Monte Carlo method. In Raytran light is modelled as rays interacting with geometric primitives in a 'scene'. The scene in this context could be a plant leaf with primitives being a cuticle layer and epidermal, mesophyll and vascular cells, and each primitive having emission, reflection, transmission and scattering functions assigned. These radiative transfer models have been used extensively to model the reflectance of a diverse range of plant leaves (Ustin *et al.*, 2004a). However, little work has been carried out to understand the interaction of light with the leaves of *Calluna*, the dwarf shrub that can be the dominant overstorey species on extensive areas of peatland.

The status and dynamics of subarctic boreal peatlands are of great interest in studies of carbon and methane flux and, hence, climate change (Dorrepaal *et al.*, 2003; Belyea and Malmer, 2004; Davidson and Janssens, 2006; Chen *et al.*, 2008; Nichol and Grace, 2010; Dorrepaal *et al.*, 2009; Harris and Bryant, 2009b). The UK's peatlands are towards the southern extreme of the global distribution (MacDonald *et al.*, 2006) and therefore may be particularly susceptible to global climate change due to the prevailing oceanic climate (Lindsay, 1995). Developing methods to monitor and measure the dynamics and direction of change of these extensive areas of peatland would be of benefit to both peatland managers and scientists (Harris and Bryant, 2009b).

Calluna vulgaris, henceforth referred to as *Calluna*, a dwarf sclerophyllous shrub, is the dominant overstorey plant species on extensive peatland and

dwarf shrub heath ecosystems in the UK, covering some 1.5 x 10^6 ha (Haines-Young *et al.*, 2000). Changes in the rate of photosynthesis, and the presence or absence of other pigments, are indicative of plant physiological processes and underlying environmental conditions which may cause stress or growth enhancement. Therefore gaining an understanding of how the reflectance of *Calluna* leaves relates to their proximate pigment content would be a first step in developing methods to measure carbon sequestration and monitor *Calluna* dominated peatlands and dwarf shrub heath by optical remote sensing methods.

It has been demonstrated that it is possible to obtain information on the physiological status of plants by acquiring hyperspectral reflectance measurements and relating these to leaf pigments through the use of spectral indices (see, for example, Lichtenthaler *et al.* (1996), Gitelson and Merzlyak (1998), Blackburn and Steele (1999), Richardson *et al.* (2002), Gitelson *et al.* (2002), Sims and Gamon (2002), Carter and Knapp (2001), Carter and Spiering (2002), Gitelson *et al.* (2003), Gitelson and Merzlyak (2004), Grace *et al.* (2007), Liu *et al.* (2007), Cho *et al.* (2008) and Blackburn and Ferwerda (2008)). Sims and Gamon (2002) offer a review of indices, developed both by themselves and by others, to determine Chlorophyll$_{(a+b)}$ content, Carotenoid:Chlorophyll ratios and Anthocyanins content from hyperspectral reflectance data. However, the Chlorophyll$_{(a+b)}$ indices presented by Sims and Gamon (2002) have not been found to be robust when applied to *Calluna* 'shoots and leaves' reflectances (Mac Arthur and Malthus, 2006) or *Calluna* canopy reflectance (Nichol and Grace, 2010) with a correlation of $r^2<0.66$ between indices and *in vitro* Chlorophyll$_{(a+b)}$ in both studies.

An alternative approach to the estimation of the leaf proximate pigment content by spectral indices is through the inversion of leaf reflectance radiative transfer models (Dawson *et al.*, 1998; Jacquemoud *et al.*, 2000; Renzullo *et al.*, 2006; Di Vittorio, 2009). The principle of a radiative transfer model inversion approach

(a) Nadir view of a continuous *Calluna* canopy

(b) *Calluna* erectophile structure

(c) *Calluna* decussate 'shoots and leaves'

Figure 2.1: The horizontal and vertical structure of a continuous *Calluna* canopy and the distribution of leaves on stems and shoots

is that if leaf reflectance spectra can be modelled from a set of state variables then when reflectance spectra are known *a priori* these spectra can be used as model inputs and the models inverted, *i.e.* run in reverse, to retrieve the set of state variables that would have generated the input spectra (Jacquemoud, 1993; Kumar *et al.*, 2001). If the reflectance of *Calluna* can be modelled from proximate pigment and leaf structural parameters then it may be possible to invert *Calluna* leaf reflectances to determine the proximate pigment content and structural parameters and, hence, measure and monitor *Calluna* photosynthesis and physiological status from remotely sensed reflectance spectra. However, as yet, modelling studies of the reflectance of *Calluna* leaves have not been conducted nor is the biophysical and biochemical content of *Calluna* leaves well documented.

This research will first investigate the biochemical content and leaf structural parameters that influence spectral reflectance of *Calluna* leaves, and the change in these parameters during growth and senescence. The investigation will then determine if a radiative transfer model can be used to model the reflectance

of *Calluna* leaves at discrete time intervals through a growth and senescence cycle. As it was considered unlikely that the optical properties of individual leaf components such as trichomes, cuticle, epidermis, mesophyll and vascular cells could be obtained, ray-tracing approaches were ruled out. The LIBERTY (Dawson *et al.*, 1998) model, developed to model the interaction of light with pine needles, was selected for this study as it was considered that the interaction of light with *Calluna* leaves is more realistically conceptualized in LIBERTY than other radiative transfer models. Continuous *Calluna* stands, when viewed from nadir, resemble (in miniature) those of conifers (Figure 2.1(a)); *Calluna* 'shoots and leaves' have an erectophile (Figure 2.1(b)) rather than the planophile orientation; and the decussate pairs of *Calluna* 'shoots and leaves' (Figure 2.1(c)) more closely resemble conifer needles than the leaves of broadleaf species. *Calluna* leaves are evergreen rather than deciduous; they are microphylls rather than megaphylls; and they tend to be rolled, at the extreme adopting a cylindrical form, rather than planar, as PROSPECT (Jacquemoud and Baret, 1990) or LEAFMOD (Ganapol *et al.*, 1998) have been developed to model. In addition, due to the complex architecture and spatial distribution of leaves in *Calluna* canopies it may be more appropriate to consider the photosynthesising elements in clumps, *i.e.* groups of individual 'shoots and leaves', each element of which may be at a different stage of growth or senescence, as has been conceptualized within LIBERTY. However, leaf cell structural representations in current radiative transfer models (such as LIBERTY) are gross simplifications (Feret *et al.*, 2008) preventing accurate estimations of leaf *in vivo* pigment absorption spectra or pigment concentrations by model inversion (Di Vittorio, 2009). Furthermore, as the spectral resolution of LIBERTY is 5 nm, absorption or reflectance features with a width < 5 nm may not be modelled and the position of the red-edge may not accurately be represented in the model (Llewellyn, 2009). In addition, the inversion accuracy of LIBERTY has been found to decrease with increasing number of modelling parameters (Moorthy *et al.*, 2008). Nevertheless, the Matlab version of LIBERTY, validated

for grassland remote sensing research by Llewellyn (2009), with the typographical error for the expression of absolute diffuse reflectance within the Melamed (1963) component of LIBERTY (acknowledged by Mandelis *et al.* (1990), Jacquemoud and Ustin (2008) and others) corrected by P. Lewis (personal communication P. Lewis 26/11/2010), has been used as the basis for the leaf reflectance model used in this research.

2.2 Research site and methodology

2.2.1 Research site

A research site, centred on 4^o 42' 18" west 55^o 51' 37" north, was established on Smeath Hill, a 120 hectare enclosure on Duchal Moor, an extensive area of *Calluna*-dominated peatland within the Renfrew Heights Special Protected Area in west central Scotland. Eight research plots were delineated and accurately located through the use of differential GPS. The *Calluna* allometry variables, age class and plot substrate type within these plots were recorded (Table 2.1). Each plot represents a particular *Calluna* age class growing in a particular substrate type. The research plots are located on a level area of moor at an altitude of 270 metres. In addition to the measurements made by the authors during the course of this research and discussed in the following sections, meteorological data was acquired from a UK Met Office station within 8 km of the research site.

2.2.2 *Calluna* spectral measurements

At approximately monthly intervals, from April to October during 2005 and 2006, three *Calluna* canopy samples were selected at random from each research plot

Table 2.1: *Calluna* allometry, age class and substrate type in each research plot

Plot	Age class	Canopy ht.$^{\Diamond}$ (mm)	Stem dia.^{o} (mm)	Substrate type
1	Building*	280	2.99	Blanket bog
2	Degenerate*	280	10.19	Dry peat
3	Mature*	350	3.82	Dry peat
4	Layering^{x}	320	7.79	Blanket bog
5	Pioneer*	150	2.10	Blanket bog
6	Pioneer*	190	2.75	Acid mineral soil
7	Mature/Degen.*	370	7.27	Blanket bog
8	Building*	320	3.13	Acid mineral soil

*After Watts 1954; ^{x}after Mac Donald 1995; $^{\Diamond}$average of 15 measurements; ^{o}average of 15 stems

using a 0.25 m^2 quadrat. The percentage of *Calluna* ground cover within each quadrat sample was estimated by counting the presence or absence of *Calluna* within each cell of a 10 cm grid placed inside the quadrat. The *Calluna* sample within each quadrat was then cut where the stems emerged from the understorey ground cover, cut stems wrapped in moist *Sphagnum* moss and samples sealed in plastic bags to minimize losses from dehydration, removed to a laboratory and processed within 24 hours. Reflectance measurement sub-samples, weighing approximately 10% of each quadrat sample, were randomly selected, weighed, then the 'shoots and leaves' stripped from the stems. This resulted in there being three reflectance samples for each *Calluna* plot, each an aggregate of leaves at different stages of their life cycle. Shoots and leaves were selected as the reflectance samples since it was not possible to strip only leaves from the shoots without causing mechanical damage because of their extremely small size (Figure 2.2(a)), complex shape and presence of trichomes (Figure 2.2(b)). The 'shoots and leaves' from each sub-sample were subsequently weighed then stacked to fill a blackened deep petri dish. Within a laboratory darkroom, each dish of stacked 'shoots and leaves' was placed in an environment with both diffuse and direct light, to better simulate natural illumination conditions, and illuminated using a 500 watt tungsten halogen light source. For each sample, a reference measurement of a

calibrated Spectralon panel was first taken, then four spectral measurements made using a GER 3700 full wavelength (350 nm to 2,500 nm) spectroradiometer fitted with a 14^o fore optic, rotating the samples through approximately 90^o between each measurement. For each spectral reflectance measurement, care was taken to ensure that the samples filled the spectroradiometer field-of-view, that the height of the spectrometer above the samples was the same at each sampling interval and that the height and illumination angle of the lamp above the samples were consistent. Therefore the area of measurement support was the same for each spectral reflectance measurement and the measurements were replicable. All spectral measurements from each research plot's samples were subsequently processed to absolute reflectance, averaged, normalized per unit weight and a Savitzky-Golay polynomial smoothing filter applied, after Mather (2004).

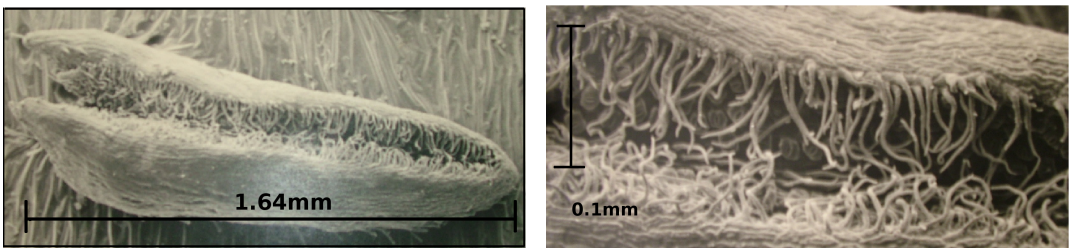

(a) Leaf protecting stoma by adopting a rolled form

(b) Trichomes over stoma on on abaxial surface of leaf

Figure 2.2: Micrograph of a *Calluna* leaf

2.2.3 *Calluna* biochemical and biophysical variable determination

A one gram sub-sample of each 'shoots and leaves' reflectance sample was randomly selected and, for each sampling interval during 2005, proximate pigments were extracted in anhydrous acetone, after Sestak *et al.* (1971). During 2006 a one

gram sub-sample of each 'shoots and leaves' reflectance sample was selected and proximate pigments extracted in anhydrous methanol, as there was an indication of the presence of Anthocyanins in the 2005 assays, although Anthocyanins are degraded in an acetone buffer (Lichtenthaler, 1987). However, an additional one gram sub-sample was selected from the 2006 samples and proximate pigments extracted in anhydrous acetone as before, to facilitate comparison with the 2005 pigment determination. A spectrophotometer, with a range of 400 nm to 800 nm and resolution of 1 nm, was used to measure the absorption spectrum of each sample and the spectra from each research plot's samples averaged. From the remainder of each reflectance sample the water content, and hence the dry matter, was determined by weighing, oven drying for 48 hours at 60^oC and weighing again. At each sampling interval the $\text{Chlorophyll}_{(a+b)}$ and total Carotenoid content of each plot was determined from the average absorption spectrum obtained from the acetone assays, after Lichtenthaler (1987), and Anthocyanins content determined from the average absorption spectrum of the methanol assays after Sims and Gamon (2002).

Table 2.2: LIBERTY leaf radiative transfer model variables

Biochemical variables$^{\#}$	**Structural variables**	**Constants**
Chlorophyll (μg/g)	Average internal cell dia. (μm)	Baseline value
Water (mg/g)	Intercellular air space value*	Albino value
Nitrogen (mg/g)	Leaf thickness (mm)	
Lignin + cellulose (mg/g)		

*A quantity with no units indicative of the radiative flux passing between cells. See Dawson, 1998. LIBERTY User Guide. $^{\#}$ per gram 'shoots and leaves'

2.2.4 *Calluna* 'shoots and leaves' reflectance modelling parameters and methods

The variables required to parameterise LIBERTY are listed in Table 2.2. The Chlorophyll$_{(a+b)}$, water content and leaf thickness values measured during 2006, the nitrogen content determined by Saebo *et al.* (2001) and the lignin plus cellulose content determined by Anderson and Hetherington (1999) were initially used to parameterize LIBERTY. An Albino value of 2 and a Baseline value of 0.0014 were selected as these were found to scale the LIBERTY infinite reflectance output spectra closest to the measured spectral reflectances and were used as constants for the remainder of the research. As LIBERTY has been noted to be sensitive to cell diameter and airspace variable changes (Moorthy *et al.*, 2008), the effect of these variables on the 700 nm to 1000 nm, near infra-red (NIR), spectral region, the region of the visible to near infra-red (VNIR) spectrum most affected by leaf internal structural parameters (Dawson *et al.*, 1998; Moorthy *et al.*, 2008; Di Vittorio, 2009), were assessed next. As will be discussed further in Section 3, the values for cell diameter and intercellular airspace were determined for each sampling interval through an iterative optimisation process by initiating LIBERTY with values considered to be realistic, running the model, comparing the model output spectrum with the corresponding measured reflectance spectrum, adjusting the cell diameter and airspace variables and repeating model runs until a minimum root mean squared error (RMSE) in the NIR region of the spectrum was achieved.

After determining the appropriate cell diameter and intercellular airspace values, LIBERTY needed to be modified to incorporate the absorption spectra of total Carotenoids and Anthocyanins, in addition to Chlorophyll$_{(a+b)}$, as the significant presence of these proximate pigments had been identified during the 2005 data

analysis. The modified LIBERTY model will be referred to as 'LIBERTY 3 pigments' (LIBERTY3P). LIBERTY3P, following Beer-Lambert's Law, defines the total absorption coefficient (*Tcoeff*) of leaf biochemical constituents at each wavelength as the sum of the products of individual constituent absorption coefficients multiplied by their concentrations per unit weight of 'shoots and leaves' and is an adaptation of LIBERTY similar to that of Vittorio's (2009) Chlorophyll$_{(a)}$, Chlorophyll$_{(b)}$ and total Carotenoids adaptation. The LIBERTY3P total absorption coefficient, T$_{coeff}$, for each wavelength with the wavelength symbol (λ) omitted for clarity, is

$$\begin{aligned} &= D\,(B + (A_{chloro}C_{chloro}) + (A_{Caroten}C_{Caroten}) + (A_{Antho}f_{Antho}) \\ &+ (A_{Albino}f_{Albino}) + (A_{LigCell}C_{LigCell}) + (A_{protein}C_{protein}) + (A_{water}C_{water})) \end{aligned} \tag{2.1}$$

In Equation 2.1, D is the average cell diameter in μm; B is the baseline absorption coefficient; A_{Chloro} the Chlorophyll$_{(a+b)}$ absorption coefficient and C_{Chloro} the Chlorophyll$_{(a+b)}$ content; $A_{Caroten}$ the Carotenoids absorption coefficient and $C_{Caroten}$ the total Carotenoids content; A_{Antho} the Anthocyanins absorption coefficient and C_{Antho} the Anthocyanins content; A_{Albino} the leaf albino absorption coefficient and f_{Albino} the albino factor; $A_{LigCell}$ the lignin and cellulose absorption coefficient and $C_{LigCell}$ the lignin and cellulose content; $A_{protein}$ the nitrogen absorption coefficient and $C_{protein}$ the nitrogen content; A_{water} the water absorption coefficient and C_{water} the water content. However, when the spectra generated by LIBERTY3P were compared with corresponding measured reflectance spectra significant spectral differences were generally noted. Subsequently, the published absorption spectra for each proximate pigment required to be modified to achieve a better fit between measured and modelled spectra, as is discussed in Section 3.

2.3 Results and discussion

2.3.1 *Calluna* 'shoots and leaves' cell diameter and intercellular airspace

Although *Calluna* proximate pigments are the primary state variables of interest in this work, the influence of cell diameter and intercellular airspace on reflectance needs to be considered. As the scattering of light due to leaf structure has the greatest influence on reflectance when absorption is low, it is especially significant in the spectral region where wavelengths are greater than 700 nm and where there is no pigment absorption (Jacquemoud and Baret, 1990; Jacquemoud *et al.*, 1996; Taiz and Zeiger, 2002; Feret *et al.*, 2008). Therefore, reflectance in the 700 nm to 2,500 nm spectral region will now be considered.

The NIR spectral reflectance of each *Calluna* sample was noted to vary at each sampling interval during both 2005 and 2006. This variance in NIR reflectance indicates that either the leaf cell diameter or intercellular airspace was varying, or both were, over the *Calluna* growth cycle. A mesophyll cell diameter of 45 μm was used in LIBERTY by Dawson *et al.* (1998) for reflectance modelldataing of *Pinus banksiana* needles and Lhotakova *et al.* (2008) and Dvoral and Stokrova (1993) report a value of 40μm for Norway spruce and Ponderosa pine mesophyll cell diameters. Nevertheless, *Calluna* leaves are considerably smaller than pine needles and Castro-Diez *et al.* (2000) reported values of 55.9 μm^2 and 374 μm^2 for *Calluna* intercellular airspace and cell areas, respectively, although these values were determined from leaves that were less than one month old (personal communication P. Castro-Diez 19/02/2010). However, as *Calluna* leaves have a 2 to 3 year life cycle (Gimingham, 1972), the stacked 'shoots and leaves' reflectance samples measured in this work are an aggregate of leaves at different stages of their life cycle. Individual leaf cells enlarge and differentiate until they assume

their function (Taiz and Zeiger, 2002) and the growth of individual cells ceases when they are physically (Tomos, 1985) and genetically (Horiguchi *et al.*, 2006) constrained. Hence, new fully grown leaves will have the optimal cell diameter for that plant species. Therefore, the mean cell diameter of the *Calluna* 'shoots and leaves' samples will increase until the maximum proportion of new fully grown leaves to older senescing leaves is achieved. However, as there is no specific data on the growth of *Calluna* mesophyll cells or development of leaf structure, the cell diameter, calculated from the cell area reported by Castro-Diez *et al.* (2000), was selected as the mean cell diameter at the time of the first sampling interval. The cell diameter was then projected to increase until the end of growth then decrease thereafter as the leaves senesce. Grant (1987) proposed that the increase in NIR reflectance observed from leaves during their growth is a result of an increase in intercellular airspace as hydrated mesophyll cells are pulled apart during leaf development. In addition, Daughtry and Biehl (1985) report that in the initial stage of senescence there is a further increase in NIR reflectance as cells separate further, again increasing the air spaces within leaves. Knipling (1970) observed that there is then a decrease in NIR reflectance as cells dehydrate and collapse during senescence, leading to a reduction in scattering from cell walls and intercellular airspace interfaces. It is therefore considered that the intercellular airspace determinant variable values will increase over the *Calluna* growth period, continue to increase for a period after growth ceases, then decrease during senescence.

The leaf structural variable values presented in Figure 2.3 were determined by modelling and adopting an iterative optimisation process. For each sampling interval a mean cell diameter and intercellular airspace variable considered to be realistic was selected and used to parameterize the model. The model was run and the modelled reflectance spectra were compared with the measured spectra. The cell diameter and airspace variable values were then adjusted and the model rerun,

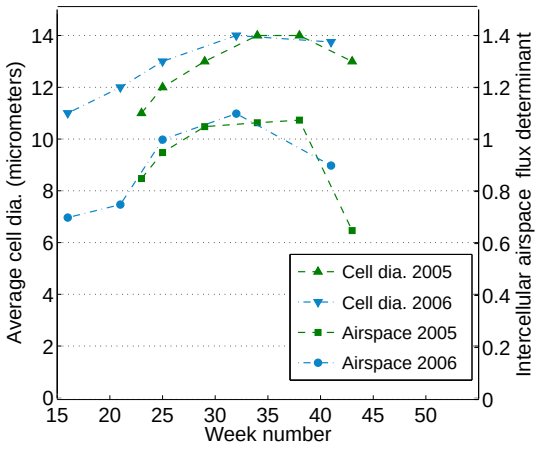

Figure 2.3: *Calluna* cell diameter and airspace determined for the 2005 and 2006 sampling periods

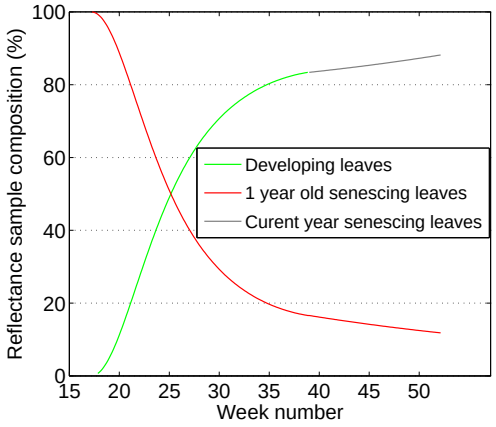

Figure 2.4: Annual modelled *Calluna* leaves growth and senescence

until a minimum RMSE was acheived for the NIR spectral region. The values in Figure 2.3 offer a numerical solution for the LIBERTY (using the 2005 data) and the LIBERTY3P (using the 2006 data) radiative transfer model outputs to approximate to the measured *Calluna* 'shoots and leaves' reflectance in the NIR region at each sampling interval.

Figure 2.3 shows that if the stacked *Calluna* 'shoots and leaves' sample has a mean mesophyll cell diameter of 11 μm at the beginning of the growth cycle in April 2006 then the mean cell diameter may rise to 14 μm by the end of the growth cycle before reducing again during senescence. In addition, from Figure 2.3, it can be noted that the intercellular airspace determinant increases, indicating that intercellular airspace scattering increases until mid June, then decreases. However, the increase in NIR reflectance proposed by Daughtry and Biehl (1985) was not observed in the intercellular airspace variables determined or in the 'shoots and leaves' samples reflectances. The physical basis for the variables presented in Figure 2.3 can be elucidated from Figure 2.4. Figure 2.4 was developed from the *Calluna* ecological growth model HeathMod (Read *et al.*, 2002), which models the foliar growth of *Calluna* and its off-take by sheep given a

set of ecological and environmental conditions, and has been parameterized with variables determined during this research but with the effects of grazing omitted. Figure 2.4 shows that from the onset of growth, approximately week 17, the proportion of senescing leaves decreases and the proportion of developing leaves increases, consequently the cell diameter and intercellular airspace determinant increase, as Figure 2.3 indicates. This increasing proportion of mature leaves begins to level off at approximately week 37, from when the proportion of mature to senescing leaves is relatively stable until growth ceases at approximately week 40. After week 40 all leaves are at stages of senescence, hence both the mean cell diameter and intercellular airspace decrease. The data presented in Figure 2.4, therefore, supports the selection of the LIBERTY and LIBERTY3P variables presented in Figure 2.3.

As can be seen in Figure 2.5, for the 25th June 2005 sampling interval, and after modelled reflectance in the NIR region was optimized, there remained significant differences between measured and modelled reflectance between the 400 nm to 700 nm and the 950 nm to 1000 nm spectral regions, and this was the case at all sampling periods. The 400 nm to 700 nm region will be considered further below. However, as the sensitivity of the monochromator in the GER3700, from 950 nm to 1000 nm, is low, the signal to noise ratio is poor in these spectral regions and this is compounded by water absorption in that region, the *in vivo* spectral absorption of which may not be accurately represented in LIBERTY, as has been found by Feret *et al.* (2008) for PROSPECT. It is, therefore, not possible to determine if errors in the 950 nm to 1,000 nm spectral region are due to the modelled or to the measured spectra and this region will not be considered further here. Further differences between measured and modelled reflectance in the 1,000 nm to 2,500 nm short-wave infra-red (SWIR) spectral region were noted, where the measured reflectance was greater than that modelled (data not shown). These differences may be due in part to absorbing compounds in leaves not being

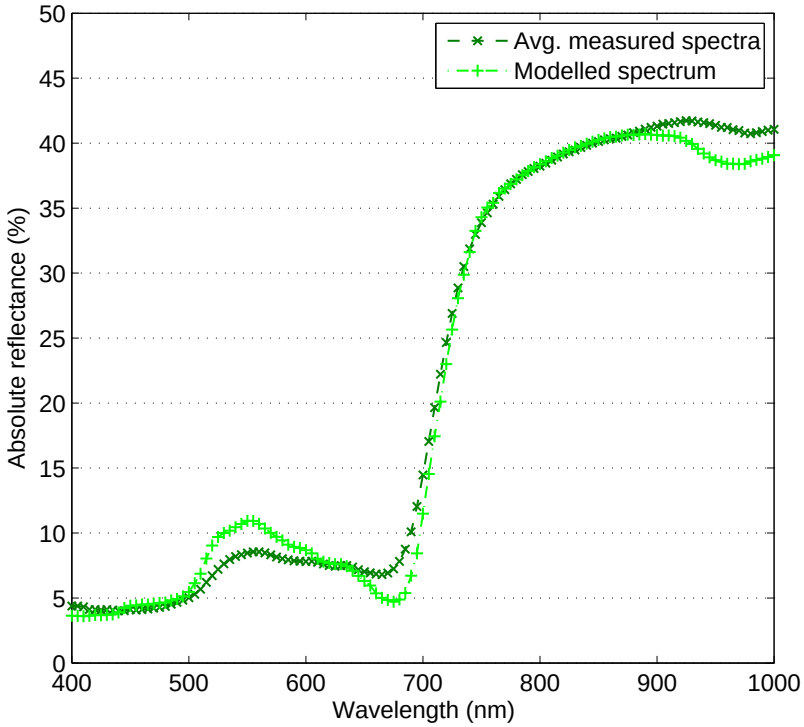

Figure 2.5: Initial measured average and modelled reflectance - June 2005 sampling interval

homogeneously distributed, as Baranoski and Rokne (2005) found that when the heterogeneous distribution of absorbers in leaves was considered the modelled reflectance in the SWIR region was greater than when their distribution was not considered. In addition, surface trichomes, present on the abaxial surface of *Calluna* leaves (Figure 2.2(b)) will influence reflectance in the NIR and SWIR spectral regions, although it is not clear if they will cause an increase (Eller, 1977; Gausman *et al.*, 1977; Wagner, 1991; Levizou *et al.*, 2005) or a decrease in reflectance (Ehleringer, 1984; Gausman *et al.*, 1969). Nor is it clear how significant the influence of trichomes will be on *Calluna* 'shoots and leaves' SWIR reflectance, given their location on the leaves. The proportion of lignin to cellulose in *Calluna* 'shoots and leaves' is also unknown and as their relative proportions will affect the lignin and cellulose absorption spectrum used in LIBERTY and LIBERTY3P, it is not possible to assess the influence these leaf structural components will have on *Calluna* 'shoots and leaves' reflectance in the SWIR region. Although it may be possible to add a correction per wavelength to LIBERTY to account for the error between measured and modelled reflectances in the 1000 nm to 2,500 nm spectral region, as this region is not influenced by proximate pigment content, the primary area of interest in this research, it will not be considered further here.

2.3.2 *Calluna* 'shoots and leaves' pigment identification, quantification and trends

The mean proximate pigment content for each 'shoots and leaves' sample of each plot and for each of the annual data sets displayed considerable variability, similar to that for Chlorophyll$_{(a+b)}$ for the 2005 sampling intervals (Figure 2.6), and where the error bars represent ± 1 standard deviation of the mean, which in some cases is close to 25% of plot mean value. One-way Analysis of Variance (ANOVA) was carried out to determine if there was a significant difference between the

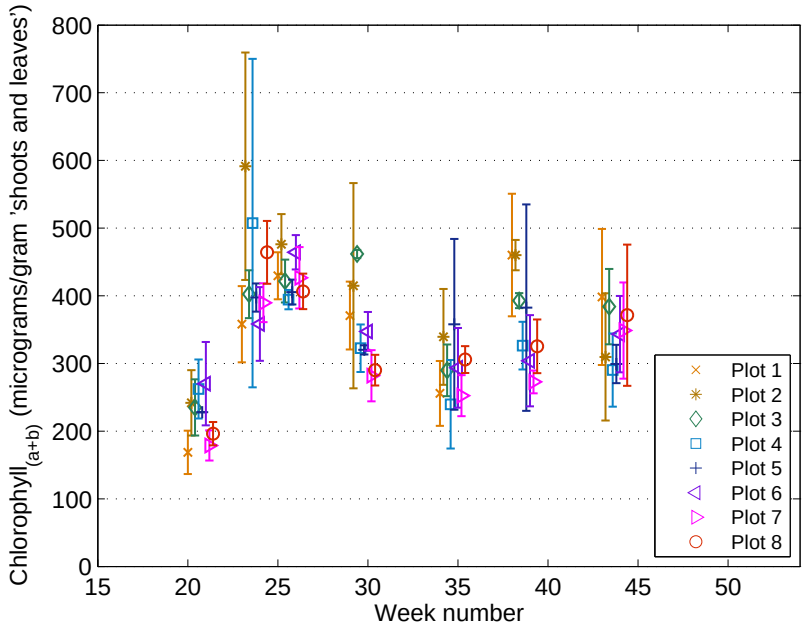

Figure 2.6: *Calluna* 'shoots and leaves Chlorophyll$_{(a+b)}$ variability 2005 sampling intervals.

means of Chlorophyll$_{(a+b)}$, total Carotenoid and Anthocyanins from each sampling interval during 2005 and 2006; no statistically significant differences were noted. Consequently, to parameterize LIBERTY and LIBERTY3P the plot proximate pigment means were averaged for each sampling interval. Although the change in *Calluna* Chlorophyll$_{(a+b)}$ and total Carotenoids and Anthocyanins have not previously been measured and published, the average values for Chlorophyll$_{(a+b)}$ content for 2005 and 2006 during the summer months were found to be comparable with those determined by Nichol and Grace (2010).

From the data acquired during 2005, Chlorophyll$_{(a+b)}$ content displayed a general increase from May through early summer, then a reduction in level, before the onset of *Calluna* flowering in late July, and an increase thereafter, followed by a reduction towards the end of the growing season (Figure 2.7). Total Carotenoid content displayed a similar trend (data not shown): a positive linear relationship

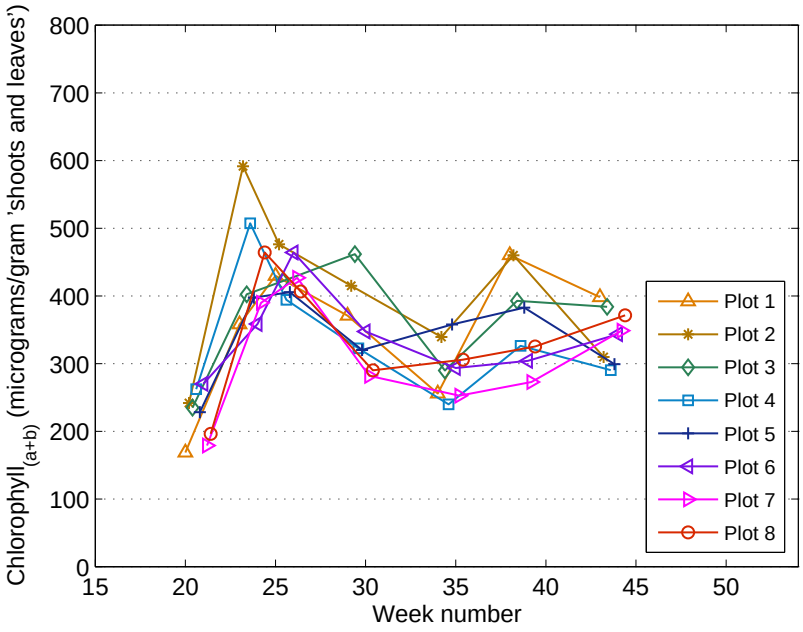

Figure 2.7: Chlorophyll$_{(a+b)}$ plot averages and trends during 2005

between Chlorophyll$_{(a+b)}$ and Carotenoids has been reported for other plant species (Sauceda *et al.*, 2008), although a negative linear relationship has been reported when light stress is induced (Demmig-Adams and Adams, 1996). From the data acquired during 2006, the Chlorophyll$_{(a+b)}$ sample averages for 6 research plots, 1; 2; 3; 4; 5; and 7 in Figure 2.8, followed the trend displayed in 2005. However, two plots, 6 and 8, did not follow the Chlorophyll$_{(a+b)}$ trend observed in the other plots but remained relatively constant from late spring until August. This difference may be due to these plots being located on a mineral soil substrate type. However, this difference was not observed for these two plots in 2005. Therefore this difference in trend may be attributable to the inherent variability of *Calluna* growing in the natural environment.

The general increase in Chlorophyll$_{(a+b)}$ and total Carotenoids from May through early summer and reduction at the end of the growing season were expected as this follows the annual growth and senescent cycle of plants. However, the reduction

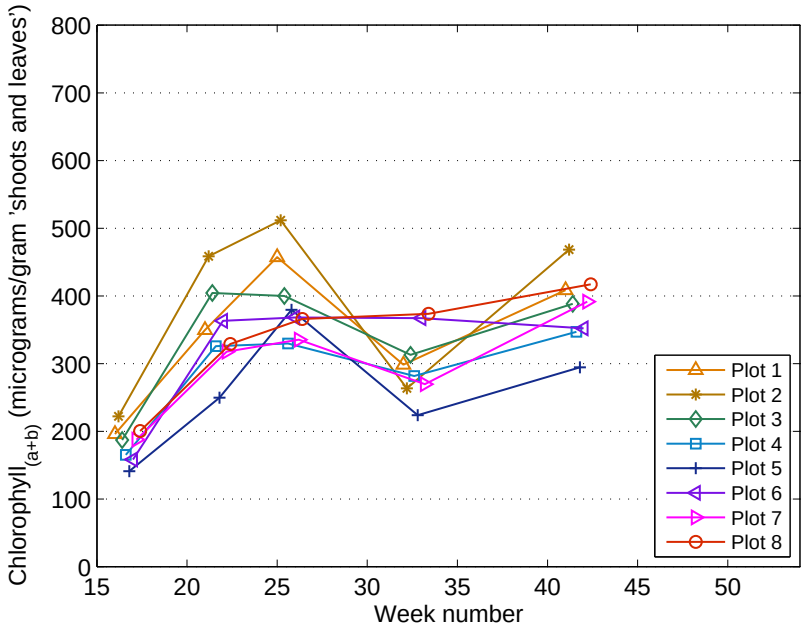

Figure 2.8: Chlorophyll$_{(a+b)}$ plot averages and trends during 2006

before the onset of flowering was unexpected. A reduction in Chlorophyll$_{(a+b)}$ content has been reported when plant species are exposed to stress. Stress, causing a reduction in Chlorophyll$_{(a+b)}$, may be induced by drought (Ma *et al.*, 2006), pollution (Carfrae *et al.*, 2004; Leith *et al.*, 2004), salt (Ma *et al.*, 2006), infestation and disease (Blanchfield *et al.*, 2006), excessive light levels (Demmig-Adams and Adams, 1996; Reddy and Raghavendra, 2006; Ma *et al.*, 2006) or high or low temperatures (Reddy and Raghavendra, 2006). At the site used in this research, drought is unlikely to be a cause of stress as the area is blanket bog, primarily National Vegetation Classifications M19, M15 and H10 in mosaic (Dayton *et al.*, 1994). The deposition of atmospheric pollutants in the area of this research site has not been quantified, although pollution inducing stress is unlikely as there is no industrialisation downwind of the site. In addition, although the prevailing wind is from the sea, salt disposition induced stress is considered unlikely as the site is approximately 10 miles upwind of the sea and sea spray,

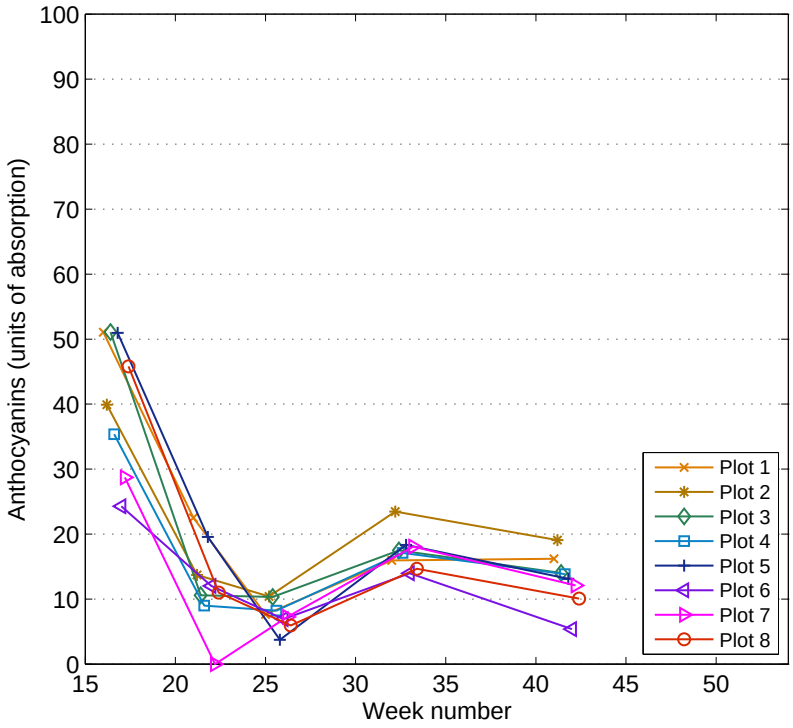

Figure 2.9: Anthocyanins plot averages and trends during 2006

carrying salt, is unlikely to travel that distance inland during the summer months when there are fewer and less severe storms than in winter months.

Foliar Anthocyanins were noted to be present during the wet chemistry proximate pigment determination, confirming the author's visual observations. The presence of Anthocyanins is known to cause leaves to turn shades of red or purple (Feild *et al.*, 2001; Neil, 2002) and *Calluna* foliage has been observed to display a purple colouration after frosts and in mid summer. Anthocyanins content determined during 2006 displays a different trend from the general trend displayed by the other pigments determined during both 2005 and 2006 (Figure 2.9). Anthocyanins content was greatest in early spring then varied through the growing season, being lowest when Chlorophyll$_{(a+b)}$ content was high and highest when

Chlorophyll$_{(a+b)}$ was low. Although the function of foliar Anthocyanins is not fully understood, they appear to perform a number of tasks such as protection from ultraviolet radiation (Holton and Cornish, 1995) and photoinhibition (Feild *et al.*, 2001; Steyn *et al.*, 2002; Neil, 2002; Close and Beadle, 2003; Merzlyak *et al.*, 2008; Hatier and Gould, 2009). The photoinhibition hypothesis proposes that when Chlorophyll$_{(a+b)}$ levels are low, or light levels are high, there is a potential for photo-oxidative damage to Chloroplasts due to an imbalance between light capture, CO_2 assimilation and carbohydrate utilisation. Anthocyanins accumulation requires and thereby attenuates light, possibly protecting Chloroplasts. The high levels of Anthocyanins at the April sampling interval correspond to low levels of Chlorophyll$_{(a+b)}$ and hence low levels of photosynthesis, expected through winter and into early spring. The elevated levels of Anthocyanins in mid summer and reduced levels of Chlorophyll$_{(a+b)}$ may be a result of light levels being higher than *Calluna* can tolerate without photo-oxidative damage to Chloroplasts, indicating support for the photoinhibition hypothesis. However, it was not possible to correlate the elevated Anthocyanins interval to specific meteorological or solar intensity events, as the lag between event and response and residence time of Anthocyanins in *Calluna* leaves is not known. Nevertheless, as the reduction in Chlorophyll$_{(a+b)}$ was observed prior to the onset of flowering, *Calluna* may be utilising its resources to set flower and seed rather than continue growth and the production of Chloroplasts, leaving it more susceptible to photo-oxidative damage, particularly as flowering coincides with the period of high annual temperature and hours of sunshine. The proximate pigment content, determined at each sampling interval in 2005 and 2006 and used to parameterize LIBERTY and LIBERTY3P, are presented in Figure 2.10.

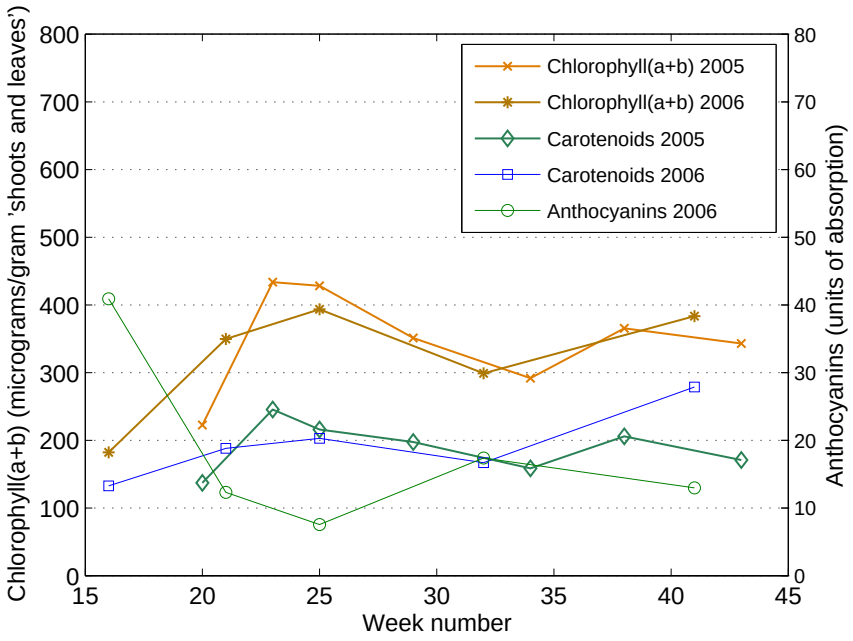

Figure 2.10: Proximate pigments - research site annual averages

2.3.3 *Calluna* 'shoots and leaves' pigment absorption

When LIBERTY was initially parameterized with the biophysical variables and Chlorophyll$_{(a+b)}$ content determined for each sampling interval during 2005 the fit between measured and modelled data was optimized for the NIR spectral region, as has previously been discussed. However, the fits between measured and modelled spectra were found to be poor or inconsistent in the 400 nm to 700 nm spectral region at each 2005 sampling interval, similar to the fit displayed in Figure 2.5 for the 25th June 2005 sampling interval. LIBERTY contains a pigment absorption spectrum derived from the pure absorption spectra of Chlorophyll$_{(a)}$ and Chlorophyll$_{(b)}$, mixed in a ratio representative of these pigments in *Pinus elliottii*, and dissolved in acetone (Dawson *et al.*, 1998). The mismatch between modelled and measured spectra in the 400 nm to 700 nm region for *Calluna* suggests that the LIBERTY Chlorophyll$_{(a+b)}$ absorption spectrum

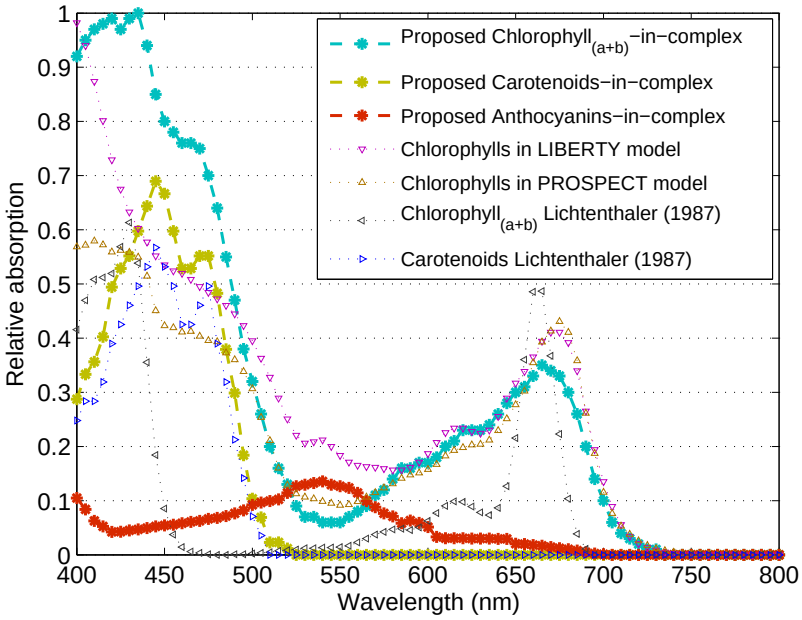

Figure 2.11: LIBERTY3P pigments and comparators

may not be representative of these pigments in *Calluna* 'shoots and leaves'. In addition, LIBERTY does not account for total Carotenoid or Anthocyanins absorption and these pigments have been identified in *Calluna*. Consequently, the absorption spectra for Chlorophyll$_{(a+b)}$ and total Carotenoids published by Lichtenthaler (1987) and Anthocyanins absorption spectra published by Neil (2002) were incorporated into LIBERTY3P in the manner presented in Equation 2.1 and measured and modelled spectra generated from the 2006 data compared. However, although there was some improvement, the fits between measured and modelled spectra remained poor.

To attempt to achieve better fits between measured and modelled spectra through the 400 nm to 700 nm spectral region for the each 2006 data, an optimisation process was again adopted. The May, June and August 2006 measured reflectance spectra were averaged and the average spectra used as the training data set. The

optimisation process was then utilized, constrained by the range of values considered likely for each pigment and sequentially modifying the Chlorophyll$_{(a+b)}$, total Carotenoid and Anthocyanins absorption spectra at each wavelength and comparing modelled with measured reflectances, until the minimum RMSE for each wavelength was achieved. The pigment absorption spectra derived through this iterative process are presented with a selection of published pigment absorption spectra for comparison in Figure 2.11. The Chlorophyll$_{(a+b)}$ absorption spectrum values between 575 nm and 650 nm developed for LIBERTY3P fall between those of PROSPECT and LIBERTY, while the values from 650 nm to 750 nm are slightly lower than both PROSPECT and LIBERTY. This indicates that the Chlorophyll$_{(a+b)}$ absorption spectrum used in LIBERTY3P is realistic. However, the difference between the LIBERTY3P Chlorophyll$_{(a+b)}$ and those of LIBERTY and PROSPECT indicate that both the pigment absorption spectra and Chlorophyll$_{(a)}$:Chlorophyll$_{(b)}$ ratio are different in *Calluna* from those represented in LIBERTY and PROSPECT. The Chlorophyll$_{(a)}$:Chlorophyll$_{(b)}$ ratio is known to vary from species to species (Taiz and Zeiger, 2002) and, for some species, within the same plant at different light levels through the canopy (Watts and Eley, 1970; Taiz and Zeiger, 2002; Boardman, 1977; Lichtenthaler *et al.*, 2007). However, the total Carotenoids absorption profile determined for LIBERTY3P was found to be generally similar to that presented by Lichtenthaler (1987). An Anthocyanins absorption maximum at 540 nm was also found to fit the measured spectra data best and agrees with the *in vivo* absorption maxima range of 537 nm to 542 nm reported by Merzlyak *et al.* (2008). It also matched the general profile of that presented by Neil (2002), although the peak was flatter.

2.3.4 *Calluna* 'shoots and leaves' measured and modelled reflectances and the influence of pigments

The modelled and measured reflectances of the *Calluna* 'shoots and leaves' at each sampling interval during 2006 are presented in Figure 2.12. At the April 2006 sampling interval (Figure 2.12(a)), the fit displayed between modelled and measured reflectances for the 400 nm to 700 nm spectral region is variable, with a wavelength dependent relative error of between +10% and −8%, and a magnitude of error greater than at the other sampling intervals. April is the sampling interval with maximum Anthocyanins content, minimum Chlorophyll$_{(a+b)}$ and minimum total Carotenoid content and with the greatest proportion of senescing 'shoots and leaves'. The pigment absorption spectra developed from the average of the May, June and August sampling interval spectra could, therefore, be less representative of the actual *in vivo* absorption spectra for this period. Better fits were achieved between measured and modelled reflectances for the May 2006 (Figure 2.12(b)), June 2006 (Figure 2.12(c)) and August 2006 (Figure 2.12(d)) sampling intervals, where the relative error per wavelength varies by approximately ±5%. As the measured reflectance spectra for May, June and August were used as the training data set in the development of the pigment absorption spectra, it could be expected that the error between measured and modelled spectra would be lower at these sampling intervals. The fit between measured and modelled reflectances, over the 550 nm to 700 nm wavelength range, for October (Figure 2.12(e)) displayed a more systematic variation with an relative error of up to +10% observed. This suggests that the Chlorophyll$_{(a+b)}$ absorption spectrum may not be as representative of the *in vivo* absorption spectrum at this period as it is during the summer months. Chlorophyll$_{(a)}$ and Chlorophyll$_{(b)}$ have been found to degrade at different rates in barley leaves during senescence (Scheumann *et al.*, 1999). Therefore the ratio of these two pigments in the Chlorophyll$_{(a+b)}$ absorption spectra may change during *Calluna* senescence and, as the degraded products

are colourless (Matile *et al.*, 1996), cause the difference between measured and modelled reflectances observed at the October sampling interval.

To assess whether the pigment absorption spectra derived from the 2006 sampling interval data were more generally representative of the absorption spectra in *Calluna* 'shoots and leaves', the 2005 reflectance spectra were modelled again. The LIBERTY3P model, with the pigment absorption spectra derived from the 2006 data and parameterized with the biophysical, biochemical and leaf structural values determined at each of the 2005 sampling intervals, was used. Subsequently, the fit between measured and modelled reflectances in the 400 nm to 500 nm spectral region where total Carotenoids and $\text{Chlorophyll}_{(b)}$ dominate absorption, and in the 600 nm to 700 nm spectral region, where $\text{Chlorophyll}_{(a)}$ dominates absorption, were improved from those modelled using the unmodified LIBERTY model. However, significant errors remained in the 500 nm to 600 nm spectral region, the region primarily affected by Anthocyanins absorption. As the Anthocyanins content had not been measured during 2005, a modelling optimisation process was again utilized, minimising the RMSE between measured and modelled reflectances in the 500 nm to 600 nm spectral region, to estimate possible Anthocyanins' content at each 2005 sampling interval. The Anthocyanins' values determined using LIBERTY3P are presented with the measured 2006 Anthocyanins values for comparison in Figure 2.13. The 2005 Anthocyanins' estimates were found to be within the range measured from the 2006 samples and follow a generally similar trend to those observed in the 2006 data.

After inclusion of the estimates for Anthocyanins in the remodelled 2005 reflectance spectra, the relative error per wavelength between measured and modelled reflectances was found to vary by up to $\pm 10\%$ for the 10th June (Figure 2.14(a)), the 25th June (Figure 2.14(b)) and the 26th August 2005 (Figure 2.14(d)) sampling intervals across the 400 nm to 700 nm spectral range. For

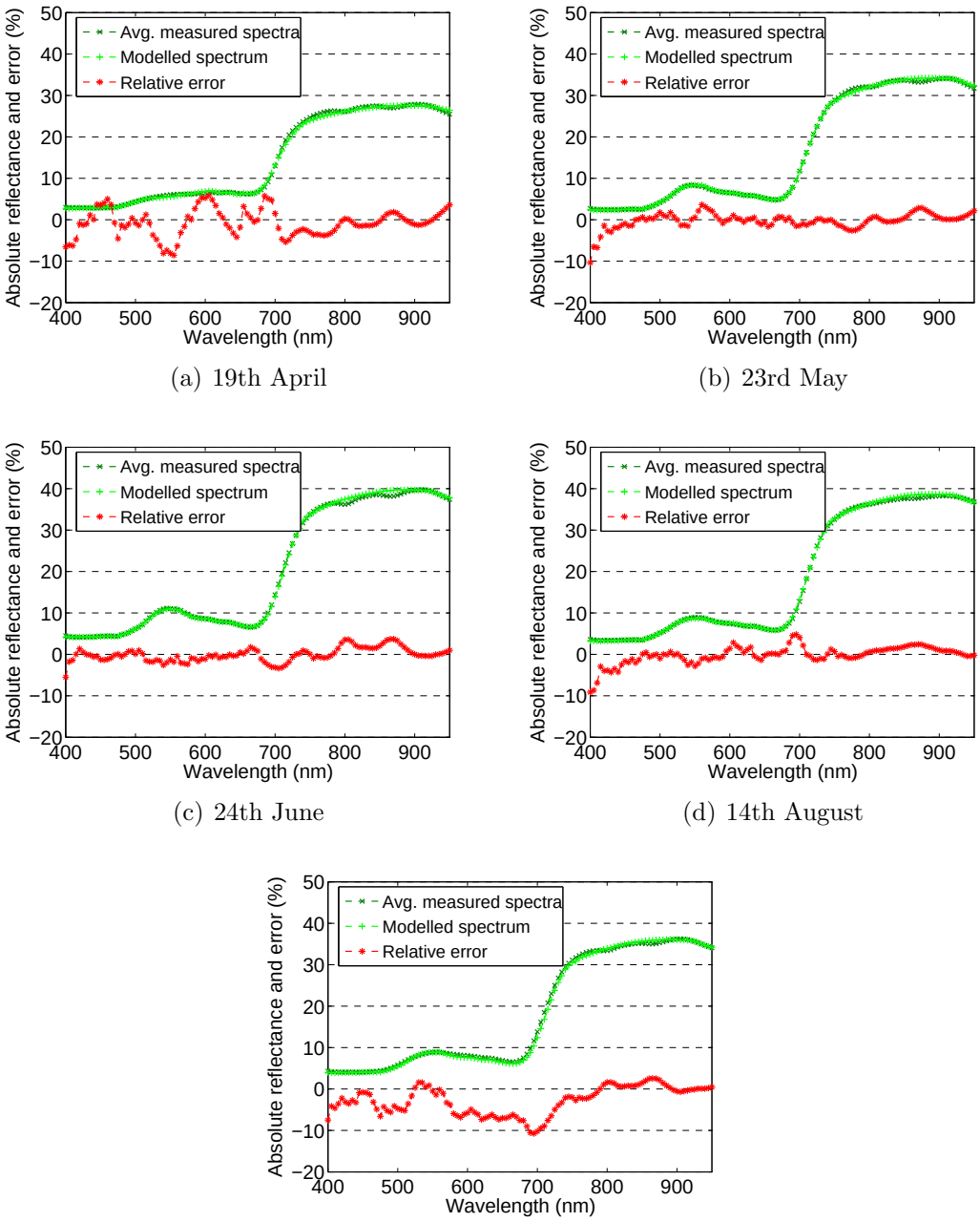

(a) 19th April

(b) 23rd May

(c) 24th June

(d) 14th August

(e) 11th October

Figure 2.12: *Calluna* 2006 'shoots and leaves' measured and modelled reflectances and relative errors

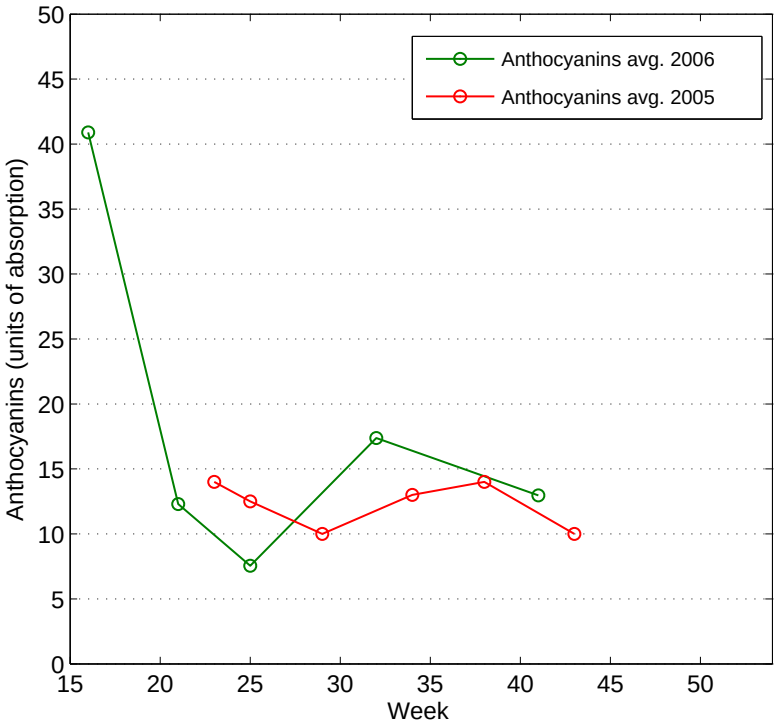

Figure 2.13: Anthocyanins content 2006 determined by wet chemistry methods and 2005 estimated using LIBERTY3P

the 24th July 2005 (Figure 2.14(c)) the error was within a ±5% range. However, for the 22nd September (Figure 2.14(e)) and 29th October (Figure 2.14(f)) sampling intervals the relative error increased up to +10% and −15%. The low relative error for the 24th July 2005 sampling date, and errors for the June and August 2005 sampling intervals are comparable with those at the corresponding 2006 sampling intervals. This indicates that the determined pigment *in vivo* absorption spectra are representative of those present in *Calluna* during the the main growth period through May, June, July and August. However, there is also a consistent over-absorption in the modelled red spectral region reflectance to varying degrees for each 2005 sampling interval, indicating that Chlorophyll$_{(a)}$ absorption spectra may be over-represented for the 2005 'shoots and leaves' samples in the derived absorption spectra. In addition, the Chlorophyll$_{(a+b)}$ absorption spectrum is even less representative at the early stages of senescence in September and October 2005, with an relative error of up to +15%, as it was for the October 2006 sampling interval.

The variability between the measured and modelled reflectances through 2005 and 2006 may be attributed to a number of factors. The Chlorophyll$_{(a+b)}$ and total Carotenoids within leaves are bound in Chlorophyll-Carotenoid-protein complexes and the light-harvesting components of these complexes, Chlorophyll$_{(a+b)}$ and Xanthophylls, are known to vary with the prevailing light environment (Lichtenthaler *et al.*, 1982). The proportions of Chlorophyll$_{(a)}$ and Chlorophyll$_{(b)}$ are also known to vary between leaves on the same plant depending on the leaves' micro light environment (Lichtenthaler *et al.*, 2007). Consequently, the Chlorophyll$_{(a+b)}$ absorption spectrum, being a composite of Chlorophyll$_{(a)}$ and Chlorophyll$_{(b)}$, may be expected to vary both over a growth cycle and inter-annually as the light environment varies (although these pigments will presumably vary within some *Calluna*-specific range). As the absorption maximas of total Carotenoids and Chlorophyll$_{(b)}$ overlap in the 400 nm to 500 nm spectral region, it has not been

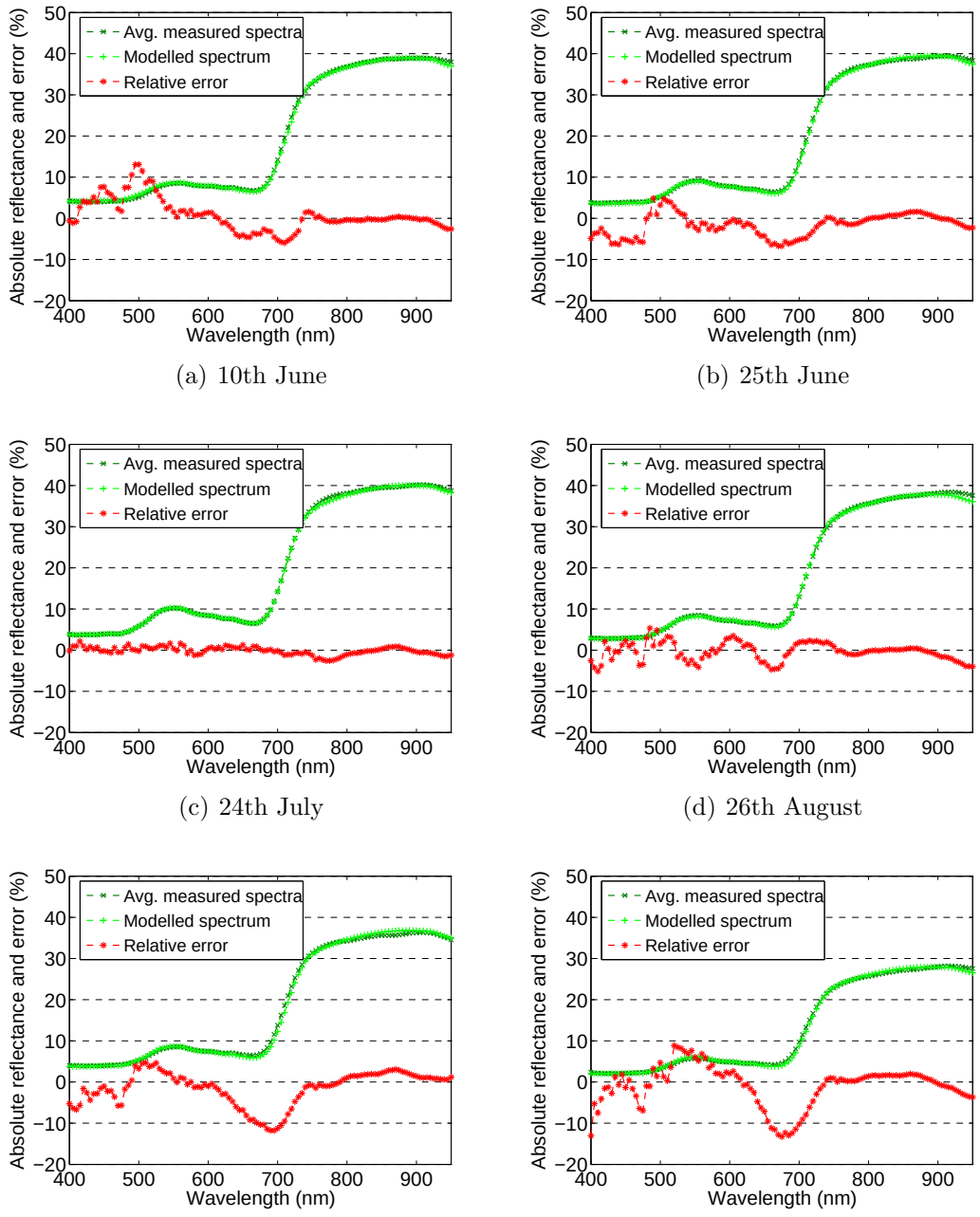

(a) 10th June

(b) 25th June

(c) 24th July

(d) 26th August

(e) 22nd September

(f) 29th October

Figure 2.14: *Calluna* 2005 'shoots and leaves' measured and modelled reflectances and relative errors

possible to resolve each absorption spectrum more fully. Therefore it has not been possible to attribute the proportion of the observed error in the 400 nm to 500 nm spectral region to each absorption spectrum and thus to specific pigments.

2.4 Conclusions

The biophysical and biochemical state variables which influence the reflectance of *Calluna* 'shoots and leaves' have been identified and quantified, or estimated where direct measurement was not possible, at approximately monthly intervals from the start of annual growth to the early stages of senescence, over two consecutive years. The change in these variables over a growth and senescent cycle has not previously been published. The estimated leaf cell diameter and intercellular airspace determinants were found to vary systematically through growth and senescence, generally following the trends expected and with a reasonable degree of inter-annual consistency. Nevertheless, the cell diameter and intercellular airspace determinant values used only represent one possible numerical solution for this element of the radiative tranfer equation modelled in LIBERTY3P and may not be representitive of those variables in *Calluna* leaves and, as the NIR reflectance modelled by LIBERTY3P is sensitive to change in these variables (Moorthy *et al.*, 2008), it may be necessary to adopt an iterative optimisation process for those parameters to achieve a good fit between measured and modelled spectra in future work. Nevertheless, a range and trend for these variables has now been presented which serve as an initiating point for future modelling studies.

From the biochemical state variables identified and quantified in this research Chlorophyll$_{(a+b)}$ were unexpectedly found to decrease prior to the onset of flowering. This reduction may be a response to elevated light and/or temperature

in mid summer, which may be compounded by stress or resource limitations in *Calluna* prior to the onset of flowering. This reduction has important implications for carbon cycle flux studies as it indicates a reduction in photosynthesis, and hence CO_2 sequestration, during this period. Total Carotenoids were also found to reduce prior to flowering and the reason for this is also not clear. Some pigments within the Carotenoid group are also reported to have a photoinhibitive function and could therefore have been expected to increase to protect Chloroplasts. However, it may be that the levels of Anthocyanins present in *Calluna* at these times of high light availability and apparent low photosynthesis capacity are such that the photoinhibitative Carotenoids are not required to modulate light energy. Nevertheless, the presence of Carotenoids significantly influences *Calluna* 'shoots and leaves' reflectance so the presence of this pigment group needs to be considered.

Ustin *et al.* (2009) advise that there is a need to determine whether individual pigments can be quantified and incorporated into remote sensing studies. This work has demonstrated that three composite pigment groups can be incorporated into a radiative transfer modelling study, leading to an increased understanding of the interaction of light with *Calluna* 'shoots and leaves' and hence of reflectance. However, given the errors between measured and modelled reflectances attributed to the variation in $\text{Chlorophyll}_{(a)}$ and $\text{Chlorophyll}_{(b)}$ content in this research, more work is required to quantify these individual pigments, then to determine the individual absorption spectrum of each pigment for inclusion in future radiative transfer modelling studies of *Calluna*. Nevertheless, the results presented in this work indicate that the proximate pigment absorption spectra derived for the 2006 measured and modelled 'shoots and leaves' reflectance data represent a reasonable first approximation of those pigments *in vivo* and may be used to model *Calluna* 'shoots and leaves' through a growth and senescent cycle within a range of prescribed errors (generally up to $\pm 10\%$).

For this work to be more widely applicable, further *Calluna* modelling studies are required to determine whether LIBERTY3P can be incorporated into a canopy reflectance model and the combined model subsequently inverted. If LIBERTY3P can be inverted, then further knowledge of *Calluna* photosynthesis and physiological processes and their change over time can be gained from 'shoots and leaves' sample reflectances without the need for wet chemistry methods. This would then enable hyperspectral remote sensing to be used to measure photosynthesis and hence monitor the status and dynamics of the dominant overstorey species on extensive areas of boreal peatlands. Canopy reflectance modelling studies of *Calluna* are now being undertaken by the authors.

Chapter 3

The fields of view and directional response functions of two field spectroradiometers

A. Mac Arthur[1], C. MacLellan[1] and T. Malthus[2]

[1] NERC Field Spectroscopy Facility, School of Geosciences, University of Edinburgh, Edinburgh, EH9 3JW UK.

[2] Environmental Earth Observation Program, CSIRO Land and Water, Black Mountain, ACT 2601, Australia.

This chapter is being published and should be cited as: Alasdair Mac Arthur, Christopher J. MacLellan and Tim Malthus (2012): The Fields of View and Directional Response Functions of Two Field Spectroradiometers, *IEEE Transactions in Geosciences and Remote Sensing*, 50:9 *in press.*

The research presented in this chapter was conducted at NERC FSF by A. Mac Arthur and C. MacLellan under the supervision of T. Malthus. A. Mac Arthur

raised the research question and defined the research domain. C. MacLellan developed the instrument characterisation method and both A. Mac Arthur and C. MacLellan conducted all measurements. A. Mac Arthur developed the analysis method and the analysis was conducted jointly. A. Mac Arthur wrote this paper, placing the work in a remote sensing context.

3.1 Introduction

Field spectroscopy is a fundamentally physically-based scientific method for the quantitative measurement of radiance or irradiance in the field (Milton, 1987). This method is used by a diverse group of researchers to gain an understanding of near-ground high spectral resolution reflected radiance of Earth surface targets (King *et al.*, 2005; Chappell *et al.*, 2006; Ferrier *et al.*, 2007; Anderson and Kuhn, 2008; Ferrier *et al.*, 2009; Croft *et al.*, 2009; Ustin *et al.*, 2009; Smith *et al.*, 2011) and underwater surfaces (Visser and Smolar-Zvanut, 2009; Hamylton, 2011); for the vicarious calibration of airborne and satellite data (Schmid *et al.*, 2005; Lavender *et al.*, 2005; Anderson *et al.*, 2006); for the validation of quantitative data derived from airborne platforms or Earth observing satellite imaging sensors (Boyd *et al.*, 2006; Huckle *et al.*, 2006; Hasselwimmer *et al.*, 2010); and for the correction of airborne or satellite acquired images for atmospheric effects (Rollin *et al.*, 2002; Aspinall *et al.*, 2002; Karpouzli and Malthus, 2003; Hadley *et al.*, 2005). The basic instrument used in this sub-discipline of hyperspectral remote sensing is the spectroradiometer, a field portable instrument capable of high spectral resolution measurements of reflected radiance, normally at a higher spatial resolution than imaging spectrometry would acquire, and from a single sampling unit (Milton *et al.*, 2009). The use of spectroradiometers to capture data, typically across the 400 nm to 1000 nm or 400 nm to 2500 nm regions of the solar spectrum in approximately 200 to 500 or more contiguous bands, offers a non-destructive method to characterise target surfaces where diagnostic absorption and reflectance features or indices derived from selected wavelength regions of acquired spectra may be related to physical and/or chemical state variables of the reflecting surfaces (Kumar *et al.*, 2001). In addition, acquired spectra may be indicative of classifications assigned to target surfaces and related to the proportions of individual reflecting surfaces or sub-classes within the area of measurement support.

To accurately estimate the reflectance of a target area in the field requires the near simultaneous measurement of two parameters: the reflected radiance from the target and the irradiance incident upon the target. The radiance reflected from the target area is normally acquired through a fixed angle fore optic, which may contain a focusing element, or through a fibre optic bundle. The irradiance incident upon the target area is normally acquired by measurement of a diffuse white reflectance reference panel by a spectroradiometer with the same fore optic arrangement as used for target measurement or by measurement using a spectroradiometer with an upward-looking cosine correcting receptor (Anderson *et al.*, 2006). Either of these measurement configurations, termed bi-conical and cos-conical respectively, require target radiance and target irradiance to be ratioed to give an estimate of reflectance of the target area in the direction from which it is being measured. Only fore optics for measuring radiance will be considered here; cosine correcting receptors for measuring irradiance will not be considered further.

The area of the Earth's surface from which radiance is recorded is normally considered to be delimited by the field-of-view (FOV) of the fore optic of the spectroradiometer, analogous to the Point Spread Function of satellite sensors (Mather, 2004; Atkinson and Aplin, 2004). The FOV is normally defined as a solid included angle through which light incident on the fore optic or fibre optic bundle enters the spectroradiometer and is considered by field spectroscopists to delineate the target area from which the reflected radiance is received, referred to as the area of measurement support (Atkinson and Aplin, 2004). The FOV is constrained by either a fore optic lens, a fore optic field stop or the numerical aperture of the fibres in a fibre optic bundle and the optical configuration of the spectroradiometer (Robinson, 1983; Schaepman, 1998). The operator can vary the size of the area of measurement support by increasing or decreasing the distance of the spectroradiometer fore optic from the target surface or by changing the fore

optic. They can also vary the orientation in space of the spectroradiometer and fore optic, thereby determining the angle from which the target surface is viewed.

The manufacturers of the most commonly used modern spectroradiometers for field spectroscopy typically only specify a nominal solid included angular value as the FOV of the fore optics supplied with their instruments (see Analytical Spectral Devices (2002) or Spectra Vista Corporation (undated), for example). However, the methods used to determine this FOV parameter are not specified and associated uncertainties are not made explicit. Moreover, the FOV is a rather nebulous term when used in field spectroscopy, unlike photogrammetry where the lens f-number or focal length is normally specified. Hence the area of measurement support cannot be calculated with any degree of certainty. To determine this area accurately the fore optic focal point needs to be known to allow height above the area of measurement support to be determined and this height, along with the included angle of the fore optic, used to calculate the radius of the FOV and hence determine the area of measurement support. For example, if a spectroradiometer with a 10^o FOV fore optic was positioned such that the front of the fore optic was 0.5 m above a target surface then the area of measurement support would vary by 12%, depending on whether the fore optic focal length was 2 cm or 5 cm, that is whether the focal point was 52 cm or 55 cm above the target surface. Analytical Spectral Devices (ASD) do suggest a method to calculate the area of measurement support but appear to indicate using the front of the fore optic as the datum rather than the focal point (Analytical Spectral Devices, 1999). Although they indicate diagrammatically that the front of the fore optic is not this datum, Spectra Vista Corporation (SVC), do not specify its location (Spectra Vista Corporation, undated). In addition, the specified nominal FOV gives no indication as to the responsivity of the spectroradiometer/fore optic system to light from different positions within the area from which radiance is being measured. With no further information supplied by the manufacturers,

the FOV of a spectroradiometer is assumed by users to be well defined by the included angle stated and to describe a circular area of measurement support, in the case of an ASD FieldSpec Pro, or an approximately rectangular area, in the case of a SVC GER 3700, for example. Furthermore, an assumption that the system has a uniform responsivity to light from different spatial locations within the area of measurement support is implicatively made. This is demonstrated in the work of Murphy *et al.* (2005); Castro-Esau *et al.* (2006); Nichol and Grace (2010) and Ferrier *et al.* (2009), to cite a few examples, where quantitative measurements have been made of state variables from an integrated sample area delineated by the FOV and relationships between these state variables and the spectrum, or specific wavelength ranges of that spectrum, established without consideration being given spatial distribution of the variables within that area or that the responsivity of the spectroradiometer may be spatially dependent. However, Painter (2011) states that when an ASD FieldSpec is used to measure the reflectance the "anisotropic distribution of the wavelength-dependent fibres that creates a sampling scenario in which different areas of the surface are observed with different parts of the spectrum" resulting in steps in spectra at the joins between each detector. Therefore, this assumption of uniformity of response is, it would seem erroneous, at least for this ASD instrument.

To relate field radiance measurements to state variables or classes of the target being measured, or to simulations of reflectance made using optical models, there is usually a need to know precisely the area of the Earth's surface from which reflected radiance is being measured. The size of this area is the sampling spatial resolution and this resolution defines the limit of spatial detail that can be recorded by a sensor system (Atkinson and Aplin, 2004). Hence knowledge of the sampling spatial resolution is critical, particularly for heterogeneous targets, such as vegetation canopies, which consist of a three dimensional structure of overlapping elements. These targets may be composed of a number of floristic

species, each of which may contain spectrally distinct reflecting surfaces and these surfaces may be present in varying proportions and with varying spatial distributions. Failure to determine the actual area of measurement support and sampling resolution and to fully characterise the system's spatial and spectral responsivity to reflected radiance from within this area, termed the directional response function (DRF), defined by the Commission Internationale de L'Eclairage (1987), may lead to uncertainties in attributing reflected radiance to state variables or classifications of the target being measured.

Few researchers have acknowledged that it is necessary to characterise the FOV of a spectroradiometer. However, using a Spectra Vista Corporation GER 1500 (which contains a single optical slit/diffraction grating/detector array spectrometer, has a spectral range of 350 nm to 1000 nm and was fitted with a 'standard' fore optic), Anderson (2005) conducted an experiment to define the extent of that instrument/fore optic system's FOV. In addition, Schaepman (1998) measured the extent of the FOV of a Spectra Vista Corporation GER 3700 spectroradiometer instrument/fore optic system (which contains three spectrometers, has a spectral range of 350 nm to 2500 nm and which was also fitted with a 'standard' fore optic). In both of these cases only the extent of the FOV along the instrument's principal axes was determined and both found that the FOV generally approximated to the manufacturer's specification. However, the FOV of spectroradiometers may have greater variability than determined by Anderson (2005) and Schaepman (1998). In the case of the full wavelength (350 nm to 2500 nm) spectroradiometric systems investigated by Schaepman (1998) the multiple spectrometers incorporated may each have an influence on the area from which radiance is recorded and on the DRF as the optical path from the entrance slit of the spectroradiometer to each spectrometer is unique. Measurements that could determine if the area of measurement support varied for each spectrometer were not made by Schaepman (1998). In addition, neither

Anderson (2005) nor Schaepman (1998) investigated the DRF of their respective instruments. In complex spectroradiometric systems the type, size and alignment of the viewing fore optic and the optical path from fore optic to spectrometer may cause significant non-uniformity of responsivity and wavelength dependencies across the area of measurement support.

Three criteria are proposed by Milton and Rollin (2006) and Fox (2001) that can be used to assess quality of field spectroscopy measurements - traceability, repeatability, and reproducibility - and they go on to discuss the calibration chain, the need for radiometric stability and the uncertainties introduced through variations in the illumination environment. However, field spectroscopy records the reflected radiance of solar radiation from an area of the Earth's surface which is spatially limited by the fore optic and characteristics of the optical path through the spectroradiometer. These also affect the traceability, repeatability and reproducibility of field spectroscopic measurements although Milton and Rollin (2006) and Fox (2001) did not address them.

This paper investigates how different fore optics and optical path designs affect the area of measurement support and the directional response function of spectroradiometers, to gain an understanding of the spatial and spectral dependence influencing spectra recorded by these field instruments.

3.2 Methods

3.2.1 Spectroradiometers

The UK Natural Environment Research Council Field Spectroscopy Facility (NERC FSF) holds a range of portable field spectroradiometers. These instruments are made available through a peer review application process to UK academics for scientific research. The spectroradiometers available include Analytical Spectral Devices (ASD) FieldSpec Pro FR #6449 and a SVC GER 3700 #1008 and both these were the instruments used in this research. Both these instruments are full wavelength systems measuring across the 350 nm to 2500 nm spectral region.

The FieldSpec Pro and GER 3700 systems use different technologies and optical designs to collect, transport and distribute light to the three spectrometers and, in the 1000 nm to 2500 nm spectral region, also different detector technologies. The ASD FieldSpec Pro uses a fore optic, either a fixed focus lens or a field stop with no focusing lens element, to collect radiance and distribute it via a fibre optic bundle to a fixed diffraction grating spectrometer for the 350 nm to 1000 nm, visible near infra-red (VNIR), spectral region, and two oscillating diffraction grating monochromators with cooled single element indium gallium arsenide (InGaAs) detectors for the 1000 nm to 1750 nm, first short wave infra-red region (SWIR-1), and 1750 nm to 2500 nm, second short wave infra-red (SWIR-2)(Figure 3.1(a)). The fibre optic bundle contains 57 individual fibres (of 110 μm and 220 μm diameter for the VNIR and SWIR fibres respectively) and the position of each fibre within the bundle is determined through a random process at the time of bundle manufacture with 19 fibres subsequently being distributed to each of the 3 spectrometers (Analytical Spectral Devices, 1999). Therefore, the ASD FieldSpec Pro optical fibre distribution may be unique to each instrument.

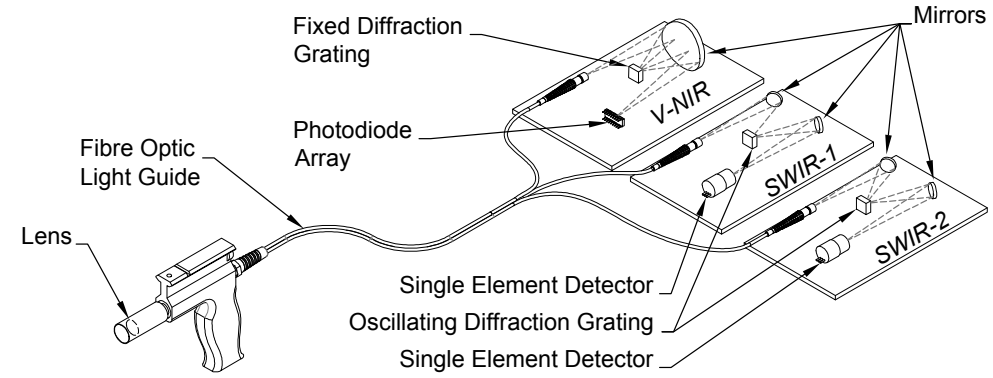

(a) ASD FieldSpec Pro

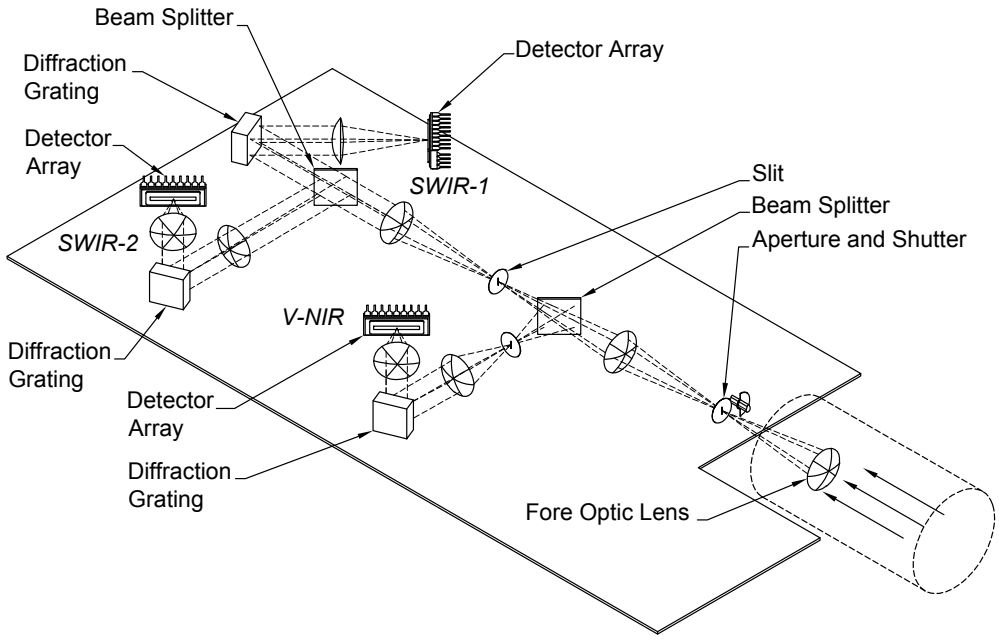

(b) GER 3700

Figure 3.1: Spectroradiometer optical path schematics

The GER 3700 is typically configured with a fixed focus fore optic lens (although a fibre optic accessory is available) attached to the spectroradiometer with radiance received distributed using lenses, mirrors, beam splitters and optical slits to a fixed diffraction grating/photodiode array spectrometer covering the VNIR spectral region and two fixed diffraction grating/lead sulphide array detector assemblies for the SWIR-1 and SWIR-2 spectral regions (Figure 3.1(b)).

3.2.2 Measurements

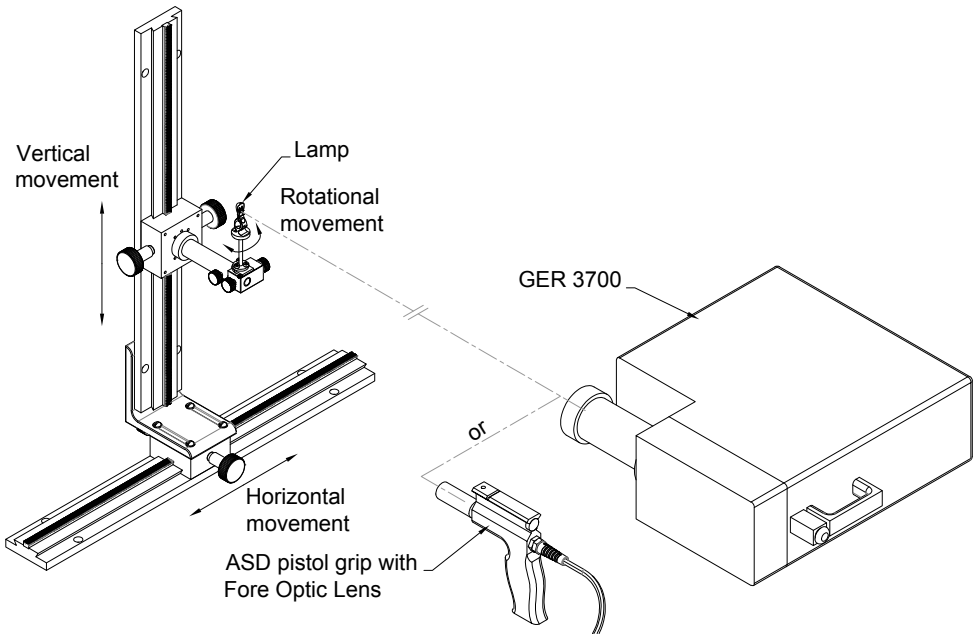

Figure 3.2: Measurement configuration showing direction of movement of linear stages, rotation of lamp and position of ASD FieldSpec Pro or GER 3700

All measurements to characterise the DRF and FOV of the two spectroradiometer systems were carried out in an optical darkroom custom built for spectroradiometric system calibration and measurements at the NERC FSF. A 55 cm linear stage, with micrometer adjustment, was mounted on an optical table within the darkroom and a second 55 cm linear stage, also with micrometer adjustment,

mounted orthogonally on the movable carriage of the first stage. A miniature 20 W quartz tungsten halogen lamp, with a 4 mm x 0.7 mm coiled filament, was then mounted on a rotary stage (also with micrometer adjustment) and secured, in the horizontal plane, to the movable carriage of the vertical linear stage (Figure 3.2). This configuration allowed the lamp to be moved vertically and horizontally across the area defined by the nominal FOV of each instrument and the lamp to be rotated horizontally. A miniature laser diode was mounted on the vertical centre line of the rotary stage and, when the stage was rotated horizontally, was used to ensure that the same point of the lamp filament was aligned with the geometric centre line of each fore optic for each measurement. A halogen lamp was selected as it emits a high-intensity, continuous light across the spectral range of interest in this research. A regulated stabilised power supply was used to ensure lamp output stability for the duration of the measurements. The darkroom walls were black and spectrally flat with a reflectance of less than 5% and black spectrally flat optical cloth, also with a reflectance of less than 5%, covered the optical table and the vertical linear stage to reduce spurious reflections from the light source. The lamp was centred on both linear stages and on the rotary stage and this position used as the reference point (the 'zero' point) for all subsequent measurements. The working distance between the lamp and the front of the fore optics was set at 1 metre and kept constant for all reference measurements, except for measurements made using the GER 3700 fibre optic bundle, where a distance of 500 mm was used. The geometric centre line of the fore optic of each spectroradiometer was aligned with the center line of the lamp, and for the ASD the optimisation routine was first initiated, then a reference spectral measurement of the lamp acquired. The reference measurement was followed by acquiring a target measurement spectrum of the lamp without moving any of the stages. The lamp was then moved in 5 mm increments, both horizontally and vertically, for both the ASD FieldSpec Pro with 10^o fore optic and the 5^o fore optic measurement

sequences and a target spectrum acquired at each point to complete a grid of measurement points. For the FieldSpec Pro/bare fibre bundle system measurements a more sparse sampling strategy was adopted as can be seen in Figure 3.7. For the GER 3700 10^o fore optic measurement sequence the lamp was moved in 1 cm increments, both horizontally and vertically, and target spectra acquired as for the ASD system. For the GER system with the 3^o fore optic and with the fibre optic accessory only the principal axes of the area defined by the nominal FOV were sampled in 1 cm increments. The spatial extent of the measurement sequences were determined by continuing to take measurements until the maximum height of any point of the spectrum measured was less than 2% of the reference measurement spectrum, when it became difficult to visually differentiate the spectra on the control computer screen. After each horizontal and vertical sequence of measurements the lamp was returned to the reference point and another reference measurement taken. In total some 7,250 spectra were acquired for analysis.

3.2.3 Post processing and data analysis methods

Processing of the ASD data required a normalisation adjustment to each spectral data file to account for the VNIR channel integration time and SWIR-1 and SWIR-2 gain settings determined by the instrument during the optimisation routine. The data from each spectroradiometer/fore optic configuration and for each wavelength selected for analysis were then normalised to the maximum amplitude for that wavelength within the measurement field. To enable the spectra to be spatially located the positional coordinates of each measurement point recorded from the linear stage micrometers were appended to the spectral data files recorded by each spectroradiometer. After initial analysis the data files were reduced to a selected number of wavebands typifying the reponsivity of each spectrometer of each instrument/fore optic, for final analysis and display.

As consideration is being given here to the spatial distribution of responsivity of spectroradiometric systems that measure from a continuous field, only varying in levels of spectral intensity and at contiguous wavelengths, the points of measurement are considered to be spatially autocorrelated. Therefore a geostatistical approach was adopted to analyse and display the data and, for each wavelength selected for display, an ordinary kriging routine was used for spatial interpolation. Ordinary kriging provides a 2-dimensional probability interpolation method using a weighted linear combination of available data with the aim of minimising errors of variance (Johnston *et al.*, 2001) and provides a unbiased estimator (Isaaks and Srivastava, 1989). In addition, kriging allows for a statistical estimation of error of the responsivity across the area of measurement displayed at the specific contour levels selected, where no measurement data may have been acquired. By adopting such a geostatistical approach a 2-dimensional graphical representation of the area of measurement support, and DRF across this area, for each instrument/fore optic combination at each selected wavelength, could be produced with contours selected for display by levels of spectroradiometric system responsivity.

3.3 Results and discussion

3.3.1 ASD Fieldspec Pro area of measurement support and DRF with a 10^o fore optic lens

The geostatistically interpolated DRFs, for this instrument/fore optic/measurement distance combination, at three wavelengths (700 nm, 1500 nm and 2200 nm), each typifying the response of the VNIR, SWIR-1 and SWIR-2 spectrometers respectively, of the ASD instrument are displayed in Figure 3.3 where a lower limiting contour of 50% of the maximum responsivity level has been chosen. The dashed

circle in Figure 3.3, with a diameter of 17.5 cm, represents the spatial extent of the nominal FOV specified by the manufacturer for this fore optic using their suggested method of calculation (Analytical Spectral Devices, 1999). The position of each area of responsivity is indicative of the position of individual fibres in the fibre optic bundle and their distribution to the individual spectrometers, where the responsivity is greater than this 50% level. The response of the instrument to radiant flux can be seen to be sparse with little or no coverage of significant areas within the area defined by the nominal FOV at this level of responsivity. The responsivity is concentrated in the lower half of the nominal FOV, with the distribution spatially dependant and highly irregular. The elongated area left of centre in Figure 3.3 indicates that three fibres attached to the VNIR spectrometer are adjacent to each other in the bundle, as does the triangular area in the bottom right quadrant nearest to the nominal FOV limit. However, given the spatial sampling resolution selected and the diameter of the fibres in the bundle the position of some fibres may possibly not be displayed at this 50% responsivity level.

To investigate the area of measurement support and the DRF of this ASD system at this measurement distance further a lower limiting contour of 5% of the maximum responsivity level for the same wavelengths as previously considered was selected and the interpolated data displayed in Figure 3.4. Again each area of responsivity indicates the position of individual fibres in the optical fibre bundle, but for each spectrometer of the ASD used in this work only 16 fibres are evident for each spectrometer, rather than the 19 specified by ASD, suggesting that 3 fibres may not be transmitting light to each spectrometer. The non-shaded areas, in Figure 3.4(a), Figure 3.4(b) and Figure 3.4(c) indicate areas where the radiance received by each of the spectrometers is less than 5% of the maximum normalised response. The VNIR spectrometer responsivity at the 5% level is largely distributed to the outer regions of the nominal FOV with little coverage

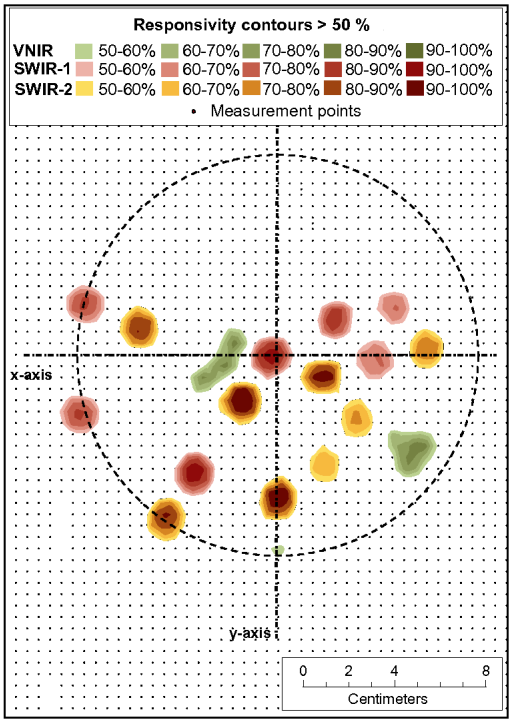

Figure 3.3: ASD FieldSpec Pro DRF greater than 50% response with the nominal 10^o fore optic

towards the centre (Figure 3.4(a)), although the concentration of coverage at the two locations where three VNIR fibres appear to be adjacent to each other is again evident. The VNIR spectrometer also has significant responsivity to areas outside the nominal 10^o fore optic FOV. The SWIR-1 spectrometer displays little responsivity in the lower right quadrant, the bias being towards the other three (Figure 3.4(b)) and with less responsivity to areas outside of the nominal FOV than displayed by the VNIR spectrometer. The SWIR-2 spectrometer responsivity is biased to the lower half of the nominal FOV with little in the upper two quadrants (Figure 3.4(c)), and also with less responsivity evident to areas outside the nominal FOV than the VNIR spectrometer. The area of measurement support normally assumed by field spectroscopists (the nominal FOV) is generally within the 5% DRF contour but for all three channels the coverage within this area varies significantly. The areas of maximum responsivity are variable for all three spectrometers and in some cases the responivity peaks are less than 50% of the maximum. The combined DRF data for the three spectrometers, with the lower limiting contour of 5% of the maximum responsivity level for each of the selected wavelengths displayed, highlights the strong spatial dependency of the spectroradiometer system responsivity (Figure 3.4(d)). The non-shaded areas in Figure 3.4(d) indicate 'blind spots' for the spectroradiometer where little or no radiance is being measured and integrated into the full wavelength (400 nm to 2500 nm) spectrum being recorded.

Cross-sectional plots of the responsivity of the system, at the selected wavelengths, along the x-axis and the y-axis of Figure 3.4(d) are displayed in Figure 3.5(a) and Figure 3.5(b), respectively. These figures highlight the strong spatial and spectral dependencies and the response of the system to radiant flux from outside of the 17.5cm diameter nominal FOV. The narrow, approximately Gaussian, response and point of maximum responsivity for each fibre receiving radiant flux is also evident from these figures.

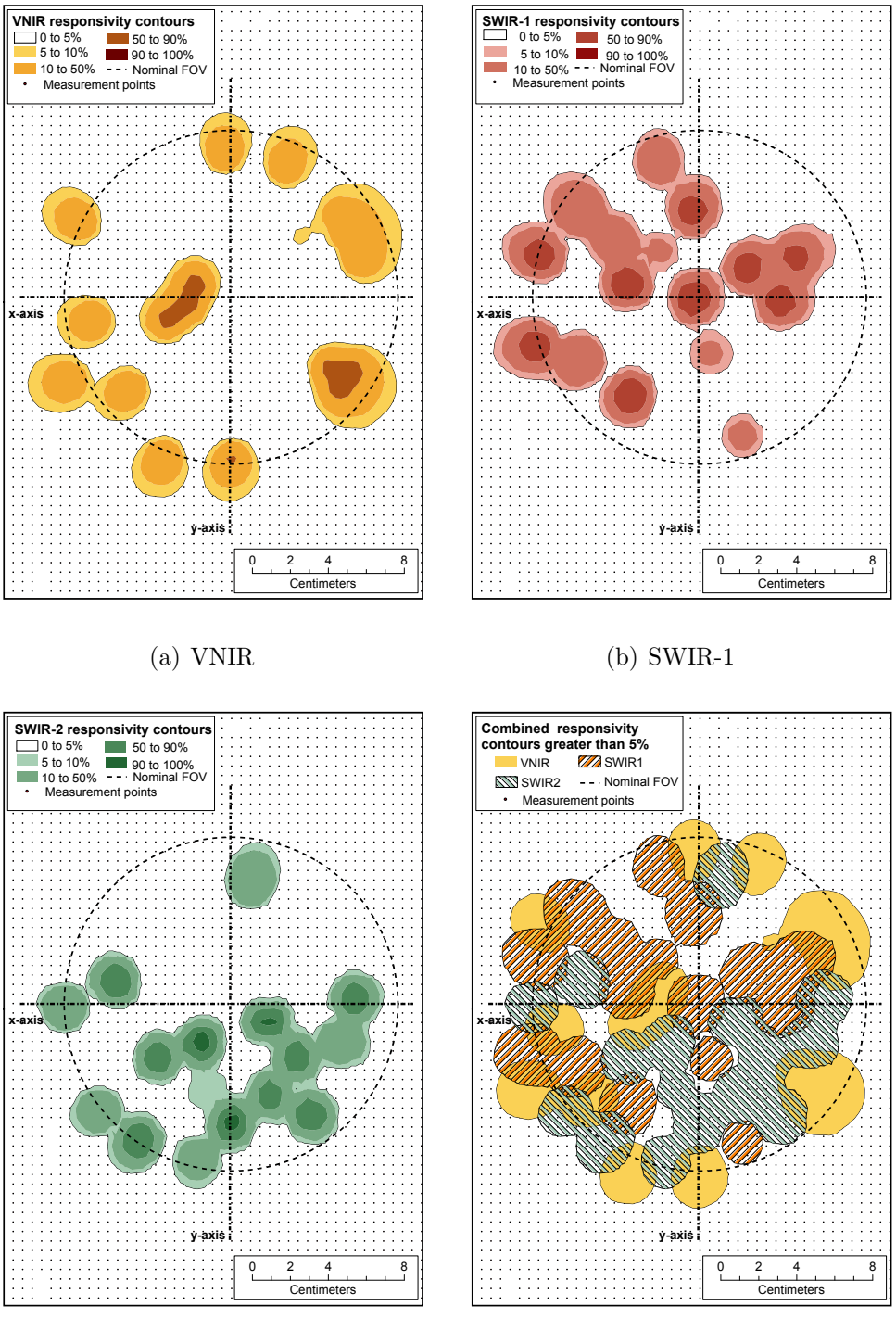

(a) VNIR (b) SWIR-1

(c) SWIR-2 (d) VNIR, SWIR-1 and SWIR-2 combined

Figure 3.4: ASD FieldSpec Pro DRF greater than 5% response with the nominal 10^o fore optic

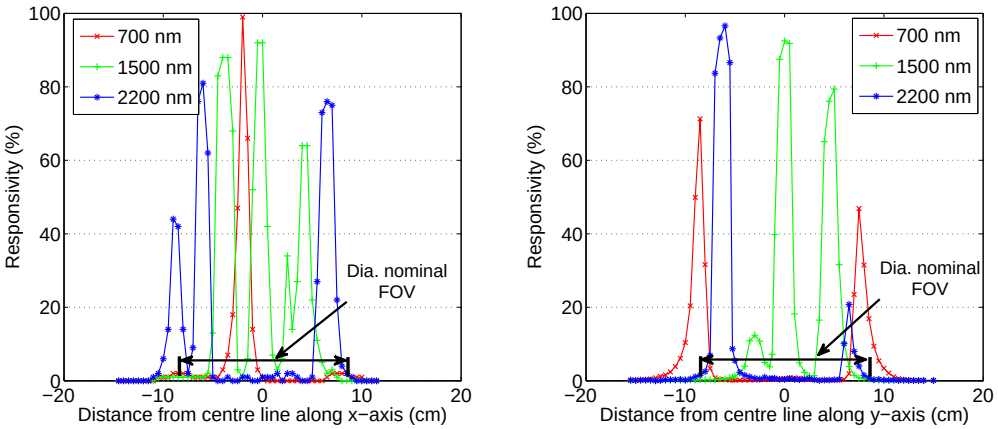

(a) x-axis (b) y-axis

Figure 3.5: ASD FieldSpec Pro selected wavelength DRF cross-sections with 10^o fore optic

When this 10^o lens-based fore optic is used the areas of responsivity for each of this ASD's three spectrometers are individually distinguishable and their spatial distribution uneven within the nominal FOV specified by the manufacturer. Therefore the area of measurement support and the area assumed from the nominal FOV are not the same. However, the number and location of the responsivity peaks appear to align with individual fibres in the fibre optic bundle and each area of response to the distribution of the fibres to the spectrometers. This indicates that the area of measurement support is being imaged by the 10^o lens onto the tip of the fibre optic bundle so that each individual fibre is receiving radiance from different spatial locations within the area of measurement support and transmitting that to the individual spectrometers to which each fibre is aligned during manufacturing. Consequently each spectrometer is measuring radiance from different spatial locations. The regions of the full wavelength spectrum measured by each spectrometer are thus from distinctly different areas, with responsivity being 'weighted' by location. At the 5% limit of peak responsivity, which contains approximately 95% of the total reflectance, there is

little overlap of the areas sampled by each spectrometer. Hence, full spectral information is acquired from few regions within the area of measurement support and it is evident that specifying an albeit nominal FOV for the ASD FieldSpec Pro with 10^o fore optic is highly misleading.

The ASD FieldSpec Pro has a number of different optical accessories available including a nominal 5^o FOV fore optic, again with focusing element, and an 18^o FOV field stop with no focusing element. The area of measurement support and the DRF of both of these fore optic accessories will now be considered.

3.3.2 ASD Fieldspec Pro area of measurement support and DRF with a nominal 5^o fore optic lens

The general design of the ASD fore optic lens accessories are the same and the DRF of the 5^o nominal FOV fore optic used in this work was found to display similar characteristics to those of the system with the 10^o lens (Figure 3.6(a)), when sampled at the same measurement distance. Spatial coverage of the area within the nominal FOV at the 5% responsivity level was not quite complete, although coverage was proportionally more extensive than with the 10^o fore optic. The responsivity of the system was again 'weighted' by location. However, the responsivity at the 5% level from outside the nominal FOV for the 5^o fore optic was minimal. The size of the areas within the area of measurement support with a responsivity greater than 50% was found to be smaller for this optic than that for the 10^o fore optic as can be seen in Figure 3.6(b) and from the width of each Gaussian response for each fibre recording radiance along the line of the x-axis of Figure 3.6(b). When this 5^o lens based fore optic is used, the areas of responsivity of each of the three spectrometers can still be differentiated, although there was significantly greater overlap between them than evident for the 10^o fore optic. Radiance was received by at least one spectrometer from all areas within the

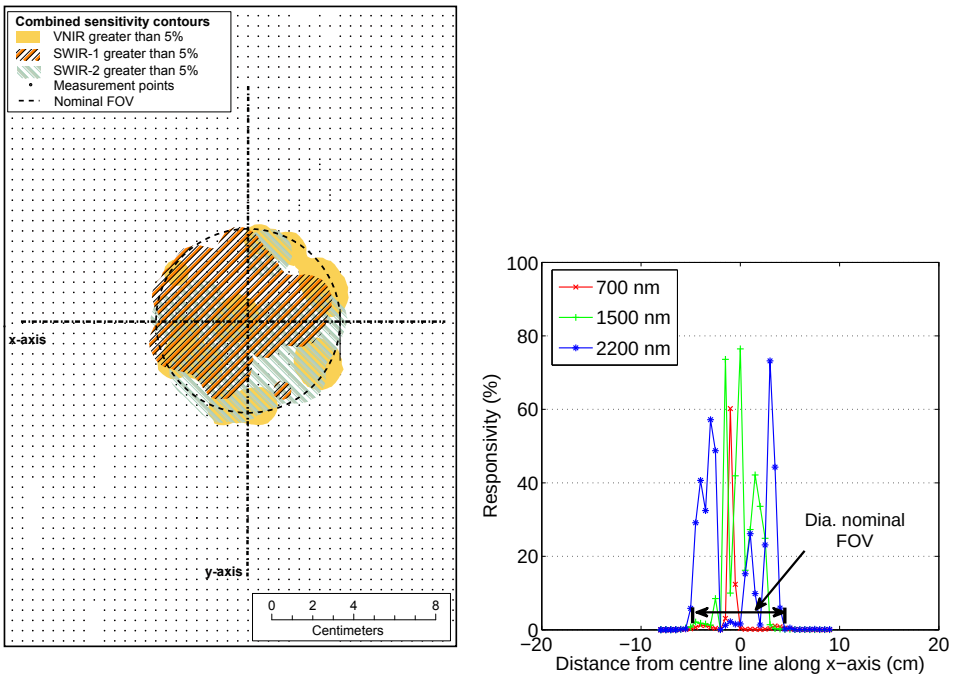

(a) 5% DRF contours

(b) x-axis cross-section

Figure 3.6: ASD FieldSpec Pro selected wavelength DRFs and cross-section with 5^o fore optic

nominal FOV. In addition, at both the 5% and 50% responsivity levels the total extent of the area of measurement support approximates more closely to that which could have been assumed from the manufacturer's specification for this lens based fore optic than for the 10^o fore optic.

3.3.3 ASD Fieldspec Pro area of measurement support and DRF with a nominal 18^o field stop fore optic

The DRF of this ASD spectroradiometer with its 18^o fore optic at this measurement distance displays different characteristics to those displayed when lens based fore optics are used. Greater spatial and spectral uniformity are evident and the areas of responsivity of the spectrometers can be seen to be primarily concentric and evenly distributed (Figure 3.7). The 18^o fore optic comprises a field stop and, as there is no focusing element present, the area of measurement support appears not to be imaged onto the tip of the fibre optic bundle. Hence each spectrometer can be considered to have a FOV rather than each fibre, as was the case for the lens based fore optics. For the VNIR spectrometer the area with a 50% responsivity level approximates to the area of that which would be assumed from nominal FOV, although the areas of measurement support of the SWIR-1 and SWIR-2 spectrometers are slightly less. At the 5% responsivity level the area of measurement support also varies for each spectrometer. At this level the area of measurement support for the VNIR spectrometer is slightly larger than the area of the nominal FOV (Figure 3.7(a)); the area of measurement support of the SWIR-1 spectrometer approximates to the nominal FOV (Figure 3.7(b)); and that of the SWIR-2 spectrometer can be seen to be significantly less than the area of the nominal FOV (Figure 3.7(c)). From Figure 3.8 it is evident that at the 50% responsivity level the area measured by the VNIR spectrometer is greater in

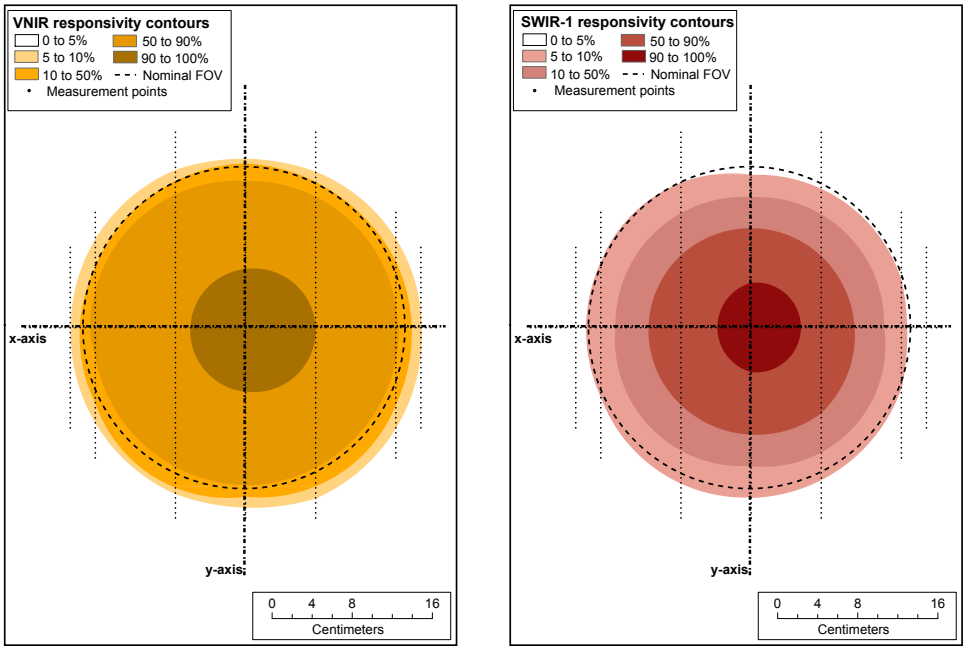

(a) VNIR

(b) SWIR-1

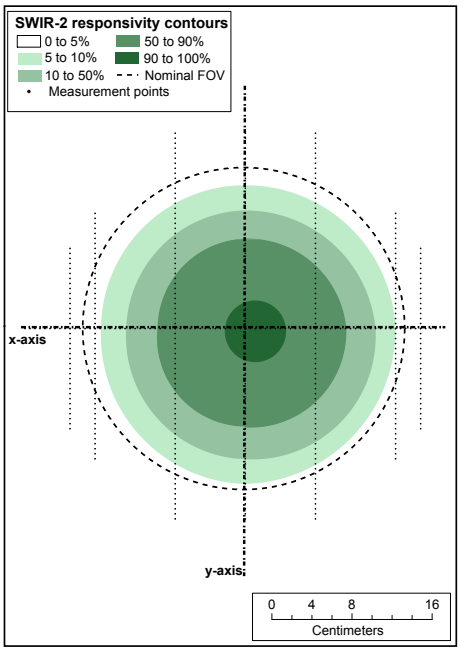

(c) SWIR-2

Figure 3.7: ASD FieldSpec Pro DRF greater than 5% response with the nominal 18^o fore optic

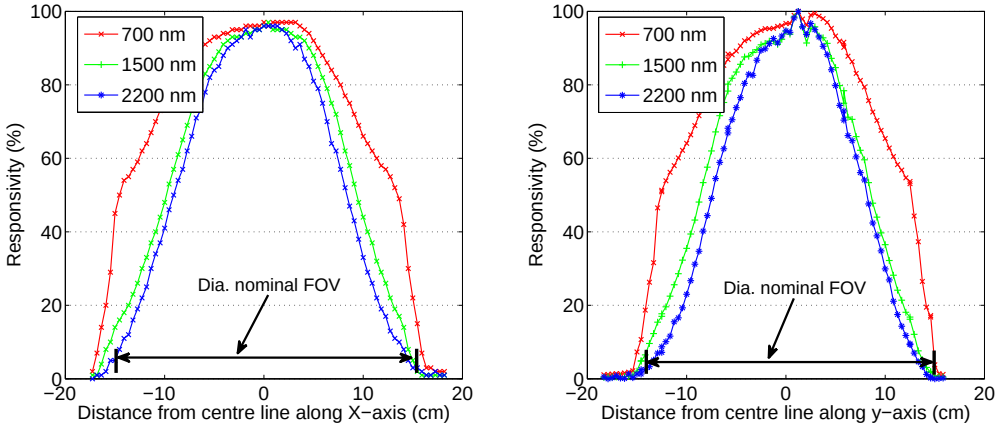

(a) (b)

Figure 3.8: The DRF cross-section along the x-axis a) and y-axis b) of the ASD FieldSpec Pro with 18^o fore optic

diameter than that of the SWIR spectrometers and that the SWIR spectrometer FOVs are closely aligned. The responsivity of the spectrometers in the ASD system with this 18^o fore optic also have approximately a Gaussian distribution as can be seen from Figure 3.8(a) and 3.8(b). From these figures it can also be observed that for the VNIR spectrometer the diameters of the 5% and the 50% sensitivity contours approximate to each other, although there are significant differences in diameter between the 5% and the 50% responsivity contours for the SWIR spectrometers.

The difference between the VNIR and SWIR spectrometer FOVs at the 50% responsivity level, and the similarities at the 5% responsivity level, may indicate that it is the field stop that is restricting the VNIR spectrometer's FOV, while the FOV of the SWIR spectrometers is possibly being restricted by the numerical aperture of the fibres. The numerical aperture of each of the fibre diameters (110 micron and 220 micron) included in the fibre optic bundle are not specified by ASD, although they do advise that the FOV of the 'bare' fibre bundle is 25^o (Analytical Spectral Devices, 1999). The apparent difference in numerical

aperture between the 110 μm and 220 μm fibres may be due to the different materials used for the fibre of the cores, and possibly the cladding, of each of the VNIR and SWIR fibres. The SWIR fibre diameter and core and cladding material may have been chosen to optimise light transmission in the SWIR spectral range, while those used for the VNIR fibres chosen to suit the spectral range of that spectrometer. However, at the 5% responsivity level the FOV of all three spectrometers are close to being in alignment. From the foregoing it is evident that the area of measurement support and DRF of the ASD FieldSpec Pro with the 18^o fore optic more closely approximates to that assumed by field spectroscopists than do the areas of measurement support and DRFs of this ASD system with lens based fore optics.

3.3.4 GER 3700 Field Spectroradiometer area of measurement support and DRF with a 10^o FOV lens

Within the GER 3700 spectroradiometer a different technological approach has been adopted to transfer light from the fore optic to the spectrometers (Figure 3.1(b)) than that used in the ASD FieldSpec Pro. Hence, the area of measurement support and the DRF of the GER 3700 display different phenomena to those of the ASD system. From Figures 3.9 and 3.10 it can be seen that the GER 3700 is responsive to radiance from contiguous areas within the nominal FOV of each of its spectrometers, although the FOVs of each spectrometer do not necessarily align with each other or match the manufacturer's specified nominal FOV for the 10^o fore optic. The VNIR spectrometer 50% responsivity contour delineates an irregular area rather than a circle, although it is completely contained within the nominal FOV of the 10^o fore optic (Figure 3.9). However, the extent of the VNIR 5% sensitivity contour exceeds the nominal FOV for approximately half its diameter at 700 nm (Figure 3.9(b)) and 900 nm

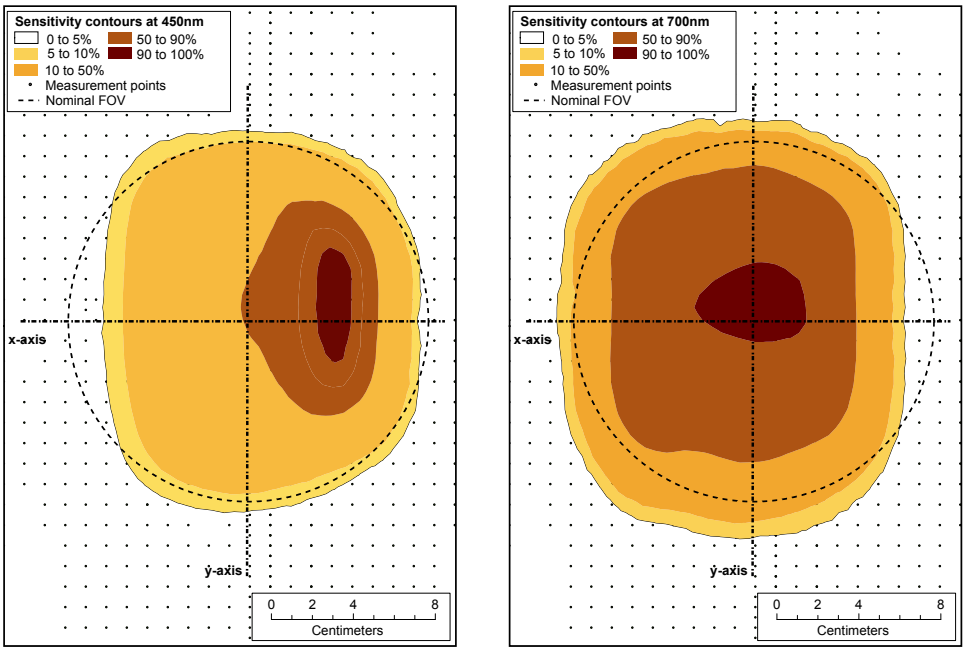

(a) 450 nm

(b) 700 nm

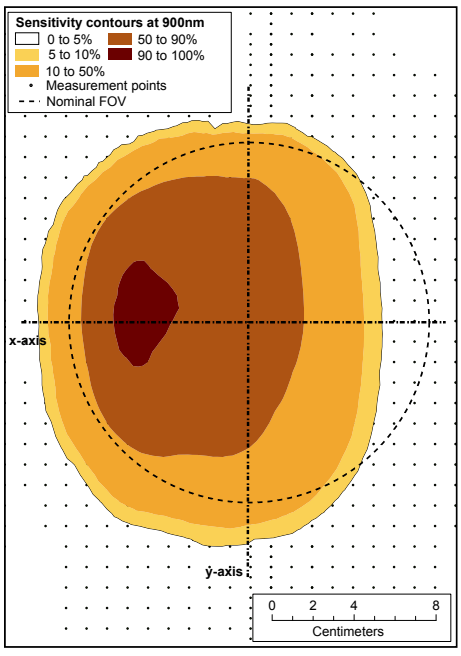

(c) 900 nm

Figure 3.9: GER 3700 with 10^o fore optic VNIR DRFs at selected wavelengths

(Figure 3.9(c)), while at 450 nm (Figure 3.9(a)) the 5% contour is mainly within the nominal FOV. The peak responsivities for each of the wavelengths displayed in Figure 3.9 are within the nominal FOV, although there is a marked shift from the left to right along the x-axis of the area of measurement support. Thus, spectral reflectance to the right side of the nominal FOV has a responsivity bias to blue wavelengths (Figure 3.9(a)) compared to the left side where the spectrometer has its maximum responsivity to infra-red wavelengths (Figure 3.9(c)), while the greatest responsivity to red wavelengths is approximately in the middle of the nominal FOV (Figure 3.9(b)). There are areas within the nominal FOV, primarily to the left for blue wavelengths (Figure 3.9(a)) and to the right for infra-red wavelengths (Figure 3.9(c)), from which little or no reflected radiance is integrated into the full wavelength spectrum recorded. The GER 3700 is responsive through its full wavelength range (400 nm to 2500 nm) to radiant flux from the central region of the nominal FOV.

However, both SWIR spectrometers have areas of responsivity to the left and to the right of the nominal FOV from which little or no radiance is integrated into the measurement recorded and both display an approximately rectangular area of measurement support (Figure 3.10(a) and 3.10(b)). The right to left bias of blue through green to infra-red wavelengths, along the x-axis of Figure 3.9 and 3.10, is evident in Figure 3.11(a) where the location of the point of maximum responsivity for each of the wavelengths displayed can be seen. From Figure 3.11(b) it is evident that the points of maximum responsivity are closer to being central on the y-axes of Figure 3.9 and 3.10, and aligned with the optical slit of the spectroradiometer.

Unlike the ASD system, each spectrometer in the GER 3700 is responsive to radiance from a significant and overlapping central region of the area of measurement support. Nevertheless, the areas from which radiance is recorded by each of the three spectrometers in the GER 3700 with 10^o fore optic are also

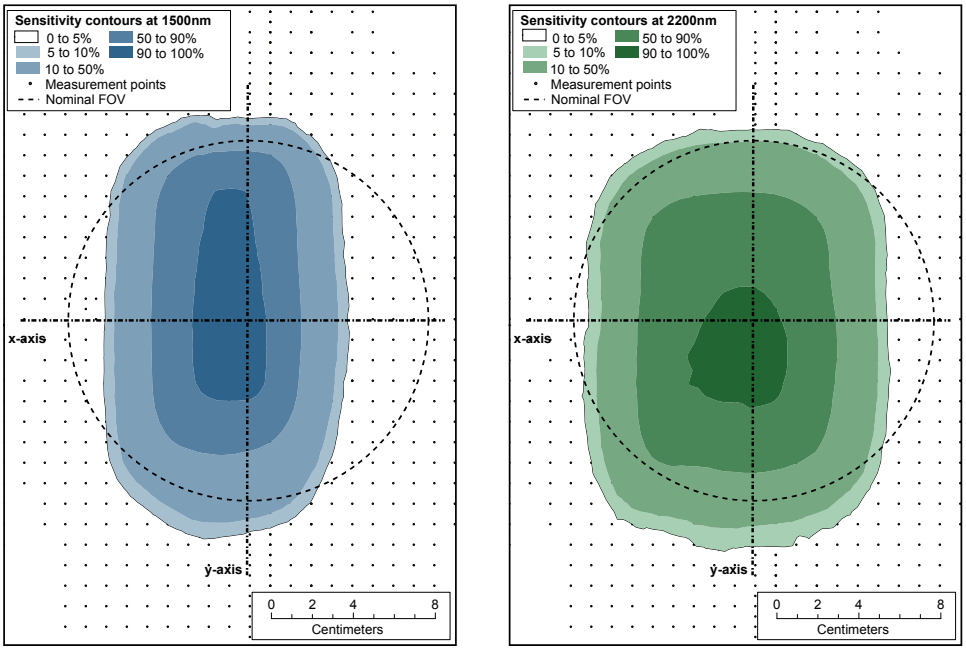

(a) 1500 nm (b) 2200 nm

Figure 3.10: GER 3700 with 10^o fore optic SWIR DRFs at selected wavelengths

individually distinguishable. There are areas within the nominal FOV from which one or other of the three spectrometers receives little or no radiant flux and the DRF of the VNIR spectrometer is wavelength dependent with a right to left/blue to infra-red responsivity bias. The design of the fore optic; the unique optical path from the instrument's entrance slit to each of the three spectrometers; the size and location of spectrograph slits; and the magnification factors of the various elements within each optical path may all influence the extent of the areas of measurement support and the DRF of each spectrometer and, hence, those of the combined GER 3700 spectroradiometric system.

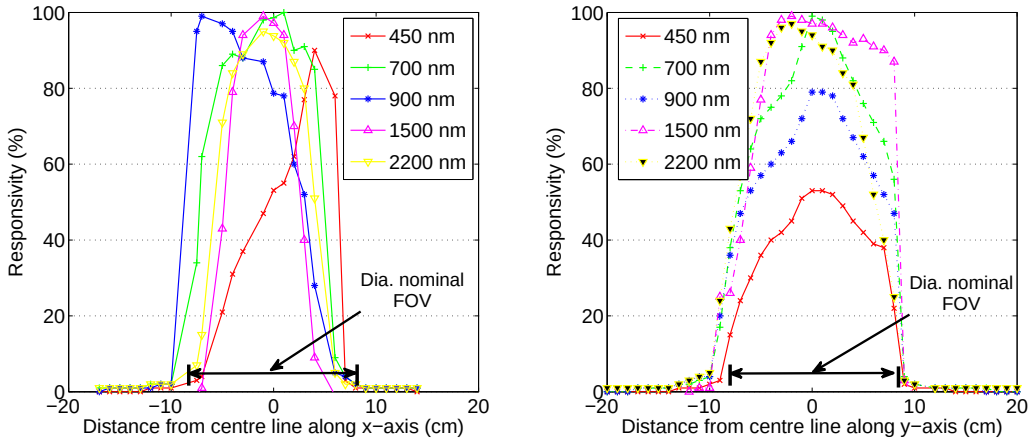

(a) (b)

Figure 3.11: The DRF cross-section along the x-axis a) and y-axis b) of the GER 3700 with 10^o fore optic

3.3.5 GER 3700 Field Spectroradiometer area of measurement support and DRF with a nominal 3^o lens

The area of measurement support and DRF of the GER 3700 fitted with its 3^o lens, the 'standard' GER fore optic, was also assessed and found to display similar, although less pronounced, characteristics to those found with the 10^o fore optic fitted. The VNIR right to left blue to infra-red spectral responsivity shift was still evident as the blue wavelengths were again found to have a maximum sensitivity towards the right of the FOV (across the optical slit) and infra-red towards the left (Figure 3.12(a)). However, response to infra-red wavelengths was more evenly distributed than observed with the 10^o fore optic fitted. Along the line of the instrument's entrance slit there appeared to be no spectral shift for VNIR wavelengths as the maximum responsivity of each was approximately aligned with the y-axis of the area of measurement support (Figure 3.12(b)), although a slight responsivity bias to the left of the y-axis was evident for the SWIR-1 wavelengths. The 5% and 50% responsivity contours were found to be

reasonably well aligned with each other along the x-axis (Figure 3.12(a)). Along the y-axis the 5% and 50% responsivity contours were less well aligned to the left of the area of measurement support (Figure 3.12(b)). The 5% and 50% responsivity contours for each spectrometer are more closely aligned for the 3^o fore optic than for the 10^o fore optic, as can be seen by comparing Figure 3.11 and 3.12. The area of measurement support is again considered to be rectangular at the 5% responsivity level as it measures approximately 8cm along the x-axis and 10cm along the y-axis, due to the influence of the optical slit. However, at the 50% responsivity level the area of measurement support is more square with axes of approximately 7cm.

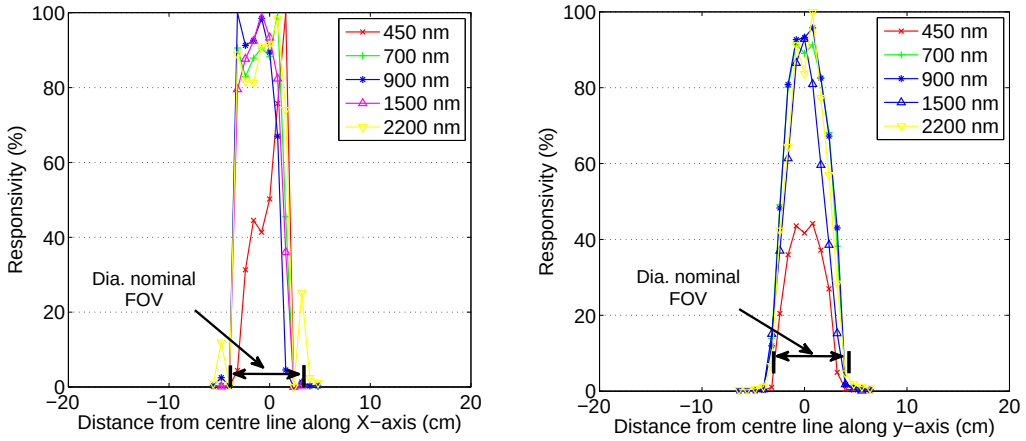

(a) Area of measurement support x-axis (b) Area of measurement support y-axis

Figure 3.12: The DRF cross-section along the x-axis a) and y-axis b) of the GER 3700 with 3^o fore optic

As was observed for the GER system with the 10^o fore optic, the response to radiance by each spectrometer overlapped in the central region of the area of measurement support, although the areas of measurement support of each of the spectrometers remained distinguishable, particularly for the VNIR detector. There remains a blue to infra-red/left to right responsivity bias, although it is less pronounced than for the 10^o fore optic. However, unlike the system with the

10^o fore optic there were no areas within the nominal FOV from which radiant flux was not received by a spectrometer. It is therefore evident that the DRF and area of measurement support more closely aligns to that which would be assumed from the specification for the 3^o fore optic, although it is more extensive at both the 5% and 50% responsivity levels.

3.3.6 GER 3700 Field Spectroradiometer area of measurement support and DRF with a fibre optic attachment

A fibre optic accessory is available for use with the GER 3700, although presently there is no FOV-limiting fore optic attachment supplied. The fibre optic bundle contains 491 individual fibres, each of the same diameter. However, the nominal FOV of this accessory has not been specified by the manufacturer. From these measurements the area of measurement support was found to be circular, measuring approximately 18 cm along each major axis at the 50% responsivity level and approximately 24 cm along each major axis at the 5% responsivity level (Figures 3.13(a) and 3.13(b)). It can also be seen that the width of the area of measurement support at the 5% responsivity level is approximately 6 cm greater than at the 50% level. Hence if the nominal FOV of the fibre optic accessory is calculated from this data, at the 5% responsivity level it is approximately 27^o and at the 50% responsivity level it is approximately 20^o. Furthermore, the responsivity was found to be approximately Gaussian and concentric for each of the wavelengths displayed, although the area of maximum responsivity is wider across the y-axis (Figure 3.13(b)) than the x-axis (Figure 3.13(a)). The fibres in the fibre optic bundle supplied for the GER 3700 are mixed during manufacture such that the position of each fibre at one end of the bundle is not the same as that fibre's position at the other end of the bundle and, as each fibre can be

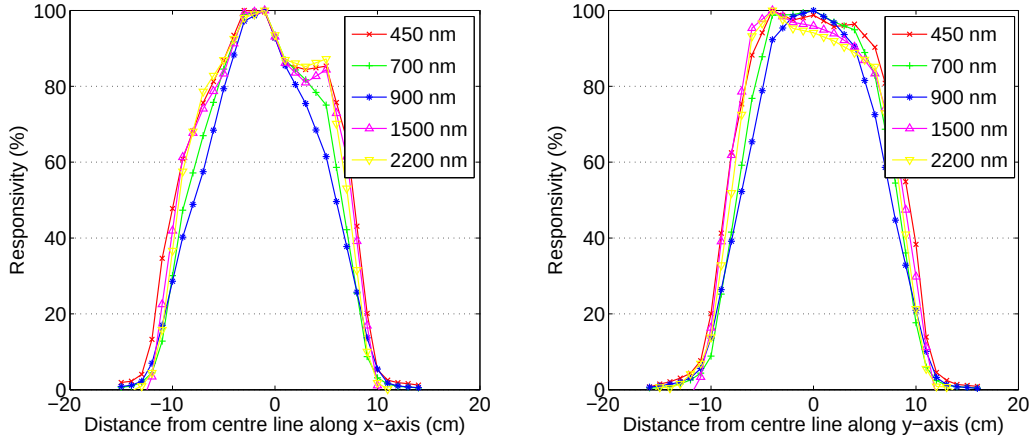

(a) Area of measurement support x-axis (b) Area of measurement support y-axis

Figure 3.13: GER 3700 DRF with fibre optic accessory at a distance of 500mm from target

assumed to have a circular FOV the area of measurement support will be circular, with little influence from the optical slit.

The GER 3700 system with fibre optic accessory displays no spectral left to right bias and the area of measurement support and DRF of each spectrometer align more closely with each other than was found with the other fore optics. The response to radiance by each spectrometer covers the full area of measurement support and there were no areas within this from which radiant flux was not received by each spectrometer. In addition, and again unlike the GER optics previously assessed, when using the fibre optic accessory the areas of measurement support of each spectrometer were primarily indistinguishable.

These area of measurement support and DRF characteristic differences between the fibre optic and lens-based fore optics for the GER 3700 system indicate that, similar to the ASD system, the area of measurement support is being imaged into the optical path by the lens-based optics. As there was no responsivity bias when using the GER 3700 fibre optic accessory, which does not have a focal point, it

would appear to be the dimensions and design of the lenses and where their points of focus fall within the optical path that are the cause of the spectral bias. This is also indicated by the DRF differences observed between the 10^o and the 3^o fore optic data, where the focal point of each will fall at different locations within the optical path. In addition, it would appear to be the shape and dimensions of slits and detector arrays that cause the area of measurement support to be elongated rather than circular for the lens based fore optics.

3.3.7 Measurement and responsivity contour uncertainties

The uncertainties associated with the extent of the areas of measurement support and DRFs displayed are dependent on both systematic and random errors introduced during measurement and from the interpolation method adopted for the analysis. Systematic errors will result from spectroradiometric uncertainties such as in wavelength position and detector response linearity and from the size of the light source used, limiting the maximum possible spatial resolution of the measurements. Random errors will result from uncertainties related to the lamp's position and rotation, relative to the fore optic geometric centre line, and from spectroradiometric dark current and thermal stability errors. Errors introduced by spatial interpolation include the number, proximity and spatial arrangement of samples, the nature of the phenomena being studied (whether it is a continuous smooth field, for example) and the interpolation model selected. Systematic spectroradiometric errors are quantified during the routine quality assurance procedures applied to both instruments and are minimised by recalibration of spectroradiometer if required, and will not be discussed further here. Uncertainties introduced through the spatial sampling resolution are quantified during the interpolation accuracy assessment.

As during the spectral measurement sequence the reference spatial location of the lamp (the measurement axis 'zero' point) was repeatedly measured, the spectral measurements at this location have been used to determine a statistical confidence level for the spectroradiometer/fore optic system responsivity which integrates both positional and spectroradiometric uncertainties. For a 95% confidence level the measurement error at the 'zero' point was calculated to be better than ± 5.5% with 35 degrees of freedom for the GER 3700 system with 10^o fore optic and for the ASD system with the 10^o fore optic. The uncertainty for each of the spectroradiometers with the other fore optics was of the same order, although with lower degrees of freedom.

There are also uncertainties related to the kriging spatial interpolation method used and these influence the position of the responsivity contours and the values predicted between the measurement points. A statistical prediction map was generated for each of the wavelengths assessed for both the ASD FieldSpec Pro and the GER 3700, each with 10^o fore optic, and the maximum root mean squared errors (RMSE) were 0.048 and 0.027, respectively. The differences between the RMSE calculated for the ASD and that for the GER instrument are due to the difference in spatial sampling resolution selected (5 mm and 10 mm, respectively) rather than any specific instrument phenomena. However, even given these uncertainties, the assessment of the extent of the area of measurement support and DRF of each spectroradiometer/fore optic combination presented here provides sufficient information on the probable shape, size and level of responsivity at spatial locations across the target area from which the spectroradiometer receives radiance to enable field spectroscopy sampling strategies to be greatly improved.

3.4 Conclusion

To enable a spectrum, or parts of a spectrum, recorded by a field spectroradiometer to be related to physical properties, or to classifications of the type of target surfaces of interest it is necessary to know the spatial extent of the surface from which radiant flux is received, that is, the area of measurement support. The responsivity of the spectroradiometer to radiant flux from within that area, i.e. the 'weighting' given to radiance from any point within the area, is assumed to be equal. However, the FOV, normally specified by spectroradiometer manufacturers, does not provide the necessary information. At best a FOV only describes one of the two parameters necessary to calculate spatial extent. These are the diameter of a circular area from which radiant flux may be received by a spectroradiometer and the distance from the apex of a triangle to the target surface, which can only be approximated as the focal point of the fore optic is unknown. In addition, the FOV gives no indication of instrument responsivity to radiant flux from different locations within the area from which that flux is received. More specifically, the use of the term FOV is misleading as it leads field spectroscopists to assume that a) the area of measurement support is circular (although in their manuals GER do advise against this assumption) b) that there is an 'edge' to this area that can be clearly defined, although a level of responsivity is never stated and c) that radiance received from any point within the area of measurement support is equally 'weighted' within the integrated spectrum recorded.

This research has shown that when the 10^o lens-based fore optic is used, the ASD system does not have a FOV but that each fibre within the fibre optic bundle receives radiance from different areas within the area of measurement support and transmits this radiance to the sole spectrometer to which that fibre is attached. Each fibre has in effect its own FOV, leading to each of the three spectrometers integrating radiance from different areas (and these areas appear

only to overlap towards the extremities of each fibre/spectrometer's responsivity) into the spectral range recorded by that spectrometer. It should also be noted that as the distribution of fibres to the spectrometers are randomised at the time of manufacture each ASD FieldSpec Pro system will have a unique DRF and hence the shape and coverage of the potential area of measurement support will be unique to each instrument. The area of measurement support has also been shown to extend well beyond that that the FOV parameter would define, yet, at the 5% responsvity level, there remain areas within the nominal FOV from which little or no radiance is received either by each or by all of the spectrometers. When the 5^o lens-based fore optic was used each fibre still receives, and hence each spectrometer measures, radiance from distinctly different areas. However, the areas of overlap are greater and the areas from which radiance is received by only one spectrometer are significantly less than found with the 10^o fore optic, when the 5% responsivity level is considered. In addition, the extent of the area from which radiance is received much more closely approximates to that which the nominal FOV would suggest and does so at both the 5% or 50% responsivity levels. This indicates a significant improvement in characteristics over the 10^o fore optic (although the term FOV still has little relevance) at a one metre sampling distance. It should be noted however, that the when the lensless 18^o fore optic is used the term FOV is less misleading as the specified FOV included angle is defined by either the field stop or the numerical aperture of the fibres or both. Each fibre still has its own FOV but as all these FOVs effectively overlap with each other each spectrometer is measuring radiance from all areas within the area of measurement support, similar to the manner described by Analytical Spectral Devices (2005) for the fibre bundle without a fore optic.

The area of measurement support and DRF measured in this research for the 18^o fore optic are thus a reasonable approximation of that assumed by field spectroscopists. It just remains for the manufacturer to state a responsivity limit

and the DRF to be defined to more fully specify the spectroradiometer/18^o fore optic combination. It should also be noted, however, that for the FieldSpec Pro model used here there was no method of determining if any fibres in the bundle were not transmitting radiance to their respective spectrometer without making DRF measurements or returning the instrument to the manufacturer for assessment. However, ASD have now incorporated a reverse illumination mechanism within their latest full wavelength spectroradiometer to allow the fibres to be checked.

For the GER 3700 system with the 10^o lens-based fore optic the area of measurement support more closely approximates a square or a rectangle, as the manufacturer suggests, than a circle. The areas of measurement support for the VNIR and SWIR spectrometers with this fore optic do display different shapes, with those of the SWIR spectrometers more rectangular than square. There is also a spatial and spectral shift in the responsivity of the VNIR spectrometer, with more 'weighting' given to blue wavelengths of light from the right and infra-red wavelengths from the left of the target surface, while along the axis in alignment with the entrance slit of the instrument no spectral shift is evident. When the 3^o fore optic is fitted, the area of measurement support of each spectrometer appeared to be square and aligned, there was little evidence of an infra-red spectral shift and the blue shift was less pronounced, indicating, as for the ASD with 5^o fore optic, an improvement over the wider angles lens-based fore optic. Again, as was observed for the ASD system, when the fibre optic accessory was used with the GER 3700 there was a significant improvement in the DRF. The DRF was found to be approximately Gaussian, concentric and overlapping for each of the spectrometers.

For Earth surface targets, the use of diagnostic spectral absorption and reflectance features, or indices derived from these, as proxies for state variables, or the use of spectra from such targets having classifications assigned in proportion of

specific elements within the target area, is dependent on the reflected radiance recorded being from a known and quantifiable target area. With heterogeneous target surfaces - and most natural Earth surface targets are heterogeneous to some degree - if the DRF is not uniform, if spatial coverage is incomplete and if the shape and area of measurement support are different from that assumed, then the components considered to be within the scene may not be quantified or correct proportions assumed. Hence the properties of the assumed target area will be inaccurately represented in the actual radiance recorded. The contribution of individual scene components to gross radiance recorded may be excluded or over emphasised leading to erroneous classification of the surface or inaccurate quantification of physical and chemical variables derived from spectral indices.

It should be noted that the DRFs reported here are for specific instrument/fore optic combinations at the specified measurement distances, sampling resolutions and for the lamp filament size used. Different results may be found if other instrument/fore optic and measurement configurations are used: the ASD instrument fibre distribution will vary, as may the SVC instrument optical path; fore optic design and materials will affect the light passing through them; measurement distances may lead to the area of measurement support being in or out of focus; and the sampling resolution will affect phenomena recorded as will the lamp filament size. However, the results reported here have significant implications for the measurement of surface reflected radiance. The wavelength dependent spatial variability of the DRF and irregularly defined areas of measurement support evident from this study indicate that the assumption that the systems have uniform and regularly defined FOVs is invalid. However, having knowledge of an instrument's DRF, and hence being able to define the area of measurement support and responsivity of a field spectroradiometer is necessary but not alone sufficient to improve field spectroscopy measurements. It is also necessary to consider the heterogeneity of the target surface and statistically assess the quantity of individual

measurements required to acquire a representative mean of the radiance spectrum of the target of interest. A practical solution which quantifies the uncertainty of radiance from heterogeneous targets resulting from a non-uniform DRF may be to include multiple measurements of radiance spectra measured from nadir while rotating the instrument fore optic about its optical axis and to indicate a standard error per wavelength for the mean spectrum determined.

This research suggests that the use of a field stop aperture in place of a lens or the optimisation of lens and, possibly, optical path design could give a more uniform DRF. However, re-positioning lenses with respect to the instrument entrance slits will cause some defocusing of the image, improving the uniformity of directional response but with a possible reduction in system responsivity. Other options for improving the uniformity of the ASD lens fore optics could possibly be in the use of optical mixers or holographic diffusers positioned between the fibre optic bundle and the lens, although, again, these options may cause some reductions in systems responsivity. Indeed, ASD now on request incorporate an optical mixer (a 'scrambler') into the ASD pistol grip. It should also be noted that the latest ASD full wavelength system, the FieldSpec 3, does incorporate a method by which the operator can check the integrity of the fibres in the optical bundle without access to a spectroscopy darkroom or returning the instrument to the manufacturer. SVC have optimised the alignment of elements in the optical path of their new instrument, the HR-1024, and make an 8^o fore optic and a bare fibre option available. Initial indications are that the DRFs of these new systems and accessories greatly improve the DRFs of each system. These improved spectroradiometric systems will now be assessed and improvements in DRFs and any consequential changes in system sensitivity reported at a later date.

Chapter 4

The effect of the directional response function of two field spectroradiometers on spectra acquired and derived vegetation biochemical indices

A. Mac Arthur[1] and T. Malthus[2]

[1]NERC Field Spectroscopy Facility, School of Geosciences, University of Edinburgh.

[2]Environmental Earth Observation Program, CSIRO Land and Water, Black Mountain, ACT 2601, Australia.

This chapter has been prepared for submission to the *IEEE Transactions in Geosciences and Remote Sensing* for review.

4.1 Introduction

Field spectroradiometers are portable non-imaging electro-optical devices used to measure spectral radiance or spectral irradiance either, normally, through the visible to near infra-red region (400 nm to 1,000 nm) or the visible to short-wave infra-red region (400 nm to 2,500 nm) regions of the solar electromagnetic spectrum in approximately 200 to 1,000 or more sampling intervals. These instruments are used by scientists primarily to gain an understanding of the interaction of light with Earth surfaces, for the validation and calibration of Earth observation data, or possibly used to measure downwelling solar flux in irradiance measurements (Milton, 1987; Curtis and Goetz, 1994; Milton *et al.*, 1995; Rollin *et al.*, 2002; Milton *et al.*, 2009). However, to be of scientific value the units of measurement and the area of the Earth surface from which field spectroradiometers measure radiant flux must be known to enable the measurements to be related to state variables and to allow other measurements acquired at spatially and/or temporally distinct intervals to be compared (Atkinson and Curran, 1995; Steven, 2004; Atkinson and Aplin, 2004; Milton *et al.*, 2009; Anderson *et al.*, 2011).

Calibration of measurement devices to national or international norms is the recognised process of standardising such measurements (Guenther, 1987). Calibration of remote sensing systems enables an accurate relationship between specific spectral regions of electromagnetic radiated flux from an Earth surface and the output of the spectrographs within the spectroradiometer to be established (Chen, 1997; Schaepman, 1998). Nevertheless, Kostkowski (1997) contests that "spectroradiometric measurements are the least reliable of all physical measurements" attributing this to instrument and calibration measurement uncertainties. Schaepman (1998) grouped the uncertainties in field spectroradiometer calibration

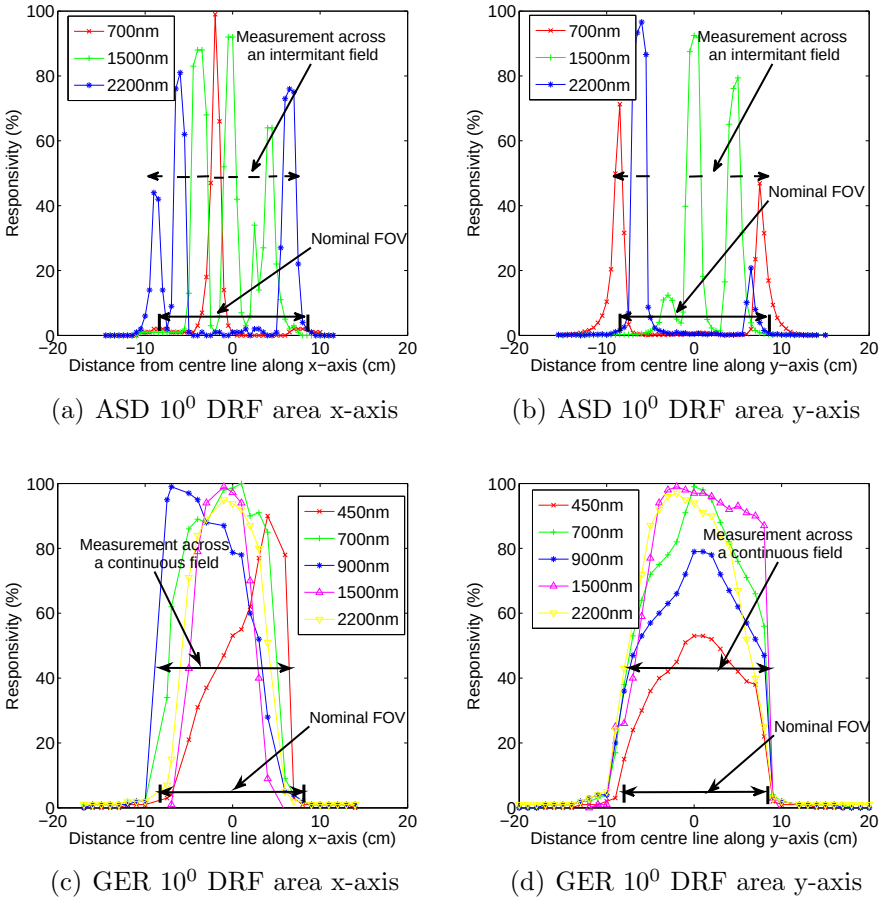

(a) ASD 10^0 DRF area x-axis

(b) ASD 10^0 DRF area y-axis

(c) GER 10^0 DRF area x-axis

(d) GER 10^0 DRF area y-axis

Figure 4.1: ASD FieldSpec Pro and GER 3700 DRFs with 10^o FOV fore optics across centre lines of the area of measurement support. Adapted from Mac Arthur *et al* (2012).

into those that are characteristic of the electronic system of the field spectroradiometer before, during and after the instrument detectors have been excited by photons; into values assigned to the detector elements within the spectroradiometer; and into those that are characteristic of the optical path that light must travel through the system prior to reaching the detector. However, the characteristics of spectroradiometer optical paths were not the focus of Schaepman's (1998) work and only preliminary investigations were carried out into optical path spectral and spatial dependencies.

Publications are available which advise on procedures for radiometric calibration and for quantification of electronic system measurement uncertainties[1] but the recommendations contained in Commission Internationale de L'Eclairage (1987) had not been applied to field spectroradiometric systems until Mac Arthur *et al.* (2012) adopted the terminology contained in these recommendations. Mac Arthur *et al.* (2012) went on to demonstrate that the FOVs of two commonly used spectroradiometers, a GER3700 and an ASD Fieldspec Pro, were not adequately or accurately defined by the nominal included solid angle specified by the manufacturers; that the responsivity to radiant flux from reflecting elements within the area of measurement support was not 'top hat', i.e. the responsivity of these spectroradiometers to radiant flux was not equal at all spatial locations within the areas of measurement support; and that when lens based fore optics were used, the responsivity was not evenly distributed radially (Figures 4.1(a), 4.1(b), 4.1(c), 4.1(d)). Mac Arthur *et al.* (2012) also demonstrated that it is the DRF that defines the area of measurement support, not the nominal FOV specified by the manufacturer, as radiant flux may be received by the spectroradiometers from outside the area delimited by the FOV and there may be regions within the FOV delimited area from which no radiant flux is received (Figure 4.1(a) and 4.1(b)). However, when fore optics with no focusing element were used with these two spectroradiometers radiant flux was received across a continuous field (Figures 4.2(a), 4.2(b), 4.2(c) and 4.2(d)), although the area of measurement support was still defined by the DRF, not the specification provided by manufacturers Mac Arthur *et al.* (2012).

In the spatial sampling of Earth surfaces the size, geometry and orientation in space of each area sampled is known as the support for measurements and subsequent analysis (Atkinson and Tate, 2000). In Earth observation, where

[1]See:- Wyatt, C. L. (1978) Radiometric Calibration: Theory and Method, Academic Press, N.Y.; CIE #53 - 1982, Methods of Characterizing the Performance of Radiometers and Photometers; or CIE #64 - 1984. Determination of the Spectral Responsivity of Optical Radiation Detectors, for example.

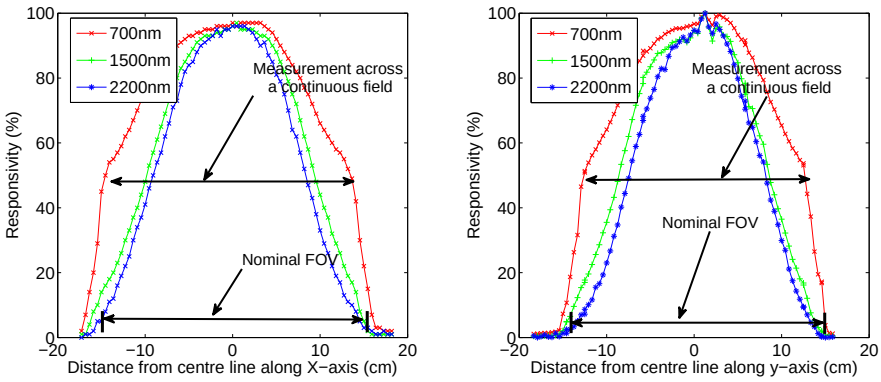

(a) ASD 18^0 DRF area x-axis

(b) ASD 18^0 DRF area y-axis

(c) GER FOP DRF area x-axis

(d) GER FOP DRF area y-axis

Figure 4.2: ASD FieldSpec Pro and GER 3700 DRFs with wide FOV fore optics across centre lines of the area of measurement support. Adapted from Mac Arthur *et al* (2012).

images are acquired by remote sensing, and where complete coverage of an area is achieved, the support for each of the sample areas is represented by pixels and the measurement of the support is affected by the point-spread function (PSF) of the sensor (Atkinson, 2004; Atkinson and Aplin, 2004). The PSF of an imaging system is reasonably well approximated by a two-dimensional Gaussian responsivity distribution and this is equally distributed radially over the plane of support (Billingsley *et al.*, 1983; van der Meer, 2001; Mather, 2004). The PSF delimits the area that is sampled and the weighting the sensor assigns to the radiant flux from each reflecting element within the defined area (Atkinson and Aplin, 2004). It has been demonstrated that the PSF has a significant influence on the information that can be derived from satellite images on a per pixel basis (Huang *et al.*, 2002).

However, although there are publications in which the characteristics of the PSF and instantaneous field-of-view (IFOV) of imaging systems are discussed[2], little research has been published describing the corresponding phenomena for field spectroradiometers[3]. The general assumption made by field spectroscopists has been that the FOV of a spectroradiometer delimits the area of measurement support and it is normally specified by instrument manufacturers as a nominal included solid angle within which the spectroradiometer/fore optic system accepts radiant flux (Spectra Vista Corporation, undated; Analytical Spectral Devices, 1999). That the area delimited by the FOV is considered to define the support for subsequent analysis is demonstrated when: elements within the FOV of the instrument (Murphy *et al.*, 2005; Smith *et al.*, 2005; Steven, 2004); the diameter of the FOV (Castro-Esau *et al.*, 2006; Ustin and Whiting, 2006; Nichol and Grace,

[2]See:- Mather, P. M., 2004. Computer Processing of Remotely-Sensed Images. Chichester, Wiley.; or Townshend, J. R. G., 1980. The Spatial Resolving Power of Earth Resource Satellites: A Review. Technical Memorandum 82020. Greenbelt, Maryland, NASA., for example.

[3]The exceptions being Schaepman, M. E., 1998. Calibration of a Field Spectroradiometer, PhD thesis, University of Zurich., and Anderson, K., 2005. Temporal variability in calibration target reflectance: methods, models and applications. Ph.D.thesis, University of Southampton.

2010); the ground FOV (Mutanga *et al.*, 2000; Harris *et al.*, 2006); the footprint (Ferrier *et al.*, 2009; Hilker *et al.*, 2009) and the area observed by the sensor (Darvishzadeh *et al.*, 2008; Sandmeier, 2000). are discussed. In these studies quantitative measurements have been made of reflecting or absorbing elements within the area of measurement support, assumed to be delineated by the FOV, and relationships between the radiant flux and these elements established.

Many studies have developed indices from the relationships between spectral absorption or reflectance features of leaves and their biochemical content[4]. These indices are proposed as proxies to quantify biochemical content without destructive sampling of the vegetation being required. Indices such as the red edge position (REP) and spectral narrow band ratios have been investigated as proxies for proximate pigment content in many studies (Horler *et al.*, 1983; Baret *et al.*, 1987; Vogelmann and Moss, 1993; Jago *et al.*, 1999; Clevers *et al.*, 2004; Baranoski and Rokne, 2005; Nichol and Grace, 2010; Ju *et al.*, 2010). Alternatively, the spectra acquired are compared to those in existing Spectral Libraries to determine surface classification or composition (Kruse, 2010), or are used as endmembers in spectral unmixing approaches for remote sensing image analysis (Plaza *et al.*, 2002; Dehaan and Taylor, 2003; Vazquez *et al.*, 2004).

Vegetation canopies and mineral surfaces are a heterogeneous mix of reflecting elements and facets. However, no studies have been carried out to investigate the effect that differences between the assumed and the actual area of measurement support and variations in responsivity across the area of measurement support have on spectra acquired from heterogeneous natural surfaces or on indices derived from spectra from such surfaces. For this work, three-dimensional data cubes of the DRFs of two field spectroradiometers were constructed for a selection of fore

[4]See:- Sims, D., Gamon, J., 2002. Relationships between leaf pigment content and spectral reflectance across a wide range of species, leaf structures and developmental stages. Remote Sensing of Environment 81, 337-354. for a review of vegetation biochemical indices.

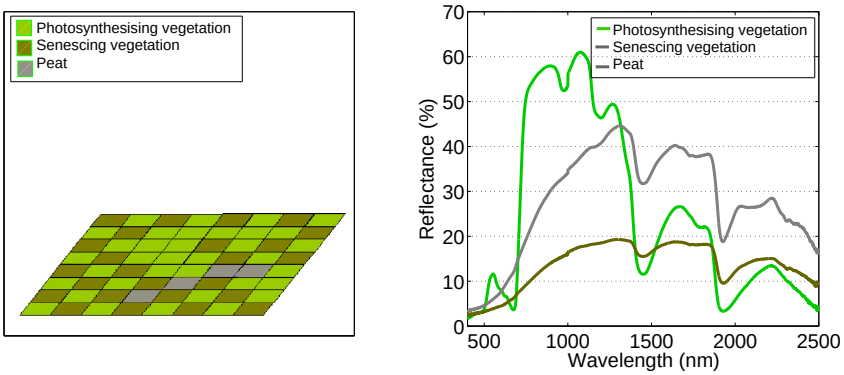

(a) Index raster surface schematic (b) Modelled surface component spectra

Figure 4.3: Components of modelled surfaces

optics, utilising the data acquired by Mac Arthur *et al.* (2012). These DRF models were then convolved with a modelled reflectance test surface and a series of modelled heterogeneous reflecting Earth surfaces to gain an understanding of the effect that each DRF of an instrument has on the spectra acquired from such surfaces and on indices, as proxies for biochemical content, derived from such spectra.

4.2 Methods

The DRFs of a GER 3700 (#1008) and of an ASD Fieldspec Pro (#6449), two full wavelength spectroradiometers held by the Natural Environment Research Council Field Spectroscopy Facility in the UK, each with a number of fore optics supplied by the manufacturers, were measured. This was achieved by passing a light source in front of each spectroradiometer/fore optic system and taking spectral measurements at discrete spatial locations on a regular measurement grid. The spectroradiometers were configured to measure in raw counts and the

measurements normalised per wavelength by ratioing each measurement with the reference point measurement, thereby converting them to relative responsivity. Each spectral measurement was subsequently indexed with the appropriate vertical and horizontal positions from the measurement grid. The method used to determine the DRF of each instrument is more fully described in Mac Arthur *et al.* (2012). The spatially referenced relative responsivity spectra were subsequently assembled into a three-dimensional data cube with the vertical and horizontal positions and wavelength scale as the three axes and the relative responsivity per wavelength interval as the attribute of each point in the data cube.

A number of raster surfaces were created with each pixel position indexed to assign one of three component reflectances, either to model a test surface, or, of a form similar to that displayed in Figure 4.3(a), to model a specific class of Earth surface and investigate DRF effects. The component reflectances selected for this research were photosynthesising *Calluna vulgaris* shoots and leaves and senescing *Calluna* shoots and leaves, as overstorey components, and peat, as the understorey component. The spectrum used for each component was acquired by making multiple spectroradiometric laboratory relative reflectance measurements of homogeneous samples, converting to absolute reflectance, then averaging each set of absolute reflectance measurements. These components were selected as each has distinctly different spectral profiles and reflectance features (Figure 4.3(b)) and can be used in combination to represent heterogeneous natural vegetation surfaces.

After the component spectra were placed in their indexed positions, each modelled surface three-dimensional data cube and each spectroradiometer/fore optic normalised DRF data cube were convolved. The sum at each wavelength interval of the convolved data cube was computed and the resulting spectrum saved (named the DRF spectrum). First a 'test surface' was created to elucidate the affects of the DRFs of each spectroradiometer and the normalised DRF data cube

was rotated through 90^o, the data cubes convolved and this repeated to derive DRF spectra from four orthogonal rotational positions. Next Earth surfaces were modelled, each normalised DRF data cube rotated in 1^o increments, convolved with each Earth surface data cube and each result saved. This rotation, convolution and saving of the resulting spectrum was repeated to give a total of 360 DRF spectra for each modelled Earth surface and spectroradiometer/fore optic combination.

A three-dimensional data cube was also created, at the same spatial and wavelength resolutions as the modelled surfaces, to represent the nominal FOV for each spectroradiometer where the responsivity across the nominal FOV was 'top hat'. The nominal FOV data cubes were also convolved with each of the modelled surface data cubes and the results saved (the nominal FOV spectra). The nominal FOV data cube did not require to be rotated and convolution repeated, as the responsivity per wavelength is the same at all spatial locations. The relative error per wavelength, derived from the difference between the nominal FOV spectrum and the DRF spectrum and expressed as a percentage per wavelength interval, was then computed for each DRF rotation and convolution. The root mean squared error (RMSE) per wavelength interval and the standard deviation (SD) per wavelength interval were calculated to give an indication of the precision and variation, respectively, of the DRF spectra, for each spectroradiometer DRF/Earth surface combination.

4.3 Results and discussion

4.3.1 Spectroradiometers with 10^o fore optics

A test surface, presented at four rotational positions in Figures 4.4(a), 4.4(d), 4.4(g) and 4.4(j), was modelled by assigning either the photosynthesising *Calluna* shoots and leaves spectrum or the bare peat spectrum to each half of an indexed raster surface to create the test surface data cube. The test surface data cube was then convolved with the DRF data cube of the GER 3700 with 10^o fore optic and of the ASD FieldSpec Pro with 10^o fore optic and the results compared.

For the GER 3700 with 10^o fore optic, the relative errors in the visible near infra-red (VNIR) (400 nm to 1,000 nm) region of the spectrum highlight the effect of the DRF wavelength dependent bias along the x-axis, that is across the optical slit of the spectroradiometer, shown in Figures 4.1(c) and 4.1(d). In this region of the spectrum, this spectroradiometer/fore optic combination has greater responsivity to blue wavelengths to the right and greater responsivity to red wavelengths to the left of the geometric centre line of a fore optic (Mac Arthur *et al.*, 2012). The effect of this bias on the spectra recorded can be seen by comparing Figures 4.4(b) and 4.4(h) where, as the peat spectrum and *Calluna* spectrum have approximately the same percentage reflectance at around 400 nm (Figure 4.3(b)), the modelled nominal FOV and DRF reflectances, and hence the relative error, should be the same at each rotational position. However, they are not. A difference of approximately 20% is evident at these two opposite rotational positions and the relative errors are approximately the inverse of each other. The DRF bias is also evident at the other two opposite rotational positions (Figures 4.4(e) and 4.4(k)), although in these cases the differences at 400 nm are less than previously observed and relative errors are not the inverse of each other.

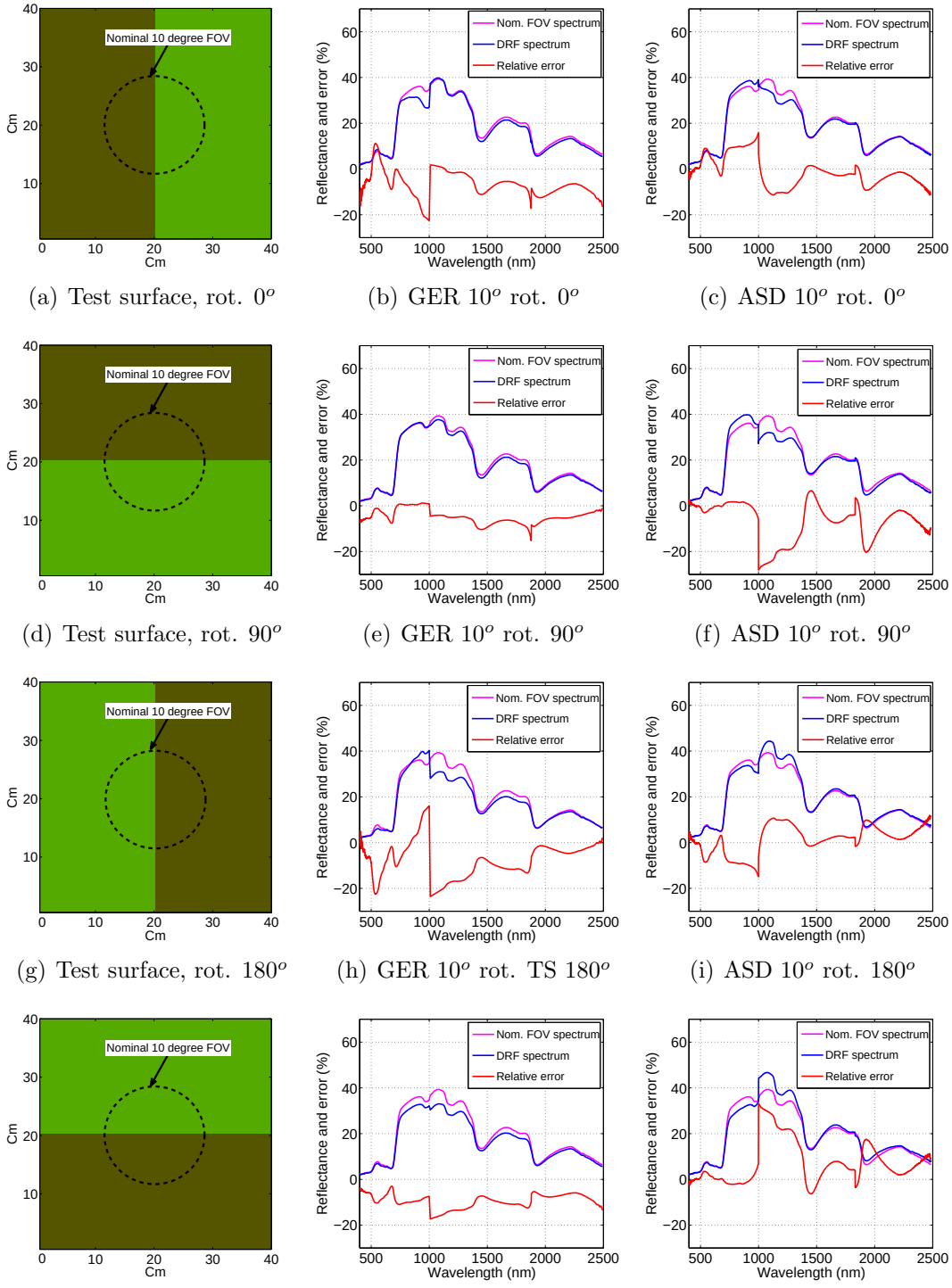

(a) Test surface, rot. 0^o (b) GER 10^o rot. 0^o (c) ASD 10^o rot. 0^o

(d) Test surface, rot. 90^o (e) GER 10^o rot. 90^o (f) ASD 10^o rot. 90^o

(g) Test surface, rot. 180^o (h) GER 10^o rot. TS 180^o (i) ASD 10^o rot. 180^o

(j) Test surface, rot. 270^o (k) GER 10^o rot. 270^o (l) ASD 10^o rot. 270^o

Figure 4.4: GER 3700 and ASD FieldSpec Pro, with 10^o fore optics, nominal FOV and DRF spectra and error from modelled *Calluna* over bare peat test surface

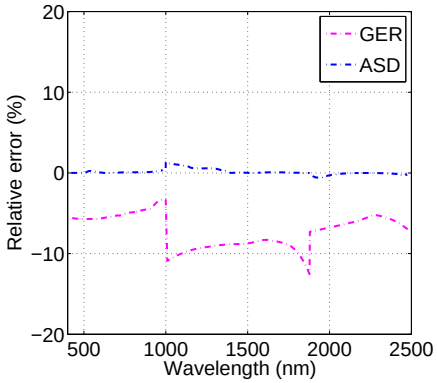

Figure 4.5: ASD and GER systems' mean relative error for 4 rotational positions

The first short-wave infra-red (SWIR-1) region, from 1,000 nm to 1,800 nm, and second short wave infared (SWIR-2) region, from 1,800 nm to 2,500 nm, of the DRF spectra also display rotational dependencies (Figures 4.4(b), 4.4(e), 4.4(h) and 4.4(k)), although these relative errors at opposite rotational positions are also not the inverse of each other. If the spectroradiometer/fore optic optical and geometric centre lines were aligned the relative error would be symmetrical about the x and y-axes of the measurement grid and would result in equal percentage error differences, either positive or negative, at opposite rotational positions, as the measurement axis datums were determined from the fore optic geometric centre line. However, it is evident from the negative displacement from the x-axis of the GER 3700 system's mean relative error per wavelength (Figure 4.5), calculated from the errors at the four rotational positions, that the optical centre line of each spectrometer within the GER 3700/10^o fore optic system is not aligned with the geometric centre line of the fore optic of the instrument. In addition, significant steps are evident in the mean relative error at the points (1,000 nm and 1,800 nm) where the spectral range of the individual spectrometers join.

The reflectance spectra derived by convolving the DRF of the ASD FieldSpec Pro/10^o fore optic system with the test surface at four orthogonal positions

also display the effects of the rotational position and wavelength dependent responsivity. The magnitude of the relative errors per wavelength interval vary greatly over the full spectral range of each of the spectrometers and between each rotational position (Figures 4.4(c), 4.4(f), 4.4(i) and 4.4(l)). However, for this instrument/fore optic combination the relative errors at opposite rotational positions do appear to be, approximately, the inverse of each other (Figures 4.4(c) and 4.4(i) and Figures 4.4(f) and 4.4(l)). From this test surface example, the DRF of the ASD system with 10^o fore optic does appear to be reasonably symmetrical around the fore optic centre line as the mean of the relative error for the 4 rotational positions is close to zero, although steps are also evident at the points (1,000 nm and 1,800 nm) where the spectral range of each spectrometer join, although of a lower magnitude than observed for the GER 3700 (Figure 4.5).

The steps evident to a greater or lesser extent, at each rotational position, in both the GER and ASD DRF spectra at 1,000 nm and at 1,800 nm, and highlighted by peaks in the relative error at these wavelengths (Figures 4.4(b), 4.4(e), 4.4(h), 4.4(k), 4.4(c), 4.4(f), 4.4(i) and 4.4(l)) have been reported as being due to each spectrometer, within a spectroradiometer, having different thermal characteristics causing a "sensitivity drift" (Salisbury, 1998) between spectrometers as temperature changes over time. However, steps in spectra at these points are often seen when measuring heterogeneous Earth surfaces with field spectroradiometers, even after adequate time has been allowed for the spectrometers to reach stable temperatures. Each component spectrum used in this research was acquired from a homogeneous sample and there were no steps present (Figure 4.3(b)). Therefore the steps observed in the spectra in Figure 4.4 and 4.5, derived by convolving the test surface data cube and the DRF data cube of each spectroradiometer system, must be due to the convolution. It is evident from the DRF of the ASD spectroradiometer with 10^o fore optic (Figures 4.1(a) and 4.1(b)) that each spectrometer will receive flux

from different areas of the test surface as each spectrometer is not measuring across a continuous field or, in the case of the GER 3700 with 10^o fore optic (Figure 4.1(c) and 4.1(d)) from areas of the same spatial extent. As each of the areas of measurement support for each individual spectrometer may have different proportions of component spectra present, the spectrum recorded by each spectrometer, within the same spectroradiometer, may not be of the same magnitude at the contiguous wavelength intervals either side of the point at which the spectrometers have been selected to join. Therefore, the steps in the DRF spectra are being caused by the combined effect of the spatial distribution of the test surface spectra and the distinctly different areas of measurement support for each spectrometer, not in these cases at least by thermal drift. It can also be noted from Figure 4.4 that there are significant differences between the DRF spectra acquired by each spectroradiometer system (highlighted by the differences between the profiles of the relative errors of each spectroradiometer) as, although the area of measurement support for each spectroradiometer defined by the nominal FOV are the same, the area of measurement support and the responsivity, defined by the DRF of each spectroradiometer, are not. Hence, each spectroradiometer will acquire a spectrum unique to that spectroradiometer/fore optic system when measuring flux from the same heterogeneous Earth surface area. If the reponsivity of both spectroradiometer/fore optic systems was equally weighted for all points from which radiant flux was received and the area of measurement support was the same for each spectroradiometer, which would be the case if the responsivity was 'top hat', then when each system had a fore optic with the same nominal FOV attached, there would be no difference between the spectrum derived from the nominal FOV and that derived from the DRF, irrespective of rotational position and/or field spectroradiometer used. However, from the results modelled from this test surface and these spectroradiometers, this is evidently not the case.

To further investigate the effect of the DRF of each spectroradiometer on spectral reflectance measurements, surfaces more representative of real world Earth surfaces were modelled and the DRF data cubes for each spectroradiometer/fore optic combination were convolved with the data cubes of each surface, as previously described. The first modelled 'natural' surface (Natural Surface 1) represents *Calluna* in the 'building' stage (Watt, 1947; Gimingham, 1960) of its growth and prior to canopy closure. For this surface photosynthesising *Calluna* and peat were again selected as the component spectra and each spectrum was assigned pixel positions representative of a *Calluna* shrub growing over a bare peat substrate such that some substrate was 'visible' through the shrub canopy. For this surface, within the area delineated by the nominal FOV of a spectrometer with a 10^o fore optic, *Calluna* represents 80% of the reflecting components and peat the remainder. Natural Surface 1, is displayed at the four rotational positions in Figures 4.6(a), 4.6(d), 4.6(g) and 4.6(j).

For the GER system the general profiles of the relative errors from Natural Surface 1 at these four rotational positions (Figures 4.6(b), 4.6(e), 4.6(h) and 4.6(k)) were similar to those found at two of the test surface rotational positions (Figures 4.4(e) and 4.4(k)), and all displayed errors of a lower value than those determined from the test surface. The maximum relative error observed was approximately 17% at the 1,000 nm wavelength interval at two rotational positions (Figures 4.6(b) and 4.6(k)), compared to approximately 22% observed from the test surface at the same wavelength (Figure 4.4(h)). The profiles displayed by the relative errors across the full spectral range at each rotational position were similar to each other, rather than the inverse at opposite rotational positions as previously observed from the test surface.

The errors determined for the ASD system and Natural Surface 1 were also not the inverse of each other at opposite rotational positions. At three positions they displayed a similar profile and percentage at each wavelength interval (Figures 4.6(c),

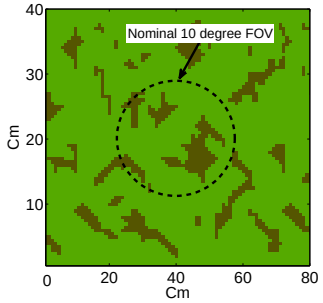

(a) Natural Surface 1, rot. 0^o

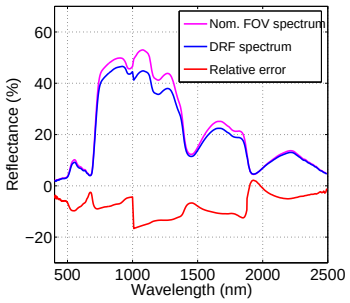

(b) GER 10^o rot. 0^o

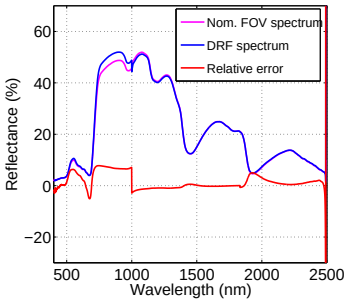

(c) ASD 10^o rot. 0^o

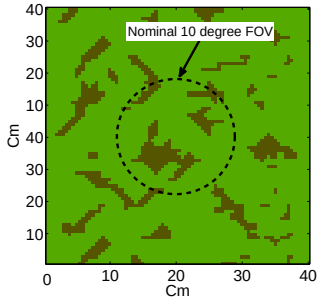

(d) Natural Surface 1, rot. 90^o

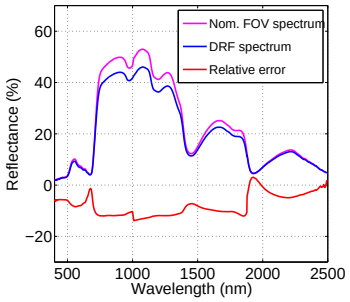

(e) GER 10^o rot. 90^o

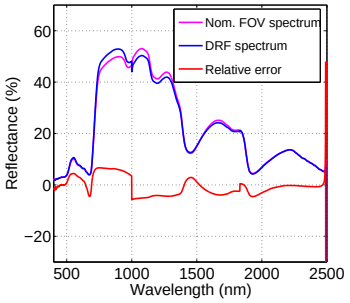

(f) ASD 10^o rot. 90^o

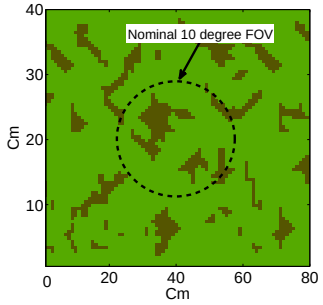

(g) Natural Surface 1, rot. 180^o

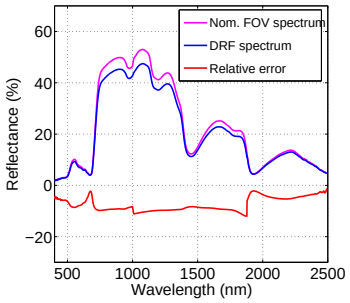

(h) GER 10^o rot.180^o

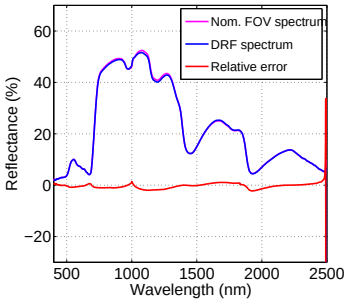

(i) ASD 10^o rot. 180^o

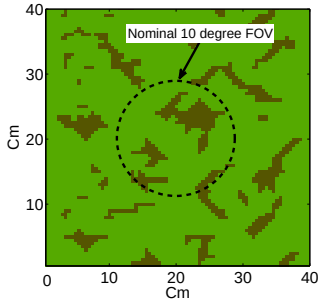

(j) Natural Surface 1, rot. 270^o

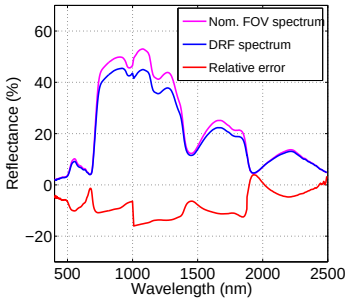

(k) GER 10^o rot. 270^o

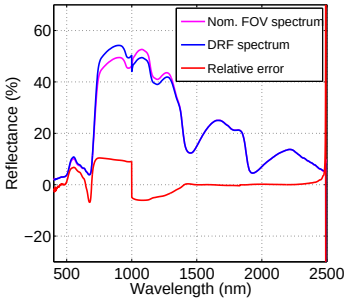

(l) ASD 10^o rot. 270^o

Figure 4.6: GER 3700 and ASD FieldSpec Pro with 10^o fore optics, nominal FOV and DRF spectra and errors from model representing 'building' *Calluna* over a bare peat Earth surface

4.6(f) and 4.6(l)) and were considerably lower than previously observed, approximately 10% (Figure 4.6(l)) compared to 25% from the test surface (Figure 4.4(l)). The errors at these three positions varied from approximately -7.5% to 14.0% depending on wavelength and rotational position, with the greatest variation being observed across the VNIR spectral range. The errors at one rotational position (Figure 4.6(i)) were minimal and displayed a significantly different profile across the full spectral range from those at the other rotational positions. It can also be noted from the relative errors of both the GER and the ASD systems that the profile of the DRF spectra (highlighted by the profile of the relative errors) acquired by each instrument again differs significantly from that acquired by the other instrument at corresponding rotational positions.

When spectra from all 360 rotational positions are considered, the errors from the GER 3700 spectra are asymmetric about the zero percent error axis (Figure 4.7(a)), as are the errors for the ASD VNIR spectrometer. However, the errors from the SWIR-1 and SWIR-2 spectral regions of the ASD appear symmetrical about the zero percent error axis (Figure 4.7(b)). The mean of the relative errors at all rotational positions (Figure 4.7(c)) gives an indication of the errors per wavelength that could be expected if an attempt was made to characterise the surface reflectance by taking measurements at each of these 360 rotational positions and averaging them. Depending on wavelength, the error would be between approximately -5% and -15% across the GER 3700 VNIR and SWIR-1, and approximately -10% and 3% across the SWIR-2, spectrometer spectral ranges. The errors across the ASD FieldSpec Pro SWIR-1 and SWIR-2 spectrometer spectral ranges would be approximately zero, while the error across the spectral range of the the VNIR spectrometer would be approximately -5% to 9% dependent on wavelength. The RMSEs per wavelength are in the main considerably higher across the full spectral range for the GER 3700 system than for the ASD system

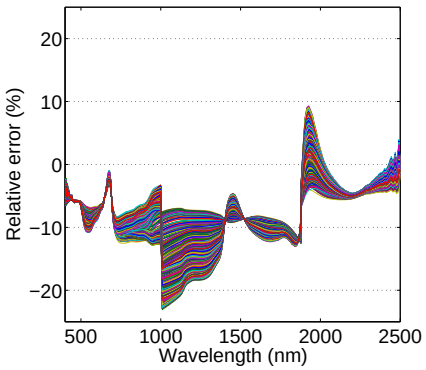

(a) GER 3700 with 10^o fore optic

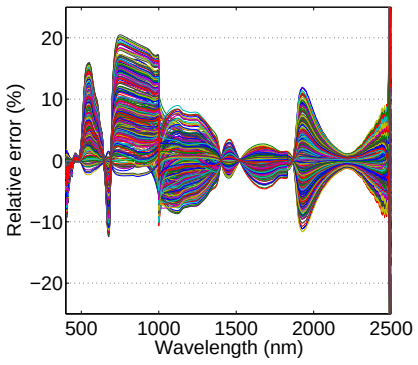

(b) ASD FS Pro with 10^o fore optic

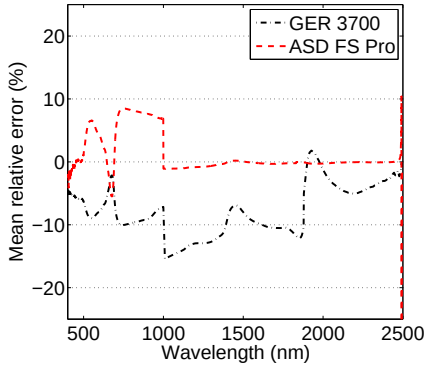

(c) GER and ASD system averages

Figure 4.7: DRF spectra relative errors and averages modelled from Natural Surface 1 at 360 rotational positions for each spectroradiometer

(Figure 4.8(a)). However, when the variability of the DRF spectra at each rotational position is considered a different picture emerges. The SD of the ASD DRF spectra per wavelength interval from 500 nm to 1,000 nm within the range of the VNIR spectrometer is much greater than for the GER DRF spectra; within the SWIR-1 range the GER 3700 DRF spectra display a greater SD from 1,000 nm to approximately 1,500 nm; and from 1,500 nm to 2,4500 nm the DRF spectra errors per wavelength interval from both instruments are similar (Figure 4.8(b)).

The precision and variability of the spectra measured by each spectroradiometric

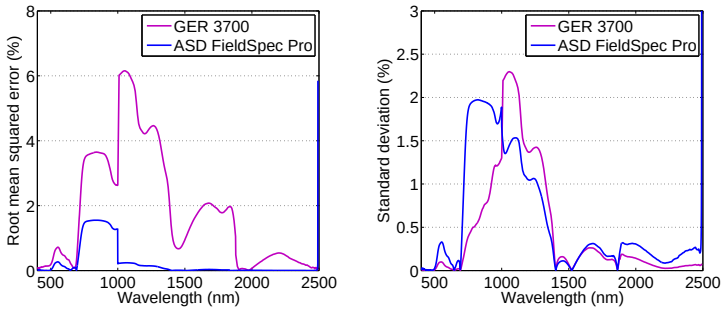

(a) GER and ASD RMSE (b) GER and ASD SD

Figure 4.8: ASD FieldSpec Pro and GER 3700 with 10^o fore optic DRF spectra RMSE and SD from Natural Surface 1

system, and modelled in this work, appear to be dependent on the radial position (distance from the centre and azimuth angle) and the spatial extent of each area (which has the same spectrum assigned to each contiguous raster position) as well as the DRF of each instrument. Hence, if the GER 3700 and ASD FieldSpec Pro systems, each with 10^o fore optic, measured the reflectance from the same area of a natural surface, of a form similar to that modelled by Natural Surface 1, all the spectra acquired would be influenced by the rotational position at which each spectrum was acquired, rather than solely an intrinsic property of the surface, for a given illumination environment.

To investigate the effect of reflecting feature size and radial position on reflectance measurement, a second surface was modelled, Natural Surface 2, this time to represent *Calluna* at a later phase of its growth cycle, the onset of the 'degenerate' stage. At this stage there is a change in the gross morphology of the *Calluna* shrub canopy as it begins to collapse radially from the centre (Gimingham, 1960) and reflectances from the substrate are integrated into the spectrum recorded. The modelled 'degenerate' *Calluna* surface over a peat substrate is presented at four rotational positions in Figures 4.9(a), 4.9(d), 4.9(g), and 4.9(j), again with 80% of the modelled surface within the nominal FOV representing *Calluna* and

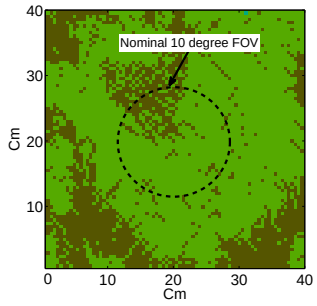

(a) Natural Surface 2, rot. 0^o

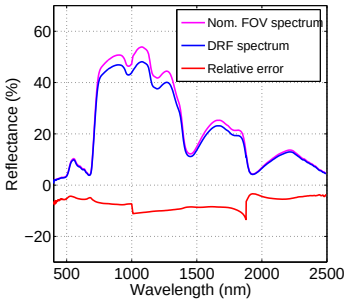

(b) GER 10^o rot. 0^o

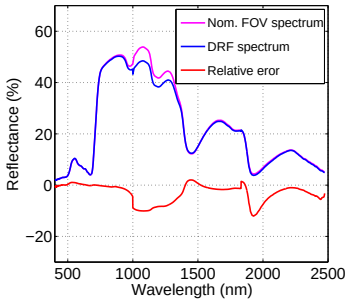

(c) ASD 10^o rot. 0^o

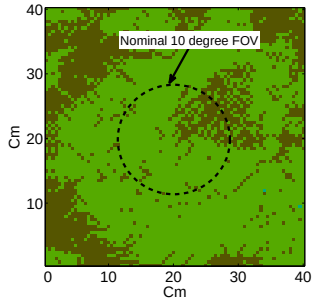

(d) Natural Surface 2, rot. 90^o

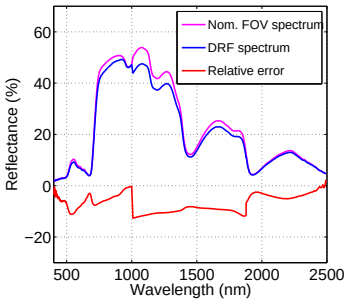

(e) GER 10^o rot. 90^o

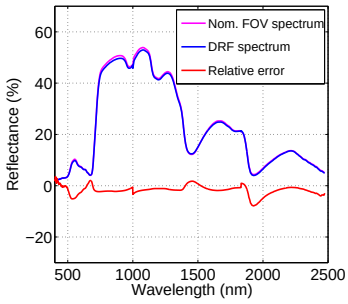

(f) ASD 10^o rot. 90^o

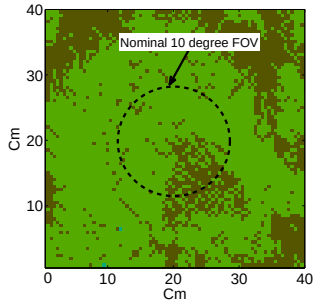

(g) Natural Surface 2, rot. 180^o

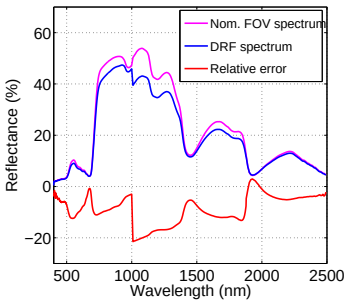

(h) GER 10^o rot. 180^o

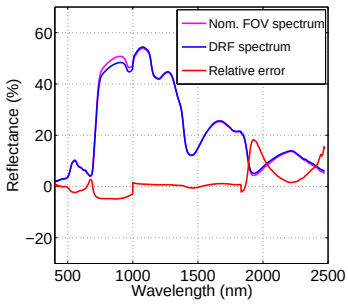

(i) ASD 10^o rot. 180^o

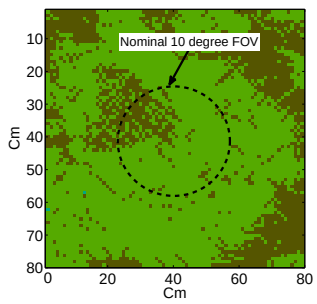

(j) Natural Surface 2, rot. 270^o

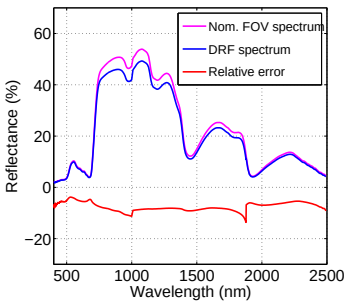

(k) GER 10^o rot. 270^o

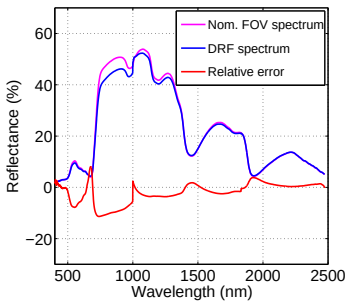

(l) ASD 10^o rot. 270^o

Figure 4.9: GER 3700 and ASD FieldSpec Pro, with 10^o fore optics, nominal FOV and DRF spectra and error from modelled *Calluna* 'degenerate' canopy over bare peat Earth surface

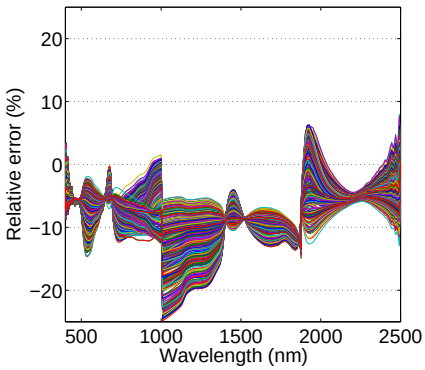

(a) GER 3700 with 10^o fore optic

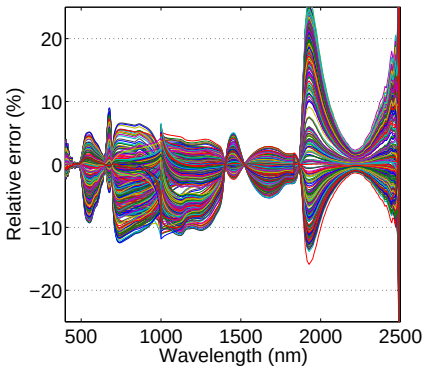

(b) ASD FS Pro with 10^o fore optic

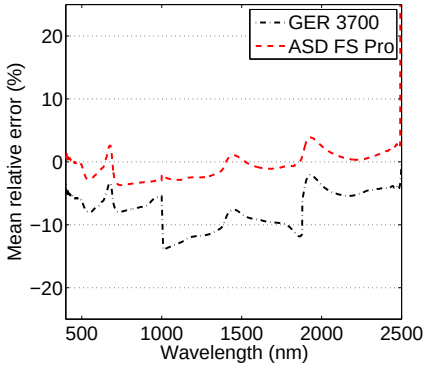

(c) GER and ASD system averages

Figure 4.10: DRF spectra relative errors and averages modelled from Natural Surface 2 at 360 rotational positions for each spectroradiometer

the remainder peat. For this surface a greater concentration of pixels indexed for the peat spectrum were modelled in one quadrant of the area delineated by the nominal FOV than in the other quadrants and this largest area of peat was interspaced with *Calluna* spectra so that it was not homogeneous, as was the case for the areas of peat in Natural Surface 1.

From the modelled DRF reflectance spectra of Natural Surface 2 for the GER system at each of the orthogonal rotational positions, the profiles of the relative errors (Figures 4.9(b) and 4.9(e) and Figures 4.9(h) and 4.9(k)) were similar to each other, to the profile of the errors from Natural Surface 1, and continued to

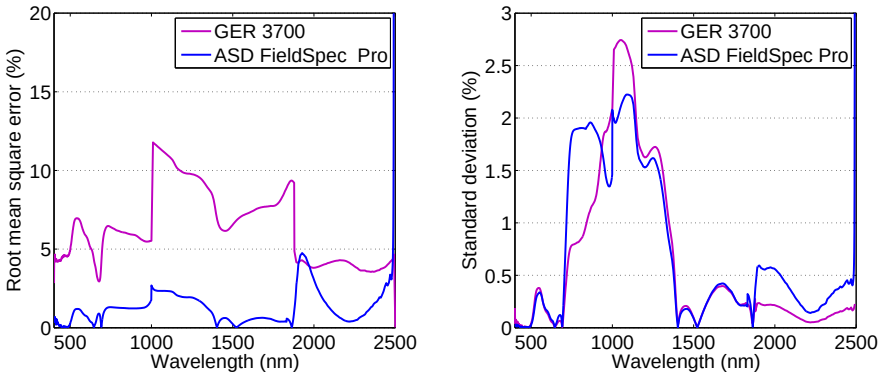

(a) GER and ASD RMSE (b) GER and ASD SD

Figure 4.11: ASD FieldSpec Pro and GER 3700 with 10^o fore optic DRF spectra RMSE and SD from Natural Surface 2

have primarily a negative offset from the zero percent error axis (Figures 4.10(a), 4.10(c)). For the ASD system, there was also primarily a negative offset from the zero percent error axis (Figures 4.9(c), 4.9(f) and 4.9(l)) except for within the SWIR-2 spectral range at one rotational position (Figure 4.9(i)) where the offset was positive. In addition, for the ASD the errors were greater in the SWIR-1 and SWIR-2 spectral regions than previously observed, as can be seen when Figure 4.10(c) and Figure 4.8(b) are compared.

When the DRF spectra from Natural Surface 2 at each 1^o rotational increment are considered the relative errors for the GER 3700 were again seen to be asymmetric about the zero percent error axis and of a generally similar form to those observed from Natural Surface 1. The errors for the ASD system were more symmetrical across the VNIR spectral range and less symmetrical for the SWIR-1 and SWIR-2 spectral ranges, around the zero percent error axis, than previously observed from Natural Surface 1. The RMSE profiles for the GER 3700 spectrometer from Natural Surface 2 also displayed a similar form to those observed from Natural Surface 1, although the magnitude per wavelength for the SWIR-1 and SWIR-2 spectrometers was lower (Figure 4.11(a)). However, for the ASD system

the profile of the RMSE from Natural Surface 2 across the VNIR and SWIR-2 spectrometer regions varied when compared to those from Natural Surface 1 and the magnitude per wavelength was generally lower, although for the SWIR-2 spectrometer the profile and magnitude were similar (Figure 4.11(a)). The SD per wavelength interval for the ASD VNIR spectral range remained reasonably consistent between the two surfaces modelled thus far. However, although the general profiles of the SD per wavelength for the other spectrometers from both systems remained similar, the magnitude varied (Figure 4.11(b)).

It is apparent then that the spectral distribution, magnitude of the errors and precision of the measurements for the ASD system are varying relative to surface characteristics, whereas those of the GER system are more consistent. These variations between the spectra recorded by each spectroradiometer system are due to the VNIR blue to red/right to left bias and the rectangularity of the area of measurement support of the SWIR-1 and SWIR-2 spectrometers in the case of the GER 3700 and; in the case of the ASD FieldSpec Pro to the fibre optic bundle arrangements where the limited number of fibres can mean a concentration of fibres for each spectrometer in different quadrants of the nominal FOV, demonstrated by Mac Arthur *et al.* (2012).

The GER 3700/fore optic system being investigated here can be considered to be measuring across a continuous field (Figures 4.1(c) and 4.1(d)), although each spectrometer does not measure the same spatial extent, while the ASD system can be considered to be measuring across an intermittent field (Figures 4.1(a) and 4.1(b)), as each fibre has its own FOV and the overlap is minimal. With the GER system all areas within this continuous field will be weighted to some degree and included in the integrated spectrum recorded. With the ASD system VNIR spectrometer areas toward the centre of the nominal FOV will be under-represented; with the SWIR-1 spectrometer areas in one quadrant will be under-represented; and with the SWIR-2 spectrometer areas in two quadrants will be

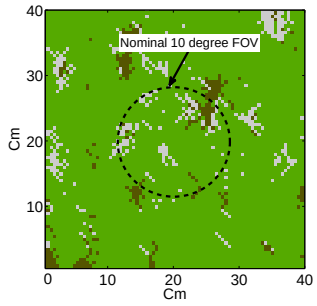

(a) Natural Surface 3, rot. 0^o

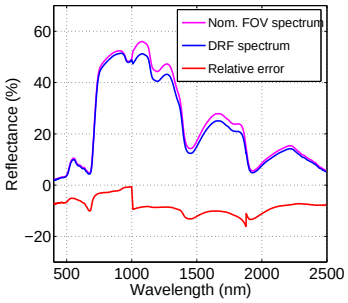

(b) GER 10^o rot. 0^o

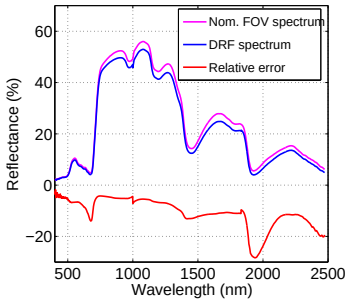

(c) ASD 10^o rot. 0^o

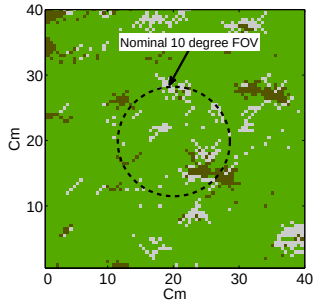

(d) Natural Surface 3, rot. 90^o

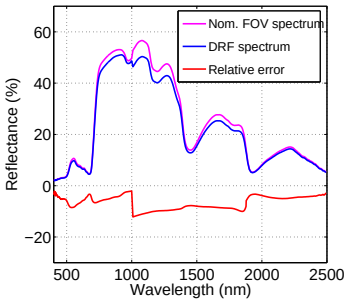

(e) GER 10^o rot. 90^o

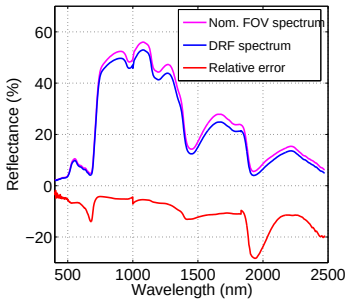

(f) ASD 10^o rot. 90^o

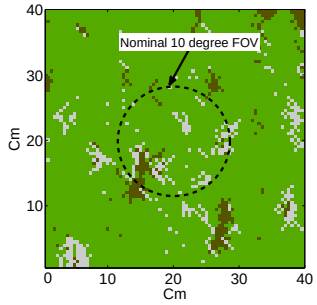

(g) Natural Surface 3, rot. 180^o

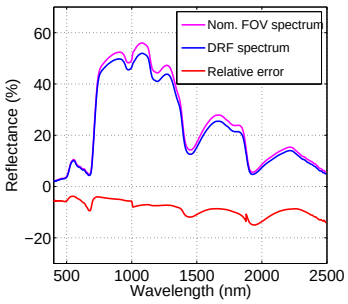

(h) GER 10^o rot. 180^o

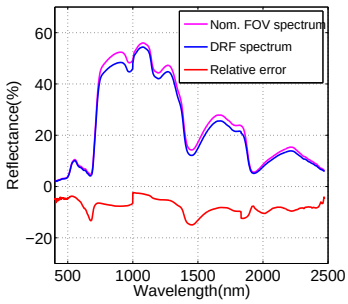

(i) ASD 10^o rot. 180^o

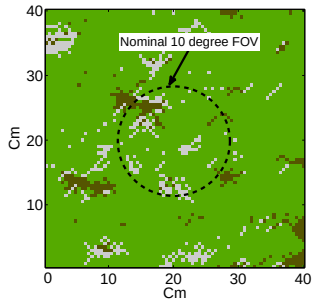

(j) Natural Surface 3, rot. 270^o

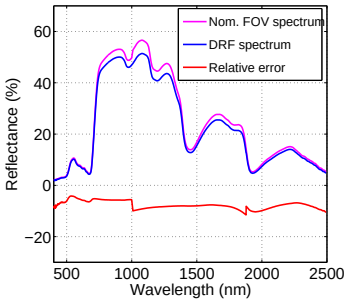

(k) GER 10^o rot. 270^o

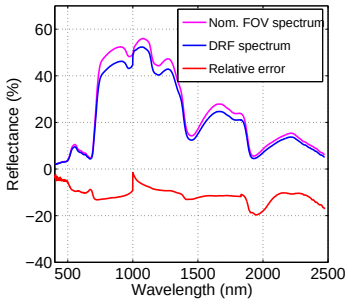

(l) ASD 10^o rot. 270^o

Figure 4.12: GER 3700 and ASD FieldSpec Pro, with 10^o fore optics, nominal FOV and DRF spectra and error from modelled *Calluna* 'senescing' canopy over bare peat Earth surface

under-represented. Therefore, with the GER 3700 system the errors are less influenced by the radial position and relative scale of the reflecting components than the ASD system. However, if it was possible to measure all rotational positions the relative errors per wavelength for the ASD system would be less than for the GER system, although the variability between each measurement would be less for the GER system.

To investigate the reflectances of a more heterogeneous surface, a surface with three distinct reflecting elements was also modelled. This surface, Natural Surface 3, displayed at four orthogonal rotational positions in Figures 4.12(a), 4.12(d), 4.12(g) and 4.12(j), represents a *Calluna* canopy at the end of a growing season when senescing shoots and leaves are present and a more heterogeneous reflecting surface exists. The relative errors of the GER 3700 DRF spectra at these rotational positions (Figures 4.12(b), 4.12(e), 4.12(h) and 4.12(k)) display a generally similar profile to the errors from the other 'natural' surfaces. The relative errors from the ASD FieldSpec Pro DRF spectra (Figures 4.12(c), 4.12(f), 4.12(i) and 4.12(l)) were more similar to those from Natural Surface 2 than Natural Surface 1, across the full spectral range. When the DRF spectral profiles at each 1^o rotational increment were considered, those from GER 3700 measurements are again asymmetric, of a similar form to those from the other 'natural' surfaces and with a negative offset from the zero percent error axis (Figure 4.10(a)). These similarities are more evident when the means of all the relative errors for each spectroradiometer from Natural Surface 3 (Figure 4.13(c)) are compared with those from Natural Surface 2 (Figure 4.10(c)). The RMSE (Figure 4.14(a)) and SD (Figure 4.14(b)) derived from the spectra for each instrument from this more heterogeneous surface are generally lower than the other natural surfaces. Furthermore, the relative difference between the SD of the ASD FieldSpec Pro DRF spectra and the GER 3700, from approximately

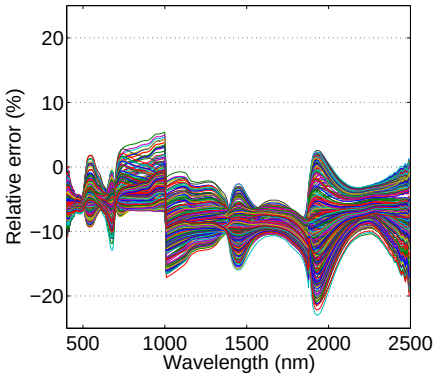

(a) GER 3700 with 10^o fore optic

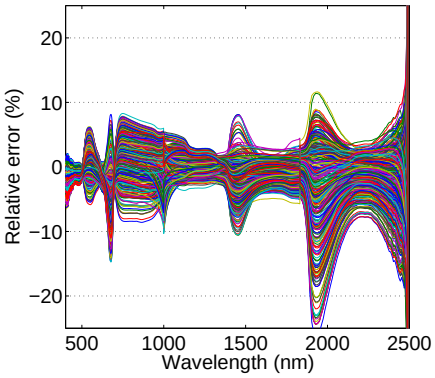

(b) ASD FS Pro with 10^o fore optic

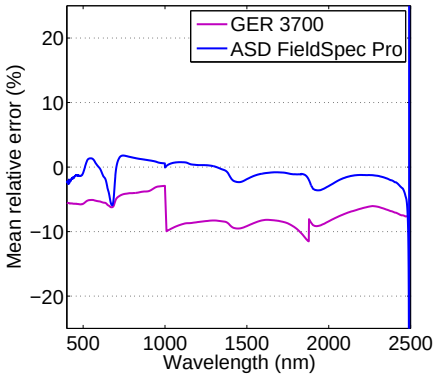

(c) GER and ASD system averages

Figure 4.13: DRF spectra relative errors and average at 360 rotational positions for each spectroradiometer from Natural Surface three using 10^o fore optics

700 nm to 1,000 nm, has increased, with that of the ASD system now being significantly higher.

From the preceding three 'natural' surface examples, it is evident that when using the 10^o lens based fore optic there will be considerable variation between the spectra that would be measured from a heterogeneous vegetation surface by each spectroradiometer used in this research dependent on the rotational position from which the measurement was acquired. It is also evident that there are significant differences between the spectra acquired by each spectroradiometer. As an alternative to field spectroradiometer fore optics containing focusing elements,

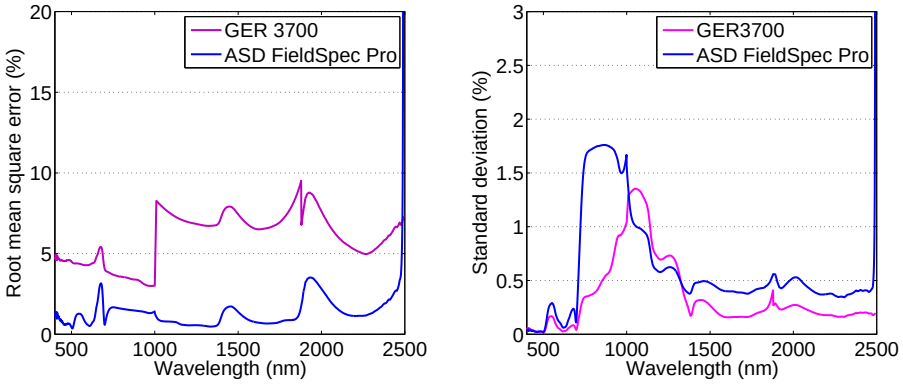

(a) GER and ASD RMSE (b) GER and ASD SD

Figure 4.14: DRF spectra RMSE and SD from Natural Surface 3 using 10^o fore optics

a fibre optic fore optic is available for the GER 3700 and a field stop without a focusing element for the ASD FieldSpec Pro and these may offer improvements over the 10^o fore optics.

4.3.2 Spectroradiometers with wide view angle fore optics

A nominal 18^o FOV field stop, without a focusing element, for the ASD FieldSpec Pro, was assessed by Mac Arthur *et al.* (2012) and the DRF across the major axes of the area of measurement support at three wavelengths is displayed in Figures 4.2(a) and 4.2(b). The DRF data cube for this spectroradiometer/fore optic was generated by linearly interpolating the data acquired by Mac Arthur *et al.* (2012) to the spatial resolution of the modelled surfaces and this data cube was subsequently convolved in 1^o rotational increments with each of the 'natural' surfaces as previously discussed. The DRF spectra were once again found to vary at each rotational position. The relative errors for each spectrometer from Natural Surface 1 were found to be asymmetric (Figure 4.15(a)) and were primarily of a lower value, varying from -7% to +12% per wavelength interval rather than the

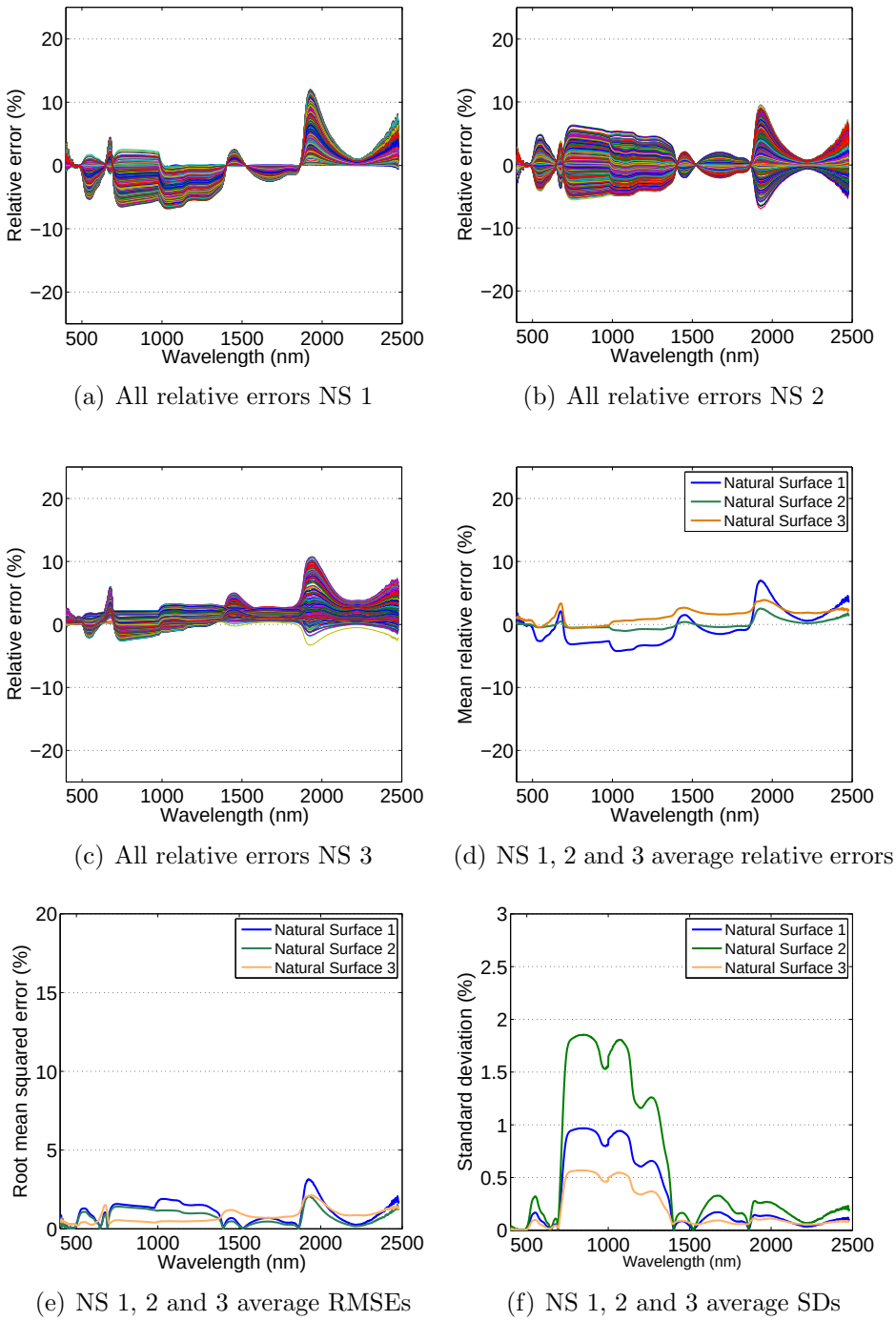

(a) All relative errors NS 1

(b) All relative errors NS 2

(c) All relative errors NS 3

(d) NS 1, 2 and 3 average relative errors

(e) NS 1, 2 and 3 average RMSEs

(f) NS 1, 2 and 3 average SDs

Figure 4.15: Relative errors, root mean square errors and standard deviations from the ASD with 18^o fore optic DRF spectra at 360 rotational positions from three modelled surfaces

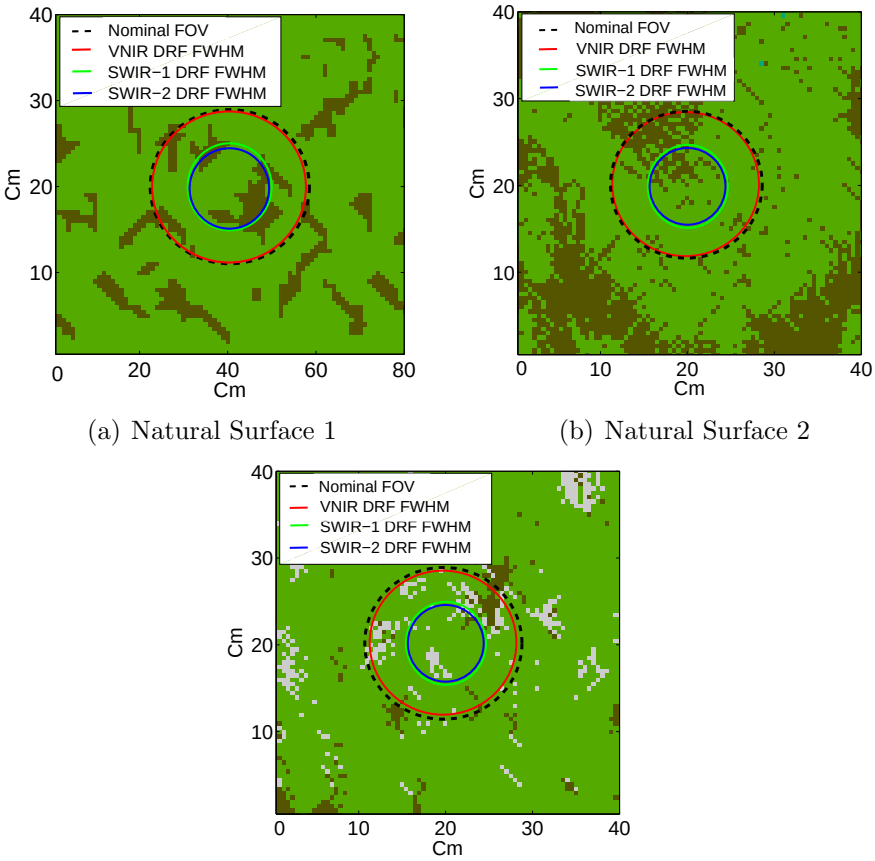

(a) Natural Surface 1

(b) Natural Surface 2

(c) Natural Surface 3

Figure 4.16: ASD FieldSpec Pro with 18^o individual spectrometer DRF and nominal FOV areas of measurement support

-10% to +20% observed when the 10^o fore optic was used, although the mean value was similar (Figure 4.15(d)), as was the RMSE (Figure 4.15(e)). For Natural Surface 3 the relative errors were again asymmetric (Figure 4.15(c)) and were of a similar magnitude (-25% to +10%) to those observed with the the 10^o fore optic (-12% to +25%), although the RMSE and SD were generally lower. However, the relative errors from Natural Surface 2 were primarily symmetrical about the zero error axis (Figure 4.15(b)), the mean value of all the errors was close to zero (Figure 4.15(d)) and the RMSE was less than 2% at all wavelengths, although the SD (Figure 4.15(f)) per wavelength was of the same order as observed from the other surfaces when the 10^o fore optic was used.

These variations between the relative errors from each surface can be explained by examining the DRF profiles presented in Figures 4.2(a) and 4.2(b). Although the DRF distribution of each of the spectrometers in ASD FieldSpec Pro with 18^o fore optic approximates more closely to a Gaussian distribution and measures across a continuous field than when lens-based fore optics are used, there is considerable difference between the responsivity distribution of the VNIR spectrometer and those of the SWIR-1 and SWIR-2 spectrometers. The responsivity of the VNIR spectrometer is approximately Gaussian from its maximum responsivity until 50% of that value, the full width half maximum (FWHM) level. At that level the area of measurement support is approximately circular and of the same diameter as the nominal FOV and from there to less than 5% responsivity it is approximately 'top hat'. The SWIR-1 and SWIR-2 responsivity is approximately a Gaussian distribution across its full width. However, the diameters of the SWIR-1 and SWIR-2 responsivities at FWHM are considerably less than the nominal FOV, each approximately 10cm rather than 17.5cm (Figures 4.2(a), 4.2(b)). For the VNIR spectrometer the relative error therefore equates to the difference between the Gaussian and 'top hat responsivities approximately across the diameter of the nominal FOV. However, for the SWIR spectrometers the relative errors are

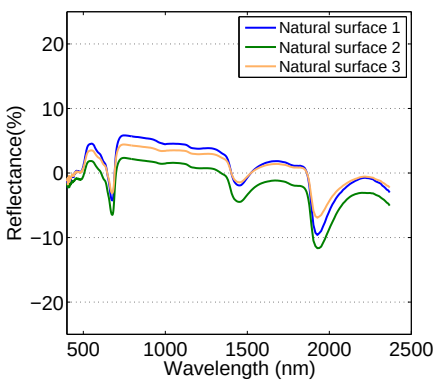

(a) NS 1, 2 and 3 average relative errors

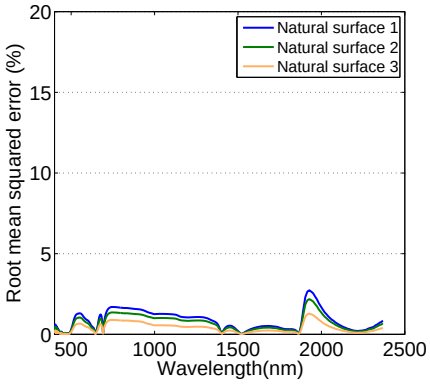

(b) NS 1, 2 and 3 average RMSEs

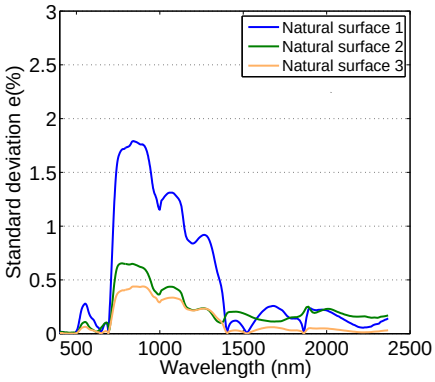

(c) NS 1, 2 and 3 average SDs

Figure 4.17: GER 3700 with FOP average relative errors, root mean square errors and standard deviations from 3 modelled surfaces

caused by the area of measurement support being considerably less for the DRF spectra than is the case for the nominal FOV, as well as the responsivity being approximately Gaussian rather than 'top hat'. The differences between the areas being sampled by the ASD VNIR and SWIR spectrometers and the variation in the proportion of reflecting components within these areas cause the relative errors observed in Figures 4.16(a), 4.16(b) and 4.16(c) for Natural Surface 1, 2 and 3, respectively.

As the manufacturer of fibre optic fore optic supplied for the GER 3700 has not specified a nominal FOV it was not possible to generate a nominal FOV 'top-hat'

responsivity data cube by the method previously used. Therefore, solely for the purposes of assessment in this research, a 'top hat' responsivity was modelled across the same spatial extent as the area of measurement support determined during the DRF measurements and this was used to construct the nominal 'FOV' data cube. This data cube was then convolved with each natural surface data cube and the resulting nominal 'FOV' spectra assessed along with the respective DRF spectra. The area of measurement support for the GER 3700 with fibre optic closely approximated to a circle (the length of the major axes can be seen to be equal in Figure 4.2(c) and 4.2(d)) and this DRF data cube and each surface data cube were convolved and rotated in 360 1^o increments, as before. The resulting error spectra for Natural Surface 1 are significantly less (-5% to +5%), except in the region of the the overlap between the SWIR-1 and SWIR-2 spectrometers (1800 nm to 1950 nm), than observed with the 10^o fore optic from the same surfaces, as were the relative errors for Natural Surface 2 and Natural Surface 3 (Figures 4.17(a)) and the relative errors from each surface presented similar profiles and magnitudes of error to each other other, as did the RMSE (Figure 4.17(b)). The RMSEs (Figure 4.17(b)) and the SDs (Figure 4.17(c)) of the spectra from each of the modelled surfaces were also of a similar magnitude to those modelled for the ASD spectroradiometer with 18^o FOV field stop.

4.3.3 Vegetation biochemical indices

As values in the VNIR region of a spectrum are often used to calculate indices related to biomass and biochemical content of leaves a number of common vegetation indices have been calculated from the DRF spectra derived from the three modelled natural surfaces used in this research. The indices selected were Simple Ratio $(SR)_{680}$, SR_{705}, Normalised Difference $(ND)_{680}$, and ND_{705} for Chlorophylls; the structure-insensitive pigment index (SIPI); the plant senescence reflectance

Table 4.1: Differences between nominal FOV spectrum index values and DRF spectrum index values for a selection of biochemical VNIR indices in general use

Natural Surface	Index	ASD 10^o FO Min. spectrum	ASD 10^o FO Max. spectrum	ASD 10^o FO Mean of 360 spectra	GER 10^o FO Min. spectrum	GER 10^o FO Max. spectrum	GER 10^o FO Mean of 360 spectra
1	SR680	2.53	-31.73	-14.4	7.55	0.3	3.69
1	SR705	0.56	-5.14	-2.49	0.47	-2.18	-0.87
1	ND680	0.5	-4.71	-2.36	1.55	0.06	0.74
1	ND705	0.5	-4.42	-2.17	0.42	-1.92	-0.77
1	SIPI	1.52	-0.16	0.78	0.67	0.25	0.48
1	PSRI	0.43	-0.75	-0.3	1.1	-0.63	0.07
1	Antho.	9.38	-1.35	4.67	4.24	0.76	2.38
2	SR680	15	-16.1	1.54	7.36	-6.12	0.49
2	SR705	2.98	-2.79	0.31	0.37	-4.09	-1.72
2	ND680	3.22	-2.6	0.37	1.46	-1.07	0.1
2	ND705	2.69	-2.42	0.28	0.32	-3.51	-1.5
2	SIPI	0.85	-1.16	-0.14	1.13	0.2	0.66
2	PSRI	0.81	-0.68	-0.03	1.45	-1.71	-0.11
2	Antho.	5.23	-6.1	-0.7	7.54	-2.41	2.88
3	SR680	15.2	-26.07	-8.2	0.58	-12.47	-5.13
3	SR705	4.1	-4.72	-1.47	-1.82	-4.4	-2.96
3	ND680	3.62	-4.33	-1.45	0.12	-2.3	-0.99
3	ND705	3.84	-4.15	-1.3	-1.63	-3.88	-2.63
3	SIPI	1.68	-1.48	0.6	1.62	0.7	1.1
3	PSRI	0.78	-0.51	0.09	0.71	-0.8	-0.07
3	Antho.	9.15	-6.17	3.3	8.39	2.34	5.33
		ASD 18^o FO Min. spectrum	ASD 18^o FO Max. spectrum	ASD 18^o FO Mean of 360 spectra	GER FOP Min. spectrum	GER FOP at Max. spectrum	GER FOP Mean of 360 spectra
1	SR680	9.23	-5.15	0.59	-5.2	2.4	-2.32
1	SR705	2.01	-1	0.14	-3.4	-0.1	-2.06
1	ND680	1.91	-0.93	0.13	-1.2	0.28	-0.4
1	ND705	1.82	-0.88	0.13	-2.75	-0.7	-1.84
1	SIPI	0.31	-0.65	-0.05	0.75	1.35	0.87
1	PSRI	0.28	-0.14	0.02	0.37	0.54	0.23
1	Antho.	1.87	-3.76	-0.26	2.3	6.1	3.76
2	SR680	19.1	-3.68	7.31	-1.0	12.10	9.03
2	SR705	4.19	-0.66	1.5	-2.1	2.77	0.39
2	ND680	3.96	-0.61	1.41	-2.9	-0.29	1.93
2	ND705	3.74	-0.57	1.33	-1.8	2.45	0.33
2	SIPI	0.19	-1.37	-0.48	-0.55	0.89	0.10
2	PSRI	0.59	-0.09	0.21	0.32	0.81	0.57
2	Antho.	1.32	-8.33	-2.99	-3.82	3.90	0.01
3	SR680	4.83	-14.52	-6.91	-1.86	12.32	7.21
3	SR705	1.14	-2.96	-1.47	-3.94	2.20	1.17
3	ND680	1.09	-2.77	-1.37	-9.24	-2.87	1.35
3	ND705	1.07	-2.68	-1.33	-1.52	2.27	1.34
3	SIPI	1.13	-0.46	0.58	-2.66	1.55	-0.45
3	PSRI	0.31	-0.08	0	-0.21	0.27	0.10
3	Antho.	5.9	-2.3	3.0	1.82	3.68	2.97

index (PSRI) for Carotenoids/Chlorophylls ratios; and the Anthocyanins index. The rationale and formula for each is presented in Sims and Gamon (2002)[5]. For the ASD FieldSpec Pro with 10^o and 18^o fore optics and the GER 3700 with 10^o fore optic the maximum, the minimum and the mean differences between indices computed from the DRF spectra and the nominal FOV spectra at all rotational positions for each modelled natural surface have been determined. For the GER 3700 with fibre optic probe (FOP) only the DRF spectral indices at two opposite rotational positions and the average of these were calculated. These differences (Table 4.1), expressed as percentages of the nominal FOV indices, indicate the percentage error that could be expected in determining biomass or biochemical content from field spectroscopy measurements.

The SR_{680} index computed from the reflectance at 800 nm divided by the reflectance at 680 nm was found to be the least reliable for each instrument and for each surface, with, in the worst case, values ranging from 2.5% to -31.7% (from Natural Surface 1) determined for the ASD with 10^o fore optic. In general, the GER 3700 offered a slight improvement; in the worst case the differences ranged from -6.1% to 7.4%. However, the mean from all rotational positions for each instrument and each surface offered some improvement for the SR_{680} index, -14.4% for the ASD with 10^o fore optic spectra from Natural Surface 1. This could be foreseen as the greatest error between wavelengths used in these indices was observed with the ASD FieldSpec Pro from Natural Surface 1 at 680 nm and 800 nm (Figure 4.10(b)). The Anthocyanins (Antho.) index was also found to be less reliable than other indices when derived from ASD with 10^o fore optic modelled measurements, with differences of -6.2% to 9.1% from NS 3. This could also have been foreseen as this index is calculated from the sum of all reflectance values from 600 nm to 699 nm divided by the sum of

[5]The PRI index was not used as it generated negative numbers, due to the presence of the peat spectrum increasing reflectance at 570 nm, for both the DRF and nominal FOV spectra above that at 530 nm, and the results for the modified indices mSR_{705},and mND_{705} were similar to those displayed for SR_{705} and ND_{705}

all reflectance values from 500 nm to 599 nm at each rotational position. The differences for the other indices derived for the ASD with 10^o fore optic were approximately ± 5%; those for the GER 3700 with 10^o fore optic and the ASD with 18^o fore optic being marginally better at approximately ± 4%, indicating some advantage in measurements across a continuous field. The GER 3700 with FOP is considered separately as the FOV was not specified by the manufacturer so no baseline for comparison could be computed. Consequently, the DRF spectra were determined at only two rotational positions and the nominal FOV spectra were integrated over the area of measurement support determined from the DRF, both less rigorous comparisons than those for the other system configurations. Nevertheless, the same trends were seen as for the other three systems. The SR_{680} and Antho. indices were the least reliable, although these differences (7.9% and 6.1%, respectively), were in the main less than those observed for the other three spectoradiometer systems and the differences for the other indices were also less, -1.1% to 3.0% being the greatest range.

4.4 Conclusions

The intention of field spectroscopists is to measure the 'true' reflectance, (the measurand defined by the Joint Committee for Guides in Metrology (2008)), of the area of support for the measurement. However, in practice this cannot be achieved as there will always be intrinsic uncertainties in any physical measurement (Joint Committee for Guides in Metrology, 2009). One method often employed to improve the accuracy of the measurement of a quantity is to make multiple measurements then determine the arithmetic mean. The standard deviation of the measurements can then also be computed to indicate the precision of these measurements. This method, to improve accuracy, assumes that the measurements are normally distributed about a mean value that is the measurand.

However, there is always uncertainty as to the offset between measurand and the mean of the measurements. To minimise this uncertainty corrections should be made to account for systematic errors introduced by measurement system biases. However, spectroradiometer DRFs introduce systematic spectral and spatially dependent biases to measurements made and these biases are different for each spectroradiometer/fore optic combination even when the spectroradiometers are of the same type and from the same manufacturer. Therefore the field spectroscopist needs to know the DRF of each spectroradiometer/fore optic system to be used to make reflectance or radiance measurements to enable systematic bias to be assessed, corrections made and uncertainties stated.

In this work to try to account for the measurement DRF bias introduced into the modelled reflectances, while maintaining the area of measurement support defined by the fore optic FOV specified by manufacturers, the spectroradiometer was in effect rotated around the centre line of its fore optic for each surface/spectroradiometer system and multiple reflectance measurements modelled. However, irrespective of the number of measurements made and averaged, significant inaccuracies remained between the modelled measurands and model measurement means. These inaccuracies were wavelength and rotational position dependent, although in some instances an individual measurement closely approximated to the measurand (the ASD with 10^o fore optic when measuring Natural Surface 1 at a rotational position of 180^o, for example). In addition, the inaccuracies were surface dependent and also, possibly, related to the relative size and number of individual reflecting classes included in the modelled surface. Hence surface heterogeneity is interacting with the DRF of each instrument and is also influencing the inaccuracies of measurements being modelled.

While making field measurements, rather than laboratory measurements, with field spectroradiometer systems it would be impractical to make measurements from all of the rotational positions modelled in this work. Over at least one

quadrant, if not more, the spectroscopist, the spectroradiometer and any frame being used to support the instrument would shadow the area of measurement support directly or alter the light environment incident on the surface of interest by blocking a significant portion of the irradiance hemisphere. In addition, it is unlikely that the rotational resolution necessary to make the measurements modelled in this research could be achieved in the field. Only a greatly reduced number of measurements and from a limited number of rotational positions would therefore, probably, be practicable. As this work has demonstrated, any spectrum measured will be dependent on the DRF of the instrument/fore optic combination used; the size of each reflecting surface, relative to the other reflecting surfaces within the area of measurement support; and the radial distribution of individual reflecting surfaces within the area of measurement support relative to the positions from which the measurements were taken. For many natural Earth surfaces measured using field spectroscopy the spatial location and orientation of individual reflecting surfaces and their position relative to the field spectroradiometer and to the Sun can be considered to be chaotically and asymmetrically distributed. However, although it could not be predicted how accurate the mean of the measurements would be, it seems likely that the fewer measurements that were made the less accurate the mean would be.

It has been demonstrated in this work that there are significant differences between a spectrum that would be expected, given the nominal FOV specified by the manufacturer, and the spectrum that would be recorded given the measured DRF of a GER 3700 and an ASD Fieldspec Pro, and that the spectrum would be different for each fore optic used. These differences are instrument specific as, in the case of the ASD Fieldspec Pro, fibres in the fibre optic bundle are randomly distributed at the time of its manufacture and then distributed to each of the three spectrographs; while the response of the GER 3700 DRF will depend on the material used, the quality of optical components and the physical alignment

of the internal optical elements and spectrographs in each instrument. The DRF is also fore optic specific as, if a focusing element is present, its focal length and refractive index define the passage of light through it and if a bare fibre or field stop is used the DRF will be defined by the numerical aperture of each fibre in the bundle.

Therefore, as has been demonstrated in this work, variations between individual instruments of the same type and between different designs of instrument will significantly influence the spectra that would be acquired by each spectroradiometer/fore optic system even although the intention of field spectroscopists may be to measure the same area of a surface. Consequently, when spectra of the same surface acquired by different spectroradiometer/fore optic systems are compared they would appear to be measurements of different surfaces. This will therefore impact on the accuracy of spectral indices used to predict biochemical variables and on the comparability of the values of these indices when derived from spectra acquired by different spectroradiometer/fore optic systems. DRFs of field spectrometers and spectroradiometers may therefore explain some of the differences noticed by Castro-Esau *et al.* (2006) and others between indices determined from spectra of the same leaf surface when different instruments have been used to make the measurements. It will also have a similar impact on the utility of diagnostic absorption and reflectance features to classify heterogeneous Earth surfaces. In addition, as the spectra measured by each spectroradiometer/fore optic system from the same surface in the same rotational position display different profiles their utility for inclusion in Spectral Libraries is compromised. This may lead to errors in pixel classifications when these spectra are selected as endmembers in pixel unmixing image analysis methods.

If the spatial extent of the area of support is ill defined; if reflecting elements within the support are over- or under-represented in the composite reflectance

recorded; and if there are wavelength dependent biases in the reflectance measurement recorded then these errors will propagate though any subsequent analysis. It should also be noted that the 'steps' in the spectra evident at the join between the individual spectrographs, often attributed to thermal instability, may also be caused by each spectrograph in spectroradiometer measuring light from different regions of the area of measurement support. This has been amply demonstrated in this work as there were no 'steps' in the component spectra used or thermal effects being modelled.

The DRFs of the spectroradiometer models used in this work can be improved by the manufacturers. Indeed ASD have included an option to purchase an optical scrambler attachment for their system, and SVC, who manufacture the instrument that supersedes the GER 3700, include a redesigned fore optic, incorporating higher quality optical components than were previously available, and align the internal optics to greater tolerances. It is believed that these improvements will alleviate the asymmetry and spatial irregularity of the DRF of each instrument but measurements to validate this have yet to be made. Nevertheless, the physical principles of the propagation of light and the requirement to split light into its constituent spectrum for spectroradiometric measurement remain and will lead to each instrument having a characteristic directional response function.

Further research is also required into the effects that surface heterogeneity has on field spectroradiometric measurements, as only very simple Earth surfaces have been represented here. Field spectroscopists would also benefit if investigations into the effects of heterogeneity were coupled with research into alternative sampling strategies, for example multiple measurements from different areas of the surface of interest by random sampling or transect methods. If surface heterogeneity was then defined this could lead to recommendations for statistically robust field sampling strategies. One approach that has been adopted by some field spectroscopists to acquire an 'average' spectrum of a heterogeneous Earth

surface is by using a 'smearing' technique. This requires the fore optic or, in the case of the GER 3700, the instrument and fore optic to be moved over the surface while the measurement is being taken. This will therefore acquire a measurement integrated over a larger area than that defined by the spectroradiotometer/fore optic system when stationary. However, it is difficult to assess how replicable these measurements would be, as the degree of surface heterogeneity and the speed of movement and distance travelled will influence the spectrum acquired and area of measurement support defined. Nevertheless, the statistical validity of this method could also be investigated through further modelling studies. Research could also usefully be conducted by comparing the modelled DRF reflectance spectra generated from modelled Earth surfaces with spectra that would be acquired from the same surfaces by satellite optical sensors, using the point spread functions of those sensors, to better inform remote sensing scaling studies.

Chapter 5

Calluna vulgaris canopy spectral reflectance modelling

A. Mac Arthur[1] and T. Malthus[2]

[1] NERC Field Spectroscopy Facility, School of Geosciences, University of Edinburgh, Edinburgh, EH9 3JW UK.

[2] Environmental Earth Observation Program, CSIRO Land and Water, Black Mountain, ACT 2601, Australia.

This chapter is being prepared for submission to the *International Journal of Remote Sensing* for review.

5.1 Introduction

Northern boreal peatlands represent a large pool of particulate organic carbon sequestered from the atmosphere over millennia (Lindsay, 1995; Belyea and Malmer, 2004; Vitt, 2006). The sensitivity of these areas to environmental change

and their significance in the global carbon cycle, and consequently to climate change, is increasingly being recognised (Harris and Bryant, 2009a; Kurbatova *et al.*, 2009), as are the other ecosystem services they provide (Alcamo and Bennett, 2003; Charman, 2002; Scottish Natural Heritage, 2011; Bonn *et al.*, 2009a, 2010; Haines-Young and Potschin, 2009).

Despite their importance, peatlands have not yet been included in many global models of terrestrial-atmosphere CO_2 exchange (Le Quéré *et al.*, 2009). Furthermore, it remains unclear whether peatlands are currently a source or sink of carbon as the issue is an intractable one (Smith *et al.*, 2004). One of the reasons for some of this uncertainty may be sparse spatial sampling as a result of current field survey methods and their cost of implementation. For example, the soil carbon analysis for the UK recently conducted by Bradley *et al.* (2005) was based on a 1:250,000 scale soil map derived from a 5 km or 10 km point sampling grid depending on region. Furthermore, whether peatlands are a source or sink of carbon may also depend on local management decisions in some regions (Billett *et al.*, 2004).

Global environmental modellers recognise that "many key processes that control climate sensitivity ... depend on very small spatial scales" (Schaepman *et al.*, 2009). Therefore an increase in both spatial sampling and scientific understanding is needed to ensure that measurements and models of carbon sources and sinks capture the fine spatial detail (Ostle *et al.*, 2009) and do so at a scale which reflects local management decisions. Measuring the current state and dynamics of peatlands at such a fine scale is therefore of importance for modelling studies and to inform direct and indirect management decisions, from farming and recreational practices to climate change and environmental policies. Hence, a method to quantifiably and replicably measure and monitor the status and dynamics of peatlands across their areal extent, and in a manner from which carbon flux can be inferred, would be of benefit. Hyperspectral remote sensing (RS) from

airborne or satellite platforms may be one such method that could meet this monitoring need.

Within the UK, *Calluna vulgaris*, a hardy dwarf shrub, is the dominant overstorey plant species across extensive upland peatlands (Haines-Young *et al.*, 2000) and it may serve as an ecological indicator species, as its physiology and morphology are influenced by its environment (Gimingham, 1960, 1972). Much recent research has focused on the biophysical (Milne and Hartlet, 2001; Milne *et al.*, 2002), ecological (Simpson *et al.*, 1998; Hester and Baillie, 1998; Hester *et al.*, 1999; Cuartas *et al.*, 2000; Milne and Hartlet, 2001; Alonso *et al.*, 2001), and agricultural and conservation functions (Grant and Armstrong, 1993; Armstrong *et al.*, 1997; Read *et al.*, 2002; Pakeman and Nolan, 2009) of *Calluna* using field study methods. The biochemical function and nitrogen status of *Calluna* have also been investigated in pollution studies using laboratory and experimental approaches (Schjoerring *et al.*, 1998; Strandberg and Johansson, 1999; Carroll *et al.*, 1999; Pitcairn *et al.*, 2001; Leith *et al.*, 2004; Carfrae *et al.*, 2004; Kalaitzidis *et al.*, 2008). In addition, extensive research has been carried out into the rate of growth of *Calluna* and a model (HillPlan) developed to model its digestible (photosynthesising) biomass production in daily increments throughout growth and senescence cycles, given a range of ecological, environmental and grazing parameters (Grant and Armstrong, 1993; Palmer, 1997; Milne *et al.*, 2002).

All of the above studies have relied on *in situ* field measurements to acquire the required data but upland *Calluna* moors are extensive (normally thousands of hectares). For practical purposes field methods sample a restricted number of locations, each of limited spatial extent (possibly less than a square metre to, at most, tens of square metres). Data are then interpolated or extrapolated, with errors possibly unknown, across the spatial extent of the moors. Standard ecological field survey methods are either subjective and, therefore, change is difficult to assess reliably over time (Cherrill *et al.*, 1995; Cherrill and McClean,

1999; Egan *et al.*, 2000; Mücher *et al.*, 2010) or objective, time consuming and expensive (Wright *et al.*, 1997); in consequence rapid, quantifiable and replicable survey methods are needed.

Hyperspectral RS has been used extensively to measure and monitor ecosystems where light is the primary driver of metabolic processes and where spectral absorption and reflectance characteristics are indicative of ecosystem biophysical and biochemical form and function and their change over time (Ustin *et al.*, 2004b, 2009; Schaepman *et al.*, 2009). Nevertheless, little has been done to investigate the utility of this technique to measure or monitor physiological processes of *Calluna*. Kooistra *et al.* (2009) and Chan *et al.* (2010) have carried out some work to classify *Calluna* cover on peatlands from hyperspectral images but their analysis relied on mixture modelling and object-based methods and a pixel based decision tree approach, respectively. They did not investigate if the biochemical or biophysical functions of *Calluna* could be measured or if the change of *Calluna* over time could be assessed, although Kooistra *et al.* (2009) observed that due to the growth and senescence cycle of *Calluna* the timing of data acquisition was critical.

Yet hyperspectral RS potentially offers a method to repeatedly and quantifiably measure the development of *Calluna* over extensive peatland areas. However, for images acquired by hyperspectral RS to be used reliably, analysis methods need to be developed which enable the data-rich content of these images to be fully utilised. The inversion of radiative transfer (RT) reflectance models, to infer biophysical and biochemical properties from the spectrum at each pixel location in hyperspectral images offers one such approach.

RT models are physically based and mathematically describe the interaction of light with key parameters influencing reflectance (Rees, 2004; Liang, 2004). One such model is the Analytical Canopy Reflectance Model (ACRM), a two-layer

model developed by Kuusk (2003) to represent multi layer heterogeneous plant canopies. Either PROSPECT (Jacquemoud *et al.*, 1996) or LIBERTY (Dawson *et al.*, 1998) leaf radiative transfer models can be coupled to ACRM canopy layers and the model parameterised with, canopy structural variables, Sun zenith, view angles and a ground layer reflectance spectrum. The combined canopy/leaf reflectance model can be parameterised with key variables influencing reflectance and run in the forward mode to generate canopy reflectance spectra. Alternatively, ACRM can be parameterised with a reflectance spectrum and a range of variables constrained then run in inverse mode to infer biochemical and biophysical state variables from the spectrum (Kuusk, 2003). As one of the input variables for these canopy/leaf models is leaf area index (LAI) it may be possible to couple the HillPlan *Calluna* growth kernel[1] photosynthesising biomass output, converted to LAI, to the corresponding canopy/leaf model input and hence model canopy reflectances at discrete temporal intervals over annual growth and senescence cycles.

One complication of this approach is that the flowers on *Calluna* canopies can dominate visible reflectance during late summer but their profusion is also an indicator of *Calluna* vigour and consequently of underlying ecological condition (Gimingham, 1972). The reflectance of these flowers also needs to be considered if *Calluna* is to serve as an indicator species through growth and senescence cycles. A linear mixture modelling approach has been adopted by some researchers for other species, for example Chen *et al.* (2009) and Shen *et al.* (2010), to convolve the reflectance of flowers and the reflectance of canopies. This approach may be appropriate in the context of this research as *Calluna* flowers were separated from the other canopy components and reflectance spectra acquired during detailed plant component reflectance measurements made by Mac Arthur and Malthus (2012).

[1]Translated into a Matlab programme script by this author

To parameterise the ACRM for forward modelling knowledge of key state variable values is necessary and these need to be acquired from physical field measurements concurrent with the field spectral measurements acquired to validate modelled reflectances. Although a number of allometric methods are used extensively in ecological surveys, only canopy height measurement has been adopted during field surveys of *Calluna* for remote sensing research and has been used as an indicator of biomass or age (Egan *et al.*, 2000). However, measurement of *Calluna* canopy height is an unreliable indicator as the gross morphology, and hence height, of *Calluna* is affected by ecological and environmental determinants and moorland management decisions such as the use of muirburn and herbivore grazing levels. In addition, reliably measuring height in the field is difficult due to gaps in *Calluna* stand ground cover, the canopy of each shrub tending to form a dome and the mobility of canopies in the wind. *Calluna* stem diameter can also be measured in the field and could be related to age using dendrochronological growth ring methods but rate of stem growth will also be affected by ecological and environmental determinants. Correlations determined between diameter and age may therefore not necessarily be transferable between different ecological communities or geographical locations. However, LAI, a key parameter in both canopy modelling and carbon flux studies, and canopy structure can be estimated using optical plant canopy analysers (Chen, 196; Breda, 2003). This approach has previously been successfully adopted for shrub LAI estimation (Frank *et al.*, 2005).

In addition to being used to validate the results of RT modelling, field spectroscopy is often used to gain an understanding of the interaction of light with Earth surfaces and to facilitate hyperspectral image analysis (Milton *et al.*, 2009). By using field spectroradiometers high spectral and spatial resolution reflectance measurements of target Earth surfaces can be made. Field spectroscopy was used by Kooistra *et al.* (2009) and Chan *et al.* (2010) to record endmembers for their linear mixture modelling analysis of hyperspectral images of *Calluna* dominated

peatlands and has lately been used to investigate the pigments in *Calluna* leaves (Mac Arthur and Malthus, 2012) and canopies (Nichol and Grace, 2010). Field spectroscopy will be used in this work to calibrate ACRM and subsequently validate the spectra generated by the model.

The aim of this research is to determine if the reflectance of *Calluna* canopies and stands can be modelled through annual and inter-annual growth and senescence cycles. To do so quantitative field survey methods will need to be developed and a photosynthesising biomass growth model coupled to a multi layer canopy and leaf radiative transfer reflectance model. If the reflectance of *Calluna* canopies and stands can be forward modelled, it is hypothesised that in future hyperspectral images will be able to be used to estimate the biological and physiological state variables influencing reflectance and their change over time through inversion of the combined model developed in this work. The inversion outputs could then be validated by the field methods also developed in this work. This may then enable *Calluna* to be used as an indicator of peatland ecological condition and consequently of environmental change.

5.2 Research site and methodology

5.2.1 Research site

On the Smeath Hill research site, more fully described in Mac Arthur and Malthus (2012), eight stands representing visually distinct physiographic units of *Calluna* have been selected for field spectroscopy and hyperspectral RT research. Each of these stands represents a particular *Calluna* age class and spatial distribution growing in three ecological communities. Areas, approximately 10 metres by 20 metres centred on each of these stands, have been fenced to exclude grazing

Table 5.1: *Calluna* age class, substrate condition, and NVC ecological classification for each research plot

	Calluna age class	Substrate type	NVC class
Plot 1	Building*	wet peat	M19a
Plot 2	Degenerate*	dry peat	H10a
Plot 3	Mature*	dry peat	H10a
Plot 4	Layering†	wet peat	M19a
Plot 7	Mature to degenerate*	dry peat	H10a
Plot 8	Mature*	thin mineral soil	None - *Calluna* mono culture

* After Watt (1947)), † after MacDonald *et al.* (1995)

herbivores and the position of these fence lines located by differential GPS measurements. Data from six of these stands has been selected for the work reported here[2]. These stands contain *Calluna* at either its building, mature, degenerate or layering growth stages in either blanket bog (NVC class M19); dry heath (NVC class H10); or a *Calluna* monoculture micro community growing on a thin mineral enriched substrate (Table 5.1).

5.2.2 *Calluna* physical variable determination and growth model parameter collection

At monthly intervals from May to September 2005 three biomass samples were selected from each stand by randomly placing a 0.25 m^2 quadrat, subdivided into twenty five 10 cm cells, to delineate an area of *Calluna*. The proportion of *Calluna* ground cover was then visually assessed and recorded. A nadir digital photograph of the area within each quadrat was taken and the canopy height in this area determined by taking 5 measurements at random and averaging them. All *Calluna* stems within the quadrat were subsequently cut where they emerged

[2]The two pioneer research plots have been excluded from this work as the spectral reflectance of the small proportion of *Calluna* within them, relative to the proportions of graminoids and bryophytes, was dominated by understorey reflectances.

from the ground vegetation layer, the cut end of the stems wrapped in wet moss to minimise drying, and then sealed in bags for transportation to a laboratory.

At the laboratory the photosynthesising *Calluna* 'shoots and leaves' were separated from the woody stems, and each fraction weighed, oven dried at 60^{o}C for forty eight hours, and weighed again. These data were used to calibrate the HillPlan growth kernel. Additional *Calluna* biomass samples were selected at points chosen at random across the research site from the NVC M19 and NVC H10 communities at the end of May 2005. These additional samples were segregated into current years green shoots, and previous years green shoots and woody biomass, then weighed, dried and weighed again. This data was used to validate the calibrated *Calluna* growth model. Subsequently, biomass samples were again collected during May and June 2009 and canopy height measurements made again from quadrat samples within the six *Calluna* stands selected for this work. This biomass data was used to adjust the number of growth days each year used in the *Calluna* growth model so that the modelled output was within the range of the measured biomass values. In addition, during May 2009, *Calluna* stem diameter, at the point where the stem emerged from the understorey, and canopy height were measured, both at approximately 10 cm intervals along the same line that the LAI measurements were to be made, that is, perpendicular to the transect rail (the position of which will be discussed in the next section).

5.2.3 *Calluna* optical field measurements

Within each of the delineated research plots, a point was selected at random and a permanent transect positioned, orientated from East to West. A transect measurement approach was adopted as change over time was of interest and this approach allowed repeated measurements, with a reasonable degree of accuracy, of the same areas of each *Calluna* stand. To form these transects wooden batons,

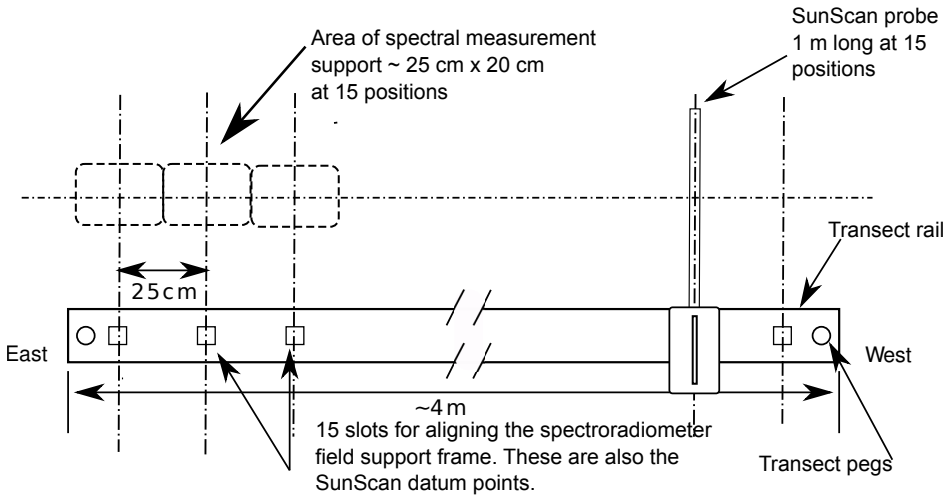

Figure 5.1: Optical measurement transect schematic

approximately four metres long with fifteen square slots, each 25 cm apart, were pegged to the ground for the duration of this research (Figure 5.1).

Field spectroscopy measurements were acquired from each of the research plots at approximately monthly intervals from April to October through the 2007 and 2009 growing seasons. A Spectra Vista Corporation (SVC) GER 3700 spectroradiometer with 10^o fore optic was used during 2007 and a SVC HR-1024 spectroradiometer with 8^o fore optic during 2009, both instruments measuring from 400 nm to 2,500 nm. The spectroradiometers were mounted, 1.5 metres and 1.8 metres respectively, above the canopy on a support frame the square foot of which was inserted into the square transect slot to ensure that spectra were acquired from approximately the same area at each measurement interval. The reflectance measurements of each plot were made in the same sequence at approximately the same time at each sampling interval to allow the change of reflectance to be compared and all measurements made within two hours of solar noon. Relative reflectance spectra were acquired, under stable illumination conditions, by first taking a calibrated reference measurement of a Spectralon reference panel then immediately taking a canopy reflectance measurement,

moving to the next transect slot datum and repeating this sequence. In addition, reflectance measurements were made of typical understorey vegetation from areas where there was no *Calluna* cover. All relative reflectance spectra were subsequently converted to absolute reflectance by convolving with the reference panel calibration coefficients.

To provide metadata for the spectral measurements, concurrent hemispherical images of sky conditions were acquired using a digital camera and simultaneously total and diffuse irradiance measurements made using a Delta-T SPN1 pyranometer. This metadata was assessed during spectral analysis to ensure that differences seen between reflectance measurements were not caused by changing irradiance conditions. The spectra from each plot were averaged to provide one mean spectrum for each plot at each sampling interval and the standard deviation (SD) per wavelength of these means calculated. These spectra and SDs were used to assess the accuracy of the modelled reflectances.

The use of a Delta-T SunScan plant canopy analyser enabled photosynthetically active radiation (PAR) penetrating *Calluna* canopies, and its spatial distribution along the length of the SunScan probe, which contained 64 individual PAR sensors, to be measured. The transect slots were also used as the datum points for these measurements. This again enabled measurements of the same area of the *Calluna* canopy to be made at each temporal sampling interval. Data from the first 17 of the 64 PAR sensors of the SunScan probe were discarded as light was found to be penetrating under the canopy from the probe insertion point due to the physical disturbance of the *Calluna* caused by inserting the probe. In the analysis only data from the remaining 47 PAR values, measured at each of the 15 transect datum points, was used. In addition, as non photosynthesising canopy components cast shadows on the photo-diodes, the measured PAR values required correcting by normalising for the proportions of woody biomass, determined during destructive sampling for each stand prior

to analysis. The SunScan measurements were not continued after the onset of flowering as these measurements were being made primarily to derive LAI and to infer photosynthesising canopy structure.

5.2.4 *Calluna* canopy reflectance modelling parameters

To investigate if *Calluna* canopy reflectance could be modelled, the coupled ACRM/LIBERTY model was used, as *Calluna* leaf reflectance has previously been modelled using LIBERTY by Mac Arthur and Malthus (2012). Attempts were first made to model the reflectance of the two *Calluna* stands with continuous ground cover (Plot 8, *Calluna* growing in mineral soil, and Plot 3, *Calluna* growing in dry peat). Then attempts were made to model the reflectance of a more heterogeneous stand (Plot 1 *Calluna* growing in wet peat). The daily biomass values for 2009 were first estimated by running the HillPlan growth kernel forward in annual runs from 2005 and then calibrated by adjusting the HillPlan kernel growth parameters so that the biomass output matched the measured biomass for the May 2009 sampling period. The LIBERTY model biochemical parameters, determined by Mac Arthur and Malthus (2012) were then scaled to the daily 2009 biomass values. Then the LAI values, determined from the SunScan data for each plot at each 2009 sampling interval (corrected for woody biomass), and the Sun zenith angle (calculated for each of the field spectroscopy sampling intervals) were used to parameterise the model. A bare peat spectrum was incorporated into ACRM as the ground layer reflectance and values for the remaining variables that were considered reasonable were used to initiate the model.

The modelled output reflectance spectra were then compared with the mean spectrum for each of the research plot transects. The ARCM Markov parameter and leaf modal angle were subsequently adjusted to determine if the modelled spectra could be matched to the measured average spectrum for each plot and

for each sampling interval, as will be discussed in the following section. This ACRM/LIBERTY canopy modelling approach was used until the mid July onset of *Calluna* flowering. From this point until the end of annual modelling the modelled daily output spectrum for each plot was linearly mixed with the average spectrum of *Calluna* flowers acquired from samples collected during the determination of *Calluna* by Mac Arthur and Malthus (2012) in proportions determined from the digital images of the plot canopies acquired at the field spectroscopy sampling intervals.

5.3 Results and discussion

5.3.1 *Calluna* stem diameter and canopy height

One-way analysis of variance (ANOVA) was carried out to determine if there were statistically significant differences between the means for the *Calluna* stem diameter data from each of the six research plots. No significant differences were found between Plots 1, 3 and 8 and Plots 4 and 7, although there were differences noted between these two groups and the means of Plot 2. This could be expected: the *Calluna* in Plots 3 and 8 visually appear from their gross morphology to be approximately the same age (mature) and Plot 1 appears to be approaching the end of the building phase; the *Calluna* in Plots 4 and 7 also appear to be approximately the same age (approaching the degenerative phase); and Plot 2 appears considerably older than the rest, in an advanced state of degeneration.

When the ANOVA was carried out on the height data from the six research plots the result was similar to that for the stem diameters, although this time the *Calluna* height mean for Plot 2 could not be differentiated from the means for Plots 4 and 7. This may be due to the *Calluna* in Plot 2 being in the degenerative

Table 5.2: *Calluna* stem diameter, canopy height and variances from July 2009 field survey data

	Mean stem dia. (mm)	Dia. Coeff. Var. (%)	Height (mm)	Height Coeff. Var. (%)
Plot 1	2.99	25	340	20
Plot 2	10.19	20	440	30
Plot 3	3.82	23	360	16
Plot 4	7.81	23	480	25
Plot 7	7.25	25	450	22
Plot 8	3.14	26	330	11

phase and its height reducing over the later stages of its life cycle as the canopy collapsed. It was observed during the course of this research that the mean height of Plot 2 fell from 620 mm, measured in July 2005, to 480 mm, measured in July 2009. However, as the height data was collected by random sampling, points where there were gaps in the canopy were recorded and a height value of zero assigned to that point. When these zero heights are included in the analysis the mean height of the canopies or stands with gaps is reduced, invalidating comparisons with canopies with either different proportions of gaps or those with no gaps. In addition, the sample size of the stem diameter and height means may not be sufficient to differentiate these plots as there were only 15 degrees of freedom for each, limiting how representative these sample means are of the population mean. Therefore, neither stem diameter or canopy height from this field survey could be used on their own to differentiate between these six *Calluna* stands.

However, when the coefficient of variation of the height data of each plot was computed these did indicate the variances expected (Table 5.2), as Plot 8 appeared to have the most homogeneous canopy cover, followed by Plots 3 and 7 (both growing in dry peat), then Plots 4 and 1 (growing in wet peat), and finally Plot 2 which, although growing in dry peat, is a degenerate *Calluna* stand. Hence, variability of inter stand canopy height may be a better indicator of *Calluna*

Table 5.3: Result of one-way analysis of variance of SunScan individual photo diode PAR values

Sampling interval	Plot 1	Plot 2	Plot 3	Plot 4	Plot 7	Plot 8	Direct irradiance (%)
April 2008	Plot 4	Yes	Yes	Plot 1	Yes	Yes	80
May 2008	Plot 2	Plot 1	Yes	Yes	Yes	Yes	80
June 2008							
April 2009	Yes	Yes	Plot 7 and 8	Yes	Plot 3 and 8	Plot 3 and 7	48
May 2009	Plot 2	Plot 1	Plot 7	Yes	Plot 3	Yes	85
June 2009	Plot 2	Plot 1	Plot 7	Yes	Plot 3	Yes	77
July 2009	Plot 2	Plot 1	Yes	Yes	Yes	Yes	80

Table note - "Yes" indicates where there were significant differences between the PAR values of the plot in the column header and the values of all other plots. The plot number in the matrix indicates the plot or plots where there were no significant differences between these and the plot listed in the column header.

growth stage and the ecological class of the area in which it is growing than mean height values.

5.3.2 *Calluna* stand classification from physical and optical data

ANOVA was again carried out to investigate if the SunScan PAR measurement values could be used to distinguish *Calluna* stands. Although significant differences between some of the PAR means were noted at some sampling intervals, not all differences were significant. The confusion matrix in Table 5.3 indicates where there were significant differences ($p<0.05$) between PAR value means for each plot and all other plots and those where the differences were not statistically significant, indicated by the respective plot number or numbers. The April 2009 ANOVA results, when measurements had been made under cloudy conditions

(the proportion of direct solar irradiance to total irradiance was relatively low), were found to be inconsistent with the other measurements made under clear sky conditions (Table 5.3). At the other sampling intervals the differences between the means of both Plots 1 and 2 and Plots 3 and 7 were not significant. However, it was noted earlier that there were significant differences between the stem diameter means for both Plots 1 and 2 and Plots 3 and 7. When two-way ANOVA was carried out on the plot mean PAR values, with mean stem diameter as the second factor, statistically significant differences ($p<0.001$) were noted between all plots at all sampling intervals except for the April 2009 one. Hence, SunScan mean PAR values with stem diameters as a second factor can be used to differentiate *Calluna* canopies at the Smeath Hill research site when the percentage of direct to total irradiance is greater than approximately 77%.

5.3.3 *Calluna* stand structural parameters inferred from optical data

The SunScan data can also be used to infer *Calluna* stand structural parameters. By comparing the statistical distribution of data from each research plot with the data from the same plot at the other sampling intervals (Figure 5.2), it can be inferred that the canopy in each research plot is closing over the growing season, as the range between the 25th and 75th percentiles reduces; and that the canopy density is increasing, as the median PAR values are decreasing, since there are a greater number of points along the Sunscan probe where little or none of the light incident on the canopy is penetrating and being recorded. It can be also be inferred from Figure 5.2 that Plot 4 is the least dense stand, as it has the highest median PAR value at each sampling interval and Plot 8 has the most dense stand, as it has the lowest median PAR value. The median values of Plots 2, 1, 3 and 7 decreasing in that order fall between these two extremes.

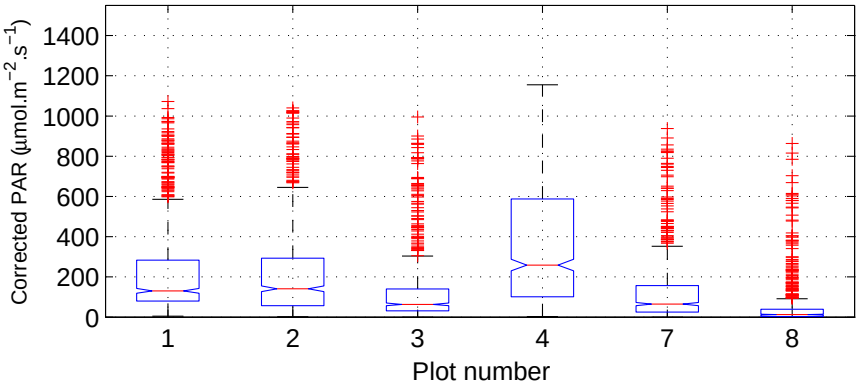

(a) May 2009

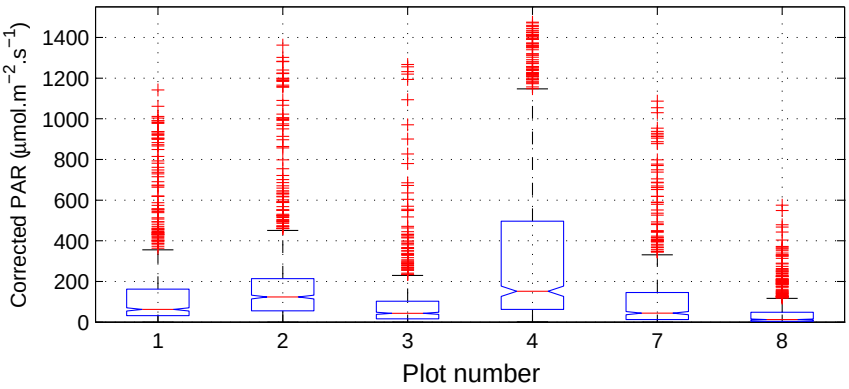

(b) June 2009

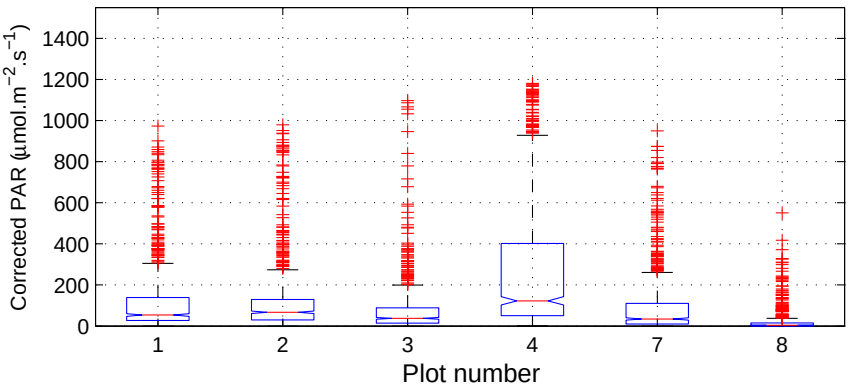

(c) July 2009

Figure 5.2: Statistical distribution of PAR values for points along the SunScan probe at each transect measurement point in each research plot

Calluna stand LAI was also determined from the SunScan data. However, as the data had been collected as PAR values these required to be converted to LAI using 'Wood's equation'[3] (Potter *et al.*, 1996). 'Woods equation' was parameterised with a leaf angle ellipsoidal distribution value of 1.00 (estimated from digital images of *Calluna* canopy vertical profiles after Potter *et al.* (1996)); the SunScan PAR values discussed previously; the fraction of total and diffuse irradiance recorded during each SunScan measurement; and the SunScan default leaf absorption coefficient of 0.85. However, corrections had to be made for the proportion of woody stems and branches present at the location of each measurement as these vary between the *Calluna* classes, with degenerate *Calluna* having the greatest proportion and building *Calluna* having the lowest. Kucharik *et al.* (1998) proposed a method to adjust for the shading effect of woody elements in indirect LAI measurements of forest canopies. However, it was considered that the close proximity of *Calluna* stems to the SunScan probe and the lack of detailed knowledge on the spatial distribution branches and other woody elements precluded the use of this method.

The SunScan LAI values for each sampling transect were therefore normalised by the respective proportion of woody biomass determined during destructive sampling in 2005. LAI was then calculated for each research plot at each sampling interval using 'Wood's Equation' (Potter *et al.*, 1996). However, the correlation observed between the LAI values and stand photosynthesising biomass (Figure 5.3) was not strong and it was noted that the LAI values for Plot 8 tended to be outliers. Gap fractions and clumping of needles in conifer canopies are known to lead to underestimates of LAI (Chen and Cihlar, 1995; Smolander and Stenberg, 2003; Simic *et al.*, 2010). It was therefore considered that the LAI values for Plot 8 may be the most accurate as this stand visually had no leaf clumping or canopy gaps evident. However, all the LAI values measured during 2009 (Figure 5.4)

[3]Provided by J. Wood of Peak Designs for use in this work

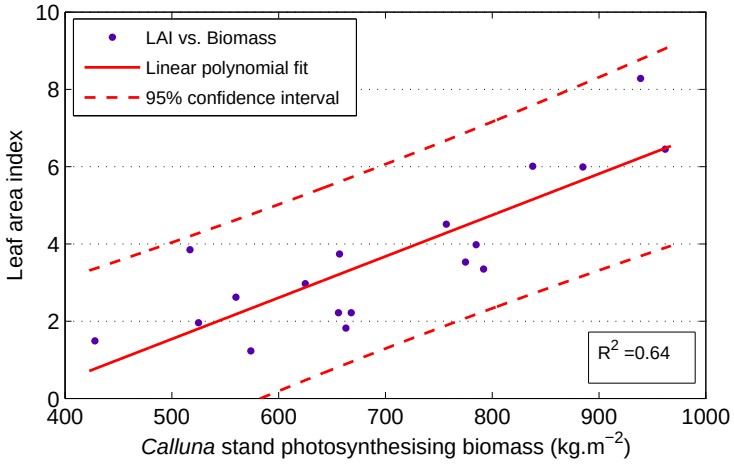

Figure 5.3: Correlation between SunScan derived LAI, corrected for woody biomass, and *Calluna* photosynthesising biomass

do follow an annual trend similar to the photosynthesising biomass values trend modelled using the *Calluna* growth kernel, initially falling until the beginning of summer then rising (Figure 5.5).

The proportion of gaps in the ground cover of each of the *Calluna* stands, delineated by each research plot, could also be assessed from the SunScan data. A range of PAR threshold values, in increments of 50, between 200 μmol/m^2/s and 800 μmol/m^2/s were selected after visual assessment of Figure 5.2 and the percentage of the total number of individual photo diode PAR values greater than these increments calculated. A PAR threshold value of 400 μmol/m^2/s was found to result in a percentage of gaps for each *Calluna* stand that reasonably closely matched those assessed visually with the aid of a quadrat during field surveys. These percentages, converted to ground cover rather than gaps in cover, are included in Table 5.4 and all, except the the estimate for Plot 1 and Plot 2, are within $\pm$5% of the visually estimated values.

As there was a four year gap between the biomass measurements and the SunScan measurements stand cover would be expected to increase and the estimated

Table 5.4: *Calluna* stand ground cover estimates from July 2005 by quadrat survey and from the July 2009 SunScan field survey

	Plot 1	Plot 2	Plot 3	Plot 4	Plot 7	Plot 8
Estimate by quadrat (%)	77	90	90	70	88	93
Quadrat coeff. var.(%)	20	32	8	23	26	4
Estimate by SunScan (%)	72	73	93	75	93	96
SunScan coeff. var (%)	24	32	12	25	28	10

ground cover be higher in 2009 than in 2005 but this is not evident for two of the stands (Table 5.4). The higher ground cover value from the 2005 visual survey than the estimate from the SunScan data for Plot 2 is probably due to it being the degenerate stand and the shrub canopy collapsing causing an increase in the number and size of stand gaps. However, the reason for the lower ground cover estimate for Plot 1 during 2009 than during 2005 is not clear, although leaf clumping, canopy gaps and proximity of the canopy to the SunScan probe may be the cause.

5.3.4 *Calluna* photosynthesising biomass growth model (HillPlan) calibration and validation

A key factor affecting the growth rate of *Calluna* is substrate type. Consequently, provision has been made within HillPlan for it to be parameterised with an appropriate variable. As three distinct soil types - thin mineral soil, dry peat, and wet peat- were identified at the Smeath Hill research site the appropriate type (Table 5.1) was used to parameterise the growth kernel to model photosynthesising biomass growth for each research plot. As no continuous meteorological data for Smeath Hill was available, data from the nearest Met Office station (Bishopton, approximately 5 km west of the research site) were extracted from the Natural Environment Research Council British Atmospheric Data Centre records. Mean

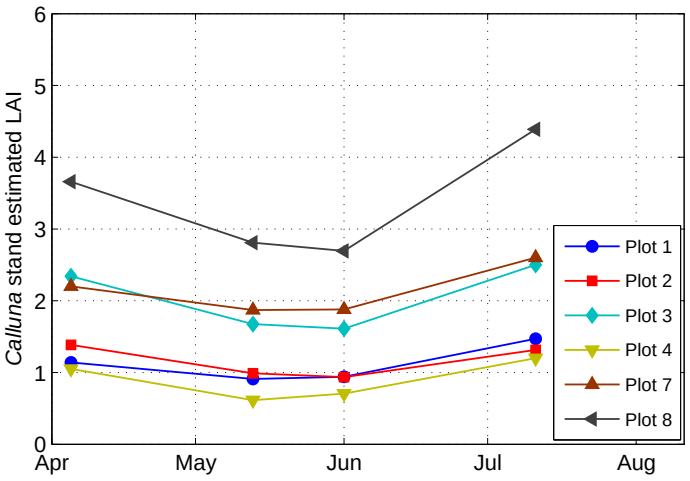

Figure 5.4: Leaf area index annual trends 2009

Table 5.5: Coefficients of variance of LAI measurements during the 2009 sampling intervals

	Plot 1	Plot 2	Plot 3	Plot 4	Plot 7	Plot 8
April	31	57	42	73	50	25
May	42	51	34	50	45	31
June	43	66	28	81	48	29
July	31	59	41	72	48	24

air temperature was corrected for differences in altitude between the Met Office station and Smeath Hill, using a lapse rate of $0.63^o/100$ m after Smithson and Atkinson (2008), as it was noted that a 0.5^o change in mean temperature caused a 5% variation in modelled annual biomass production. The initiating photosynthesising dry matter biomass value for each substrate type was selected to match that measured at the May 2005 sampling interval, as the biomass measurement SDs were lowest at that time.

As the LAI data for each of the *Calluna* stands appear to form three distinct groups (Figure 5.4) and each group corresponds to a soil type, data from one

of each was selected for *Calluna* stand reflectance modelling. The selected plots were Plot 1 and Plot 3 as they had the lowest coefficient of variance in their groups (Table 5.5) and Plot 8. The *Calluna* growth kernel was first initiated for these three plots, for the 2005 modelling period, using the growth start and end dates and growth and senescence constants contained within the model. However, it was observed that the projected *Calluna* biomass for each of the three soil types then did not fall within one SD of the mean of the measured values at the corresponding sampling intervals and these differences became progressively worse through the growing season. Consequently, through an iterative process of model parameterisation, analysis of output, parameter adjustment and output reassessment, the optimal values for the growth start and end dates and growth and senescence constants were determined for the Smeath Hill research site.

This iterative process resulted in the growth initiation date supplied with the model being used. However, the growth end date needed to be adjusted for each soil type, with an end date two weeks earlier than that provided with the model found to result in the best fit for the dry and wet peat substrates, while an end date one weeks later was required for the mineral soil substrate. In addition, a production constant of 0.99425 for new biomass growth was required rather than 0.997739, the value provided with the model, indicating that the *Calluna* is less productive per unit time at Smeath Hill than in the areas used to develop the model. That productivity of *Calluna* is lower at Smeath Hill, at a higher altitude and on the wetter west coast of Scotland, seems reasonable given that the model was derived from data collected on the east coast of Scotland and the more productive English uplands. However, the senescing biomass constant provided was found to give reasonable results. When the revised growth end dates and production constant were used a reasonable fit was achieved between the measured and modelled data, as can be seen from Figure 5.5. In this figure an indication of the total photosynthesising biomass modelling error, determined

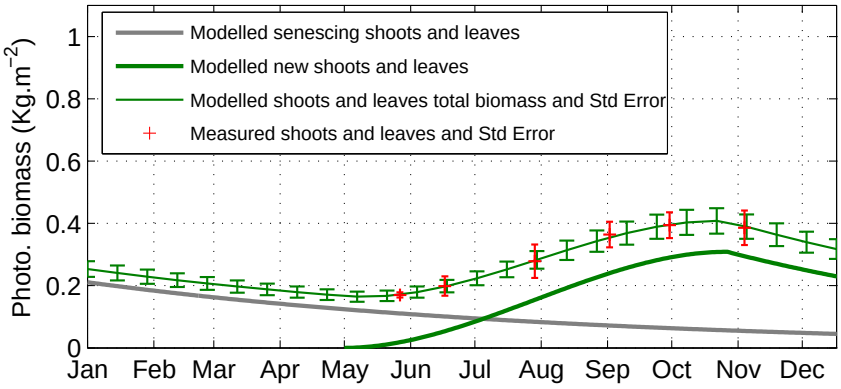

(a) Plot 8 - mineral soil

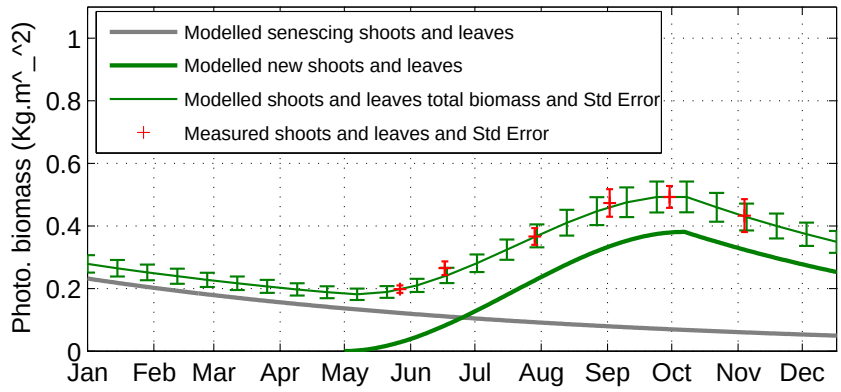

(b) Plot 3 - NVC H10

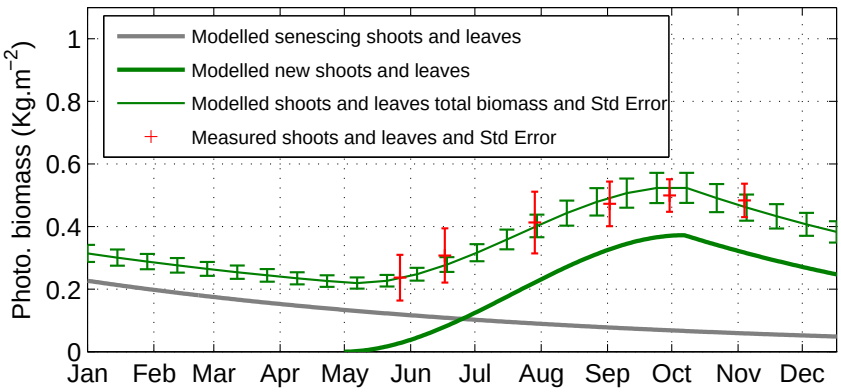

(c) Plot 1 - NVC M19

Figure 5.5: Modelled and measured photosynthesising biomass 2005 with error bars of one standard error either side of the mean shown, after model adjustment

from the data provided by MLURI and used to produce the *Calluna* growth kernel, has been included.

The greatest annual production of photosynthesising biomass was found for *Calluna* growing in the dry peat substrate (Figure 5.5(b)). *Calluna* growing in the wet peat substrate (Figure 5.5(c)) produced slightly less than that in dry peat and the lowest annual production was noted for *Calluna* growing in the mineral soil (Figure 5.5(a)). The differences between modelled and measured biomass were greatest for the wet peat *Calluna* stand (NVC M19) (Figure 5.5(c)) where the maximum difference was 10% and the measurement SD was also greater than that modelled. The annual growth start and end dates supplied with the model are subjective as these parameters are difficult to determine and are influenced by annual weather. Hence differences between the values used to develop HillPlan and those required to parameterise the *Calluna* biomass growth model for Smeath Hill were to be expected. That *Calluna* may have a longer growing season on mineral soil than on the other soil types was not expected and the reasons for this are unknown.

Although the *Calluna* photosynthesising biomass model was now calibrated for annual use, to be of use in phenological studies and the long term monitoring of *Calluna* dominated peatlands it is necessary to validate the annual outputs of the model over successive inter-annual cycles. To achieve this the model was parameterised with the variables previously determined for the Smeath Hill research site, initiated with the measured 2005 biomass values and the mean annual temperature for each year, determined as previously discussed, and the model run for the years 2006, 2007, 2008 and 2009 for each of the three soil classes. The 2009 modelled photosynthesising biomass production for each soil class was then compared with the field sampled biomass carried out during May of that year and the growth start and end dates again adjusted until the modelled 2009 biomass for each plot approximated to the mean measured biomass and the

modelled values were within one SD of the mean. This required adjustment of up to a maximum of ±7 days for the growth start and end dates. These values were considered reasonable, given annual meteorological change.

5.3.5 *Calluna* canopy reflectance modelling and measurements

A control graphical user interface (GUI) for ACRM/LIBERTY, developed during this research[4], was used to determine which of the variables included in the model had the greatest influence on reflectance. LAI and the Markov canopy scattering parameter, along with the parameters previously noted by Mac Arthur and Malthus (2012) to be of importance in the LIBERTY model, were then included as parameters which could be varied within the ACRM/LIBERTY component of the *Calluna* growth and senescence reflectance model being developed. Values for these and the other variables used to parameterise the canopy reflectance model were then determine as described in the following paragraphs.

LAI values for inclusion in ACRM were determined by fitting a cubic polynomial, as *Calluna* growth was not linear (Figure 5.5), to the biomass values modelled for Plot 8 (Figure 5.5) then scaling this data to the corresponding LAI measurement values (Figure 5.4) to give LAI values in daily increments. This resulted in a maximum LAI value of 9 in October. This was considered reasonable as when the LAI value was increased above this in ARCM it had no further effect on reflectance. Therefore at this LAI value the canopy is an infinite reflector (analogous to that for stacked needles described by Dawson *et al.* (1998)) and all light is either being absorbed or reflected by the canopy. That little or no light

[4]This interface was developed by M. Hagdorn of the School of Geosciences, University of Edinburgh with assistance from this author.

penetrates through to the understorey of Plot 8 was evident from there being no higher plants at that level, only bare peat.

The LAI values determined from the SunScan data for the other plots, were not considered reliable due to the effect of canopy gaps and leaf clumping previously discussed. Therefore the biomass to LAI conversion coefficients derived for Plot 8 were used to derive LAI values for the other plots from their modelled biomass. These values were corrected for the percentage canopy ground cover for the stand being modelled and were used to parameterise ACRM for the respective stands.

The leaf ellipsoidal distribution used to calculate LAI from the SunScan PAR data; an average Ångström turbidity coefficient value of 0.2, determined from the solar total:diffuse ratio recorded during SunScan measurements after Pinazo *et al.* (1995); and a nadir view angle were used to parameterise ACRM and these values kept constant for each modelling interval and for each *Calluna* stand being modelled. In addition, the Sun zenith angle at solar noon on the day of each modelling increment and the leaf size parameter (average leaf length of 1.5 mm divided by the respective plot average canopy height) were used. Subsequently, a Python programming script was written[5] to link the *Calluna* growth model to the ACRM/LIBERTY canopy reflectance model. This resulted in a ACRM/LIBERTY/*Calluna* growth and senescence model which could generate *Calluna* reflectance in daily increments from April through to the beginning of October for each year chosen to be modelled.

The combined ACRM/LIBERTY/*Calluna* growth reflectance model was first parameterised with the LIBERTY values, incorporating the photosynthesising biomass (kg/m^2) for Plot 8 (the most homogeneous *Calluna* stand) and the pigment content ($\mu g/g$ photosynthesising biomass) determined by Mac Arthur and Malthus (2012); the LAI values determined in this work for Plot 8; the

[5]This was written by M. Hagdorn with assistance from the author.

remaining ACRM parameters discussed previously; and a bare peat spectrum for the ACRM ground reflectance layer. The model was then run in daily increments from the beginning of April 2009 to mid July 2009 (just before the onset of flowering). Significant differences were noted between modelled and mean reflectances measured at each field spectroscopy sampling interval during 2009 across the near infra-red (NIR) region of the spectrum. These differences were in both percentage reflectance and in the shape of the slope of the NIR plateau between 800 nm and 900 nm.

The slope of the NIR plateau had been found during sensitivity analysis to be influenced by the Markov parameter, a scattering property related to canopy vertical geometry and leaf clumping (Kuusk, 1995). The vertical structure of *Calluna* canopies varies, with dead and senescing leaves being concentrated in the lower layers, and canopy density decreases while height through the canopy increases as adventurous individual long shoots project upwards. By manipulating the Markov parameter, a value was determined that allowed the slope of the modelled reflectance across the NIR plateau to approximate to that of the reflectances measured at each sampling interval.

However, the percentage reflectance of the modelled spectra across the NIR region was also lower than that measured. The NIR region has been reported by Moorthy *et al.* (2008) and Mac Arthur and Malthus (2012) to be most sensitive to changes in the LIBERTY inter-cellular airspace parameter. This parameter was subsequently adjusted and, although the values followed the same trend, and started from and ended with those values determined by Mac Arthur and Malthus (2012), they increased gradually to a maximum in mid July, approximately 100% greater than Mac Arthur and Malthus (2012) had determined for stacked 'shoots and leaves' (Figure 5.6). This difference in NIR scattering may be due to the leaves adopting a rolled form, after having been removed from the plant, resulting in less scattering (at a scale related to the inter cellular airspace parameter) than when the leaves

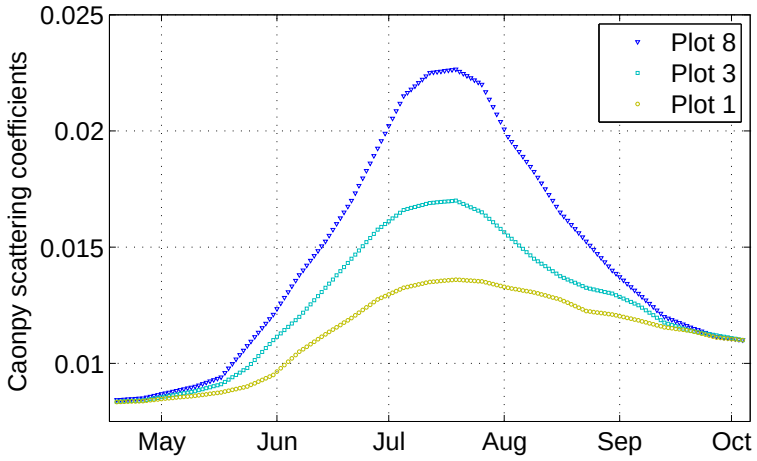

Figure 5.6: Canopy and leaf scattering coefficients

are attached to the plant. *Calluna* leaves have evolved a degree of tolerance to drought by being able to adopt a rolled form which protects the stoma on the abaxial surface of the leaves (Albert *et al.*, 2011). The abaxial surface also has trichomes which shade the stoma and may increase the NIR scattering when the leaves are not rolled. Therefore the form of, and the presence of trichomes on, *Calluna* leaves when they are not experiencing drought or have been removed from the stems may necessitate this increase in the LIBERTY inter cellular airspace values.

As *Calluna* is a flowering species, the influence of flowers on reflectance from July to October, the period when flowers are present, also requires to be considered. Nadir digital photographs taken of the *Calluna* canopies at each spectral measurement point during the late August 2009 sampling interval (the period of maximum flower cover) allowed the proportion of the canopy covered by flowers to be visually estimated. The mean spectrum of 'purple' flowers, measured during laboratory work by Mac Arthur and Malthus (2012), was linearly mixed in increasing proportions with the reflectance spectra modelled for Plot

8 from mid July to mid August, when the estimated maximum proportion of flower was reached. Similarly, the mean spectrum of 'senescencing' flowers was introduced at the beginning of September and gradually replaced the 'purple' flower spectrum through to the end of modelling. These mixture modelled reflectance spectra for Plot 8 were then compared with the measured reflectances and the corresponding sampling intervals and the inter-cellular airspace variable again adjusted to provide a set of values which enabled the modelled reflectances to be within the measured reflectance ranges, as indicated by reflectance at 800 nm in Figure 5.7(a), for this stand from April to October 2009. In Figure 5.7(a) modelled reflectance at 800 nm can be seen to rise only very gradually from the beginning of modelling until early June, rises more rapidly until early August, then gradually falls to the end of modelling.

The LAI values, estimated for Plot 3 from its modelled biomass data; a bare peat spectrum as the ground layer reflectance; and the inter-cellular airspace values determined previously were subsequently used to model the reflectance of *Calluna* growing in Plot 3. However, again the modelled NIR reflectances were not within the range of the measured reflectances. The inter-cellular airspace variable was again adjusted as previously discussed and values were determined which followed the same trend as for Plot 8 but this time reached a maximum approximately 50% greater than that determined by Mac Arthur and Malthus (2012) for the mid July sampling interval (Figure 5.6). When these values were used, and the 'purple' and 'senescing' flower spectra linearly mixed with the modelled stand spectrum, following the method used for Plot 8, in the proportions visually assessed from digital photographs for Plot 3, a reasonable match was again achieved between modelled and measured reflectance in the NIR region, indicated at 800 nm in Figure 5.7(c), for this stand from April to October 2009. For Plot 3 modelled reflectance at 800 nm (Figure 5.7(c)) can be seen to rise only very gradually from the beginning of modelling until early June then rise more rapidly until early

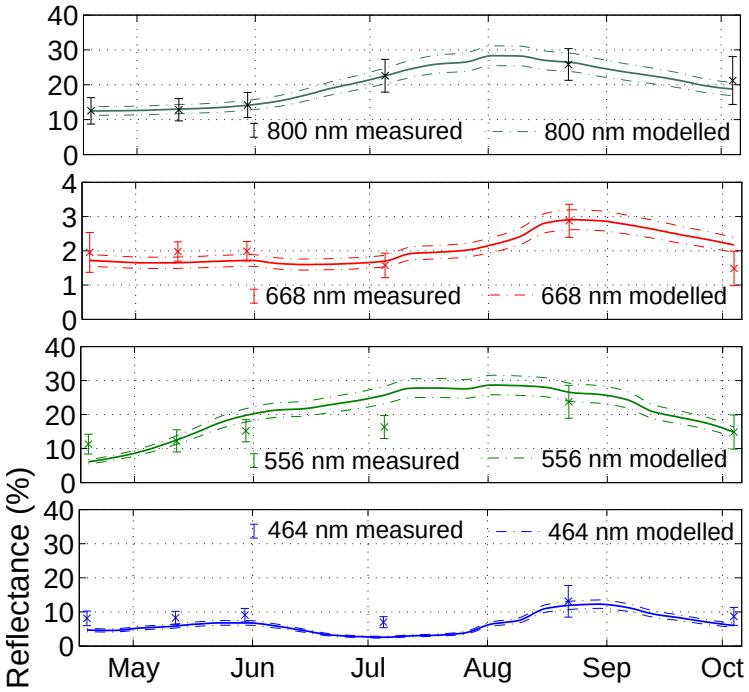

(a) Mature *Calluna* on mineral soil 2009 (Plot 8)

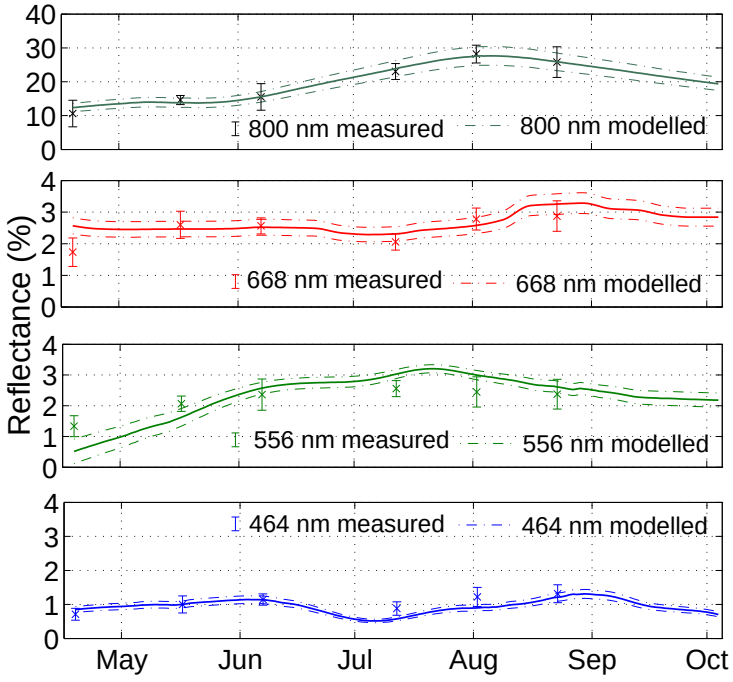

(b) Mature *Calluna* on mineral soil 2007 (Plot 8)

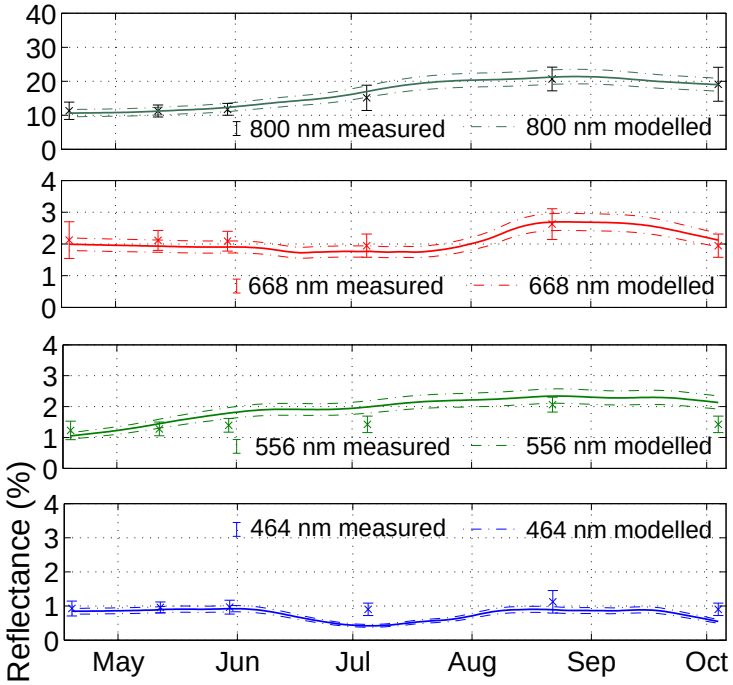

(c) Mature *Calluna* NVC H10 2009 (Plot 3)

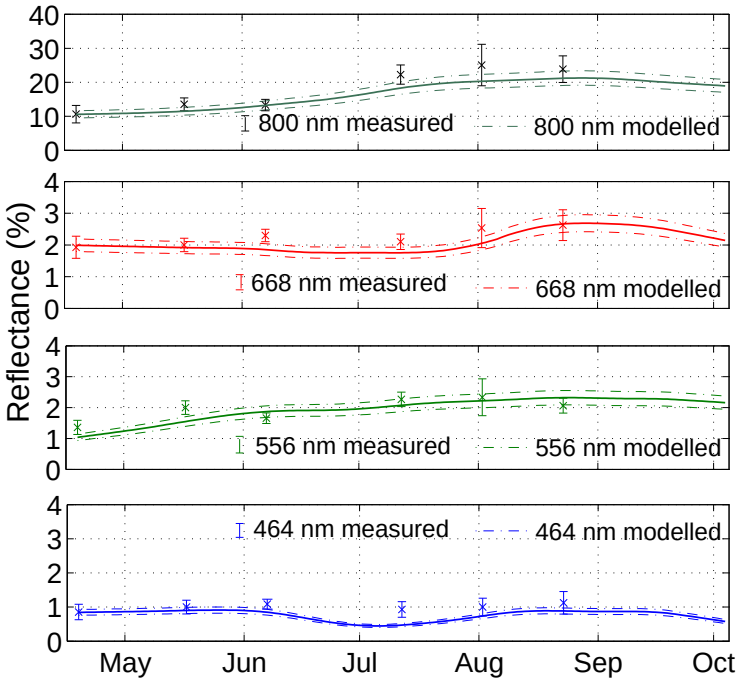

(d) Mature *Calluna* NVC H10 2007 (Plot 3)

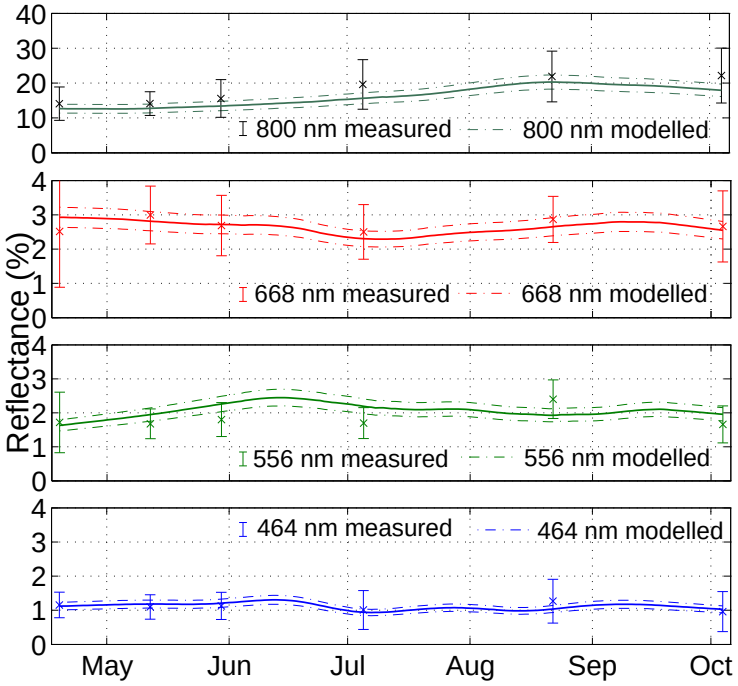

(e) Building *Calluna* NVC M19 2009 (Plot 1)

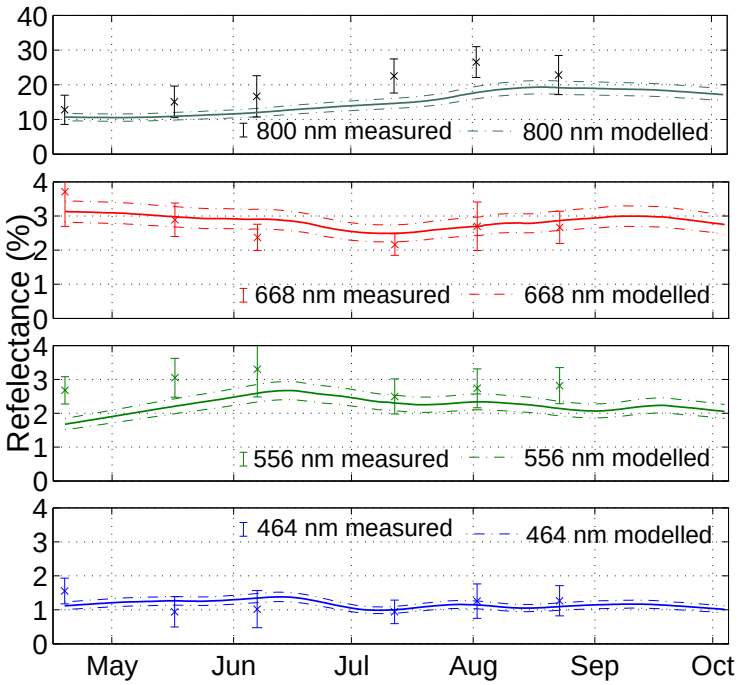

(f) Building *Calluna* NVC M19 2007 (Plot 1)

Figure 5.7: Modelled *Calluna* reflectance at four wavelengths, with a confidence interval, and with the mean measured reflectances and error bars of one standard deviation either side of mean, for three research plot types

August and gradually fall to the end of modelling, although both the rise and fall are more gradual than for Plot 8 and the maximum reflectance is also lower.

As ground cover was incomplete in Plot 1 (the stand containing building *Calluna* growing in wet peat) understorey graminoids and bryophytes contributed to the gross reflectance recorded. Understorey spectra had been acquired from Plot 1 at each field spectroscopy sampling interval during 2009 and, after linear interpolation per wavelength interval to daily increments, these were included in ACRM as the ground layer reflectances. LAI was again determined from the modelled biomass and adjusted for canopy cover. The inter-cellular airspace values were scaled from those used for Plot 3 by the differences in LAI, as it was considered that the scattering influencing NIR reflectance was a function of the leaf area present (Figure 5.6). The 'purple' and 'senescing' flower spectra were then linearly mixed in the observed proportions as before. When the NIR reflectance at 800 nm, from April to October 2007 for Plot 1, is compared to the measured reflectance the means are not as well aligned (Figure 5.7(e)) as they were for the two continuous cover *Calluna* stands. The mean reflectance spectra from this plot contain a contribution from understorey directly below the *Calluna* canopy, in a proportion related to the LAI; areas where only understorey reflectance was measured and composite measurements of both understorey and canopy, determined by the stand structure along the line of the transect. This variability of reflecting surface is evident for the increased range of the measured reflectance indicated by the error bars being longer for these reflectance measurements at 800 nm (Figure 5.7(e)) than displayed from the stands with more homogeneous cover (Figure 5.7(a) and 5.7(c)). The reflectance at 800 nm for this plot also followed the same trend as Plot 8 and Plot 3 but its rise and fall were more gradual and the maximum lower than that modelled for Plot 3.

The modelled biomass values for 2007 for each plot, the pigment content and LAI values derived from this and the other model parameters previously described

were subsequently used to parameterise the ACRM/LIBERTY *Calluna* growth and senescence model, to investigate if inter-annual change in reflectance could be modelled. A reasonable fit between modelled NIR reflectances and measured reflectances for the most homogeneous stands, displayed for Plot 8 at 800 nm (Figure 5.7(b)), was again achieved. However, the modelled reflectances for Plot 3 for 2007 were an underestimate when compared with the measured reflectances (Figure 5.7(d)) and the underestimate for Plot 1 reflectances was even greater (Figure 5.7(f)). The measured reflectances at 800 nm for Plot 1 during both 2007 and 2009 are generally higher than the modelled reflectances indicating that, possibly, either inter cellular airspace values scaled from those determined for Plot 3 or the LAI values derived from the modelled biomass were an underestimate, or both were. Both the airspace and LAI values for Plot 3 and Plot 1 were estimated from those of Plot 8 by assuming linear relationships and this may not be the case as canopy density decreases. Furthermore, as Plot 1 is the most open canopy being modelled, the stand ground cover value may be an underestimate as it was derived from the SunScan PAR values and these are affected by canopy gaps and leaf clumping effects previously discussed for LAI derivation, although Potter *et al.* (1996) consider this less likely.

To further investigate the influence of LAI on the contribution made by understorey reflectances, data from the mid July 2009 sampling interval were selected, as this is before the influence of flowers on reflectance. When a LAI value of 2.5 was used to model Plot 1 canopy reflectance, and the graminoids and bryophytes understorey reflectance was excluded, the reflectance at 800 nm reduced from 18.7% to 17.4%, a change of approximately 7%. When a LAI value of 5, the value at the mid July 2009 modelling interval, was used to model Plot 1 reflectance, and understorey reflectance was excluded, reflectance at 800 nm fell from 24.7% to 24.0% a change of approximately 3%. This indicates the importance of including an understorey reflectance spectra within the ACRM/LIBERTY *Calluna* growth

and senescence reflectance model when LAI values are lower than approximately 7.5 but that for LAI values greater than this understorey reflectance does not contribute when there is complete *Calluna* ground cover.

Only the NIR region of the spectrum, the region most influenced by biomass and leaf structure, has been discussed so far. However, the visible region of the solar spectrum, the region in which leaf pigments dominate reflectance, was also modelled and measured.

The modelled reflectance in the red region of the spectrum, is displayed in Figures 5.7(a), 5.7(c), and 5.7(e) at the wavelength of maximum Chlorophylls absorption (668 nm) determined by Mac Arthur and Malthus (2012). The modelled reflectances follow the same trend as the measured reflectances and the range of measured reflectances, indicated by the error bars, overlap the modelled reflectance confidence bounds at each of the 2009 sampling intervals. The reflectance at this wavelength at first decreases slightly, as the Chlorophylls content per gram 'shoots and leaves' increases at a greater rate than leaf biomass per unit areas, then reflectance increases to mid July. Reflectance then increases more rapidly as flowers begin to dominate through August and falls again as the flowers senesce. This indicates that the convolution of the *Calluna* growth kernel modelled photosynthesising biomass and the Chlorophylls content, interpolated from the work of Mac Arthur and Malthus (2012), were able to be used to predict Chlorophylls content through the *Calluna* growth and senescent annual cycle. It also indicates that the linear mixture modelling approach used to incorporate *Calluna* flower reflectances is a reasonable one.

The modelled reflectances in the blue region of the spectrum, the region of maximum Carotenoids absorption and displayed at 464 nm in Figures 5.7(a), 5.7(c), and 5.7(e) is less consistent. It has not followed the same trend as the measured reflectances for the *Calluna* stands growing in mineral soil and dry

peat substrate (there was no reduction in measured reflectance in July), although it does for the stand growing in wet peat. In addition, the range of measured reflectances does not overlap the modelled reflectance confidence bounds. For the soil (Figure 5.7(a)) and dry peat (Figure 5.7(c)) stands, measured reflectance is approximately constant at each of the field spectroscopy sampling intervals while the modelled reflectance reduces appreciably from June to July before rising again until mid August. However, the modelled and measured reflectances from the *Calluna* stand in wet peat do follow generally the same trend, reducing slightly in July but then not rising significantly. Measured reflectance in the green region of the spectrum displayed at 556 nm in Figures 5.7(a), 5.7(c), and 5.7(e) - the wavelength of maximum Anthocyanins absorption determined by Mac Arthur and Malthus (2012) - also does not display the same trend and the modelled reflectance.

These differences between modelled and measured reflectances at both 464 nm and 556 nm may be because some Carotenoids, Xanthophylls for example, serve a photoprotective function. Anthocyanins also serve a photoprotective function as well as being a response to leaf tissue damage. The rate of Anthocyanins response to initiating events is unknown as is the duration or longevity of leaf colour changes it causes. Therefore as the prevalence of both these pigments may depend on meteorological events, such as bright sun or frost, or on physical damage or disease, it may not be possible to predict future values of reflectance in the blue and green region of the spectrum, and hence the content of these pigment groups, by modelling.

When the visible region of the spectra for each plot was modelled for 2007, the modelled reflectances in the red region, 668nm in Figure 5.7(b), for Plot 8 were in the main within the modelled confidence bounds, while there was a mismatch at some of the sampling intervals for Plots 3 and 1. The modelled and measured reflectances at 556 nm, (Figure5.7(b)) and at 464 nm (Figure5.7(b)) were again

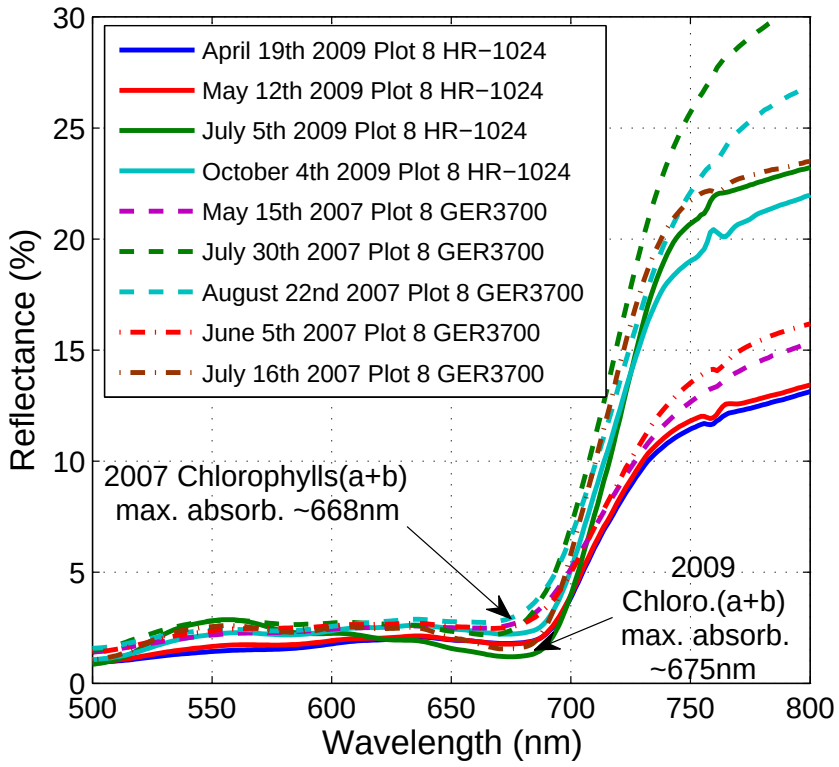

Figure 5.8: Differences between Chlorophylls absorption maximum measured from mean field spectra during 2007 and 2009

,

in general not well matched, although there was some overlap at some sampling intervals.

However, when the reflectance spectra for each plot measured in 2007 were compared with those measured in 2009 a subtle shift in the Chlorophylls absorption maximum feature was noted. The spectra from 2007 had a Chlorophylls absorption maximum at 668 nm while the absorption maximum for those measured during 2009 was 675 nm (Figure 5.8). The reasons for this are unclear. Although a GER 3700 was used for field spectroscopy during 2007 and a SVC HR-1024 during 2009, an instrument bias seems unlikely as mercury argon lamp emission features at 696.5 nm and 546.1 nm were used during instrument quality assurance

checks and the wavelength calibration of each instrument was within ±0.5 nm of those points. In addition, SVC have advised that the same interpolation method was used to derive the wavelength calibration of both instruments and that this was done using features at the same wavelengths.

An event such as wide scale nitrogen disposition which could increase the acidity of the environment and possibly alter the acidity of the xylem sap, which could effect the profile of pigment absorption spectra (personal communication Prof.H. Lichtenthaler, 21/09/2009), seems unlikely as there are no industrial sources of nitrogen downwind of the research site. Another possible cause is weather. During 2009 there were a greater number of accumulated hours of sunshine than during 2007 and there were some temperature extremes. However, due to the limited number of spectral sampling intervals and the lack of knowledge of time lag between a meteorological event and a biological response in *Calluna* it would not be possible to establish a direct relationship. Therefore, although the cause of this discrepancy remains unresolved, it may well be an no more than an indication of natural variability and the change in pigment composition and individual pigment absorption spectra in-complex through the natural growth and senescence cycle of *Calluna* and through annual and inter-annual temporal cycles. However, despite the discrepancy being unresolved it may still be possible to infer Chlorophylls, Carotenoids and Anthocyanins content from inversion of the measured spectra using RT models, with the range of values being constrained for specific temporal intervals *a posteriori* by *Calluna* growth and senescent photosynthesising biomass modelling as forward modelling has been demonstrated here.

5.4 Conclusions

A combined optical and allometric method for differentiating *Calluna* stands which complements remote sensing and radiative transfer modelling has been developed. This method uses a SunScan plant canopy analysis system to record PAR penetrating through a canopy and combines these data in statistical analysis with *Calluna* stem diameter to enable the *Calluna* stands delineated on the Smeath Hill research site to be differentiated. As each of the stands used in this research was of a defined *Calluna* age and ecological community class, then it would seem possible to infer these classes from these optical and allometric data. However, wider validation of this method for stands outside the research site is required. The relationships between these optical/allometric classifications and the classifications normally used by ecologists also need to be more rigorously established. Investigations into the validity of this method for other moorlands could then be conducted. In addition, an empirical relationship between stem diameter and woody biomass needs to be established, rather than the direct measurement of woody biomass (sampled at a different temporal interval) used in this work. This would then allow the *Calluna* growth model biomass production to be verified using a non-destructive allometric method.

The use of the SunScan probe also allowed the *Calluna* canopy and stand structural parameters (LAI and ground cover) to be inferred from the PAR values recorded. However, the LAI values were not considered to be reliable for Plot 3 and Plot 1 as the ground cover of these stands tended to be less continuous and the shoots and leaves more clumped together than in Plot 8. Leaf clumping and canopy gaps are acknowledged to cause LAI estimation errors for forest canopy cover when estimated using optical methods. Nevertheless, it was possible to use the spatial distribution of PAR values recorded using the SunScan to estimate the proportion of canopy gaps and hence derive an estimate of the percentage

of *Calluna* ground cover in each stand. Furthermore, it was also possible to infer canopy development from these PAR values when time series measurements were made. Therefore when coupled to stem diameter measurements the use of this SunScan survey method will enable objective and replicable surveys of *Calluna* stands to be made and, although further verification work is required, will assist both *Calluna* field surveys and remote sensing studies. Work remains to be done, however, to determine if the LAI/leaf inter cellular air space parameter relationship is a linear one and to further investigate the contribution that woody elements make to the values recorded by optical plant canopy analysers.

The HillPlan *Calluna* growth kernel was able to be calibrated, its outputs validated and uncertainties in the model output values estimated for the Smeath Hill research site. To enable reasonable results to be achieved, however, required the growth start and end date for each year to be adjusted to influence the modelled *Calluna* photosynthesising biomass productivity. This adjustment was within a reasonable range, given that the onset and end of growth can fluctuate annually as they are influenced by meteorological conditions (White *et al.*, 2003). The growth kernel was subsequently dynamically coupled to a canopy/leaf radiative transfer model which enabled the reflectance of *Calluna* stands to be reasonably modelled in daily increments through annual and inter-annual growth and senescence cycles. However, and in addition, a linear mixture modelling approach also had to be adopted for the August to October modelling intervals to enable the reflectance of *Calluna* flowers to be incorporated into the gross canopy reflectances modelled.

The accuracy of the reflectances generated by the coupled canopy/leaf/*Calluna* growth model, when compared to reflectances measured in the field, varied depending on heterogeneity of the *Calluna* canopy and the spectral wavelengths being compared. Wavelengths in the red and NIR regions could be most reliably modelled as reflectances in these regions varied systematically with the annual

and inter-annual development of *Calluna*. These are the regions of the spectrum influenced by photosynthesising biomass and Chlorophylls content, two plant parameters of primary interest to climate modellers. Wavelengths in the blue and green regions could be predicted less reliably perhaps as reflectances in these regions are significantly affected by short term weather events and other phenomena, such as disease infestations, that may not follow a temporal cycle that can be predicted.

Nevertheless, by adopting an iterative and ongoing approach it would appear possible to calibrate this *Calluna* reflectance model using: spectra acquired at opportune temporal periods (when sky conditions permitted, for example); readily available meteorological data; data on annual pigment content trends reported by Mac Arthur and Malthus (2012); and canopy structural and scattering parameters quantified in this work allowing continued refinement of the modelled reflectances over time. This would be especially advantageous in remote sensing peatland studies as it is difficult, in the northern temperate oceanic climates in which peatlands are typically found, to acquire images of the same area on the same day in successive years. The modelling method developed here enable reflectances acquired from either field spectroscopy or from sensors on airborne or satellite platforms at one annual time interval to be used to calibrate the model and then to model reflectances at other time intervals in successive or preceding years, for comparison with spectra acquired when weather conditions have permitted data acquisition. This may then enable inter-annual changes in photosynthesising biomass, Chlorophylls content and flower profusion, and their changes over time, to be assessed thus allowing the monitoring of ecological, and consequent environmental change to *Calluna* dominated peatlands.

It would also appear now to be possible to use the *Calluna* growth model to determine LAI and photosynthesising biomass parameter values required to constrain the inversion of the coupled ACRM/LIBERTY canopy reflectance model.

By defining and narrowing the range of values for these model parameters the inversion can be constrained so that the results achieved more closely estimate actual canopy state variables at each modelling increment (Lewis, 2007). The coupled *Calluna* growth/ACRM/LIBERTY canopy reflectance model could then be used in the analysis of hyperspectral images to potentially infer photosynthesising biomass and contents of Chlorophylls, Carotenoids and Anthocyanins. However, if images were acquired during the *Calluna* flowering period a linear unmixing approach would first have to be adopted to separate the rest of the canopy reflectances from the flower reflectances. A *Calluna* flowering index could be developed from hyperspectral data to identify this period.

A series of hyperspectral images of the Smeath Hill research site were acquired during the course of this research using the AISA the Eagle/Hawk sensors mounted on the Natural Environment Research Council Airborne Research and Survey Facility aircraft. These images could be used to determine if the coupled *Calluna* growth/ACRM/LIBERTY canopy reflectance model can potentially be inverted and thus if the state variables significantly influencing reflectance can be estimated. In addition, as further field spectroscopy data of the Smeath Hill research plots were acquired during 2009 in random point surveys, these could be used to refine the model calibration prior to the hyperspectral images being used in the model inversion process. However, from the forward modelling work reported here it would appear that only spectra from areas of continuous *Calluna* cover may be able to be reliably inverted. Nevertheless, it may be possible to differentiate these areas from those stands with incomplete cover by analysing the variability of the spectra at contiguous pixel locations, adopting the object-based image analysis method used by Mac Arthur *et al.* (2007) to analyse aerial photographic images. Further work will now be carried out to determine if the coupled *Calluna* growth/ACRM/LIBERTY canopy reflectance model can be

inverted, and to assess both its sensitivity to varying parameters and the validity of results from the the analysis of the hyperspectral images.

Chapter 6

General discussion

It has been proposed in this thesis that it may be possible to use *Calluna vulgaris* as an indicator of ecological and environmental change to peatlands. Knowledge of the condition of these environments and the rate and direction of their change is of interest to climate scientists and land managers alike (Harris and Bryant, 2009b). However, it is acknowledged that data need to be acquired at spatial resolutions that can reflect local management decisions (Ostle *et al.*, 2009). Optical imaging sensors on satellite platforms currently operational are able to acquire data at ground sampling resolutions of a few metres and Mehner *et al.* (2004) has reported on the utility of data from one such satellite to classify upland areas. However, Mehner *et al.* (2004) noted that the "low spectral resolution ... was a ... weakness".

Hyperspectral imaging sensors are now available on airborne platform and similar sensors are scheduled to be deployed on satellite platforms in the coming decade. Hyperspectral images offer a "quantum jump" in data content (Lillesand *et al.*, 2004) from that used by Mehner *et al.* (2004) and others in remote sensing research of peatlands. Schaepman *et al.* (2009) reports the "exponential" growth

of imaging spectroscopy over the last two decades and highlights its use for investigating leaf metabolic regulation and biochemistry through a continuum of temporal and spatial scales to global biogeochemical cycles.

Hyperspectral images acquired from sensors on airborne platforms have been used; to assess the relationship between optical and ecological classifications (Thomas *et al.*, 2002), bare peat composition (McMorrow *et al.*, 2004), peatland fire damage (McMorrow *et al.*, 2005), surface wetness (Teh *et al.*, 2011) and hydrological processes (Harris and Bryant, 2009b), to build spectral libraries of species and identify the optimal time for hyperspectral field surveys (Lowe *et al.*, 2010), and to map to biotype classifications (Middleton *et al.*, 2009) in peatland environments. High spatial resolution hyperspectral images have also been used to map general ground cover classes in *Calluna* dominated peatlands (Kooistra *et al.*, 2009), as previously discussed in Chapter 1 of this thesis. This diversity of application indicates the utility of these high spectral and spatial resolution data for peatland research.

A significant amount of research has also been carried out measuring and monitoring the biological and physiological processes of forests using airborne hyperspectral imaging sensors. For example Thomas *et al.* (2009) used hyperspectral images to infer and map leaf physiology at a four metre ground sampling interval and Goodenough *et al.* (2009) and Sampson *et al.* (2003) report on similar work, although both used secondary remotely sensed data sources to assist their analysis. However, there have been no attempts to measure and monitor biological and physiological process of the overstorey vegetation on peatlands by hyperspectral remote sensing.

The use of radiative transfer modelling may significantly increase the information that can be extracted from hyperspectral images (Ustin *et al.*, 2009) than can be extracted through the analysis methods used by Kooistra *et al.* (2009),

for example. Furthermore, future hyperspectral satellite sensors will have the capacity to acquire data at high temporal frequencies. The hyperspectral EnMap satellite sensor will offer a 4 day revisit time, for example (Kaufmann *et al.*, 2010). Although this sensor will not have a high spatial resolution, higher spatial resolution satellite sensors may follow in future. Schaepman *et al.* (2009) suggest that radiative transfer modelling may enable analysis at these temporal and spatial scales (airborne and satellite) to be combined and Weiss *et al.* (2001) highlights the utility of combining these models with models of plant functioning and growth. Therefore developing radiative transfer modelling methods coupled to plant growth models may enable the data content of hyperspectral images acquired from sensors on airborne platform to be more fully utilised to measure and monitor annual and inter-annual growth and senescence cycles of plants. This would then make it possible for hyperspectral images acquired by future satellite sensor to be used to monitor ecological change to peatlands and inform climate scientists, ecologists and peatland managers.

This thesis sets out to gain an understanding of the properties of *Calluna vulgaris* influencing reflectance and from this develop a canopy radiative transfer model that can model the reflectance of *Calluna* through annual and inter-annual growth and senescence cycles. This may then enable hyperspectral remote sensing and radiative transfer reflectance modelling to be used to monitor the status and dynamics of *Calluna*, which would facilitate its use as an indicator species of environmental change to peatlands where it dominates. Hyperspectral remote sensing of these *Calluna* dominated peatlands could then also provide data for global environmental change studies and be used to inform local and regional environmental management decisions.

The research presented in this work has identified and quantified three photosynthetically active pigment groups (Chlorophyll$_{(a+b)}$, Carotenoids and Anthocyanins) and two leaf structural variables (inter-cellular airspace and cell diameter) in *Calluna* shoots and leaves and quantified the change of these five variables through two annual growth and senescence cycles. The presence of one of these pigments, Anthocyanins, and the influence of leaf structural parameters on reflectance had not previously been presented in the remote sensing literature discussing *Calluna*. It was shown that these five variables significantly influenced the reflectance of *Calluna* shoots and leaves through the visible-near infra-red region of the solar spectrum and that they changed through annual growth and senescence cycles. The research then went on to quantify the photosynthetically active biomass and canopy structural parameters that influenced reflectance. By doing so, it has enabled changes to *Calluna* canopy reflectance through annual and inter-annual growth and senescence cycles to be modelled.

This *Calluna* photosynthesising biomass, canopy structure and spectral reflectance research has been carried out by adopting field and laboratory measurements and modelling studies. At a field research site a combination of *in situ* measurements of *Calluna* structural and optical parameters were made and physical samples collected. Then in a laboratory further optical measurements were made prior to destructive sampling to determine additional physical and optical parameters. Subsequently, using the data acquired in the field and in the laboratory both radiative transfer reflectance modelling and *Calluna* photosynthesising biomass growth modelling were conducted.

It was noted during the course of this research that the area of measurement support for the field spectroscopy reflectance measurements did not appear to be well defined by the nominal included angle used by manufacturers to specify the field-of-view (FOV) of the spectroradiometer lens based fore optics being used. Detailed knowledge of the areal extent and shape of the area of

measurement support is required to attribute the reflectance of individual surface classes within the area of interest to the integrated reflectance recorded by the spectroradiometer. Knowledge of the extent and shape of the area of measurement support is also required to inform field spectroscopy sampling strategies and develop statistically robust methods, particularly when heterogeneous Earth surfaces are being measured (Atkinson and Curran, 1997; Curran and Atkinson, 1999; Rahman *et al.*, 2003; Atkinson and Aplin, 2004).

Consequently, the research also investigated, in an optical laboratory, the characteristics of two full wavelength (400 nm to 2,500 nm) field spectroradiometers, namely the area of measurement support from which reflectances are received by these instruments to enable field sampling strategies to be developed. The areas of measurement support for the two systems investigated were found not to be as assumed by field spectroscopists from the specifications provided by manufacturers. Furthermore, during this work spatially determined wavelength, or wavelength region specific, variations in spectroradiometer responsivity to reflected radiances from the area of measurement support were quantified. This spatially dependent responsivity, named the directional response function (DRF), of each of the spectroradiometers was quantified and found not to be as implicitly assumed by field spectroscopists.

As it was unclear what effect the differences between the assumed and the actual area of measurement support, and the differences between the assumed responsivity and the actual responsivity, would have on spectra acquired a numerical modelling study was conducted. Three dimensional models of Earth surface targets were developed (x and y dimensions and reflectance per wavelength) and convolved with three dimensional models of the DRF (x and y directions and responsivity per wavelength) for each spectroradiometer/fore optic system available for this research. The results of this showed that there were significant differences between the spectra that would be measured by specific instrument/fore optic

combinations and those that would have been assumed given the specifications for these fore optics provided by manufacturers. These differences were wavelength specific for the SVC system and wavelength region specific for the ASD system and depended on the fore optic used and instrument orientation specific for all systems.

6.1 Addressing the aims of this research

The intention of the research presented in this thesis has been to gain a better understanding of the interaction of light with *Calluna vulgaris*; to develop near ground optical measurement methods to measure its canopy structure and spectral reflectance; and to develop methods that may be used in the analysis of hyperspectral images.

The aims of this research, presented in Section 1.6 of Chapter 1, were:

- to investigate the pigment content and optical properties of *Calluna* shoots and leaves to enable the reflectance of these, and their change in reflectance over time, to be modelled

This research has determined the biophysical and biochemical content of *Calluna* shoots and leaves influencing reflectance across the visible-near infra-red region of the solar spectrum through laboratory destructive sampling and spectrophotometric and spectroradiometric measurements. The work identified and quantified Chlorophyll$_{(a+b)}$, Carotenoids and Anthocyanins, found to be present in *Calluna* shoots and leaves and measured the change of these pigments over time. It was found that the absorption spectrum of Chlorophyll$_{(a+b)}$ was not the same as that presented in the remote sensing literature for other plant species. A *Calluna*

specific absorption spectrum for Chlorophyll$_{(a+b)}$ was subsequently derived by an iterative radiative reflectance modelling approach during this work. When this absorption spectrum, and those for Carotenoids and Anthocyanins, also derived in this work, were incorporated into a leaf radiative transfer reflectance model, the reflectance of *Calluna* shoots and leaves could be modelled through a growth and senescent cycle. However, the degree of accuracy with which reflectances were modelled, when compared to those measured, varied temporally, with the lowest errors observed in the mid summer period. In addition, the structural variables (cell diameter and inter cellular air space) within *Calluna* shoots and leaves, which also significantly influenced spectral reflectance, were also quantified and found to vary systematically, and by similar amounts, through the two growth and senescence cycles investigated. It was not possible in this work to determine the physical accuracy of these structural variables. Nevertheless, they did enable a numerical solution for radiative transfer reflectance modelling of *Calluna* shoots and leaves to be developed. Therefore it has been possible to model the reflectance of *Calluna* shoots and leaves and the change in their reflectance over time, and the accuracy of these modelled reflectances, when compared to measured reflectances, has been quantified.

However, it is evident from this work that the absorption spectra of the leaf pigments used in radiative transfer modelling in remote sensing research are not a constant. The *Calluna* specific absorption spectra that were developed to enable modelled 'shoots and leaves' reflectances to match measured reflectances with a reasonable degree of accuracy at a specific measurement interval, did not result in accurately modelled reflectances at all the other measurement intervals. This is probably due to the absorption spectra of photo active pigments being affected by the type and concentration of the other pigments present and by the acidity of the xylem sap of leaves (personal communication Prof.H. Lichtenthaler, 21/09/2009). It also appears from this work and the work of Di Vittorio (2009)

and others that the relative proportions of Chlorophyll$_{(a)}$ and Chlorophyll$_{(b)}$ may also change through annual growth cycles. These individual pigments were not initially quantified in this work. However, when an attempt was subsequently made to quantify them, it proved not to be possible to derive the individual *in vivo* absorption spectra for Chlorophyll$_{(a)}$ and Chlorophyll$_{(b)}$ using the data available and the iterative optimisation modelling method used in this research. However, it would appear necessary to derive *in vivo* absorption spectra of both Chlorophyll$_{(a)}$ and Chlorophyll$_{(b)}$ to enable the reflectances of *Calluna* shoots and leaves to be more accurately modelled through all periods of annual growth and senescence cycles. Nevertheless, a leaf radiative transfer reflectance model that used the *in vivo* absorption spectra for Chlorophyll$_{(a+b)}$, Carotenoids and Anthocyanins derived in this work was successfully incorporated into the *Calluna* canopy reflectance model which will be discussed next.

- to link a *Calluna* ecological growth model to a canopy reflectance model and model reflectance through a number of annual and inter-annual growth and senescence cycles

During the course of this research, a quantifiable optical method of characterising *Calluna* canopies and stands was developed by measuring the PAR penetrating through to the canopy understorey. This enabled canopy ground cover, necessary for canopy reflectance model parameterisation, to be estimated and, when coupled with stem diameter measurements, the *Calluna* stands in the research plots to be differentiated. This ability to differentiate stands may enable this method to be used to derive *Calluna* stand classifications that could be directly related to the commonly used *Calluna* age classes and ecological classes, facilitating quantitative and replicable moorland surveys for conservation and management purposes. However, estimates of leaf area index (LAI) derived from these PAR measurements were found to be less reliable. Nevertheless, this ability to

differentiate stands and quantify ground cover will assist remote sensing studies and provide qualitative data for inclusion into the HillPlan grazing ecology model, developed by the Macaulay Land Use Research Institute. This will enable more reliable prescriptions for upland hill farm sheep grazing and muirburn to be developed, enhancing agricultural, sporting and conservation use.

The photosynthesising biomass growth kernel was extracted from a *Calluna* ecological growth and herbivore utilisation model (HillPlan) modified, calibrated for the research site being used for this work, and its outputs verified. A relationship was then established between the growth model biomass output values and the LAI values determined by the optical survey method. Using this relationship, the modelled biomass values were converted to LAI values in the modified growth model. However, the data used to derive these LAI values and the field spectroscopy data, used to compare modelled reflectances, were acquired at different scales. The PAR-based LAI sensors measure from the whole irradiance hemisphere above them and the cosine response and responsivity of these sensors were not quantified during this work. On the other hand, field spectra were acquired from a planar area of measurement support the areal extent of which was defined by the spectroradiometer/fore optic system used. The growth model was then dynamically linked to a canopy reflectance model, which contained the leaf reflectance model used previously in this thesis. The growth model, therefore, provided the LAI input parameter values and the photosynthesising biomass values necessary to convert the leaf pigments content measured in μg/g shoots and leaves in the leaf model to g/m^2 required by the canopy model, and could do so in daily increments.

The combined biomass growth/canopy/leaf model was then shown to be able to generate canopy reflectances in daily increments through a series of growth and senescence cycles for the range of *Calluna* age classes and the ecological conditions at the *Calluna* dominated peatland site used for this research. It was subsequently

determined from this work that the reflectance of *Calluna* canopies and stands could be modelled through annual and inter-annual growth and senescence cycles. However, the accuracy, when modelled and measured reflectances were compared, depended on the wavelength region being considered and the homogeneity of the *Calluna* stands. This homogeneity was related to the age class of the *Calluna* and the ecological conditions in which the *Calluna* was growing.

The wavelengths selected for analysis in the near infra-red (NIR) and the red regions of the spectrum were the most accurately modelled and these are the regions where reflectance changes systematically through annual growth and senescence cycles. Therefore the change in reflectance of these regions can be predicted reasonably well if the model is parameterised with the necessary environmental and ecological variables. However, of particular interest to studies of environmental change to peatlands, and to climate induced phenological change, may be the ability to monitor inter-annual changes in the timing of the onset, and in the extent and density of, flowering, with which this modelling may also assist.

Most RS research has focused on monitoring *Calluna* when it is at its greenest. During this period all other vegetation is also predominantly green, making differentiation difficult and leading to confounding variables for remote sensing research. However, *Calluna* has spectrally distinct flowers. The profusion of these flowers is determined by the vigour of each shrub and this vigour is indicative of the shrub age and the ecological community in which it is growing (Gimingham, 1972). This research has demonstrated that a mixture modelling method when combined with radiative transfer reflectance modelling can be used to model *Calluna* canopies when in flower and the transitions in reflectance from the period when there are no flowers, through flowering and on through to winter dormancy. The onset of flowering caused a significant and distinct change in reflectance in the red region of the spectrum. From the data for the three plots analysed,

this was most pronounced for the most homogeneous stand (Plot 8), slightly less so for the less homogeneous stand (Plot 3) and least distinct for the most heterogeneous stand (Plot 1). Consequently, it may be possible to monitor any ecological change to *Calluna* dominated peatlands using hyperspectral remote sensing to measure the profusion of flowers, possible with the development of a *Calluna* flowering index, and use flowering as an indicator of stand condition. Then the *Calluna* growth/canopy reflectance radiative transfer modelling method developed in this work could be used to compare data from different annual and inter-annual temporal sampling intervals.

However, reflectance in the blue and green regions of the spectrum were not able to be predicted reliably. The reflectance of these regions is dominated by pigments which respond to short term allogenic influences. In addition, the reflectance of one of these pigment group, Anthocyanins, may confound *Calluna* flower reflectances as they also appear purple, although Anthocyanins leaf colouration does not normally dominate canopy reflectances. Nevertheless, model inversion studies can now be conducted and from these it may be possible to infer the biomass and pigment content from hyperspectral images of *Calluna* dominated peatlands.

- to investigate the spatial extent of the area of measurement support for field spectroradiometric measurements, the uniformity of spectral response across this area and to compare these with those assumed by field spectroscopists, given the specifications provided by instrument manufacturers

The fields-of-view (FOV) of two full wavelength spectroradiometer systems, with a range of fore optic accessories, were investigated in an optical laboratory, and the nominal FOV was found to be a wholly inadequate parameter to define the extent of the area from which reflected radiance would be received by these spectroradiometers during field spectroradiometric measurements. In

addition, the responsivity of each system to reflected radiance from different areas within the area of measurement support was found to display wavelength, or wavelength region, specific dependencies. Furthermore, each spectroradiometer system was found to display significantly different characteristics from the other systems related to their optical design. The directional response function (DRF, (Commission Internationale de L'Eclairage, 1987)) of a spectroradiometer/fore optic system provides a more appropriate and scientific approach to specify the characteristics of each system. The DRF was shown to capably define each area of measurement support and hence, spatial sampling resolution, and wavelength, or wavelength region, specific dependent responsivity to reflected radiance from within this area. A key conclusion from the work is that field spectroscopists should determine the DRF of the spectroradiometer/fore optic systems to be used prior to conducting field measurements as, due to the optical design (for ASD FieldSpec Pros) and manufacturing tolerances for (SVC GER 3700s), each spectroradiometer/fore optic system will have a different DRF. This may significantly influence the spectra recorded, particularly heterogeneous surfaces and surfaces with anisotropic reflectances.

The findings of this research should also be considered when the selection of field spectroradiometers and choice of appropriate fore optic is being made. As field spectroscopists are trying to approximate the bidirectional reflectance distribution function (BRDF) of a surface, selecting as narrow a view angle as possible would seem appropriate (Milton *et al.*, 2009). However, this probably requires a spectroradiometer fitted with a fore optic containing a lens focusing element. In the ASD system it is the lens that is causing the area of measurement support to be 'imaged' onto the tip of the fibre optic bundle. As this tip has up to 57 individual fibres, each is receiving light from a different area of this 'image'. Then, as these fibres are then randomly distributed to the three detectors (with each detector covering a different region of the VNIR-SWIR spectrum), each detector

is recording reflectance from different areas of the area of measurement support and there may or may not be any overlap between these areas. It should also be noted that as the fibres in the fibre optic bundle of each ASD FieldSpec Pro are randomly distributed to the detectors, each ASD FieldSpec Pro may have a unique DRF. Hence, possibly, no two instruments would record the same reflectance from the same area of a heterogeneous Earth surface target.

In the SVC system it is a combination of both the lens 'imaging' the area of measurement support into the instrument through a rectangular optical slit and the fore optic lens that determines the DRF. The optical slit imposes the rectangularity on the area of measurement support and it appears that the fore optic lens is the primary cause of the chromatic aberration due to its refractive index, although other optical elements may contribute, leading to the right/left blue/NIR bias in reflectance recorded when lens based fore optics are used.

If measurements are being made of a heterogeneous target it may therefore be more appropriate to select the ASD 18^o fore optic or use the instrument without a fore optic in 'bare fibre' configuration and, if using the GER 3700, fit the fibre optic attachment. However, it is acknowledged that, although the DRF of both of the fibre options measure across a continuous field and the responsivities are approximately Gaussian, the view angle to the edge of the area of measurement support is greatly increased, which may introduce other errors to the measurement being recorded due to the BRDF of the surface. Therefore Earth surface anisotropy should also be considered when making fore optic selection.

Both the ASD FieldSpec Pro and the SVC GER 3700 used in this work are over ten years old, and both manufacturers have recently upgraded their systems after being advised of the results of this research. On request, ASD will now supply an optical mixer, named a "scrambler". This can be fitted within the pistol grip of the instrument between the fore optic and the fibre optic bundle. It, in

effect, defocuses the image so that the light that reaches the fibre bundle tip is incoherent. Hence there should be no wavelength region spatial bias. However, a slight loss in responsivity should be expected, due to transmission losses at the lens/scrambler and scrambler/fibre bundle tip interfaces. SVC have also improved the optical design of their instruments and higher quality optical components are now available and have been used. SVC can provide on request a lens based fore optic that has been optimised to minimise any wavelength spatial bias. Nevertheless, as a different technological approach is used to measure reflectance in each of these instruments the reflectances recorded by each may not be the same even after these improvements. Furthermore, due to manufacturing tolerances, and in the case of ASD instrument the random distribution of fibres to the detectors, each spectroradiometer/fore optic system of the same make and model may record a different spectrum from the same Earth surface to that recorded by another instrument of the same make and model and this may be the case when heterogeneous or anisotropic Earth surfaces are being measured.

- determine the impact of actual measurement support on assumed spectral response, given the specifications provided by instrument manufacturers

A series of reflectance modelling studies were conducted by convolving the DRFs of the two spectroradiometers, each with a selection of fore optics characterised during this research, with a number of modelled heterogeneous Earth surface targets. Significant differences were highlighted between the spectra that would have been assumed to be recorded if the specified nominal FOV limited the area of measurement support (and if there were no spatially determined wavelength/wavelength region specific responsivity dependencies) and those that would be recorded given the DRF of each spectroradiometer/fore optic system. The profiles of the modelled spectra were found to vary depending on: the spatial distribution of individual reflecting elements within the area of measurement

support; the rotational position of the spectroradiometer relative to the modelled surface; and the specific field spectroradiometer fore optic used. Biochemical indices were also calculated from the modelled spectra and these were found to vary significantly from those that would have been expected if the area of measurement support had been defined by the FOV and if there had been no wavelength or wavelength region specific spatial dependencies.

It is not possible to know the measurand, the 'true' value (which in this work is the reflectance of an Earth surface), as the Joint Committee for Guide in Metrology advise there will always be measurement uncertainties (Joint Committee for Guides in Metrology, 2008). Earth surfaces are illuminated by the whole sky hemisphere and the presence of the spectroradiometer being used to make measurements will interfere with this, even when the spectroscopists remove themselves from the scene. There will also be spectroradiometer introduced biases, some known and possibly quantified and others unknown; and even the wavelength scale is a discrete classification system imposed by scientists and the spectroradiometer technologies available on a continuous phenomenon, therefore detail is lost. Consequently, the accuracy, the offset between the measurand and the value measured, cannot be known definitively. Even when only the inherent reflectance of a surface (that is the reflectance solely dependent on the surface properties and independent of illumination) is considered, a further level of complexity is evident as most (if not all) Earth surfaces are anisotropic rather than Lambertian (Milton, 1987). Therefore the radiant flux would need to be measured over the whole of the hemisphere into which it radiates and this should be done from all possible angles and with infinitely small included solid view angles which cannot be achieved in practice. Spectroscopists should develop methodologies that minimise the errors that they introduce to improve the accuracy of their measurements but can only ever make measurements that approximate to the measurand reflectance when viewed from a specified position, with a particular

spectroradiometer/fore optic system configuration, under specific illumination conditions and subject to the calibration of their instrument.

One method that could be adopted to improve the accuracy of field spectroscopic measurements is to try to account for spectroradiometer induced bias. In the context of this work that is bias introduced to the reflectance recorded by the DRF of the instrument. In this modelling study a synthetic 'true' reflectance was modelled which represents the measurand; then the accuracy of the modelled 'measured' reflectance (the reflectance that would be measured given the DRF of an instrument) could be determined. This work has demonstrated that, due to the spatially dependent wavelength and wavelength region biases of the DRF and the difference in the area of measurement support between that which would have been assumed (used to model the measurand reflectance) and that defined by the DRF, significant but quantifiable inaccuracies can be attributed to the DRF of the specific instrument/fore optic systems measured and modelled in this thesis.

6.2 Implications of this research

The influence which the three pigment groups and the two leaf structural parameters, identified and quantified in this work, have on the reflectance of *Calluna* has not previously been presented in the literature. These pigment absorption spectra were found not to be constant but depend on the type and quantity of other leaf pigments in-complex. Therefore, there is a degree of inaccuracy in the absorption spectra derived in this work as they were estimated from a number of samples acquired at a limited number of temporal intervals hence only represent a limited number of the possible pigment combinations. Although an attempt has been made to quantify the inaccuracy that will result in the reflectance spectra modelled using the five parameters selected, the comparison of

modelled and measure reflectance spectra shows that uncertainties remain. These *in vivo* absorption spectra were estimated from *in vitro* pigment quantification and spectra acquired in a laboratory by reflectance spectroscopy of shoots and leaves removed from plants and where the physical dimensions of leaf cells and airspaces are unknown.

Nevertheless, this work indicates that it may be possible to measure and monitor environmental change to *Calluna* dominated peatlands using hyperspectral remote sensing as future or past *Calluna* canopy reflectance can possibly be predicted from current reflectance through the use of the combined *Calluna* growth/canopy reflectance model developed in this research. This model could be calibrated and validated for hyperspectral data analysis using the optical field surveys to measure LAI and canopy spectra acquired by field spectroscopy using the methods demonstrated in this work. It could then be applied to different temporal periods or geographical locations if parameterised with the appropriate environmental, ecological and graphical variables. Of particular interest to climate change studies may be monitoring potential phenological change of *Calluna* flowering by hyperspectral remote sensing. It may be possible to do this by adopting the combined radiate transfer reflectance and linear mixture modelling approach proposed in this thesis.

Currently the model developed in this work could only be used with a reasonable degree of accuracy for stands where there was continuous *Calluna* cover and with an LAI of greater than 7.5, so that understorey reflectances did not contribute significantly to the reflectance recorded. The heterogeneity of *Calluna* canopies and stands where these conditions are not met makes modelling their reflectance intractable at the present time and the results of future radiative transfer model inversions would probably be unreliable. There could be some improvement if radiative transfer models of the understorey species could be developed and if

individual absorption spectra for Chlorophyll$_{(a)}$ and Chlorophyll$_{(b)}$ were incorporated into the model.

The *Calluna* stands on these peatlands are burnt (muirburn) in succession on a 20-year to 30-year rotation to provide a succession and mosaic of *Calluna* age classes. However, current recommendations for the management of *Calluna* dominated peatlands by cyclical burning advise that *Calluna* stands 20 metres to 30 metres wide (Scottish Government, 2011) be left between areas that are burnt. The *Calluna* stands that regenerate in these areas, when on favourable substrate, may have continuous canopy cover from when they are approximately 10 until 20 years old (Gimingham, 1972). Therefore these areas would provide a succession of areas of reasonable areal extent and duration of growth for phenological change to be monitored by hyperspectral remote sensing. However, as even the two homogeneous *Calluna* stands used in this modelling and analysis are anisotropic reflecting surfaces, due to their irregular surfaces and inter-canopy shadowing, there may still be biases introduced into reflectance recorded and used to validate modelled spectra due to the DRF characteristics of field spectroradiometer/fore optic systems, which will be discussed next.

The information provided by spectroradiometer manufacturers would lead field spectroscopists to believe that the area of measurement support was round, in the case of ASD instruments/fore optic systems, or rectangular, although this is often overlooked, in the case of SVC instrument/fore optic systems. This research found that when using a fore optic with a focusing element the area of measurement support for the ASD used was not round; it extended significantly beyond the area defined by the information supplied by the manufacturer; and there was not complete coverage of the area of measurement support at all wavelengths being measured by the instrument. It provided an irregular intermittent field of responsivity. Although the GER 3700 did have a continuous field of responsivity

the level was not the same for all points within the area of measurement support for all wavelengths recorded.

The canopy reflectance spectra modelled at each sampling interval in this work were compared with spectra acquired in the field and the field spectroscopy methodology was developed and measurements started using information provided by the spectroradiometer manufacturers. This information was subsequently found to be insufficient to define the area of measurement support of the field spectroscopy measurements. As will be discussed in more detail in the following paragraph, there was a blue/near infra-red wavelength responsivity bias oriented across the width of the optical slit of the GER 3700 spectroradiometer. This GER 3700 was the instrument used to make the field measurements during 2007. During field measurements the instrument was oriented so that it was aligned with the solar principal plane. However, this meant that the optical slit of the instrument was perpendicular to the solar principle plane. Consequently, canopy elements towards the edge of the area of measurement support closest to the Sun would have a blue wavelength region bias and those furthest away from the Sun a near infra-red wavelength bias. There would then be a further bias introduced as the elements towards the edge of the area of measurement support closest to the Sun would tend to be in shade and those away from the Sun more fully illuminated. If the DRF of this instrument had been known in advance, the instrument slit could have been aligned with the Sun and the height of the instrument above the canopy set in such a way that the edge of each of the areas of measurement support overlapped in an attempt to balance out this bias, as there is no wavelength bias along the length of the slit, or another fore optic could have been used.

When using a fore optic with no focusing element (a field stop) the area of measurement support for the ASD spectroradiometer/fore optic system was round, support for all three detectors was concentric but the extent of the area

was detector specific. It was also found that for the SVC instrument used in this research, when used with a fore optic with focusing element, the area of measurement support was approximately rectangular, although it extended beyond that defined by the 'nominal' FOV included angle in some regions of the area of measurement support and did not cover others. Furthermore, although it provided a continuous field of responsivity, there was a blue/near infra-red wavelength responsivity bias across the area of measurement of support and this bias was oriented across the optical slit of the instrument. When the SVC instrument with fore optic with no focusing element, in this case a fibre optic probe, was used, the area of measurement support was found to be round; to have a continuous field of responsivity across the area; and for its responsivity to be equal radially. From the foregoing it is evident that the field-of-view, specified as a 'nominal' included angle, is misleading and does not adequately define the area of measurement support of these spectroradiometers.

These characteristics of the instrument/fore optic systems and their DRFs are fundamentally due to the design of each instrument and its fore optics and are dictated by physical principles (although much can be done to minimise unwanted attributes). Therefore, users should characterise the DRF of the spectroradiometer/fore optics they propose to use and develop appropriate field sampling strategies if the intention is to make good quality reflectance measurements of heterogeneous or anisotropic Earth surfaces.

Chapter 7

Conclusions

Field spectroscopy has greatly assisted in increasing our understanding of the interaction of light with Earth surfaces and has aided the development and use of optical remote sensing from airborne and satellite sensors to gain a better understanding of the processes and dynamics of the Earth. Field spectroscopy has enabled the reflectance of Earth surfaces to be characterised from data acquired close to the ground and features of these reflectance spectra related to state variables, measured by other methods, of spatially and temporally defined surfaces. By doing so field spectroscopy has enabled state variables measured *in situ* and at high spatial resolutions, such as at eddy covariance flux tower sites, to be spatially extrapolated or inferred from hyperspectral images acquired form airborne or satellite sensors, hence, providing local, regional or global coverage (Gamon *et al.*, 2006a,b; Schaepman *et al.*, 2010; Balzarolo *et al.*, 2011). It has also been used, as in this work, to gain an understanding of the biochemical and biophysical processes of plants that influence reflectance enabling the development of models which may be used to further assist analysis of data acquired in future from hyperspectral airborne or satellite sensors. In addition it has been used to "validate models and to maintain *(airborne and satellite)* sensor calibration"

(Milton *et al.*, 2009). However, although the use of field spectroscopy has furthered our understanding of Earth systems, from the work reported in this thesis some recommendation can be made to further improve spectroscopy field methodologies and analysis methods in each of these application domains.

7.1 Recommendations

Spectral reflectance modelling and state variable inference of photosynthesising Earth surfaces

If the *in vivo* spectral profile and the wavelengths of maximum absorption of leaf pigments can vary seasonally and with the presence of other leaf pigments-in-complex, as this work and the work of Di Vittorio (2009) has demonstrated, then the generally published *in vivo* pigment spectral absorption profiles should not be taken as a constant or as an accurate representation of the pigments in a particular species of interest at a particular point in time. This variation in pigment absorption spectra may be compounded by the responsivity per wavelength interval of the spectrometer/fore optic system used being spatially dependent. Consequently, spectroscopists and radiative transfer modellers should determine or verify the *in vivo* proximate pigments, and their change through growth and senescence cycles, in the species of interest in their research. Researchers should also to consider the use of wavelength bands (for correlation between state variables and spectral bands) which are determined over the possible range of pigment feature wavelength variability rather than at specific individually measured wavelength intervals, thereby integrating over a wavelength region and averaging variability for comparison with other data. Researchers should also exercise caution when using wavelength regions, particularly the blue and (to a lesser extent) the near infra-red, where spatially determined wavelength biases could be pronounced.

Spatial sampling and extrapolation

The area of measurement support is a fundamental measurement statistics in geosciences (Atkinson *et al.*, 2000; Atkinson and Aplin, 2004). Much effort has been expended in understanding the area of measurement support (the 'footprint') of eddy covariance measurements at sites where carbon dioxide flux between the Earth's surface and atmosphere are being measured and modelled (see Vesala *et al.* (2004), Kljun *et al.* (2004) or Göckede (2004) and many others for examples) or in understanding the Earth surface area represented by pixels in imaging spectroscopy and remote sensing (see Atkinson and Aplin (2004), Lillesand *et al.* (2004) or Mather (2004) and many others for examples). However, in field spectroscopy little effort has been expended to understand the corresponding support for field spectroscopic measurements. It has been demonstrated in this thesis that the field-of-view of spectrometer fore optics does not adequately define the area of measurement support, the systems responsivity to flux from within that area or if the responsivity is across a continuous or intermittent field. Consequently, field spectroscopists should require manufacturers define the DRF of each spectrometer/fore optic system they supply or researchers should determine it for themselves to aid the development of appropriate measurement methodologies. For example, at flux tower sites where measurements are often made from a fixed location the areal extent of the area of measurement support needs to be known to assess if the area being measured is representative of the wider Earth surface area within the 'foot print' of the flux tower. Particularly as the contribution of "component parts" can not be determined using eddy covariance methods (Moncrieff *et al.*, 1995) and Gamon *et al.* (2006b) has proposed using spectroscopic measurements to bridge this gap. However, there may be spatially dependent wavelength biases or the responsivity of the spectrometer/fore optic system may be spatially 'weighted' as the responsivity could be across a continuous field with a Gaussian responsivity distribution as may be the case for systems with a lens based fore optic and optical slit, systems

with a single optical fibre or systems with a fore optic without a focusing element. Alternatively the responsivity may be across an intermittent field as may be the case with multiple fibre/lens based fore optic systems. It is recommended that these responsivity distributions should also be taken into account when determining spatial sampling strategies, particularly from heterogeneous Earth surfaces where the comparative scales of DRF features and surface heterogeneity needs to be considered. In addition, spectral measurement uncertainties should be determined by making multiple measurements using a statistically defined spatial sampling strategy (random, grid or transect, for example), using the same spectrometer/fore optic system used for the fixed point measurements, and these uncertainties made explicate if interpolations or extrapolations are being made and state variable of other areas inferred from spectral data. The adoption of fore optics and accessories such as optical scramblers or integrating spheres with lens attachment should also be considered as there are indications that these will improve responsivity distribution (provide Gaussian or 'top hat' responsivity respectively) and minimise wavelength spatial dependencies.

Validation of airborne or satellite sensor calibration

Indirect methods have been developed to verify the calibration of optical sensors mounted on airborne or satellite platform or provide calibration correction coefficients. These methods are independent of the methods used for primary calibration before deployment, or of on-board calibration sources, and are of importance as the sensor will then be in its data acquisition mode (Anderson, 2005). These indirect methods mainly rely on making multiple spectral measurements using field spectrometers, preferably simultaneous with airborne or satellite over pass data acquisitions, of natural or artificial Earth surfaces. These surfaces should be spectrally and spatially homogeneous (Anderson, 2005) and spectra acquired of them averaged to provide a representative spectrum for comparison with the spectrum measured by the airborne or satellite sensor of the same surface. If the surfaces

used are spectrally and spatially homogeneous and Lambertian then multiple field measurements may only be necessary to account for changes in atmospheric composition and solar position. However, if the surfaces are not homogeneous and/or are anisotropic, and most Earth surfaces used for vicarious calibration probably are to a greater of lesser extent at some scale, then consideration will need to be given to the DRF characteristics of the spectrometer/fore optic system being used. To make some account for these biases the spectrometer should be rotated around its optical axis between measurements and multiple measurements made, hence, averaging any systematic wavelength dependent spatial bias introduced by the DRF of the system being used.

General recommendation Finally, the recommendation made by Schaepman-Strub *et al.* (2006) to standardise reflectance terminology should be followed and, as this work has shown, international standards developed by other agencies such as Commission Internationale de L'Eclairage be used to develop a common vocabulary and robust standards for field spectroscopy and optical remote sensing.

To further investigate the issues raise in this section a number of areas where future research could usefully be pursued to improve field spectroscopy have been identified. Research should be conducted to develop radiative transfer reflectance models more representative of the surfaces they are being used to model; to advance knowledge of the interaction of light with the biochemical and biophysical processes and dynamics of photosynthesising Earth surfaces; and develop statistical robust field spectroscopy sampling strategies for heterogeneous Earth surfaces.

7.2 Further work

***Calluna* photo active pigments and leaf structural parameters**

The absorption spectrum of Chlorophyll$_{(a+b)}$ is composed of the individual Chlorophyll$_{(a)}$ and Chlorophyll$_{(b)}$ absorption spectra. These individual *in vivo* spectra could possibly be determined through further time series laboratory destructive sampling, spectrophotometry, high performance liquid chromatography, and spectroradiometric and modelling studies, although an automated numerical optimisation method would also require to be developed to enable this to be completed within a reasonable time due to the additional complexity. The relative proportions of each of these pigments and their change over time could then be quantified in *Calluna* leaves. Determining the time lag between stress inducing events, such as unseasonal extreme cold, and Anthocyanins production in *Calluna* shoots and leaves would also be of benefit to future remote sensing and reflectance modelling of Calluna. Remote sensing and reflectance modelling of *Calluna* would also benefit from investigations into the effect that different proportions of the three primary pigments quantified in this work have on their in-complex absorption spectra. The results of research into these three topics would enable *Calluna* reflectance to be more accurately modelled through growth and senescent cycles and enable photosynthetic processes to be more accurately quantified from remote sensing studies.

***Calluna* canopy and stand reflectance modelling**

Additional research could usefully be carried out to quantify the distribution of photosynthetically active biomass through the vertical structure of *Calluna* canopies, as this affects scattering in the near infra-red region of the spectrum and hence the slope of the near infra-red plateau. This could possibly be done *in situ* using optical methods, for example by inserting a PAR sensor into the *Calluna* canopy to make measurements and create a vertical light profile. In addition,

with the deployment of full waveform Light Detection And Ranging (LIDAR) systems on airborne platforms achieving vertical resolutions of approximately 10 cm, it maybe possible to infer the vertical structure of some *Calluna* canopies using airborne remote sensing. As it appears from this work that the flowering phase of *Calluna* is spectrally most distinct, further work could usefully be done to quantify, both physically and by using hyperspectral remote sensing, the profusion of flowers on different canopies and stands to determine if these quantities are correlated with the stand structure and ecological community in which each stand was growing.

The reflectance of the graminoids understorey layer could also be modelled using the canopy and leaf radiative transfer models used in this work if the parameters required for model input were quantified. A radiative transfer model of Bryophyte reflectance could also usefully be developed to assist remote sensing of peatland environments. Further work is also needed to understand why there was a wavelength shift in the Chlorophyll$_{(a+b)}$ absorption maximum between the 2007 and the 2009 sampling periods and whether this was caused by a natural or anthropogenic event or by an instrument bias.

Spectroradiometer directional response functions

The DRFs of other ASD and SVC full wavelength spectroradiometers could be measured and studies undertaken to investigate the differences between the spectra that could be modelled by these instruments and those that were modelled in this research. The single spectrograph spectrometers provided by these and by other manufacturers should have their DRFs measured to more fully complete the information available to enable field spectroscopists to select the instruments most appropriate for their work and to develop more statistically robust field sampling strategies.

Spectroradiometric measurement of heterogeneous and anisotropic

Earth surfaces

The influence that the DRF of field spectroradiometers has on the reflectances recorded from heterogeneous surfaces could be more fully investigated by modelling the reflectances of real Earth surfaces, rather than the stylised surfaces modelled in this work, and this could be verified by laboratory and field spectroradiometric measurements of the same Earth surface target area with different spectroradiometers. Further work could also be carried out to investigate the effect that the areal extent of different reflecting classes within the area of measurement support has on modelled reflectances. The effect that the DRF of spectroradiometers has on measuring reflectances of anisotropic surfaces when measuring their hemispherical conical (or directional) reflectance distribution function would be another area of research that could usefully be pursued.

7.3 Concluding statement

This work has demonstrated how radiative transfer modelling and field spectroscopy can be used to gain an understanding of the complex interactions between light and *Calluna vulgaris*. That pigment absorption spectra are not a constant but are dynamic and change through annual growth and senescence cycles has been emphasised by this work. It has also highlighted the importance of more fully characterising field spectroradiometers than is normal practice when heterogeneous and anisotropic Earth surfaces are to be measured. Nevertheless, a method has been developed which may allow the rich content of spectra acquired by field spectroscopy or hyperspectral images of *Calluna* dominated peatlands to be more fully utilised through the inversion of the canopy growth and reflectance model developed in this thesis. Work will now commence to determine if hyperspectral images acquired during the course of this research by airborne sensors on the Natural Environment Research Council Airborne Research and Survey

Facility aircraft can be inverted, using the growth and reflectance model developed in this thesis, and the properties and processes of *Calluna vulgaris* canopies inferred. If this can be done it will enable hyperspectral remote sensing to be used to monitor ecological change across extensive areas of *Calluna* dominated boreal peatlands and to provide data for climate research, and may assist in these peatlands being included in climate models.

Appendix A

Verification of instrument calibration records

During the course of the work presented in Chapter 2 of this thesis a Perkin Elmer UV/Vis 40 scanning spectrophotometer was used to measure the *in vitro* absorption spectra of *Calluna* 'shoots and leaves' pigments assays extracted in acetone and methanol. The wavelength accuracy and absorption linearity were verified by measuring laboratory calibration standards purchased from Hellma Analytics. The results for both absorption linearity (Figure D) and (Figure A.1(b)) were within the tolerances specified by Hellma for these standards.

A GER 3700 (#1008) full wavelength (400 nm to 2,500 nm) spectroradiometer was used during 2005 and 2006 to measure the relative reflectance spectra of stacked *Calluna* 'shoots and leaves', which were subsequently converted to absolute reflectance. This instrument was also used during field work in 2007. The GER 3700 is owned by NERC FSF and routine quality assurance (QA) tests are carried out prior to and following each loan. The QA test results

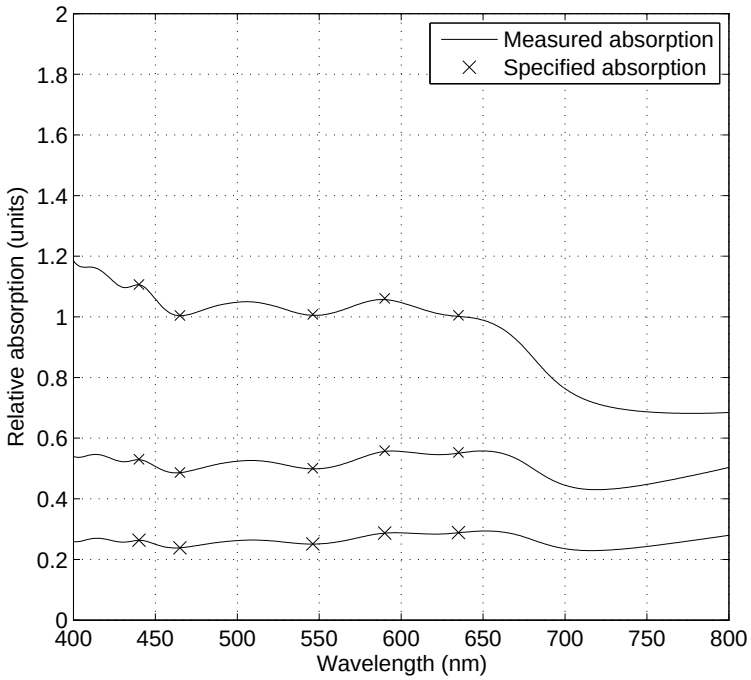

(a) Absorption calibration linearity

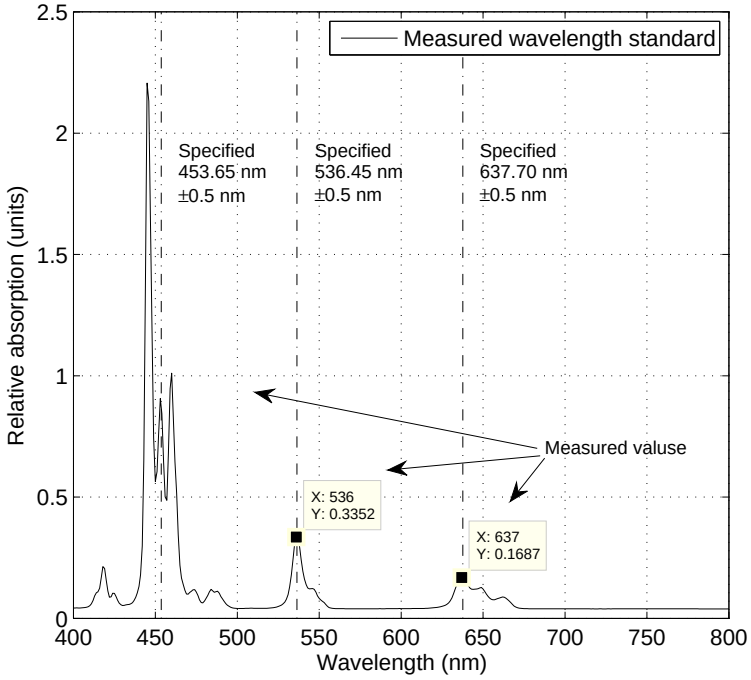

(b) Wavelength accuracy

Figure A.1: Verification of calibration of Perkin Elmer UV/Vis 40 Spectrophotometer

for the 25^{th} October 2007, shown in Figure A.2(a), are typical for of the QA results at each test period during this research. A ASD FieldSpec Pro full spectroradiometer wavelength was used during 2006 for some field measurements and a Spectra Vista Corporation HR-1024 full spectroradiometer wavelength was used for all field work during 2009: the QA records for these instruments are in Figures A.2(b) and A.2(c), respectively. Note the term "Fail" in the records is to bring the value to the attention of QA assessor; it does not necessarily constitute rejection of the instrument and is to be used for critical assessment. A judgement is required to be made by comparing the values stated, their wavelength location, the standards against which they are measured and the instruments' characteristics over successive QA assessments before deciding if the instrument calibration status is currently fit for purpose.

The Spectralon reference panel calibration coefficients for the panel used to convert relative to absolute reflectance during this research. Panel SRT #007 was used during 2006 and 2007 and SRT #019 during 2009 and the calibration files are available from the calibration archive on the FSF web site <http://fsf.nerc.ac.uk/resources/post-processing/calfile_archive/calfile_archive.shtml>.

A Tanita Model 1210 digital balance with an accuracy specified by the manufacturer of ±0.002 g was used to measure the weights of *Calluna* 'shoots and leaves' samples. The accuracy of this balance was verified by comparison with the School of Geosciences Sartorios MC 2105 calibrated balance and all samples measured with the Tanita balance were within ±.001 g of the measurement made with the Sartorios balance. In addition, a Salter Brecknell Electrosamson digital field balance was used to measure biomass samples in the field. The accuracy and precision of this instrument was verified by making repeated measurement of the same sample in a stable environment and comparing values attained from it with those obtained using a new School of Geosciences Sentiment Laboratory balance.

NERC Field Spectroscopy Facility

GER 3700 Quality Assurance Test Result

Instrument:	GER 3700
Serial #:	1008
Test Date:	Thursday, October 25, 2007
Benchmark Filename:	3ER 3700 #1008 Wide Angle L
Benchmark Cal. Date:	Friday, October 26, 2007

SENSORS TEMP	Min. Temp	Average Temp	Max. Temp	Pass/Fail
VNIR Temp Sensor	29.31	30.4685	32.4	Pass
SWIR1 Temp Sensor	31.94	32.991	34.6	Pass

DARK NOISE TEST	Peak - Peak	Std. Dev. Limits	Std.Dev	Pass/Fail
DC Test (VNIR)	0.946	< 1	0.137	Pass
DC Test (SWIR1a)	2.65	< 1	0.569	Pass
DC Test (SWIR1b)	7.48	< 2	1.964	Pass
DC Test (SWIR2)	24.98	< 5	3.882	Pass

NOISE EQUIVALENT RADIANCE TEST	Limits	N.E.R.	Pass/Fail
N.E.R. @ 400-450nm	< 3.000E-02	1.396E−02	Pass
N.E.R. @ 700-800nm	< 3.000E-02	2.040E−02	Pass
N.E.R. @ 940-960nm	< 1.500E-01	7.412E−02	Pass
N.E.R. @ 1450-1500nm	< 2.000E-01	1.031E−01	Pass
N.E.R. @ 1550-1600nm	< 4.000E-01	1.564E−01	Pass
N.E.R. @ 2000-2050nm	< 9.000E-01	6.031E−01	Pass
N.E.R. @ 2440-2460nm	< 3.000E+00	2.112E+00	Pass

WAVELENGTH TEST	Results	Limits ± nm	Error	Pass/Fail
Hg-Ar (365nm)	363	3	−2.0	Pass
Hg-Ar (404.7nm)	404	2	−0.7	Pass
Hg-Ar (435.8nm)	435	2	−0.8	Pass
Hg-Ar (546.1nm)	546	2	−0.1	Pass
Hg-Ar (696.5nm)	697	2	0.5	Pass
Hg-Ar (750.9nm)	750	2	−0.9	Pass
Hg-Ar (763.5nm)	764	2	0.5	Pass
Hg-Ar (811.5nm)	812	2	0.9	Pass
Hg-Ar (841.8nm)	842	2	0.2	Pass
Hg-Ar (912.3nm)	912	2	−0.3	Pass
Hg-Ar (965.8nm)	968	3	2.2	Pass
Mylar (1128.7nm)	1129	10	0.3	Pass
Mylar (1659.9nm)	1661	10	1.1	Pass
Mylar (1904.6nm)	1904	10	−0.6	Pass
Mylar (2130.8nm)	2138	10	7.2	Pass
Mylar (2253.3nm)	2258	10	2.7	Pass
Mylar (2331.0nm)	2333	10	2.0	Pass
Mylar (2444.5nm)	2445	10	0.5	Pass

SIGNAL to NOISE TEST With 1000fL SOURCE	Limits	Results	Pass/Fail
Signal:Noise @ 400nm	> 250	393	Pass
Signal:Noise @ 750nm	> 2,500	4729	Pass
Signal:Noise @ 950nm	> 1000	1534	Pass
Signal:Noise @ 1100nm	> 450	755	Pass
Signal:Noise @ 1500nm	> 300	494	Pass
Signal:Noise @ 1750nm	> 80	157	Pass
Signal:Noise @ 1840nm	> 40	84	Pass
Signal:Noise @ 2490nm	> 2.5	3	Pass

VERIFICATION OF SYSTEM RESPONSE CAL.	Limits	Parameter	Pass/Fail
		Max Abs. Deviation	
Radiance Cal VNIR	< 5%	0.5%	Pass
Radiance Cal SWIR1	< 5%	2.4%	Pass
Radiance Cal SWIR2	< 5%	2.8%	Pass
		Average % Change	
Radiance Cal Visible	< 1%	0.3%	Pass
Radiance Cal NIR	< 3%	0.2%	Pass
Radiance Cal SWIR1a	< 2%	1.9%	Pass
Radiance Cal SWIR1b	< 4%	2.1%	Pass
Radiance Cal SWIR2a	< 4%	1.9%	Pass
Radiance Cal SWIR2b	< 5%	1.5%	Pass

(a) GER 3700 #1008

NERC Field Spectroscopy Facility

SVC HR 1024 Quality Assurance Test Result Sheet

Instrument:	SVC HR 1024
Serial #:	811011
Test Date:	Tuesday, February 10, 2009
Benchmark Filename:	05. SVC HR1024 #0811011 Lens #7
Benchmark Cal. Date:	Thursday, January 15, 2009

SENSORS TEMP	Min. Temp	Average Temp	Max. Temp	Pass/Fail
VNIR Temp Sensor	22.6	25.8	31.6	Pass
SWIR1 Temp Sensor	−0.3	−0.2	−0.1	Pass
SWIR2 Temp Sensor	−5.6	−5.3	−5.2	Pass

)ARK NOISE (Scaled DN	Peak - Peak	Std. Dev. Limits	Std.Dev	Pass/Fail
DC Test (Silicon)	256.667	< 60	36.540	Pass
DC Test (InGaAs-1)	780.00	< 150	110.909	Pass
DC Test (InGaAs-2)	6677.78	< 1000	861.361	Pass

NOISE EQUIVALENT RADIANCE TEST	Limits	N.E.R.	Pass/Fail
N.E.R. @ 400-450nm	< 2.000E-03	1.808E−09	Pass
N.E.R. @ 700-800nm	< 5.000E-03	2.738E−09	Pass
N.E.R. @ 940-960nm	< 5.000E-02	2.192E−08	Pass
N.E.R. @ 1200-1250nm	< 1.000E-01	4.825E−08	Pass
N.E.R. @ 1550-1600nm	< 5.000E-02	1.484E−08	Pass
N.E.R. @ 2000-2050nm	< 5.000E-02	2.339E−08	Pass
N.E.R. @ 2440-2460nm	< 7.500E-02	2.757E−08	Pass

WAVELENGTH TEST	Results	Limits ± nm	Error	Pass/Fail
Hg-Ar (365nm)	365.5	3	0.5	Pass
Hg-Ar (404.7nm)	404.2	2	−0.5	Pass
Hg-Ar (435.8nm)	436.2	2	0.4	Pass
Hg-Ar (546.1nm)	545.9	2	−0.2	Pass
Hg-Ar (696.5nm)	696.4	2	−0.1	Pass
Hg-Ar (750.9nm)	750.6	2	−0.3	Pass
Hg-Ar (763.5nm)	763.4	2	−0.1	Pass
Hg-Ar (811.5nm)	811.1	2	0.0	Pass
Hg-Ar (841.8nm)	841.5	2	−0.3	Pass
Hg-Ar (912.3nm)	923.6	2	11.3	Fail
Hg-Ar (965.8nm)	967.5	3	1.7	Pass
Mylar (1128.7nm)	1127.5	4.5	−1.2	Pass
Mylar (1659.9nm)	1660.5	4.5	0.6	Pass
Mylar (1904.6nm)	1903.8	4.5	−0.8	Pass
Mylar (2130.8nm)	2130.6	4.5	−0.2	Pass
Mylar (2253.3nm)	2254.0	4.5	−1.3	Pass
Mylar (2331.0nm)	2329.7	4.5	−1.3	Pass
Mylar (2444.5nm)	2445.2	4.5	0.7	Pass

SIGNAL to NOISE TEST With 1000fL SOURCE	Limits	Results	Pass/Fail
Signal:Noise @ 400nm	> 1000	2960	Pass
Signal:Noise @ 750nm	> 10,000	37177	Pass
Signal:Noise @ 950nm	> 1000	5739	Pass
Signal:Noise @ 1100nm	> 200	2393	Pass
Signal:Noise @ 1500nm	> 500	3264	Pass
Signal:Noise @ 1700nm	> 500	1670	Pass
Signal:Noise @ 1900nm	> 500	976	Pass
Signal:Noise @ 2490nm	> 50	150	Pass

VERIFICATION OF FSF SYSTEM RESPONSE CAL.	Limits	Parameter	Pass/Fail
		Max Abs. Deviation	
Radiance Cal VNIR	< 5%	4.9%	Pass
Radiance Cal SWIR1	< 5%	6.5%	Fail
Radiance Cal SWIR2	< 5%	7.6%	Fail
		Average % Change	
Radiance Cal Visible	< 1%	1.5%	Fail
Radiance Cal NIR	< 3%	1.4%	Pass
Radiance Cal SWIR1a	< 2%	3.2%	Fail
Radiance Cal SWIR1b	< 4%	4.4%	Fail
Radiance Cal SWIR2a	< 4%	4.6%	Fail
Radiance Cal SWIR2b	< 5%	2.2%	Pass

ERIFICATION OF INTERNAL SYSTEM RESPONSE CA	Limits	Parameter	Pass/Fail
		Max Abs. Deviation	
Radiance Cal VNIR	< 5%	4.0%	Pass
Radiance Cal SWIR1	< 5%	6.2%	Fail
Radiance Cal SWIR2	< 5%	7.6%	Fail
		Average % Change	
Radiance Cal Visible	< 1%	0.9%	Pass
Radiance Cal NIR	< 3%	1.6%	Pass
Radiance Cal SWIR1a	< 2%	3.0%	Fail
Radiance Cal SWIR1b	< 4%	4.2%	Fail
Radiance Cal SWIR2a	< 4%	4.4%	Fail
Radiance Cal SWIR2b	< 5%	2.1%	Pass

(b) SVC HR-1024 #1011

Figure A.2: Field spectroradiometer quality assurance records

The results from the field balance were within ±0.5% of each other and the mean of these within 2% of those measured by the laboratory balance.

Appendix B

Laboratory spectroradiometric measurements sample light environment

The *Calluna* shoots and leaves were stacked in a 100 mm diameter blacked petri dish, the dish placed at the centre of a Portable Soft Lighting Studio ($http://www.maplin.co.uk/portable-soft-lighting-studio$) box and all measurements were made from nadir. The Lighting box, had an optical cloth base (spectrally flat from 400 nm to 2,500 nm and with reflectance less than 5%), three white translucent sides, one side open and an open top. This measurement set up provided direct illumination and a proportion of diffuse illumination, to more closely represent stable natural illumination conditions. The Lighting box was illuminated using a 500 watt double ended tungsten halogen lamp angled towards the sample at 55^o and positioned 60 cm from the centre line and 100 cm above the base of the box. See Figure B.1 for the laboratory reflectance measurement configuration. The light environment across the base of the box was measured with a photographic Lux meter at 4 cm intervals in a grid. The normalised distribution

of the light across the base is shown in Figure B.2. All points within the area where the petri dish was positioned had a level of illumination greater than 96% of the maximum measured illumination level measured. To measure the ratio of total to diffuse illumination and verify that there were no wavelength dependent influences in the diffuse light environment being caused by the translucent sides an integrating sphere designed to measure irradiance was attached to the SVC HR-1024 spectroradiometer and 10 measurements made at the centre point on the base of the box. A 2 cm diameter shading disc on the end of a 20 cm long 1.5 mm diameter arm was then used to shade the input port of the sphere and further 10 measurements made. As can be seen from Figure B.3, the direct:diffuse ratio was approximately 9.3:0.7 from 400 nm to 1,000 nm although there was a linear 1% wavelength dependent increase across this spectral range. It was considered that for practical purposes this 1% variation was within the spectral reflectance measurement error and could be discounted.

Figure B.1: Laboratory spectral reflectance measurement configuration

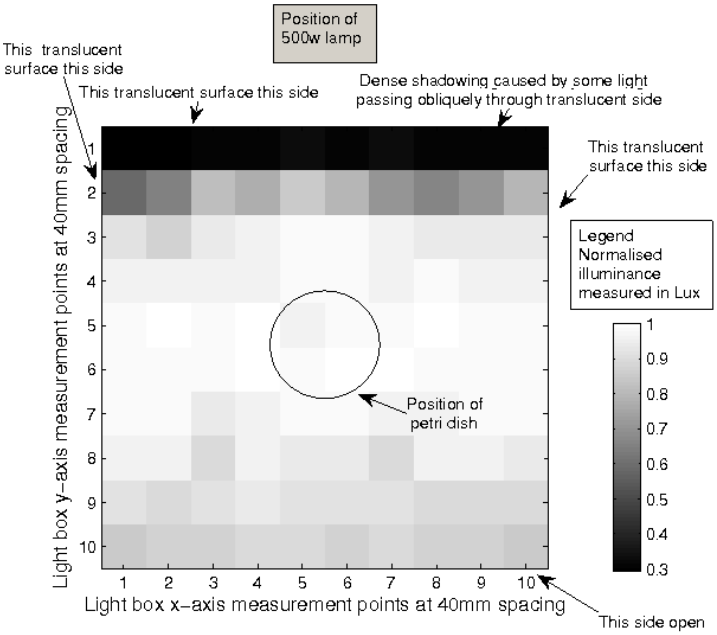

Figure B.2: Laboratory spectral reflectance measurement light environment

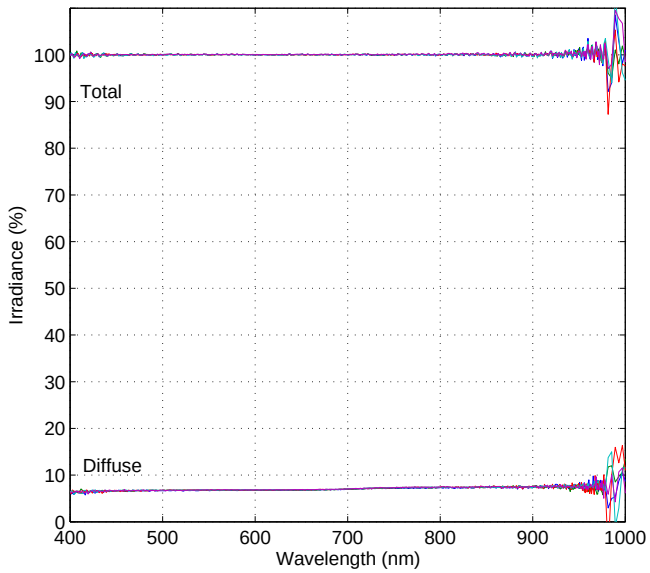

Figure B.3: Wavelength dependent proportions of total and diffuse illumination at central area of Light box where the spectral reflectance measurements of *Calluna* shoots and leaves were measured

Appendix C

Selected meteorological records Bishopton Met Office 2005 to 2009

No continuous meteorological data was acquired at the Smeath Hill research site during the course of this research. Data was therefore acquired from the Met Office MIDAS Land Surface Station at Bishopton (Latitude: 55.9^o; Longitude: -4.533^o; Altitude: 59 m), approximately 12 km North West of Smeath Hill. The temperature (Figure C.1) data were adjusted for lapse rate using 0.63^o/100 m, as the research site was at an altitude of 270 m. The annual daily hours of sunshine are calculated by the Met Office using the Campbell-Stokes method. The rainfall data from the Bishopton station has not been included here as rainfall was considered to be the most unreliable of the meteorological data analysed since rain events may be more site specific than temperature and sunshine, particularly when an elevated site is being considered.

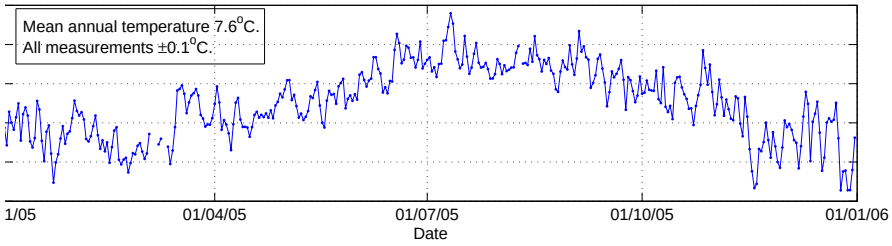

(a) 2005

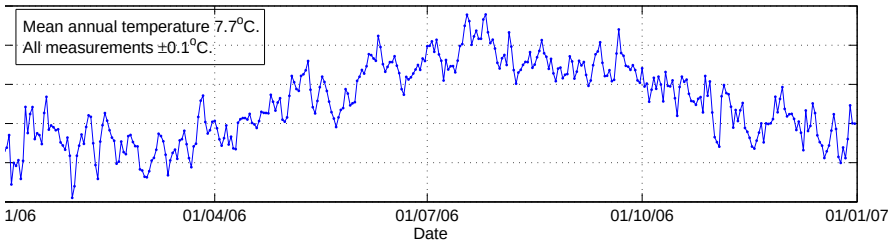

(b) 2006

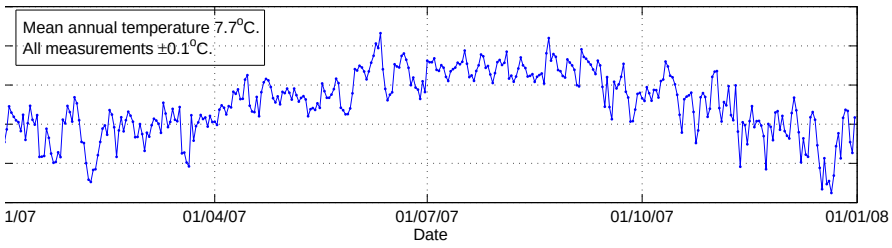

(c) 2007

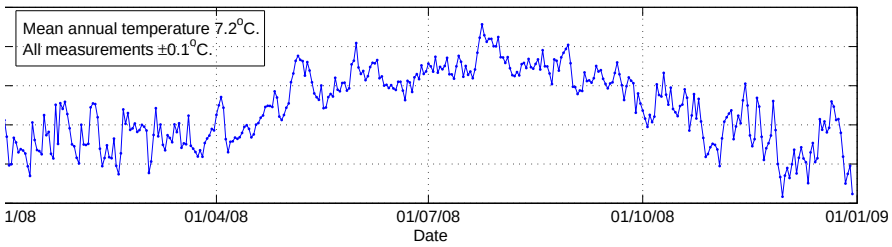

(d) 2008

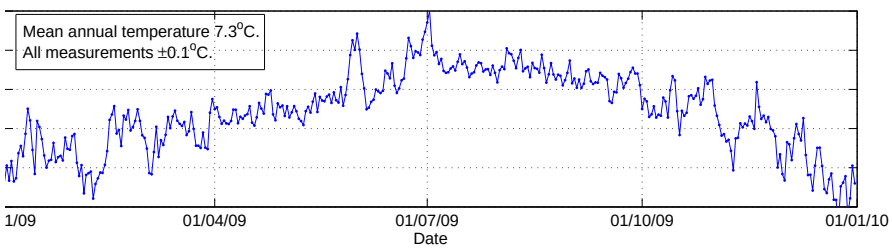

(e) 2009

Figure C.1: Estimated mean daily temperature for Smeath Hill research site

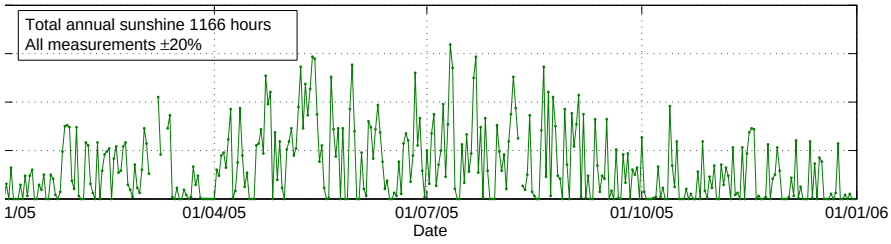

(a) 2005

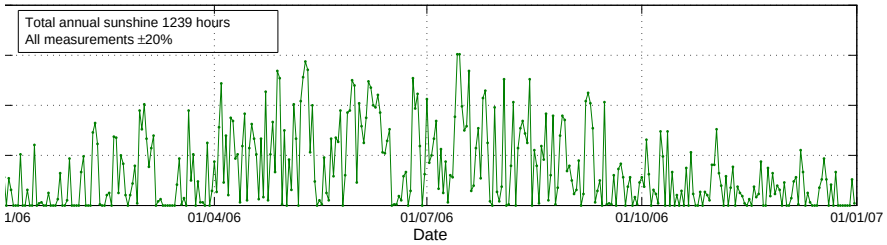

(b) 2006

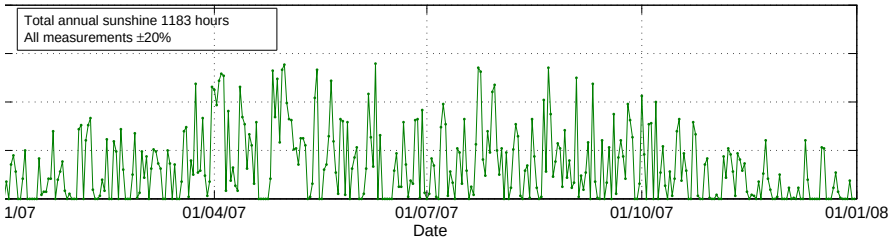

(c) 2007

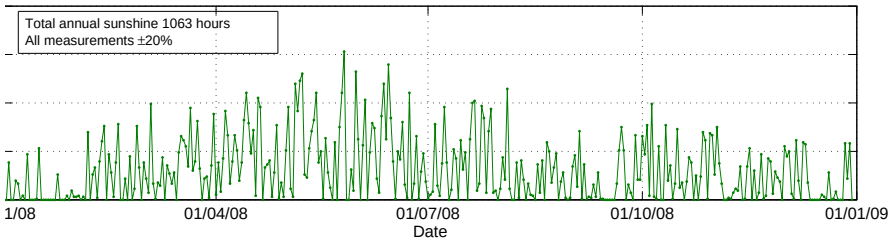

(d) 2008

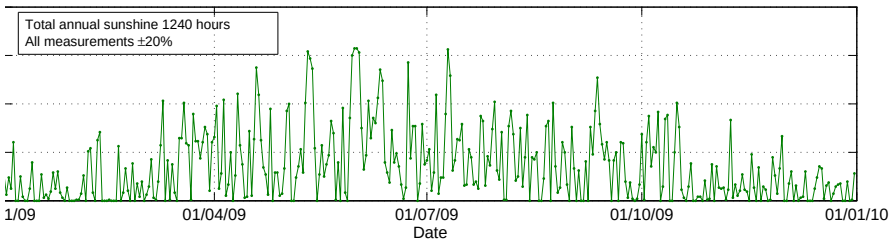

(e) 2009

Figure C.2: Daily hours sunshine recorded at Met Office station, Bishopton

Appendix D

SunScan transect PAR spatial distribution data

The data included in the analysis in Chapter 5 is shown in Figures C.1,2 and 3. The growth and development of the *Calluna* canopy and stand structures can be seen. It can be inferred from the increasing number of data points with a low value that the canopy density is increasing and inferred from the reduction in the number of points with very high values that the canopies are closing. In addition, the differences between each plot at of the three sampling intervals May, June and July 2009 can be seen from this data. However, although it was possible to infer canopy structure and stand ground cover it was not possible to determine LAI from these data.

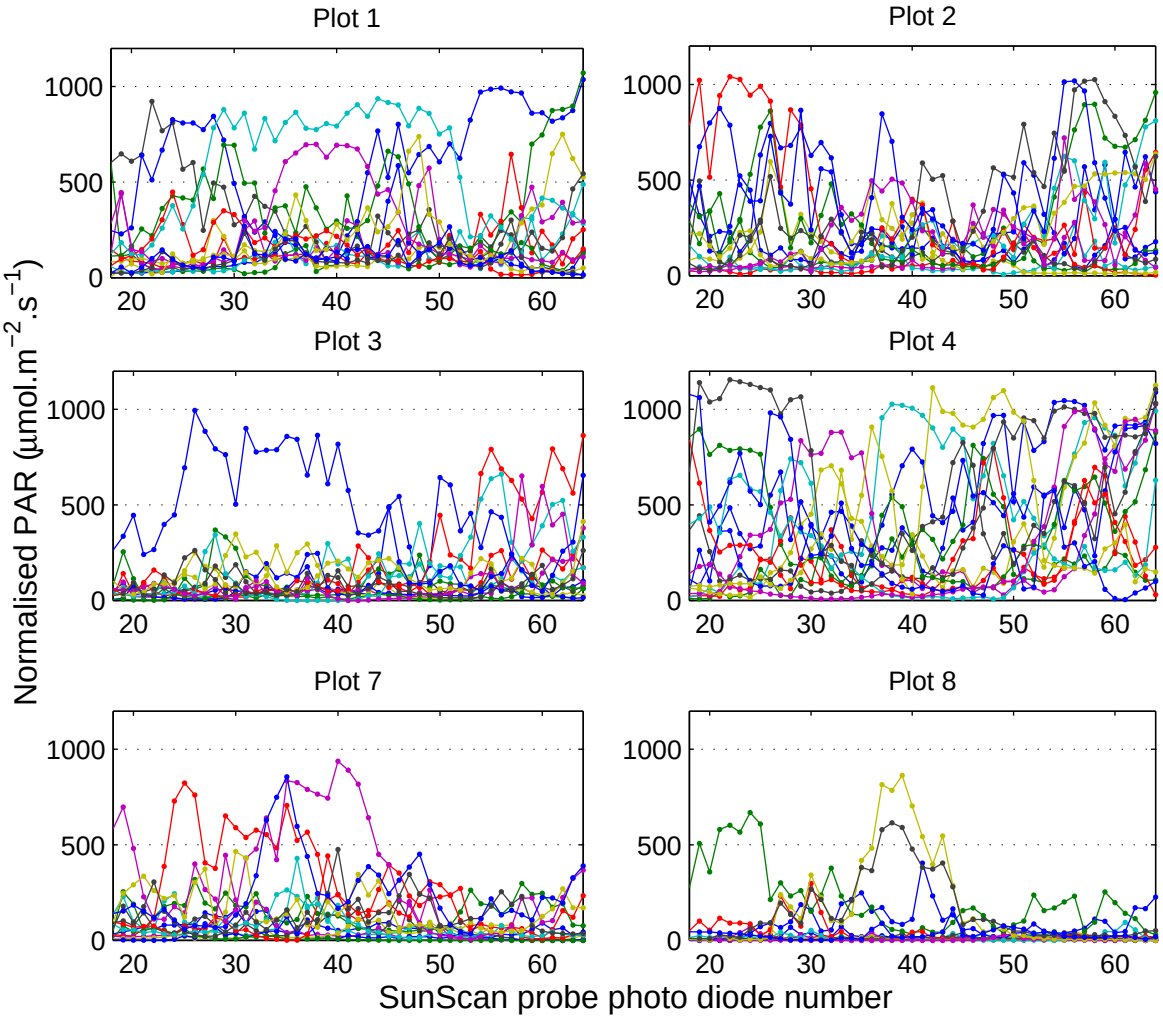

Figure D.1: SunScan PAR data May 2009

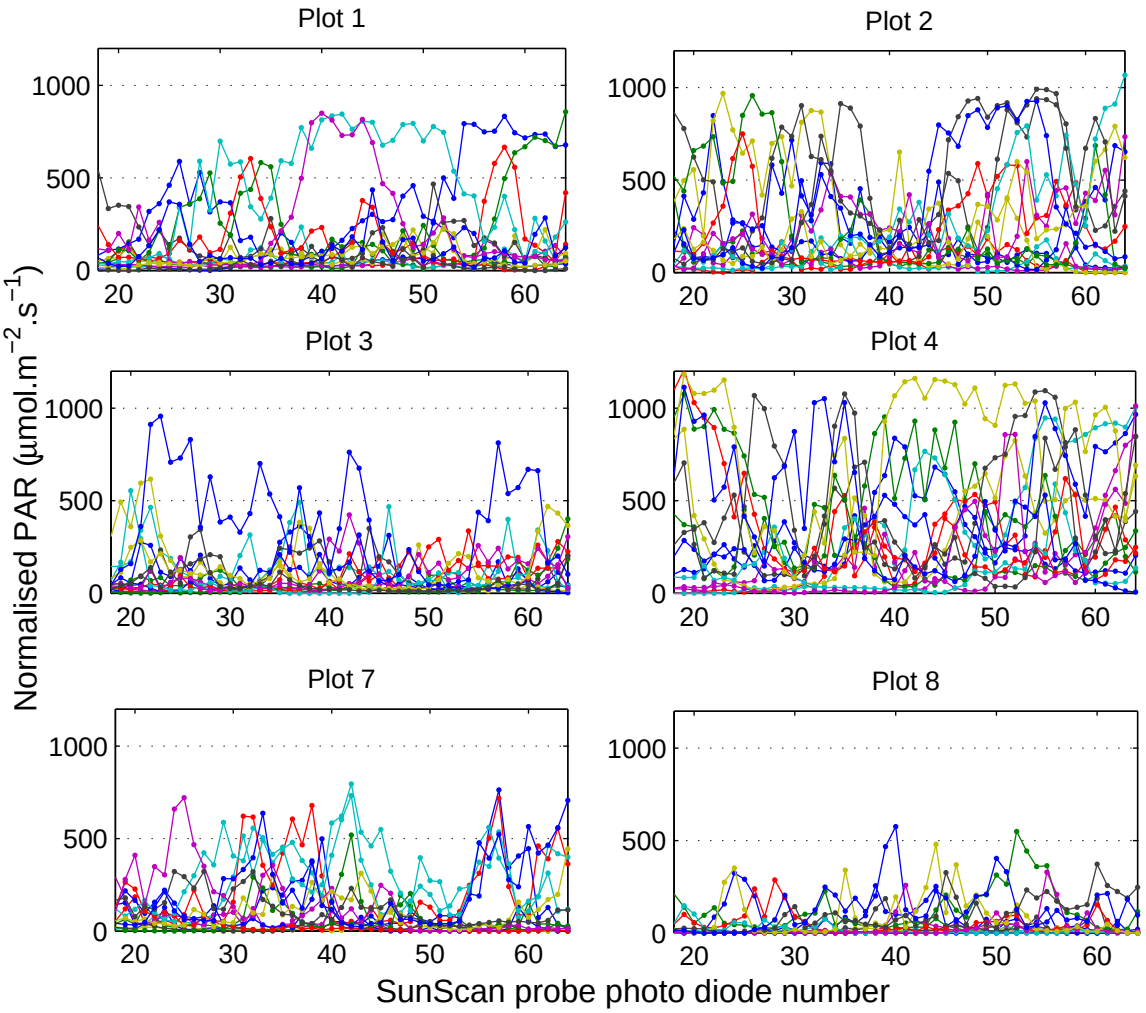

Figure D.2: SunScan PAR data June 2009

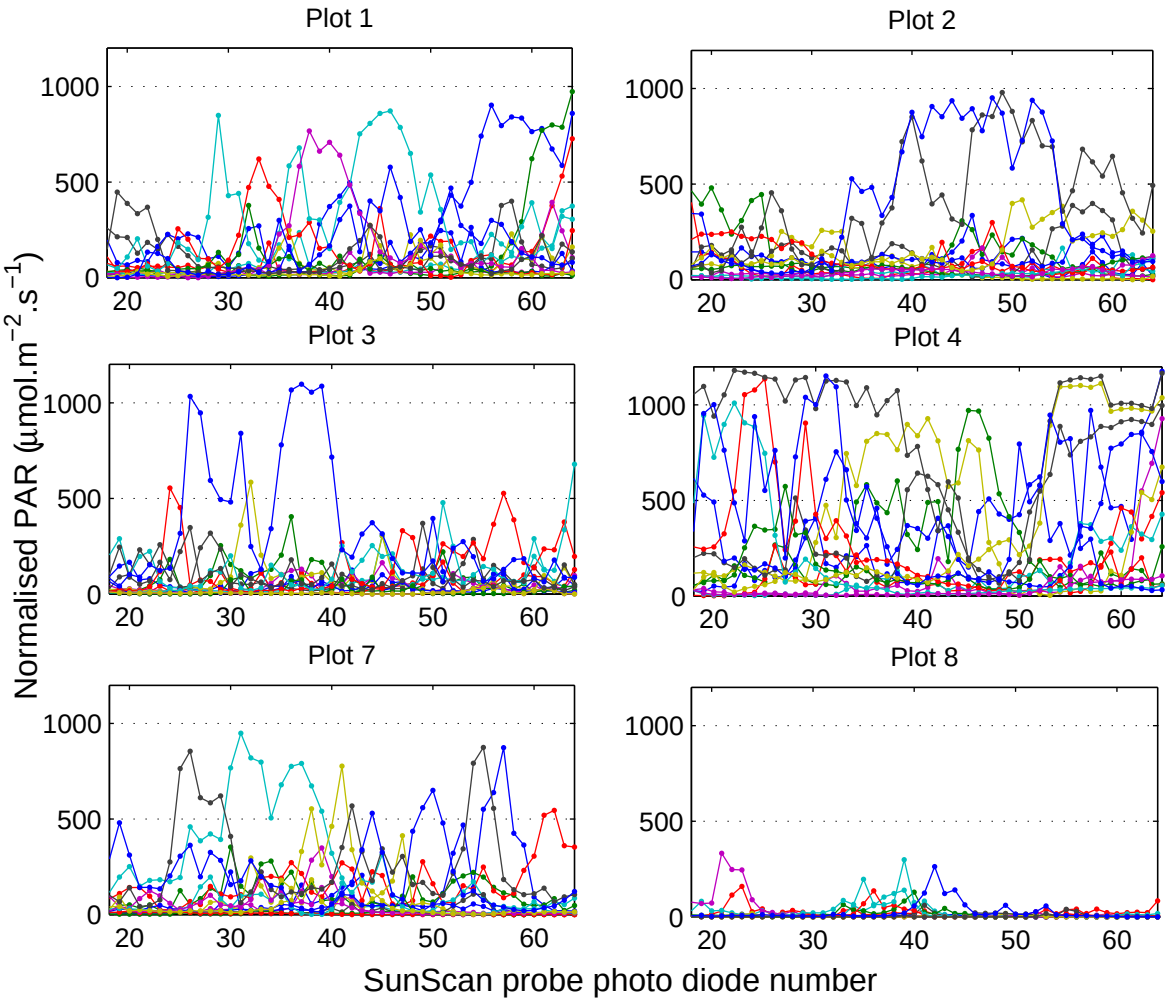

Figure D.3: SunScan PAR data July 2009

Appendix E

Positional accuracy and precision of research plot transect field spectroscopy measurements

The intention was to measure the same area of measurement support for each spectral measurement at each transect measurement point at each temporal sampling interval. This required that the spectroradiometer, mounted on its support frame, be repeatedly located at the same transect measurement point, using the slots cut in the transect for this purpose. To assess the positional accuracy and precision of making these repeat measurements with the SVC HR-1024 spectroradiometer, a white board was placed on top of a *Calluna* canopy and obscured from the instrument user's view. The mounting frame with HR-1024 attached was mounted in a transact slot 30 times, each time being levelled only using the x and y direction spirit level attached to the frame. Each time the frame was mounted in the transect the sighting laser on the HR-1024 was activated, a field assistant marked the centre point of the laser spot on the board and the location of each of these points was subsequently measured. From Figure

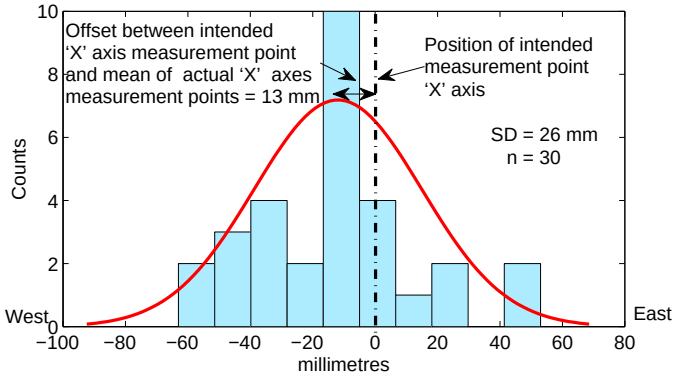

(a) Measurement x-axis

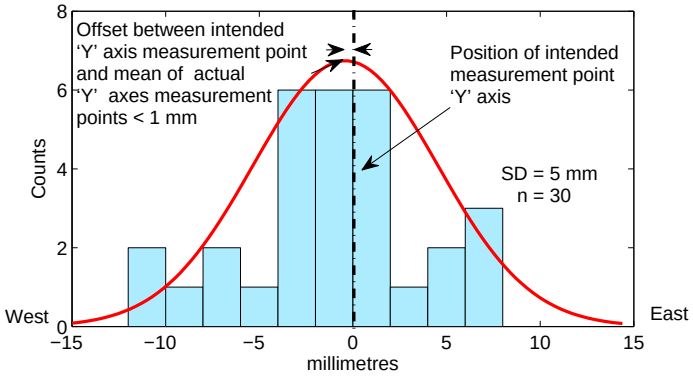

(b) Measurement y-axis

Figure E.1: Positional accuracy and precision of repeated field spectroscopy measurements of the same area

E.1(a) it can be seen that the mean of 30 measurement was offset to the left of the intended measurement central point by 13 mm and 95% of the measurements were within ±26 mm of that point in the East/West direction (x-axis). In the North/South direction (y-axis) (Figure E.1(b)) the mean of 30 measurements was offset to the North but within 1 mm of the intended measurement point and 95% of the measurements were within ±10 mm of that point.

References

Albert, K.R., Ro-Poulsen, H., Mikkelsen, T.N., Michelsen, A., van den Linden, L. and Beier, C. (2011). Effects of elevated CO_2 warming and drought episodes on plant carbon uptake in a temperate heath ecosystem are controlled by soil water status. *Plant, Cell & Environment*, **34**, 1207–1222.

Alcamo, J. and Bennett, E.M. (2003). Ecosystems and their services. In J. Alcamo and E.M. Bennett, eds., *Ecosystems and human well-being: a framework for assessment*, 49–71, Island Press.

Alonso, I., Hartley, S.E. and Thurlow, M. (2001). Competition between heather and grasses on scottish moorlands: Interacting effects of nutrient enrichment and grazing regime. *Journal of Vegetation Science*, **12**, 249–260.

Analytical Spectral Devices (1999). *Technical Guide*. Analytical Spectral Devices, Inc, Boulder, Colorado, 4th edn.

Analytical Spectral Devices (2002). *ASD FieldSpec Pro: User's Guide*. Analytical Spectral Devices, Inc., Boulder, Colorado, rev. c 08-10-2005 edn.

Analytical Spectral Devices (2005). *FieldSpec 3 User Manual, Revision C*. Analytical Spectral Devices, Inc., Boulder, Colorado.

Anderson, J.M. and Hetherington, S.L. (1999). Temperature, nitrogen availability and mixture effects on the decomposition of heather [*Calluna vulgaris* (l.) Hull] and bracken [*Pteridium aquilinum* (l.) Kuhn] litters. *Functional Ecology*, **13**, 116–124.

Anderson, K. (2005). *Temporal variability in calibration target reflectance: methods, models and applications.*. Ph.D. thesis, University of Southampton.

Anderson, K. and Kuhn, N. (2008). Variations in soil structure and reflectance during a controlled crusting experiment. *International Journal of Remote Sensing*, **29**, 3457–3475.

Anderson, K., Milton, E.J. and Rollin, E.M. (2006). Calibration of dual-beam spectroradiometric data. *International Journal of Remote Sensing*, **27**, 975–986.

Anderson, K., Bennie, J.J., Milton, E.J., Hugh, P.D., Lindsay, R. and Meade, R. (2010). Combining lidar and ikonos data for eco-hydrological classification of an ombrotrophic peatland. *Journal of Environmental Quality*, **39**, 260–273.

Anderson, K., Dungan, J. and Mac Arthur, A.A. (2011). On the reproducability of field reflectance factors in the context of vegetation studies. *Remote Sensing of Environment*, **115**, 1893–1905.

Archer, D. (2010). *The Global Carbon Cycle*. Princeton Primers in Climate, Princeton University Press, Princeton, New jersey.

Armitage, R.P., Kent, M. and Weaver, R.E. (2004). Identification of the spectral characteristics of british semi-natural upland vegetation using direct ordination: a case study from dartmoor, uk. *International Journal of Remote Sensing*, **25**, armitage2004.

Armstrong, H.M., Gordon, I.J., Grant, S.A., Hutchings, N.J., Milne, J.A. and Sibbald, A.R. (1997). A model of the grazing of hill vegetation by sheep in the uk .1. the prediction of vegetation biomass. *Journal of Applied Ecology*, **34**, 166–185.

Aspinall, R.J., Marcus, W.A. and Boardman, J.W. (2002). Considerations in collecting, processing, and analysing high spectral resolution hyperspectral data for environmental investigations. *Journal of Geophysical Systems*, **4**, 15–29.

Atkinson, P.M. (1999). Spatial statistics. In A. Stien, F.D. van der Meer and B. Gorte, eds., *Spatial Statistics for Remote Sensing*, Kluwer, Dordrecht.

Atkinson, P.M. (2004). Resolution manipulation and sub-pixel mapping. In S. de Jong and F.D. van Der Meer, eds., *Remote Sensing Image Analysis: Including the Spatial Domain*, vol. 5, 51–70, Kluwer, London.

Atkinson, P.M. and Aplin, P. (2004). Spatial variation in land cover and choice of spatial resolution for remote sensing. *International Journal of Remote Sensing*, **25**, 3687–3702.

Atkinson, P.M. and Curran, P.J. (1995). Defining an optimal size of support for remote-sensing investigations. *IEEE Transactions on Geoscience and Remote Sensing*, **33**, 768–776.

Atkinson, P.M. and Curran, P.J. (1997). Choosing an appropriate spatial resolution for remote sensing investigations. *Photogrammetric Engineering and Remote Sensing*, **63**, 1345–1351.

Atkinson, P.M. and Tate, N.J. (2000). Spatial scale problems and geostatistical solutions: A review. *Professional Geographer*, **52**, 607–623.

Atkinson, P.M., Foody, G.M., Curran, P.J. and Boyd, D.S. (2000). Assessing the ground data requirements for regional scale remote sensing of tropical forest biophysical properties. *International Journal of Remote Sensing*, **21**, 2571–2587, 345FP INT J REMOTE SENS.

Baird, A.J., Comas, X., Slater, L.D., Belyea, L.R. and Reeve, A.S. (2009). *Understanding Carbon Cycling in Northern Peatlands: Recent Developments and Future Prospects*, vol. 184 of *Geophysical Monograph Series*, chap. 1.

Balzarolo, M., Anderson, K., Nichol, C., Rossini, M., Vescovo, L., Arriga, N., Wohlfahrt, G., Calvet, J.C., Carrara, A., Cerasoli, S., Cogliati, S., Daumard, F., Eklundh, L., Elbers, J.A., Evrendilek, F., Kaduk, J., Klumpp, K., Matteucci, G., Meroni, M., Montagnani, L., Ourcival, J.M., Sánchez-Cañetem, E.P., Pontailler, J.Y., Juszczak, R., Scholes, B. and Martín, M.P. (2011). Ground-based optical measurements at european flux sites: A review of methods, instruments and current controversies. *Sensors*, **11**, 7954–7981.

Baranoski, G.V.G. and Rokne, J.G. (2005). A practical approach for estimating the red-edge position of plant leaf reflectance. *International Journal of Remote Sensing*, **26**, 503–521.

Barclay-Estrup, P. and Gimingham, C.H. (1969). The description and interpritation of cyclical processes in a heath community: I. vegetational change in relation to the calluna cycle. *Journal of Ecology*, **57**.

Baret, F., Champion, I., Guyot, G. and Podaire, A. (1987). Monitoring wheat canopies with a high spectral resolution radiometer. *Remote Sensing of Environment*, **22**, 367–378.

Baret, F., Houlès, V. and Guérif, M. (2007). Quantification of plant stress using remote sensing observations and crop models: the case of nitrogen management. *Journal of Experimental Botany*, **58**, 869–880.

Barrett, E. and Curtis, L.F. (1999). *Environmental Remote Sensing*. Stanley Thornes, Cheltenham, 4th edn.

Barton, C. (2001). A theoretical analysis of the influence of heterogeneity in chlorophyll distribution on leaf reflectance. *Tree Physiology*, **21**.

Belward, A.S., Taylor, J.C., Stuttard, M.J., Bignal, E., Mathews, J. and Curtis, D. (1990). An unsupervised approach to the classification of seminatural vegetation from landsat thematic mapper data - a pilot-study on Islay. *International Journal of Remote Sensing*, **11**, 429–445.

Belyea, L.R. and Malmer, N. (2004). Carbon sequestration in peatland: patterns and mechanisms of response to climate change. *Global Change Biology*, **10**, 1043–1052.

Biewer, S., Erasmi, S., Fricke, T. and Wachendorf, M. (2009). Prediction of yield and the contribution of legumes in legume-grass mixtures using field spectrometry. *Precision Agriculture*, **10**, 128–144.

Billett, M.F., Palmer, S.M., Hope, D., Deacon, C., Storeton-West, R., Hargreaves, K.J., Flechard, C. and Flower, D. (2004). Linking land-atmosphere-stream carbon fluxes in a lowland peatland system. *Global Biogeochemical Cycles*, **18**, 1–12.

Billett, M.F., Charman, D.J., Clark, J.M., Evans, C.D., Ostle, N.J., Worral, F., Burden, A., Dinsmore, K.J., Jones, T., McNamara, N., Parry, L., Rowson, J.G. and Rose, R. (2010). Carbon balance of uk peatlands: current state of knowledge and future research challenges. *Climate Research*, **45**, 13–29.

Billingsley, F.C., Anutu, P.A., Carr, J.L., McGillem, C.D., Smith, D.M. and Strand, T.C. (1983). Data processing and reprocessing. In R.N. Colwell, ed., *Manual of Remote Sensing*, vol. 1, 719–788, American Society of Photogrammetry, Falls Church, Virginia.

Bird, A.C., Taylor, J.C. and Brewer, T.R. (2000). Mapping national park landscape from ground, air and space. *International Journal of Remote Sensing*, **21**, 2719–2736.

Blackburn, G.A. (1998). Quantifying chlorophylls and caroteniods at leaf and canopy scales: An valuation of some hyperspectral approaches. *Remote Sensing of Environment*, **66**, 273–285.

Blackburn, G.A. (2007). Hyperspectral remote sensing of plant pigments. *Journal of Experimental Botany*, **58**, 855–867.

Blackburn, G.A. and Ferwerda, J.G. (2008). Retrieval of Chlorophyll concentration from leaf reflectance spectra using wavelet analysis. *Remote Sensing of Environment*, **112**, 1614–1632.

Blackburn, G.A. and Steele, C. (1999). Towards the remote sensing of matorral vegetation physiology: Relationships between spectral reflectance, pigment, and biophysical characteristics of semiarid bushland canopies. *Remote Sensing of Environment*, **70**, 278–292.

Blanchfield, A.L., Robinson, S.A., Renzullo, L. and Powell, K. (2006). Phylloxera-infested grapevines have reduced chlorophyll and increased photoprotective pigment content-can leaf pigment composition aid pest detection? *Functional Plant Biology*, **33**, 507–514.

Boardman, N. (1977). Comparative photosynthesis of sun and shade plants. *Annual Review of Plant Physiology*, **28**, 355–377.

Bonn, A., Allott, T., Hubacek, K. and Stewart, J. (2009a). *Introduction: Drivers of environmental change in upland environments: concepts, threats and opportunities*, chap. 1, 1–10. Routledge Studies in Ecological Economics, Routledge.

Bonn, A., Rebane, M. and Reid, C. (2009b). *Ecosystem services: a new rationale for conservation of upland environments*, 448–474. Routledge.

Bonn, A., Holden, J., Parnell, M., Worrall, F., Chapman, P.J., Evans, C.D., Termansen, M., Beharry-Borg, N., Acreman, M., Rowe, E., Emmett, B. and

Tsuchiya, A. (2010). Ecosystem services of peat – phase 1. Tech. Rep. Project code: SP0572, DEFRA.

Boyd, D.S., Entwistle, J.A., Flowers, A.G., Armitage, R.P. and Goldsmith, P.C. (2006). Remote sensing the radionuclide contaminated Belarusian landscape: a potential for imaging spectrometry? *International Journal of Remote Sensing*, **27**, 1865–1874.

Bradley, R.I., Milne, R., Bell, J., Lilly, A., Jordan, C. and Higgins, A. (2005). A soil carbon and land use database for the United Kingdom. *Soil Use and Management*, **21**, 363–369.

Breda, N. (2003). Ground-based measurements of leaf area index: a review of methods, instruments and current controversies. *Journal of Experimental Botany*, **54**, 24032417.

Bullock, J. (2006). Plants. In W. Sutherland, ed., *Ecological Census Techniques: a handbook*, 186–212, Cambridge University Press, Cambridge, 2nd edn.

Carfrae, J.A., Sheppard, L.J., Raven, J.A., Leith, I.D., Stein, W., Crossley, A. and Theobald, M. (2004). Early effects of atmospheric ammonia deposition on *Calluna vulgaris* (L.) Hull growing on an ombrotrophic bog. *Water, Air, & Soil Pollution Focus*, **4**.

Carroll, J.A., Caporn, S., Cawely, L., Read, D.J. and Lee, J.A. (1999). The effect of increased deposition of atmospheric nitrogen on *Calluna vulgaris* in upland Britain. *New Phytologist*, **141**, 423–431.

Carter, G.A. and Knapp, A.K. (2001). Leaf Optical Properties in Higher Plants: Linking Spectral Characteristics to Stress and Chlorophyll Concentration. *Journal of Botany,*, **88**, 677–684.

Carter, G.A. and Spiering, B.A. (2002). Optical Properties of Intact Leaves for Estimating Chlorophyll Concentration. *Journal of Environmental Quality*, **31**, 1424–1432, chlorophylls.

Castro-Diez, P., Puyravaud, J. and Cornelissen, J. (2000). Leaf structure and anatomy as related to leaf mass per area variation in seedlings of a wide range of woody plant species and types. *Oecologia*, **124**, 476–486.

Castro-Esau, K., Sánchez-Azofeifa, G. and Rivard, B. (2006). Comparison of spectral indices obtained using multiple spectroradiometers. *Remote Sensing of Environment*, **103**, 276–288.

Castro-Esauand, K.L. and Kalacska, M. (2008). *Tropical Dry Forest Phenology and Discrimination of Tropical Tree Species Using Hyperspectral Data*, 2–22. CRC Press, Taylor & Francis, eBook ISBN: 978-1-4200-5343-2 Accessed 09-09-2010.

Chan, J.C.W., Spanhove, T., Ma, J., Vanden Borre, J., Paelinckx, D. and Canters, F. (2010). Natura 2000 habitat identification and conservation status assessment with superresolution enhanced hyperspectral (CHRIS/Proba) imagery. In *Proceedings of Geographic Object-Based Image Analysis conference (GEOBIA)*, The International Archives of the Photogrammetry, Remote Sensing and Spatial Information Sciences Vol. XXXVIII-4/C7.

Chappell, A., Zobeck, T.M. and Brunner, G. (2006). Using bi-directional soil spectral reflectance to model soil surface changes induced by rainfall and wind-tunnel abrasion. *Remote Sensing of Environment*, **102**, 328–343.

Charman, D. (2002). *Peatlands and Environmental Change*. John Wiley & Sons Ltd, Chichester.

Chase, T.N., Pielke Sr, R.A., Kittel, T.G.F., Nemani, R.R. and Running, S.W. (2000). Simulated impacts of historical land cover changes on global climate in northern winter. *Climate Dynamics*, **16**, 93–105.

Chen, H. (1997). *Remote Sensing Calibration Systems: An introduction*. A. Deepak, Hampton, Virginia.

Chen, J., Shen, M., Zhu, X. and Tang, Y. (2009). Indicator of flower status derived from in situ hyperspectral measurement in an alpine meadow on the Tibetan Plateau. *Ecological Indicators*, **9**, 818–823.

Chen, J.M. (196). Optically-based methods for measuring seasonal variation of leaf area index in boreal conifer stands. *Agricultural and Forest Meteorology*, **80**, 135–163.

Chen, J.M. and Black, T.A. (1992). Defining leaf area index for non-flat leaves. *Plant Cell Environment*, **15**, 421–429.

Chen, J.M. and Cihlar, J. (1995). Plant canopy gap-size analysis theory for improving optical measurements of leaf-area index. *Applied Optics*, **34**, 6211–6221.

Chen, Y., McNamara, N., Dumont, M., Bodrossy, L., Stralis-Pavese, N. and Murrell, J. (2008). The impact of burning and *Calluna* removal on below-ground methanotroph diversity and activity in a peatland soil. *Applied Soil Ecology*, **40**, 291–298.

Cherrill, A. and McClean, C. (1999). The reliability of 'Phase 1' habitat mapping in the UK: The extent and types of observer bias. *Landscape and Urban Planning*, **45**, 131–143.

Cherrill, A.J., McClean, C., Lane, A. and Fuller, R.M. (1995). A comparison of land-cover types in an ecological field survey in northern england and a

remotely-sensed land-cover map of great-britain. *Biological Conservation*, **71**, 313–323.

Cho, M., Skidmore, A. and Atzberger, C. (2008). Towards red-edge positions less sensitive to canopy biophysical parameters for leaf Chlorophyll estimation using properties optique spectrales des feuilles (PROSPECT) and scattering by arbitrarily inclined leaves (SAILH) simulated data. *International Journal of Remote Sensing*, **28**, 2241–2255.

Clevers, J.G.P.W., Kooistra, L. and Salas, E.A.L. (2004). Study of heavy metal contamination in river floodplains using the red-edge position in spectroscopic data. *International Journal of Remote Sensing*, **25**, 3883–3895.

Close, D. and Beadle, C. (2003). The ecophysiology of foliar Anthocyanin. *The Botanical Review*, **69**, 149–161.

Commission Internationale de L'Eclairage (1987). Methods of characterizing illuminance meters and luminance meters. Tech. Rep. 69, Commission Internationale de L'Eclairage.

Cournède, P.H., Mathieu, A., Houllier, F., Barthélémy, D. and de Reffye, P. (2007). Computing competition for light in the greenlab model of plant growth: A contribution to the study of the effects of density on resource acquisition and architectural development. *Annals of Botany*, **101**, 1207–1219.

Croft, H., Anderson, K. and Kuhn, N. (2009). Characterising soil surface roughness using a combined structural and spectral approach. *European Journal of Soil Science*, **60**, 431–442.

Csaplovics, E. (1992). Analysis of Color Infrared Aerial-Photography and Spot Satellite Data for Monitoring Land Cover Change of a Heathland Region of the Causse Du Larzac (Massif-Central, France). *International Journal of Remote Sensing*, **13**, 441–460.

Cuartas, P., Gordon, I.J., Hester, A.J., Perez-Barberia, F.J. and Hulbert, I.A.R. (2000). The effect of heather fragmentation and mixed grazing on the diet of sheep *Ovis aries* and red deer *Cervus elaphus*. *Acta Theriologica*, **45**, 309–320.

Curran, P.J. and Atkinson, P.M. (1999). Issues of scale and optimal pixel size. In A. Stien, F.D. van der Meer and B. Gorte, eds., *Spatial Statistics for Remote Sensing*, Kluwer, Dordrecht.

Curtis, B. and Goetz, A.F.H. (1994). Field spectrometry: Techniques and instrumentation. 195–203, Procceding of an International Symposium on Spectral Sensing Research, ASD, Boulder, Colorado.

Darvishzadeh, R., Skidmore, A., Schlerf, M. and Atzberger, C. (2008). Inversion of a radiative transfer model for estimating vegetation LAI and Chlorophyll in a heterogeneous grassland. *Remote Sensing of Environment*, **112**, 2592–2604.

Daughtry, C. and Biehl, L. (1985). Changes in spectral properties of detached birch leaves. *Remote Sensing of Environment*, **17**, 281–289.

Davidson, E. and Janssens, I. (2006). Temperature sensitivity of soil carbon decomposition and feedbacks to climate change. *Nature*, **440**, 165–173.

Davies, G.M., Hamilton, A., Smith, A. and Legg, C.L. (2008). Using visual obstruction to estimate heathland fuel load and structure. *International Journal of Wildland*, **17**, 380–389.

Dawson, T.P., Curran, P.J. and Plummer, S.E. (1998). LIBERTY - Modeling the Effects of Leaf Biochemical Concentration on Reflectance Spectra. *Remote Sensing of Environment*, **65**, 50–60.

Dayton, N., Clarke, I. and Arnott, D. (1994). A vegitation survey of Clyde Muirshiel Regional Park, Strathclyde. Tech. rep., Scottish Natural Heritage.

Dehaan, R. and Taylor, G.R. (2003). Image-derived spectral endmembers as indicators of salinisation. *International Journal of Remote Sensing*, **24**, 775–794.

Delalieux, S., Somers, B., s. Hereijgers, Verstraeten, W.W., Keulemans, W. and Coppin, P. (2008). A near-infrared narrow-waveband ratio to determine leaf area index in orchards. *Remote Sensing of Environment*, **112**, 3762–3772.

Demmig-Adams, B. and Adams, W. (1996). Chlorophyll and Carotenoid composition in leaves of *Euonymus kiautschovicus* acclimated to different degrees of light stress in the field. *Australian Journal of Plant Physiology*, **23**, 649–659.

Di Vittorio, A. (2009). Enhancing a leaf radiative transfer model to estimate concentrations and *in vivo* specific absorption coefficients of total Carotenoids and Chlorophylls *a* and *b* from single-needle reflectance and transmittance. *Remote Sensing of Environment*, **113**, 1948–1966.

Disney, M., Lewis, P. and Saich, P. (2006). 3D modelling of forest canopy structure for remote sensing simulations in the optical and microwave domains. *Remote Sensing of Environment*, **100**, 114–132.

Dorrepaal, E., Aerts, R., Cornelissen, J., Callaghan, T. and van Logtestijn, R. (2003). Summer warming and increased winter snow cover affect *Sphagnum fuscum* growth, structure and production in a sub-arctic bog. *Global Change Biology*, **10**, 93–104.

Dorrepaal, E., Toet, S., van Logtestijn, R., Swart, E., Martine J. van de Weg, M., Callaghan, T. and Aerts, R. (2009). Carbon respiration from subsurface peat accelerated by climate warming in the subarctic. *Nature*, **460**, 616.

Dvoral, J. and Stokrova, J. (1993). Structure of needles in the early phases of development in *Pinus ponderosa* P. et C. Lawson with special reference to plastids. *Annals of Botany*, **72**, 423–431.

Earth Observation for Natura (2000). Earth observation for natura 2000. Tech. Rep. EN/61201/DC/Final, National Remote Sensing Centre Limited for the European Commission DGXII / Framework IV.

Egan, S., Smith, A., Robertson, D. and Waterhouse, A. (2000). Estimation of heather biomass using ground based methods for the calibration of remotely sensed data. *Aspects of Applied Biology*, **58**.

Ehleringer, J.R. (1984). Intraspecific competitive effects on water relations, growth and reproduction in *Encelia farinosa*. *Oecologia*, **62**, 151–162.

Eller, B.M. (1977). Leaf pubescence: The significance of lower surface hairs for the spectral properties of the upper surface. *Journal of Experimental Botany*, **28**, 1054–1059.

Erwin, K. (2009). Wetlands and global climate change: the role of wetland restoration in a changing world. *Wetlands Ecological Management*, **17**, 71–84.

Feild, T., Lee, D. and Holbrook, N. (2001). Why leaves turn red in autumn. the role of Anthocyanins in senescing leaves of red-osier dogwood. *Plant Physiology*, **127**, 566–574.

Feret, J.B., Francois, C., Gitelson, G.P., Asnerand, A., Bidel, R.E., Martin, L., Ustin, S.L., le Maire, G. and Jacquemoud, S. (2008). PROSPECT-4 and 5: Advances in the leaf optical properties model separating photosynthetic pigments. *Remote Sensing of Environment*, **112**, 3030–3043.

Ferrier, G., Rumsby, B.T. and Pope, R.J. (2007). Application of hyperspectral remote sensing data in the monitoring of the environmental impact of hazardous waste derived from abandoned mine sites. *Journal of the Geological Society of London, special publications,*, **283**, 107–116.

Ferrier, G., Hudson-Edwards, K. and Pope, R. (2009). Characterisation of the environmental impact of the Rodalquilar mine, Spain by ground-based reflectance spectroscopy. *Journal of Geochemical Exploration*, **100**, 11–19.

Foody, G.M. and Trodd, N.M. (1993). Non-classificatory analysis and representation of heathland vegetation from remotely sensed imagery. *GeoJournal*, **29**, 343–350.

Fox, N.P. (2001). Traceability to SI for EO measurements. *CEOS WGCV Cal/Val Newsletter,*, **9**, 1–9.

Frank, T.D., Tweddale, S.A. and Lenschow, S.J. (2005). Non-destructive estimation of canopy gap fractions and shrub canopy volume of dominant shrub species in the Mojave desert. *Journal of Terramechanics*, **45**, 231–244.

Gamon, J.A., Huemmrich, K.F., Peddle, D.R., Chen, J., Fuentes, D., Hall, F.G., Kimball, J.S., Goetz, S., Gu, J., McDonald, K.C., Miller, J.R., Moghaddam, M., Rahman, A.F., Roujean, J.L., Smith, E.A., Walthall, C.L., Zarco-Tejada, Fernandes, R. and Cihlar, J. (2004). Remote sensing in boreas: Lessons learned. *Remote Sensing of Environment*, **89**, 139–162.

Gamon, J.A., Cheng, Y., Claudio, H., MacKinney, L. and Sims, D.A. (2006a). A mobile tram system for systematic sampling of ecosystem optical properties. *Remote Sensing of Environment*, **103**, 246–254.

Gamon, J.A., Rahman, A.F., Dungan, J.L., Schildhauer, M. and Huemmrich, K.F. (2006b). Spectral network (SpecNet)what is it and why do we need it? *Remote Sensing of Environment*, **103**, 227–235.

Ganapol, B.D., Johnson, L.F., Hammer, P.D., Hlavka, C.A. and Peterson, D.L. (1998). LEAFMOD: A New Within-Leaf Radiative Transfer Model. *Remote Sensing of Environment*, **63**.

Gausman, H.W., Menges, R.M., Escobar, D., Everitt, J. and Bowen, R. (1969). Effect of leaf pubescence of *Gynura aurantiaca* on light reflectance. *Botanical Gazette*, **130**, 158–162.

Gausman, H.W., Menges, R.M., Escobar, D., Everitt, J. and Bowen, R. (1977). Pubescence affects spectra and imagery of silverleaf sunflower (*Helianthus argophyllus*). *Weed Science*, **25**, 437–440.

Ge, S., Everett, J., Carruthers, R., Gong, P. and Anderson, G. (2006). Hyperspectral characteristics of canopy components and structure for phenological assessment of an invasive weed. *Environmental Monitoring and Assessment*, **120**, 109–126.

Gimingham, C.H. (1960). Biological Flora of the British Isles: *Calluna Salisb.* A monotypic genus. *Journal of Ecology*, **48**.

Gimingham, C.H. (1972). *Ecology of Heathlands*. Chapman and Hall, London.

Gimingham, C.H. (1975). *An Introduction to Heathland Ecology*. Oliver & Boyd, Edinburgh, Scotland.

Gimingham, C.H. (1989). Heather and heathlands. *Botanical Journal of the Linnean Society*, **101**, 263–268.

Gitelson, A., Gritz, Y. and Merzlyak, M. (2003). Relationships between leaf Chlorophyll content and spectral reflectance and algorithms for non-destructive Chlorophyll assessment in higher plant leaves. *Journal of Plant Physiology*, **75**, 272–282.

Gitelson, A.A. and Merzlyak, M. (1998). Remote sensing of Chlorophyll concentration in higher plant. *Advances in Space research*, **22**.

Gitelson, A.A. and Merzlyak, M. (2004). Non-destructive assessment of Chlorophyll, Carotenoid and Anthocyanin content in higher plant leaves: Principles and algorithms. In S. Stamatiadis, J.M. Lynch and J.S. Schepers, eds., *Remote sensing for Agriculture and Environment*, 78–94, Ella.

Gitelson, A.A., Zur, Y., Chivkunova, O. and Merzlyak, M. (2002). Assessing Carotenoid content in plant leaves with reflectance spectroscopy. *Photochemistry and Photobiology*, **160**, 271–281.

Glime, J. (2007). Bryophyte ecology. Ebook sponsored by Michigan Technological University and the International Association of Bryologists. http://www.bryoecol.mtu.edu. Accessed 18th March 2011.

Göckede, M. (2004). *Adoption of Footprint Method for the Quality Control of Edd-Covariance Measurements*. Ph.D. thesis, Faculty of Biology, Chemistry and Geosciences, University of Bayreuth.

Goodenough, D.G., Niemann, K.O., Dyk, A., Gordon, P. and Quinn, G.S. (2009). Mapping high resolution forest chemestry with AISA. In *6th EARSeL IS SIG workshop. Imaging Spectroscopy: Innovative tool for scientific and commercial environmental applications.*, University of Tel-Aviv, Israel.

Gordon, J.E., Thompson, D.B.A. and Horsfield, D. (2001). Geo-ecology and the conservation management of sensitive upland landscapes in scotland. *Catena*, 323–332.

Gorham, E. (1991). Northern peatlands: Role in the carbon cycle and probable responses to climatic warming. *Ecological Applications*, **1**, 182–195.

Govaerts, Y.M. and Verstraete, M. (1998). Raytran: a monte carlo ray tracing model to compute light scattering in three-dimensional heterogeneous media. *IEEE Transactions on Geoscience and Remote Sensing*, **36**, 493–505.

Grace, J., Nichol, C., Disney, M., Lewis, P., Quaife, T. and Bowyer, P. (2007). Can we measure terrestrial photosynthesis from space directly, using spectral reflectance and fluorescence? *Global Change Biology*, **13**, 1484–1497.

Grant, L. (1987). Diffuse and specular characteristics of leaf reflectance. *Remote Sensing of Environment*, **22**, 309–322.

Grant, S.A. and Armstrong, H.M. (1993). Grazing ecology and the conservation of heather moorland - the development of models as aids to management. *Biodiversity and Conservation*, **2**, 79–94.

Grant, S.A. and Hunter, R.F. (1962). Ecotypic Differentiation of *Calluna vulgaris (L.)* in Relation to Altitude. *New Phytologist*, **61**, 44–55.

Gu, L., Post, W.M., Baldocchi, D.D., Black, T.A., Suyker, A.E., Verma, S.B., Vesala, T. and Wofsy, S.C. (2009). *Characterising the Seasonal Dynamics of Plant Community Photosynthesis Across a Range of vegetation Types*. Springer, Dordrecht, Netherlands.

Guenther, B. (1987). Practical aspects of achieving accurate radiometric field measurements. *Remote Sensing of Environment*, **22**, 131–143.

Hadley, B.C., Garcia-Quijano, M., Jensen, J.R. and Tullis, J.A. (2005). Empirical versus model-based atmospheric correction of digital airborne imaging spectrometer hyperspectral data. *Geocarto International*, **20**, 21–28.

Haines-Young, R.H. and Potschin, M. (2009). Upland Ecosystem Services. Report to Natural England. Tech. rep., Natural England, NE Project Code: PTY02/10/002.27 CEM Report No 10.

Haines-Young, R.H., Barr, C.J., Black, H., Briggs, D., Bunce, R., Clarke, R., Cooper, A., Dawson, F., Firbank, L., Fuller, R., Furse, M., Gillespie, M.K., Hill, R., Hornung, M., Howard, D.C., McCann, T., Morecroft, M., Petit, S., Sier, A., Smart, S., Smith, G., Stott, A., Stuart, R. and Watkins, J. (2000). Accounting for nature: assessing habitats in the UK countryside. Tech. rep., DETR, London.

Hamylton, S. (2011). Estimating the coverage of coral reef benthic communities from airborne hyperspectral remote sensing data: Derivatives, multiple discriminant function analysis and linear spectral unmixing,. *International Journal of Remote Sensing*, **32**, 9673–9690.

Hansen, J., Sato, M., Ruedy, R., Lo, K. and Medina-Elizade, M. (2006). Global temperature change. *Proceedings of the National Academy of Science USA*, **103**, 14288–14293.

Harris, A. and Bryant, B. (2009a). A multi-scale remote sensing approach for monitoring northern peatland hydrology: Present possibilities and future challenges. *Journal of Environmental Management*, **90**, 2178–2188.

Harris, A. and Bryant, B. (2009b). Northern peatland vegetation and the carbon cycle: A remote sensing approach. In A. Baird, L.R. Belyea, X. Comas, S. Reeves and L. Slater, eds., *Carbon Cycling in Northern Peatlands*, 79–98, American Geophysical Union, Washington DC.

Harris, A. and Bryant, R.G. (2008). A multi-scale remote sensing approach for monitoring northern peatland hydrology: Present possibilities and future challenges. *Journal of Environmental Management*, **90**, 2178–2188.

Harris, A., Bryant, R.G. and Baird, A.J. (2006). Mapping the effects of water stress on *Sphagnum*: Preliminary observations using airborne remote sensing. *Remote Sensing of Environment*, **100**, 363–378.

Hasselwimmer, C.E., Riley, T.R. and Liu, J.G. (2010). Assessing the potential of multispectral remote sensing for lithological mapping on the antarctic peninsula: case study from eastern adelaide island, graham land. *Antarctic Science*, **22**, 299–318.

Hatier, J. and Gould, K. (2009). Anthocyanin function in vegetative organs. In K. Gould, K. Davies and C. Winefield, eds., *Anthocyanins : biosynthesis, functions, and applications*, 1–19, Springer.

Heimann, M. and Reichstein, M. (2008). Terrestrial carbon dynamics and climate feedbacks. *Nature ecosystem*, **45**, 289–292.

Hester, A.J. and Baillie, G.J. (1998). Spatial and temporal patterns of heather use by sheep and red deer within natural heather/grass mosaics. *Journal of Applied Ecology*, **35**, 772–784.

Hester, A.J., Gordon, I.J., Baillie, G.J. and Tappin, E. (1999). Foraging behaviour of sheep and red deer within natural heather grass mosaics. *Journal of Applied Ecology*, **36**, 133–146.

Hilker, T., Coops, N.C., Coggins, S.B., Wulder, M.A., Brown, M., Black, T.A., Nesic, Z. and Lessard, D. (2009). Detection of foliage conditions and disturbance from multi-angular high spectral resolution remote sensing. *Remote Sensing of Environment*, **113**, 421–434.

Hobbs, S. (2003). Linear mixture modelling solution methods for satellite remote sensing. Tech. rep., College of Aeronautics, Cranfield University, Cranfield, Bedford, UK.

Holden, J., Chapman, P.J. and Labadz, J.C. (2004). Artificial drainage of peatlands: hydrological and hydrochemical process and wetland restoration. *Progress in Physical Geography*, **28**, 95–123.

Holden, J., Shotbolt, L., Bonn, A., Burt, T.P., Chapman, P.J., Dougill, A.J., Fraser, E.D.G., Hubacek, K., Irvine, B., Kirkby, M.J., Reed, M.S., Prell, C., Stagl, S., Stringer, L.C., Turner, A. and Worral, F. (2007). Environmental change in moorland landscapes. *Earth-Science Reviews*, **82**, 75–100.

Holton, T. and Cornish, E. (1995). Genetics and biochemistry of Anthocyanin biosynthesis. *The Plant Cell*, **7**, 1071–1083.

Horiguchi, G., Ferjani, A., Fujikura, U. and Tsukaya, H. (2006). Coordination of cell proliferation and cell expansion in the control of leaf size in *Arabidopsis thaliana*. *Journal of Plant Research*, **119**, 37–42.

Horler, D.N.H., Dockray, M. and Barber, J. (1983). The red edge of plant leaf re ectance. *International Journal of Remote Sensing*, **4**, 273–288.

Huang, C., Townshend, J.R.G., Laing, S., Kalluri, S. and Defries, R. (2002). Impact of sensor's point spread function on land cover characterization: assessment and deconvolution. *Remote Sensing of Environment*, **80**, 203–212.

Huckle, J.M., Marrs, R.H. and Potter, J.A. (2006). Characterising the salt-marsh resource using multi-spectral remote sensing: a case study of the dee estuary in north-west england. *Journal of Practical Ecology and Cons*, **6**, 1–22.

Hudson, I.L. and Keatley, M.R. (2010). *Introduction and Overview*, 1–23. Springer, New York.

Isaaks, E.H. and Srivastava, R.M. (1989). *An Introduction to Applied Geostatistics*. Oxford University Press, Oxford.

Jacquemoud, S. (1993). Inversion of the PROSPECT + SAIL canopy reflectance model from AVIRIS equivalent spectra: Theoretical study. *Remote Sensing of Environment*, **44**, 281–292.

Jacquemoud, S. and Baret, F. (1990). PROSPECT: A model of leaf optical properties spectra. *Remote Sensing of Environment*, **34**, 75–91.

Jacquemoud, S. and Ustin, S.L. (2001). Leaf optical properties: A state of the art. 223–232, 8th Int. Symp. Physical Measurements & Signatures in Remote Sensing.

Jacquemoud, S. and Ustin, S.L. (2008). Modeling leaf optical properties. http://www.photobiology.info/Jacq_Ustin.html. Accessed 26th February 2010.

Jacquemoud, S., Ustin, S.L., Verdebout, J., Schmuck, G., Andreoli, G. and Hosgood, B. (1996). Estimating leaf biochemistry using the PROSPECT leaf optical properties model. *Remote Sensing of Environment*, **56**, 194–202.

Jacquemoud, S., Bacour, C., Poilve, H. and Frangi, J.P. (2000). Comparison of four radiative transfer models to simulate plant canopies reflectance: Direct and inverse mode. *Remote Sensing of Environment*, **74**, 471–481.

Jacquemoud, S., W., V., Baret, F., Bacour, C., Zarco-Tejada, P.J., Asner, G.P., François, C. and Ustin, S.L. (2009). PROSPECT+SAIL models: A review of use for vegetation characterization. *Remote Sensing of Environment*, **113**, S55–S66.

Jago, R.A., Cutler, M.E.J. and Curran, P.J. (1999). Estimating canopy chlorophyll concentration from field and airborne spectra. *Remote Sensing of Environment*, **68**, 217–224.

Johnson, I.R. and Thornley, J.H.M. (1983). Vegetative crop growth model incorporating leaf area expansion and senescence, and applied to grass. *Issue Plant, Cell & Environment Plant, Cell & Environment*, **6**, 721–729,.

Johnston, K., Ver Hoef, J.M., Krivoruchko, K. and Lucas, N. (2001). *Using ArcGIS Geostatistical Analyst: GIS by ESRI*. ESRI, Redlands, CA.

Joint Committee for Guides in Metrology (2008). *Evaluation of measurement data; Guide to the expression of uncertainty in measurement*. Joint Committee for Guides in Metrology (ISO), 1st edn.

Joint Committee for Guides in Metrology (2009). *Evaluation of measurement data An introduction to the "Guide to the expression of uncertainty in measurement" and related documents*. Joint Committee for Guides in Metrology (ISO), 1st edn.

Joosten, H. (2010). The global peatland CO_2 picture: Peatland status and drainage related emissions in all countries of the world. Tech. rep., Greifswald University, http://www.wetlands.org/. Accessed 18th March 2011.

Joosten, H. and Clarke, D. (2002). *Wise use of mires and peatlands - Background and principles including a framework for decision-making*. International Mire Conservation Group and International Peat Society, Totnes, Devon.

Jordan, C.F. (1969). Derivation of leaf-area index from quality of light on the forest floor. *Ecology*, **50**, 663–666.

Ju, C.H., Tian, Y.C., Yao, X., Cao, W.X., Zhu, Y. and Hannaway, D. (2010). Estimating leaf chlorophyll content using red edge parameters. *Pedosphere*, **20**, 633–644.

Kalaitzidis, C., Caprorn, S.J.M. and Cotler, M.E.J. (2008). Estimating foliar nitrogen concentration of heather (*Calluna vulgaris*) from field and laboratory spectra. *Water Air Soil Pollution*, **194**, 57–66.

Karpouzli, E. and Malthus, T. (2003). The empirical line method for the atmospheric correction of IKONOS imagery. *International Journal of Remote Sensing*, **24**, 1143–115.

Kaufmann, H., Guanter, L., Segl, K., Chabrillat, S., Hofer, S., Foerster, K., Sang, B., Stuffer, T., Müeller, A., Müeller, R., Richter, R., Chlebek, C. and Rossner, G. (2010). EnMAP – An Advanced Optical Payload for Earth Observation. In *Art, Science and Applications of Reflectance Spectroscopy Symposium*, ASD.

King, M.D., France, J.L., Fisher, F.N. and Beine, H.J. (2005). Measurement and modelling of UV radiation penetration and photolysis rates of nitrate and hydrogen peroxide in Antarctic sea ice: An estimate of the production rate of hydroxyl radicals in first-year sea ice. *Journal of Photochemistry and Photobiology, A: Chemistry,*, **176**, 39–49.

Kljun, N., Kastner-Klein, P., Fedorovich, E. and Rotach, M.W. (2004). Evaluation of lagrangian footprint model using data from wind tunnel convective boundary layer. *Agricultural and Forest Meteorology*, **127**, 189–201.

Knipling, E. (1970). Physical and physiological basis for the reflectance of visible and near-infrared radiation from vegetation. *Remote Sensing of Environment*, **1**, 155–159.

Kooistra, L., Mücher, C.A., Chan, J.C.W., Vanden Borre, J. and Haest, B. (2009). Use of spectral mixture analysis for characterisation of function and structure of heathland habitat types. In *6th EARSeL IS SIG workshop. Imaging Spectroscopy: Innovative tool for scientific and commercial environmental applications.*, University of Tel-Aviv, Israel, Tel-Aviv, Israel.

Kostkowski, H. (1997). *Reliable Spectroradiometry*. Spectroradiometry Consulting, La Plata, MA.

Kruse, F.A. (2010). Mineral Mapping Using Spectroscopy - From Field Measurements to Airborne Satellite-Based Imaging Spectrometry. In *Art, Science and Applications of Reflectance Spectroscopy Symposium*, ASD Inc. and IEEE GRSS.

Kucharik, C.J., Norman, J.M. and Gower, S.T. (1998). Measurement of branch area and adjusting leaf area index indirect measurements. *Agricultural and Forest Meteorology*, **91**, 69–88.

Kuhry, P. and Turunen, J. (2006). *The Postglacial Development of Boreal and Subarctic Peatlands*, 25–41. Ecological Studies, Springer.

Kumar, L., Schmidt, K., Dury, S. and Skidmore, A. (2001). *Imaging Spectrometry and Vegetation Science*, vol. 4. Kluwer, London.

Kurbatova, J., Li, C., Tatarinov, F., Varlagin, A., Shalukhina, N. and Olchev, A. (2009). Modeling of the carbon dioxide fluxes in European Russia peat bogs. *Environmental Research Letters*, **4**, 1–5.

Kuusk, A. (1995). A markov chain model of canopy reflectance. *Agricultural and Forest Meteorology*, **76**, 221–236.

Kuusk, A. (2001). A two-layer canopy reflectance model. *Journal of Quantitative Spectroscopy & Radiative Transfer*, **71**, 1–9.

Kuusk, A. (2003). *Two-Layer Canopy Reflectance Model ACRM User Guide*. Tartu Observatory, 08th edn.

Kuusk, A., Lang, M., Kuusk, J., Lükk, T., Nilson, T., M., M., Rautiainen, M. and Eenmäe, A. (2008). Database of optical and structural data for the validation of radiative transfer models. Tech. Rep. 09.2009, Tartu Observatory, Estonia.

Kuusk, A., Kuusk, J. and Lang, M. (2009). A dataset for the validation of reflectance models. *Remote Sensing of Environment*, **113**, 889–892.

Lang, M., Kuusk, A., Lükk, T., Pehk, M. and Alm, G. (2002). Reflectance spectra of ground vegetation in sub-boreal forests. http://www.aai.ee/bgf/ger2600/frspec.html. Accessed 8th February 2012.

Lavender, S.J., Pinkerton, M., Moore, G., Aiken, J. and Blondeau-Patissier, D. (2005). Modification to the atmospheric correction of SeaWiFS ocean colour images over turbid waters. *Continental Shelf Research*, **25**, 539–555.

le Maire, G., François, C., Soudani, K., Berveiller, D., Pontailler, J.Y., Bréda, N., Genet, H., Davi, H. and Dufrêne, E. (2008). Calibration and validation of hyperspectral indices for the estimation of broadleaved forest leaf Chlorophyll content, leaf mass per area, leaf area index and leaf canopy biomass. *Remote Sensing of Environment*, **112**, 3846–3864.

Le Quéré, C., Raupach, M.R., Canadell, J.G., Marland, G. *et al.* (2009). Trends in the sources and sinks of carbon dioxide. *Nature Geoscience*, **2**, 831–836.

Leith, I.D., Sheppard, L., Fowler, D., Cape, J., Jones, M., Crossley, A., Hargreave, K., Tang, Y.S., Theobald, M. and Sutton, M.R. (2004). Quantifying dry NH_3 deposition to an ombrotrophic bog from an automated NH_3 field release system. *Water, Air, and Soil Pollution Focus*, **4**, 207–218.

Levizou, E., Drilias, P., Psaras, K. and Manetas, Y. (2005). Blackwell publishing, ltd. nondestructive assessment of leaf chemistry and physiology through spectral reflectance measurements may be misleading when changes in trichome density co-occur. *New Phytologist*, **165**, 463–472.

Lewis, P. (2007). 3d canopy modelling as a tool in remote-sensing research. In J. Vos, L.F.M. Marcelis, P.H.B. Visser, P.C. Struick and P.C. Evers, eds., *Functional-Structural Plant Modelling in Crop Production*, vol. 22 of *Wageningen UR Frontis Series*, 219–229, Springer, The Netherlands.

Lhotakova, Z., Alberechtova, J., Janac, J. and Kubinova, L. (2008). Advantages and pitfalls of using free-hand sections of frozen needles for three-dimensional analysis of mesophyll by stereology and confocal microscopy. *Journal of Microscopy*, **232**, 56–63.

LI-COR (1992). *LAI-2000 Plant Canopy Analyzer*. LI-COR, Inc., Lincon, Nebraska, 2nd edn.

Liang, S. (2004). *Quantitative Remote Sensing of Land Surfaces*. John Wiley & Sons Ltd, New Jersey.

Lichtenthaler, H.K. (1987). *Chlorophyll and Carotenoids: Pigments in photosynthetic biomembranes*, vol. 148. Academic press, Inc., London.

Lichtenthaler, H.K., Prenzel, U. and Kuhn, G. (1982). Adaptation of Chloroplast-ultrastructure and of Chlorophyll-protein levels to high-light and low-light growth conditions. *Z. Naturforsch*, **37c**, 464–475.

Lichtenthaler, H.K., Gitelson, A.A. and Lang, M. (1996). Non-destructive determination of Chlorophyll concentration of leaves of a green and aurea mutant of Tabacco by reflectance measurement. *Journal of Plant Physiology*, **148**, 483–493.

Lichtenthaler, H.K., Babani, F. and Langsdorf, G. (2007). Chlorophyll fluorescence imaging of photosynthetic activity in sun and shade leaves of trees. *Photosynthesis Research*, **93**, 235–244.

Lillesand, T.M., Kiefer, R.W. and Chipman, J.W. (2004). *Remote sensing and image interpretation*. Wiley, New York, 5th edn.

Limpens, J., Berendse, F., Blodau, C., Canadell, J.G., Freeman, C., Holden, J., Roulet, N., Rydin, H. and Schaepman-Strub, G. (2008). Peatlands and the carbon cycle: from local processes to global implications – a synthesis. *Biogeosciences Discussions*, **5**, 1379–1419.

Lindsay, R. (1995). *Bogs: The Ecology, Classification and Conservation of Ombrotrophic mires*. Scottish Natural Heritage, Battleby, Perth.

Lindsay, R. (2010). Peatbogs and carbon: A critical synthesis to inform policy development in oceanic pet bog conservation and restoration in the context of climate change. Tech. rep., Environmental Research Group, University of East London, London.

Liu, Z., Huang, J., Xin-Hong Wu, X. and Dong, Y. (2007). Comparison of vegetation indices and red-edge parameters for estimating grassland cover from canopy reflectance data. *Journal of Integrative Plant Biology*, **49**, 299–306.

Llewellyn, G.M. (2009). *Remote sensing of grassland with contaminated soil using the spectral red-edge*. Ph.D. thesis, School of Geography, Faculty of Engineering, Science and Mathematics, University of Southampton.

Lowe, B., McMorrow , J.M., Evans, M.G. and Walker, J. (2010). Phenology of moorland plants; towardsestimating temporal window for remote sensing of peatland restoration. In *Proceedings of RSPSoc and Irish Earth Observation Symposium*, 223–230, University College Cork.

Ma, Q.Q., Wang, W., Li, Y., Li, D. and Zou, Q. (2006). Alleviation of photoinhibition in drought-stressed wheat (*Triticum aestivum*) by foliar-applied glycinebetaine. *Journal of Plant Physiology*, **163**, 165–175.

Mac Arthur, A.A. and Malthus, T.J. (2006). The hyperspectral and phenological characterisation of upland heather dominated ecological communities: Preliminary results. In *RSPSoc Annual Conference 2006. Understanding a Changing World: Integrated approaches to monitoring, measuring and modelling the environment*, University of Cambridge.

Mac Arthur, A.A. and Malthus, T.J. (2012). *Calluna vulgaris* foliar pigment and spectral reflectance modelling. *International Journal of Remote Sensing*, **33**, 5214–5239.

Mac Arthur, A.A., MacLellan, C. and Malthus, T.J. (2007). Determining the fov and directional response field of spectroradiometers. In *Imaging Spectroscopy: innovation in environmental research*, Bruges, Belgium.

Mac Arthur, A.A., MacLellan, C. and Malthus, T.J. (2012). The fields of view and directional response functions of two field spectroradiometers. *IEEE Transactions on Geoscience and Remote Sensing*, **50**, *in press.*

Macaulay Institute (2003). *HILLPLAN Field Guide Part 1: Data Collection*. Macaulay Land Use Research Institute, Craigiebuckler, Aberdeen, Sept. 2001 edn.

MacDonald, A., Stevens, P., Armstrong, H., Immirizi, P. and Reynolds, P. (1998). *A Guide to Upland Habitats: Surveying land management impacts*. Scottish Natural Heritage, Battleby.

MacDonald, A.J., Kirkpatrick, A.H., Hester, A.J. and Sydes, C. (1995). Regeneration by natural layering of heather (*Calluna-Vulgaris*) - frequency and characteristics in Upland Britain. *Journal of Applied Ecology*, **32**, 1.

MacDonald, G., Beilman, D., Kremenetski, K., Sheng, Y., Smith, L. and Velichko, A. (2006). Rapid early development of circumarctic peatlands and atmospheric CH_4 and CO_2 variations. *Science*, **314**, 285–288.

Mackey, E.C., Shaw, P., Holbrook, J., Shewry, M.C., Saunders, G., Hall, J. and Ellis, N.E. (2001). *Natural Heritage Trends: Scotland 2001*. Scottish Natural Heritage, Battleby, Perth.

Mandelis, A., Boroumand, F. and vanden Bergh, H. (1990). Quantitative diffuse reflectance spectroscopy of large powders: the melamed model revisited. *Applied Optics*, **29**, 2853–2860.

Mather, P.M. (2004). *Computer Processing of Remotely-Sensed Images*. Wiley, Chichester, 3rd edn.

Matile, P., Hortensteiner, S., Thomas, H. and Krautler, B. (1996). Chlorophyll breakdown in senescent leaves. *Plant Physiology*, **112**, 1403–1409.

McMorrow, J., Cutler, M., Al-Roichi, A. and Evans, M. (2005). Hyperspectral remote sensing of peat humification. In *4th EARSeL Workshop on Imaging Spectroscopy. New quality in environmental studies.*, Warsaw University, Warsaw.

McMorrow, J.M., Cutler, M.E.J., Evans, M.G. and Al-Roichdi, A. (2004). Hyperspectral indices for characterizing upland peat composition. *International Journal of Remote Sensing*, **25**, 313–325.

Mehner, H., Cutler, M.E.J., Fairbairn, D. and Thompson, G. (2004). Remote sensing of upland vegetation: the potential of high spatial resolution satellite sens. *Global Ecology and Biogeography*, **13**, 359–369.

Melamed, N.T. (1963). Optical properties of powders. Part 1. Optical absorption coefficients and the absoute value of diffuse reflectance. *Journal of Applied Physics*, **34**, 560–570.

Merzlyak, M., Chivkunova, O., Solovchenko, A. and Naqvi, K. (2008). Light absorption by Anthocyanins in juvenile, stressed, and senescing leaves. *Journal of Experimental Botany*, **59**, 3903–3911.

Middleton, M., Arkimaa, H., Hyvönen, E., Närhi, P., Kuosmanen, V. and Sutinen, R. (2009). Classification of boreal mire biotypes with hyperspectral airborne HyMap Finland. In *6th EARSeL IS SIG workshop. Imaging Spectroscopy: Innovative tool for scientific and commercial environmental applications.*, University of Tel-Aviv, Israel.

Mills, H. (2005). *The Potential of High Spatial Resolution Remote Sensing for Mapping Upland Vegetation using Advanced Classification Methods*. Ph.D. thesis, University of Newcastle.

Milne, J., Pakeman, R.J., Kirkham, F.W., Jones, I.P. and Hossell, J.E. (2002). Biomass production of upland vegetation types in England and Wales. *Grass and Forage Science*, **57**, 373–388.

Milne, J.A. and Hartlet, S.E. (2001). Upland plant communities - sensitivity to change. *Catena*, **42**, 333–343.

Milton, E.J. (1987). Principles of field spectroscopy. *International Journal of Remote Sensing*, **8**, 18071827.

Milton, E.J. (2009). *Field Spectroscopy*, vol. 1. EOLSS Publishers/ UNESO.

Milton, E.J. and Rollin, E.M. (1988). The directional reflectance of heather canopies: Towards a descriptive model. Proceedings of IGARSS 1988 Symposium.

Milton, E.J. and Rollin, E.M. (2006). Estimating the irradiance spectrum from measurements in a limited number of spectral bands. *Remote Sensing of Environment*, **100**, 348 – 355.

Milton, E.J., Rollin, E.M. and Emery, D.R. (1995). *Advances in field spectroscopy*, 9–32. John Wiley & Sons Ltd.

Milton, E.J., Hughes, E.J., Anderson, K., Schulz, J., Lindsay, R., Kelday, S.B. and Hill, C.T. (2005). Remote sensing of bog surfaces. Tech. Rep. 366, JNCC, Peterborough.

Milton, E.J., Schaepman, M., Anderson, K., Kneubühler, M. and Fox, N. (2009). Progress in field spectroscopy. *Remote Sensing of Environment*, **113**, S92–S109.

Moncrieff, J.B., Malhi, Y. and Leuning, R. (1995). The propagation of errors in long-term measurements of land-atmosphere fluxes of carbon and water. *Global Change Biology*, **2**, 231–240.

Moorthy, I., Miller, J., Zarco-Tejada, P.J. and Noland, T.L. (2003). Needle chlorophyll content estimation: A comparative study of prospect and liberty. 1–3, Proceedings IEEE International Geoscience and Remote Sensing Symposium.

Moorthy, I., Miller, J. and Thomas L. Noland, T. (2008). Estimating Chlorophyll concentration in conifer needles with hyperspectral data: An assessment at the needle and canopy level. *Remote Sensing of Environment*, **112**, 2824–2838.

Mücher, C.A., Kooistra, L., Vermeulen, M., Haest, B., Spanhove, T., Delalieux, S., Vanden Borre, J. and Schmidt, A. (2010). Object identification and characterization with hyperspectral imagery to identify structure and function of natura 2000 habitats. In *Proceedings of the Geobia conference*, The International Archives of the Photogrammetry, Remote Sensing and Spatial Information Sciences Vol. XXXVIII-4/C7.

Murphy, R.J., Tolhurst, T.J., Chapman, D.J. and Underwood, A.J. (2005). Estimation of surface chlorophyll-a on an exposed mudflat using field spectrometry: accuracy of ratios and derivative-based approaches. *International Journal of Remote Sensing*, **26**, 1835–1859.

Mutanga, O., Skidmore, A. and Pins, H.H.T. (2000). Predicting in situ pasture quality in the Kruger National Park, South Africa, using continuum-removed absorption feature. *Remote Sensing of Environment*, **73**, 257–269.

Myneni, R.B. and Running, S.W. (1997). Estimation of global leaf area index and absorbed PAR using radiative transfer models. *IEEE Transactions on Geoscience and Remote Sensing*, **35**, 1380–1393.

Naumann, J.C., Anderson, J.E. and Young, D.R. (2008). Linking physiological responses, Chlorophyll fluorescence and hyperspectral imagery to detect salinity stress using the physiological reflectance index in the coastal shrub, *Myrica cerifera*. *Remote Sensing of Environment*, **112**, 3865–3875.

Neil, S. (2002). *The functional role of Anthocyanins in leaves*. Ph.D. thesis, School of Biological Sciences, University of Auckland.

Nichol, C. and Grace, J. (2010). Determination of leaf pigment content in *Calluna vulgaris* shoots from spectral reflectance. *International Journal of Remote Sensing.*, **31**, 5409–5422.

Nilson, T., Kuusk, A., Lang, M. and Luik, T. (2003). Forest reflectance modeling: Theoretical aspects and applications. *Ambio*, **32**.

Ostle, N.J., Levy, P.E., Evans, C.D. and Smith, P. (2009). UK land use and soil carbon sequestration. *Land Use Policy*, **26S**, S274–S283.

Painter, T.H. (2011). Correspondence. *Journal of Glaciology*, **57**, 183–185.

Pakeman, R.J. and Nolan, A.J. (2009). Setting sustainable grazing levels for heather moorland: a multi-site analysis. *Journal of Applied Ecology*, **46**, 363–368.

Palmer, S.C.F. (1997). Prediction of the shoot production of heather under grazing in the uplands of Great Britain. *Grass and Forage Science*, **52**, 408–424.

Paterson, A. (2002). *Scotland's Landscape: Endangered Icon*. Polygon at Edinburgh, Edinburgh.

Peddle, D.R., Johnson, R.L., Cihlar, J. and Latifovic, R. (2004). Large area forest classification and biophysical parameter estimation using the 5-scale canopy reflectance model in multiple-forward-mode. *Remote Sensing of Environment*, **89**, 252–263.

Petoukhov, V. and Semenov, V.A. (2010). A link between reduced barents-kara sea ice and cold winter extremes over northern continents. *Journal of Geophysical Research*, **115**, 1–11.

Pinazo, J.M., Canada, J. and Bosca, J.V. (1995). A new method to determine Ångström's turbidity coeficient: its application for Valencia. *Solar Energy*, **54**, 219–226.

Pitcairn, C.E.R., Leith, I.D., Fowler, D., Hargreaves, K.J., Moghaddam, M., Kennedy, V.H. and Granat, L. (2001). Foliar nitrogen as an indicator of nitrogen deposition and critical loads exceedance on a European scale. *Water, Air, and Soil Pollution*, **130**, 1037–1042.

Plaza, A.J., Martinez, P., Pérez, R. and Plaza, J. (2002). Spatial/Spectral Endmember Extraction by Multidimensional Morphological Operations. *IEEE Transactions on Geoscience and Remote Sensing*, **40**, 2025–2041.

Potter, E., Wood, J. and Nicholl, C. (1996). *SunScan Canopy Analysis System*. Delta-T, Cambridge, England, 1st edn.

Price, J.S., Heathwaite, A.L. and Baird, A.J. (2003). Hydrological processes in abandoned and restored peatlands: An overview of management approaches. *Wetlands Ecology and Management*, **11**, 65–83.

Rahman, A.F., Gamon, J.A., Sims, D.A. and Schmidts, M. (2003). Optimum pixel size for hyperspectral studies of ecosystem function in southern California chaparral and grassland. *Remote Sensing of Environment*, **8**, 192–207.

Read, J.M., Birch, C.P.D. and Milne, J.A. (2002). Heathmod: a model of the impact of seasonal grazing by sheep on upland heaths dominated by *Calluna vulgaris* (heather). *Biological Conservation*, **105**, 279–292.

Reddy, A. and Raghavendra, A.S. (2006). Photooxidative stress. In Z.M. Rao, A.S. Raghavendra and K. Reddy, eds., *Physiology and molecular biology of stress tolerance in plants*, 157–186, Springer.

Rees, W.G. (2004). *Physical Principles of Remote Sensing*. Cambridge University Press, Cambridge, 2nd edn.

Ren, H.Y., Zhaung, D.F., Pan, J.J., Shi, X.Z. and Wang, H.J. (2008). Hyperspectral remote sensing to monitor vegetation stress. *Journal of Soils Sesdiments*, **8**, 323–326.

Renzullo, L., Blanchfield, A.L., Guillermin, R., Powell, K.S. and Held, A.A. (2006). Comparison of PROSPECT and HPLC estimates of leaf Chlorophyll contents in a grapevine stress study. *International Journal of Remote Sensing*, **27**, 817–823.

Rich, T., Peterken, G., Tucker, G., McMeechan, F. and Dobsan, D. (2005). *Handbook of biodiversity methods: survey, evaluation and monitoring*. Cambridge University Press, Cambridge.

Richardson, A.D., Duigan, S.P. and Berlyn, G.P. (2002). An evaluation of noninvasive methods to estimate foliar Chlorophyll content. *New Phytologist*, **153**, 185–194.

Robertson, D., Waterhouse, A., Holland, J.P., Gooding Hill, R.F., Egan, S. and Smith, A. (2003). Characterisation of *Calluna vulgaris* dominant moorland using remote sensing with Landsat TM. Http://www.sac.ac.uk/envsci/external/Hill&Mountain/eobem/Publications/dresden.pdf. Accessed 29th October 2003.

Robinson, B. (1983). *Electro-optical non-imaging sensors*, vol. 1. American Society of Photogrammetry.

Rochdi, N. and Fernandes, R. (2004). How do current GORT models describe the Bidirectional Reflectance Distribution Function of Forests? vol. 3, 1815–1818, Geoscience and Remote Sensing Symposium.

Rochefort, L. and Lode, E. (2006). *Restoration of Degraded Boreal peatlands*, vol. 188 of *Ecological Studies*, 381–417. Springer, New York.

Rodwell, J. (1991). *British Plant Communities: Mires and Heaths*. Cambridge University Press, Cambridge.

Rollin, E.M., Milton, E.J. and Anderson, K. (2002). The role of field spectroscopy in airborne sensor calibration: the example of the NERC CASI. 21pp, Proceedings of a conference on Field Spectral Measurements in Remote Sensing, University of Southampton.

Saebo, A., Haland, A., Skre, O. and Mortensen, L. (2001). Influence of nitrogen and winter climate stresses on *Calluna vulgaris* (l.) hull. *Annals of Botany*, **88**, 823–828.

Salisbury, J.W. (1998). Spectral measurements field guide. Tech. Rep. ADA362372, Defense Technology Information Centre.

Sampson, P.H., Zarco-Tejada, P.J., Mohammed, G.H., Miller, J.R. and Noland, T.L. (2003). Hyperspectral Remote Sensing of Forest Condition: Estimating Chlorophyll Content in Tolerant Hardwoods. *Forest Science*, **49**.

Sandmeier, S.R. (2000). Acquisition of Bidirectional Reflectance Factor Data with Field Goniometers. *Remote Sensing of Environment*, **73**, 257–269.

Sauceda, J., Rodreguez, H., Lozano, R., Silva, I.C. and Meza, M. (2008). Seasonal trend of Chlorophylls *a* and *b* and Carotenoids in native trees and shrubs of northeastern mexico. *Journal of Biological Science*, **8**, 258–267.

Schaepman, M.E. (1998). *Calibration of a Field Spectroradiometer: Calibration and Characterization of a Non-Imaging Field Spectroradiometer Supporting Imaging Spectrometer Validation and Hyperspectral Sensor Modelling*. Ph.D. thesis, Remote Sensing Laboratories, University of Zurich.

Schaepman, M.E., Ustin, S.L., Plaza, A.J., Painter, T.H., Verrelst, J. and Liang, S. (2009). Earth system science related imaging spectroscopy: An assessment. *Remote Sensing of Environment*, **113**, S123–S137.

Schaepman, M.E., Kneubühler, M., Bartholomeus, H., Malenovský, Z., Damm, A., Schaepman-Strub, G. and Hueni, A. (2010). Scaling spectroscopic approaches – from leaf albedo to ecosystems mapping. Proceedings of ASD and IEEE GRS; Art, Science and Applications of Reflectance Spectroscopy Symposium, Vol. II, 19pp, Boulder, CO.

Schaepman-Strub, G., Schaepman, M.E., Painter, T.H., Dangel, S. and Martonchik, J.V. (2006). Reflectance quantities in optical remote sensing-definitions and case studies. *Remote Sensing of Environment*, **103**, 27–42.

Schaepman-Strub, G., Limpens, J., Menken, M., Bartholomeus, H.M. and Schaepman, M.E. (2008). Towards spatial assessment of carbon sequestration in peatlands: spectroscopy based estimation of fractional cover of three plant functional types. *Biogeosciences Discussions*, **5**, 1293–1317.

Scheumann, V., Schoch, S. and Rudiger, W. (1999). Chlorophyll *b* reduction during senescence of barley seedlings. *Planta*, **209**, 364–370.

Schjoerring, J., Husted, S. and Poulson, M.M. (1998). Soil-plant-atmosphere ammonia exchange associated with *Calluna vulgaris* and *Deschampsia flexuosa*. *Atmospheric Environment*, **32**, 507–512.

Schlerf, M. and Atzberger, C. (2006). Inversion of a forest reflectance model to estimate structural canopy variables from hyperspectral remote sensing data. *Remote Sensing of Environment*, **100**, 281 – 294.

Schmid, T., Koch, M. and Gumuzzio, J. (2005). Multi-sensor approach to determine changes of wetland characteristics in semi-arid environments (Central Spain). *IEEE Transactions on Geoscience and Remote Sensing*, **43**, 2516–2525.

Schumann, M. and Joosten, H. (2008). Global peatland restoration manual. Tech. rep., Germany.

Schwartz, M.D. (2003). Introduction. In M.D. Schwartz, ed., *Phenology: An integrative Environmental Science*, Kluwer Academic Publishers, London.

Scottish Government (2011). Prescribed burning on moorland, Supplement to the Muirburn Code: A Guide to Best Practice.

http://www.scotland.gov.uk/Resource/Doc/158521/0042977.pdf. Accessed 6th August 2011.

Scottish Natural Heritage (2002). *Hills and Moors*. Natural heritage Futures, Scottish Natural heritage, Battleby, Perth.

Scottish Natural Heritage (2003). Principles of moorland management. http://www.snh.org.uk/pdfs/publications/heritagemanagement/moorlandforum.pdf. Accessed 6th August 2011.

Scottish Natural Heritage (2005). The Peatlands of Caithness & Sutherland Management Strategy 2005 - 2015. Battleby, Perth.

Scottish Natural Heritage (2011). Hills and Moors. http://www.snh.org.uk/futures/Data/pdfdocs/Hills_and_Moors.pdf. Accessed 3rd January 2011.

Sestak, Z., Catsky, J. and Jarvis, P. (1971). *Plant Photosynthetic Production*. DR W. Junk N.V, The Hague.

Shen, M., Chen, J., Zhu, X., Tang, Y.S. and Chen, X. (2010). Do flowers affect biomass estimate accuracy from NDVI and EVI? *International Journal of Remote Sensing.*, **31**, 2139–2149.

Simic, A., Chen, J.M., Freemantle, J.R., Miller, J.R. and Pisek, J. (2010). Improving Clumping and LAI Algorithms Based on Multiangle Airborne Imagery and Ground Measurements. *IEEE Transactions on Geoscience and Remote Sensing*, **48**, 1742–1759.

Simpson, I.A., Kirkpatrick, A.H., Scott, L., Gill, J.P., Hanley, N. and MacDonald, A.J. (1998). Application of a grazing model to predict heather moorland utilization and implications for nature conservation. *Journal of Environmental Management*, **54**, 215–231.

Sims, D.A. and Gamon, J.A. (2002). Relationships between leaf pigment content and spectral reflectance across a wide range of species, leaf structures and developmental stages. *Remote Sensing of Environment*, **81**, 337–354.

Smith, A.M.S., Wooster, M.J., Drake, N.A., Dipotso, F.M., Falkowski, M.J. and Hudak, A.T. (2005). Testing the potential of multi-spectral remote sensing for retrospectively estimating fire severity in African Savannahs. *Remote Sensing of Environment*, **97**, 92–115.

Smith, L., MacDonald, G., Velichko, A.A., Beilman, D.W., Borisova, O.K., Frey, K.E., Kremenetski, K. and Sheng, Y. (2004). Siberian Peatlands a Net Carbon Sink and Global Methane Source Since the Early Holocene. *Science*, **303**, 353–355.

Smith, M., Stevens, T., Mac Arthur, A.A., Malthus, T. and Lu, H. (2011). Characterising Chinese loess stratigraphy and past monsoon variation using field spectroscopy. *Quaternary International*, **234**, 146–158.

Smithson, P. and Atkinson, K. (2008). *Fundamentals of the Physical Environment*. Routledge, New York, 4th edn.

Smolander, S. and Stenberg, P. (2003). A method to account for shoot scale clumping in coniferous canopy reflectance models. *Remote Sensing of Environment*, **88**, 363 – 373.

Spectra Vista Corporation (undated). *GER 3700 Spectroradiometer User Manual*. Spectra Vista Corporation, Poughkeepsie, New York, 2nd edn.

Steiner, D. and Gutermann, T. (1966). Russian data on spectral reflectance of vegetation, soil and rock types: Final technical report. Tech. rep., Department of Geography, University of Zurich and European Research office, United States Army.

Steven, M.D. (2004). Correcting the effects of field of view and varying illumination in spectral measurements of crops. *Precision Agriculture*, **5**, 55–72.

Steyn, W.J., andHolcroft D. M. Wand, S.J.E. and Jacobs, G. (2002). Anthocyanins in vegetative tissues: A proposed unified function in photoprotection. *New Phytologist*, **155**, 349–361.

Strahler, A.H., Woodcock, C.E. and Smith, J.A. (1986). On the nature of models in remote sensing. *Remote Sensing of Environment*, **20**, 121–139.

Strandberg, M. and Johansson, M. (1999). Uptake of nutrients in *Calluna vulgaris* seed plants grown with and without mycorrhiza. *Forest Ecology and Management*, **114**, 129–135.

Taiz, L. and Zeiger, E. (2002). *Plant Physiology*. Sinauer Associates, Inc., Sunderland, Massachusetts, 3rd edn.

Teh, Y.A., Silver, W.L., Sonnentag, O., Detto, M., Kelly, M. and Baldocchi, D.D. (2011). Large greenhouse gas emissions from a temperate peatland pasture. *Ecosystems*, **14**, 311–325.

Thenkabail, P.S., Smith, R.B. and De Pauw, E. (2000). Hyperspectral vegetation indices and their relationships with agricultural crop characteristics. *Remote Sensing of Environment*, **71**, 158–182.

Thomas, V., Treitz, P., Jelinski, D., Miller, J., Lafleur, P. and McCaughey, J.H. (2002). Image classification of a northern peatland complex using spectral and plant community data. *Remote Sensing of Environment*, **84**, 83–89.

Thomas, V., McCaughey, J.H., Treitz, P., Finch, D.A., NewAuthor5 and Rich, L. (2009). Spatial modelling of photosynthesis for a boreal mixedwood forest by integrating micrometeorological, lidar and hyperspectral remote sensing data. *Agricultural and Forest Meteorology*, **149**, 639–654.

Thompson, D.B.A., MacDonald, A.J., Marsden, J.H. and Galbraith, C.A. (1995). Upland Heather Moorland in Great-Britain - a Review of International Importance, Vegetation Change and Some Objectives for Nature Conservation. *Biological Conservation*, **71**, 63–178.

Tomos, A.D. (1985). The physical limitations of leaf cell expansion. In N. Baker, W. Davies and C. Ong, eds., *Control of leaf growth*, 1–33, Cambridge University Press.

Trenbeth, K.E. (1990). Recent observed interdecadal climate change in the northern hemisphere. *American Meteorological Society*, **71**, 988–993.

Trodd, N. (1996). Analysis and representation of heathland vegetation from near-ground level remotely-sensed data. *Global Ecology and Biogeography Letters*, **5**, 206–216.

Usher, M.B., MacKey, E.C. and Curran, J.C. (2001). *The State of Scotland's Environment and Natural Heritage*. The Stationary Office, Edinburgh, Scotland.

Ustin, S.L. and Whiting, M.L. (2006). Determination of crop residue cover using field spectroscopy. In *Soil Carbon and California's Terrestrial Ecosystems, Final Report*, Kearney Foundation of Soil Science, Davis, California.

Ustin, S.L., Jacquemoud, S., Zarco-Tejada, P.J. and Asner, G.P. (2004a). *Remote sensing of the environment: state of the science and new directions*, 679–729. Remote Sensing for Natural Resource Management and Environmental Monitoring, John Wiley and Sons, New York.

Ustin, S.L., Roberts, D.A., Gamon, J.A., Asner, G.P. and Green, R.O. (2004b). Using imaging spectroscopy to study ecosystem processes and properties. *Biosciences*, **54**, 523–534.

Ustin, S.L., Gitelson, A.A., Jacquemoud, S., Schaepman, M., Gregory, P., Asner, G.P., Gamon, J.A. and Pablo Zarco-Tejada, P. (2009). Retrieval of foliar information about plant pigment systems from high resolution spectroscopy. *Remote Sensing of Environment*, **113**, S67–S77.

van der Meer, F.D. (2001). Basic physics of spectrometry. In F. van der Meer and S.M. de Jong, eds., *Imaging Spectroscopy: Basic principles and Prospective Applications*, vol. 4, Kluwer Academic Publishers, London.

van der Meer, F.D., de Jong, S.M. and Bakker, W.H. (2001). Basic analytical techniques. In F. van der Merr and S.M. de Jong, eds., *Imaging Spectrometry: basic principles and prospective applications*, vol. 4, Kluwer Academic Publishers, London.

Vazquez, J.M., Arquero, A., Martinez, E. and Gonzalo, C. (2004). Efficient methodology for endmembers selection by field radiometry: an application to multispectral mixture model. In *Image and Signal Processing for Remote Sensing X*, vol. 5573, 435–443, Proc. of SPIE.

Verhoef, W. (1984). Light scattering by leaf layers with application to canopy reflectance modeling: The SAIL model. *Remote Sensing of Environment*, **16**, 125–141.

Verhoef, W. and Bach, H. (2003). Simulation of hyperspectral and directional radiance images using coupled biophysical and atmospheric radiative transfer models. *Remote Sensing of Environment*, **87**, 23–41.

Verhoef, W. and Bach, H. (2007). Coupled soil–leaf-canopy and atmosphere radiative transfer modeling to simulate hyperspectral multi-angular surface reflectance and toa radiance data. *Remote Sensing of Environment*, **109**, 166–182.

Vesala, T., Rannik, Ü., Leclerc, M., Foken, T. and Stabelfeld, K. (2004). Flux and concentration footprints. *Agricultural and Forest Meteorology*, **127**, 111–116.

Visser, F. and Smolar-Zvanut, N. (2009). Detecting submerged macrophytes in a uk chalk stream using field spectroscopy. 541–547, Proceedings of the Annual Conference of the Remote Sensing and Photogrammetry Society.

Vitt, D.H. (2006). Functional characteristics and indicators of boreal peatlands. In R.K. Wieder and D.H. Vitt, eds., *Boreal peatland Ecosystems*, Ecological Studies, 9–21, Springer.

Vogelmann, J.E. and Moss, D.M. (1993). Spectral Reflectance Measurements in the Genus *Sphagnum*. *Remote Sensing of Environment*, **45**, 273–279.

Voßbeck, M., Clerici, M., Kaminski, T., Lavergne, T., Pinty, B. and Giering, R. (2010). An inverse radiative transfer model of the vegetation canopy based on automatic differentiation. *Inverse Problems*, **26**, 1–15.

Wagner, G.J. (1991). Secreting glandular trichomes: More than just hairs. *Plant Physiology*, **96**, 675–679.

Wardley, N.W., Milton, E.J. and Hill, C.T. (1987). Remote sensing of structurally complex semi-natural vegetation an example from heathland. *International Journal of Remote Sensing*, **8**, 31–42.

Warren, C. (2002). *Managing Scotland's Environment*. Edinburgh University Press, Edinburgh, Scotland.

Watt, A.S. (1947). Pattern and process in the plant community. *Journal of Ecology*, **35**, 1–22.

Watts, D. and Eley, J. (1970). Changes in the Chlorophyll a:b ratio during autumn coloration of *Populus sargentii*. *Bulletin of the Torrey Botanical Club*, **108**, 379–382.

Weiss, M., Troufleau, D., Baret, F., Chauki, H., Prévot, L., Olioso, A., Bruguier, N. and Brisson, N. (2001). Coupling canopy functioning and radiative transfer models for remote sensing data assimilation. *Agricultural and Forest Meteorology*, **108**, 113–128.

White, M.A., Brunsell, N. and Schwartz, M.D. (2003). Vegetation phenology in global cahnge studies. In *Phenology: An integrative Environmental Science*, 453–446, Kluwer Academic Publishers.

Widlowski, J.L., Taberner, M., Pinty, B., Bruniquel-Pinel, V., Disney, M., Fernandes, R., Gastellu-Etchegorry, J.P., Gobron, N., Kuusk, A., Lavergne, T., Leblanc, S., Lewis, P., Martin, E., Mottus, M., North, P., Qin, W., Robustelli, M., Rochdi, N., Ruiloba, R., Soler, C., Thompson, R., Verhoef, W., Verstraete, M.M. and Xie, D. (2007). Third radiation transfer model intercomparison (RAMI) exercise: Documenting progress in canopy reflectance models. *Journal of Geophysical Research*, **112**, 1–28.

Wieder, R.K. and Vitt, D.H. (2006). *Preface*, vol. 188 of *Ecological Studies*, v–vi. Springer, Berlin, Germany.

Wright, G.G., Sibbald, A.R. and Allison, J.S. (1997). The integration of a satellite spectral analysis into a heather moorland management model (HMMM): the case of Moidach More, northeast Scotland, U.K. *International Journal of Remote Sensing*, **18**, 2319–2336.